STATIC AND DYNAMIC LOAD, STRESS, AND DEFLECTION CYCLES IN SPUR-GEAR SYSTEMS

by

Herbert H. Richardson

S.B., Massachusetts Institute of Technology
(1955)

S.M., Massachusetts Institute of Technology
(1955)

SUBMITTED IN PARTIAL FULFILLMENT OF THE REQUIREMENTS FOR THE DEGREE OF DOCTOR OF SCIENCE

AT THE

MASSACHUSETTS INSTITUTE OF TECHNOLOGY

June, 1958

Signature of Author _____
Department of Mechanical Engineering, May 19, 1958

Certified By _____
Thesis Supervisor

Accepted By _____
Chairman, Departmental Committee on Graduate Students

STATIC AND DYNAMIC LOAD, STRESS, AND DEFLECTION CYCLES IN SPUR-GEAR SYSTEMS

by

Herbert H. Richardson

Submitted to the Department of Mechanical Engineering on May 19, 1958, in partial fulfillment of the requirements for the degree of Doctor of Science.

ABSTRACT

A rigorous analysis of the static behavior of spur-gear systems is presented. Curves, data, and equations are given which permit computation of the static load, stress, and deflection cycles for any gear system, real or proposed. The effects of nonlinear elasticity, elastic deformation during load transfer, manufactured errors and friction are included in the analysis, and the results of the analysis are verified by comparison with measured stress cycles for actual gears.

General equations for the dynamic behavior of spur-gear systems are derived, and simplified forms of the equations are suggested. Two simplified analyses of dynamic loads and stresses are presented; the first analysis considers dynamic loads to occur as the result of single-load-transfer disturbances, and the second analysis considers dynamic load to be excited through the action of the effective time-varying elasticity of the gear mesh. Solutions for both of these cases are presented in the form of nondimensional charts.

A simple experimental technique which employs wire strain gages for measuring dynamic loads and stresses in operating gear systems is described.

Comparison is made between preliminary measured dynamic-stress cycles and the predictions of the two simplified analyses presented. This comparison indicates that a single-load-transfer analysis based on idealized gear-tooth geometry will give somewhat conservative predictions of dynamic load and stress for lightly-loaded, inaccurately-machined gearing. However, in the case of heavily-loaded, accurately-machined gearing, the qualitative behavior was predictable only by the variable-elasticity analysis. For the precision gears tested in this investigation, no dynamic increment loads were observed that were in excess of 15 per cent of the static loads.

Thesis Supervisor: Robert W. Mann
Title: Assistant Professor
Mechanical Engineering

ACKNOWLEDGMENTS

The author wishes to express his sincere appreciation for the guidance, advice, assistance, and cooperation which has been contributed to this investigation from many sources, not all mentioned specifically here.

First of all, thanks are due to Dr. John A. Hrones and the staff of the Dynamic Analysis and Control Laboratory for the inspiration and the stimulating environment which made this work possible. The interest shown by Dr. Thomas Searle and Mr. James Coakley of the laboratory staff is particularly appreciated.

Sincere thanks are expressed to Professor Robert W. Mann, who acted as thesis supervisor, and to Professors N. C. Dahl, T. P. Goodman, J. B. Reswick and W. A. Wilson of the Mechanical Engineering Department for their interest in this investigation and for their generous contributions of technical and personal advice and counsel throughout all phases of this thesis project.

The competent help of Mr. Helge Heen of the Dynamic Analysis and Control Laboratory staff during the initial analytical and experimental phases of this project is gratefully acknowledged.

Outside of M. I. T. several individuals and organizations contributed to this investigation. The author wishes to acknowledge his indebtedness to the Caterpillar Tractor Company for its generous contributions to this project in terms of test equipment, and particularly to Mr. Bruce Kelley of this company's research staff for his interest in this study and for his competent advice and assistance in connection with the experimental work. Thanks also are due to Mr. Jake Jaeger and the Pratt and Whitney Tool Company for the careful and precise grinding of two sets of test gears for use in this project.

The financial support for this investigation was provided by the Office of Ordnance Research, Army Ordnance Corps, under Contract No. DA-19-020-ORD-3697, Ordnance R and D Project No. TB2-0001.

Finally, a special acknowledgement is due to Miss Grace Lynch of the Dynamic Analysis and Control Laboratory staff, not only for her meticulous preparation of this manuscript, but also for her capable handling of many of the administrative aspects of this research project.

TABLE OF CONTENTS

TABLE OF CONTENTS (Continued)

TABLE OF CONTENTS (Continued)

LIST OF FIGURES

LIST OF FIGURES (Continued)

LIST OF FIGURES (Continued)

LIST OF FIGURES (Continued)

LIST OF FIGURES (Continued)

CHAPTER 1. INTRODUCTION

1. Statement of the Problem

Gearing, one of the most universally used machine elements, is applied in mechanical systems of every size and description, from the tiny pinions in a watch or a computer system to the high-speed, heavily-loaded reduction gears of an aircraft gas turbine. Modern trends toward high speeds, minimum weights and volumes, great precision, and high-temperature operation, have accentuated, increased in importance, and made more difficult the problems of gear design.

Classical methods of gear design, developed between the years 1850 to 1931, involve the use of semi-empirical equations developed from early service tests carried out on gearing. These tests covered the ranges of most parameters involved in transmission gearing for steam and internal-combustion engines or electric motors and laid a firm basis for the conservative design of similar gearing. However, in modern aircraft, missile, and space-vehicle applications, where test data on comparable gears do not exit, these semi-empirical equations generally are inadequate. Virtually all new critical gear designs must be evolved at least in part through operational testing and trial-and-error refinement, owing to the lack of reliable design information.

Thus the need is becoming more and more acute to re-examine gear technology in the light of present and future needs, and to develop rigorous methods, based on fundamental principles, for predicting and optimizing gear performance.

This thesis deals only with one phase of the general gear design problem: that of predicting the contact loads and significant stresses that exist between mating gear teeth under operational conditions. The objectives of the thesis are to achieve a thorough understanding of the load and stress behavior under static or low-speed conditions of gear operation, and to initiate careful investigation of the dynamic loads

and stresses which occur under conditions of high-speed operation in the presence of appreciable inertia.

2. Resume of Past and Current Work Concerning Gear-Tooth Loads

2.1. Early History

Literature on the subject of gear-tooth loads and the strength and durability of gears dates back at least to 1796. In 1879, an investigation by John H. Cooper revealed the existence of over 48 well-established rules for the horsepower capacity and working strength of gears, differing by as much as a factor of five. In a subsequent study by William Harkness in 1886, differences of 15 to 1 were found in the predicted power capacity of a given pair of gears[8+].

The first attempt to apply engineering analysis to the strength of gear teeth was set forth by Wilfred Lewis[1] in a paper presented at the Engineers' Club of Philadelphia in 1892. Lewis, through application of simple-beam theory to a gear tooth, related the allowable transmitted load for low speed operation to an allowable working stress for the material, and to the geometry of the tooth. The Lewis formula, Eq. (1.1) expresses the allowable tooth load in terms of the bending stress induced at the root of the tooth:

$$W = \frac{\sigma f Y}{p_d \cos \theta} \tag{1.1}$$

where

W = allowable load, normal to the tooth profile

σ = allowable bending stress

f = face width

p_d = diametral pitch = number of teeth ÷ pitch diameter

θ = pressure angle.

+Superscript numbers are appended in the Bibliography, Appendix E.

The factor Y in Eq. (1.1) has become known as the Lewis form factor, and is a function of the number of teeth in the gear and of the position of the load along the tooth surface. Tables of this factor have been worked out by Lewis and others, for conditions of loading at the tip and near the middle of the tooth[11].

In connection with his proposed design equation, Lewis discussed the effects of gear speed or pitch-line velocity in terms of a reduced allowable stress, and presented velocity factors recommended for pitch-line velocities up to 2400 ft/min. These factors subsequently were put into the following equation form by Carl Barth[8]

$$\sigma = \frac{600\ \sigma_s}{600 + v} \tag{1.2}$$

where σ_s is the allowable static stress, v is the pitch-line velocity in ft/min., and σ is the stress to be used in Eq. (1.1).

Oscar Lasche, in 1899, suggested the concept of a dynamic increment load, which results from the combined action of the gear inertia and geometrical errors in the gear teeth[2]. Lasche reasoned that the actual peak load on a particular tooth would be greater at high speeds than its average or static value, and that the maximum value of the actual dynamic load should be used in Eq. (1.1) in place of the stress modification factor, Eq. (1.2), of Lewis and Barth. A special research committee was formed under A.S.M.E. about 1920 to investigate gear-tooth loads and to establish standard design criteria for gearing. A test machine was designed by Lewis,[6,7] was manufactured, and was shipped to M.I.T. in 1924, where a series of tests under the direction of Earle Buckingham was initiated to determine the effects of accuracy and velocity on the load capacity of gears[8, 10, 11, 12, 13, 14, 16, and 18]. The method of measuring dynamic loads on the gear teeth was an indirect one which involved determination of the speed at which the teeth of a load-transmitting gear pair would separate. A separation was taken as an indication that the dynamic increment load had become equal

to the average transmitted load. Separation was indicated by an increase of electrical resistance through the test-gear mesh. During the course of these studies, the Lewis Equation (Eq. (1.1) was found inadequate to predict allowable loads, even at low speeds. Failure of gears tested was observed to occur principally by severe and progressive pitting of the tooth surfaces near the pitch point. Following suggestions by Logue and Jandesek, Buckingham applied the Hertz equation for the maximum surface compressive stress between contacting rollers to measure wearing quality of gear tooth surfaces. The so-called wear equation, as derived by Buckingham[29], takes the form

$$W = 2R_p f \frac{2\,ig}{ig + ip} K \tag{1.3}$$

where R_p is the pitch radius of the pinion, ip and ig are numbers of teeth on the pinion and gear, respectively, f is face width, and K is termed a "wear factor". A table of wear factors[29] was developed empirically for use in Eq. (1.3).

The data on dynamic tooth loads which resulted from the test program carried out on the Lewis machine was put in the form of an empirical equation:

$$T_d = T_t + T_i = T_t + \frac{T_t + C\,ef}{1 + \frac{20}{v}(T_t + C\,ef)^{\frac{1}{2}}} \tag{1.4}$$

where

T_d = tangential component of dynamic load, lbs.

T_t = average transmitted tangential load, lbs.

C = tabulated materials coefficient related to tooth flexibility, lbs/in.^{2}

e = manufactured error (equivalent constant value), in.

v = pitch-line velocity, ft/min.

With the publication, in 1931, of the results of this test program in a Special Research Bulletin of A.S.M.E.[19], the classical method of gear design was established, and Eqs. (1.1), (1.3) and (1.4) became widely accepted as a design basis for gearing. Even today these results appear in almost every standard textbook on machine design[47], and over many years have proven satisfactory for the solution of many ordinary gear design problems.

2.2. Recent Developments and Current Practice.

After completion of the work carried on by the A.S.M.E. Special Research Committee on the Strength of Gear Teeth, very little research in gearing was reported until after the outbreak of World War II. The impetus provided by vital needs for high-performance, light-weight gearing in military aircraft resulted in the initiation of many gear-research programs. The design methods of Lewis and Buckingham proved grossly inadequate in predicting gear performance to the desired degree of accuracy, and areas of investigation were broadened to such things as gear-tooth lubrication under conditions of non-rigid teeth,[40] non-uniform load distribution on tooth surfaces,[25] power loss and efficiency[29], and effects of mode of loading on fatigue life[46]. Since discussion of all these factors lies somewhat outside the scope of this thesis, the reader is referred to the bibliography for detailed references concerning these and other specific gear problems.

2.21. Current Failure Criteria

At the present time, most gear designs are based on three major criteria which now appear to control gear failure.

2.211. Bending Stress Criterion

The Lewis Equation (Eq. (1.1)) is almost universally employed, modified by a suitable "stress correction factor," n, which takes account of the stress concentration at the root of the tooth and corrects errors in theory involved in assuming a gear tooth is a simple cantilever beam[9, 20, 23]. The most widely used stress correction factor is that of Dolan and Broghamer[24], which was derived from studies of photoelastic models of gear teeth.

$$n = 0.18 + \left(\frac{t_o}{r_f}\right)^{0.15} \left(\frac{t_o}{h}\right) \tag{1.5}$$

where t_o, r_f, and h, refer to tooth thickness at the root, fillet radius, and height of the load above the tooth, respectively. Equation (1.1) for the allowable load normal to the profile then assumes the form, known as the Modified Lewis Equation,

$$W = \frac{\sigma f Y}{n\ p_d \cos \theta} \tag{1.6}$$

For critical gear designs, where an error of 10 per cent or so is undesirable, more refined and more complex methods of computing the maximum bending stress in a gear tooth have been developed. In a recent publication[48], Kelley and Pedersen have developed a new formula for computing the maximum bending stress in the root of any gear tooth. The formula presented was derived using photoelastic data, and was verified by experimental evidence using carburized and hardened test gears. Good correlation between the formula and all known photoelastic data was found for positions from the tip of the tooth down to the lowest point at which load can occur. Application of the Kelley-Pedersen formula involves first a layout of the tooth, as shown in Fig. 1. A parabola is then inscribed in the gear-tooth outline as indicated. At the point of contact between the tooth fillet and the parabola, a tangent is drawn to the parabola making an angle α with the tooth centerline. A second line is then drawn through the point of contact with the fillet, making an angle ϵ with the tangent previously drawn. The angle ϵ, called a stress-shift angle, is given by the empirical equation

$$\epsilon = 25^{\circ} - \frac{\alpha}{2}\,. \tag{1.7}$$

In terms of the remaining quantities shown on Fig. 1, the final equation for the maximum bending stress is:

$$\sigma = \frac{W}{f}\left[1 + 0.26\left(\frac{e'}{r_f}\right)^{0.7}\right]\left[\frac{1.5a'}{e'^2} + \frac{\sin\beta}{2\,e'} + \frac{0.45}{(b'e')^{\frac{1}{2}}}\right] \tag{1.8}$$

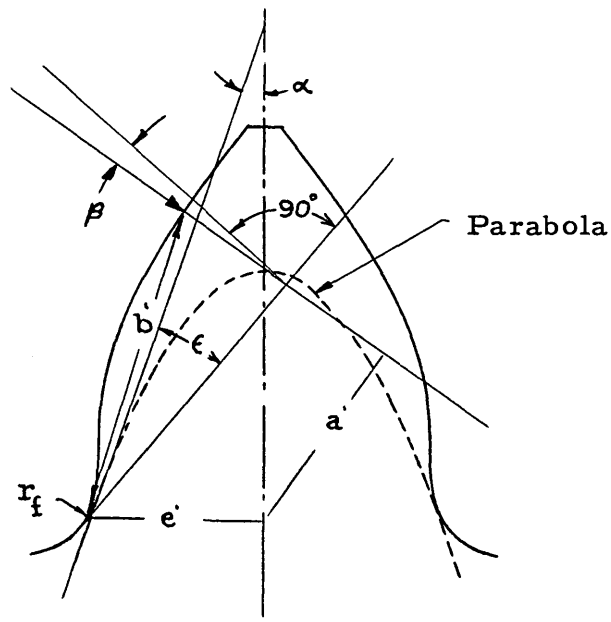

Fig. 1. Construction for Kelley-Pedersen Beam Strength Formula

When the magnitude and direction of the load on a gear tooth is known, Eq. (1.8) can be used to compute the maximum bending stress in the tooth to a high degree of accuracy. This stress then can be compared with limiting fatigue or yield stresses for the material in a proposed gear design. Due to the complexity of this method, it normally would be employed only in highly critical designs. Even then, the simpler Lewis equation probably would be used in the initial phases of the design process.

2.212. Wear Strength Criterion

When two spur-gear teeth are in contact but are not loaded, the contact occurs only along a single line. However, as load is applied to the gears, this line broadens out into a narrow contact band over which the transmitted load is distributed. This distributed force gives rise to local stresses which, if excessive, will cause failure of the tooth surfaces by a progressive and destructive pitting and breakdown. Such failures were termed "wear" failures by Buckingham, and are to be distinguished from scoring or scuffing which results from breakdown of lubrication between the mating members.

The original wear equation of Buckingham, Eq. (1.3), is generally used, with the tabulated wear factors (K), presented by Buckingham in 1949[29]. For applications where finite gear life is permissible, much higher wear factors than those given by Buckingham have often proved satisfactory[47]. In some instances, the surface compressive stress is calculated, without reference to an empirical wear factor, directly from the theoretical Hertz equation

$$\sigma_c^{\,2} = \frac{0.35W \left(\frac{1}{R_p} + \frac{1}{R_g}\right)}{f \sin\theta \left(\frac{1}{E_p} + \frac{1}{E_g}\right)} \tag{1.9}$$

where σ_c is compressive stress, R_p, R_g and E_p, E_g are pitch radii, and Young's moduli, respectively, for the pinion and the gear[33]. Because the actual wear failures are influenced by factors other than the stress computed from Eq. (1.9), notably the viscosity and viscosity characteristics of the lubricant, theoretical predictions of wear strength based on Eq. (1.9) usually are considerably in error.

2.213. Scoring Resistance Phenomena

When gearing is operated under conditions of high speed, heavy loads, or high temperatures, failure of the tooth surfaces has been found to occur by local seizing or welding and tearing of the metal. Such failures are known as scoring, scuffing, or tearing, and depend on variables such as

lubricant properties, sliding velocity of the tooth surfaces, friction, temperature, surface finish, and tooth load.

Initial attempts to predict scoring in gears took the form empirical "P. V. T." factor[37]; the product of the Hertz compressive stress σ_c from Eq. (1.9), in psi, the sliding velocity V between mating teeth, in ft/sec., and the distance T along the line of action from the pitch point to the point of contact, in inches. Some success has been experienced in correlating incipient scoring with this empirical factor, and it is widely used in the gear industry today.

The best currently available design information on gear scoring involves a comparison between the flash temperature of the lubricating oil and a calculated peak temperature in the contact region between mating teeth. Blok[21, 28] derived the following equation for this maximum temperature T_f by considering the generation of heat by friction and the transient flow of heat away from the contact region

$$T_f - T_o = \frac{k \mu W(V_1 - V_2)}{\sqrt{b}\left(S_1\sqrt{V_1} + S_2\sqrt{V_2}\right)} \tag{1.10}$$

where T_o is the gear blank temperature, k is a constant, μ is the coefficient of friction, W is the tooth load, V_1 and V_2 are linear velocities of the gear teeth at their contact point, S_1 and S_2 are properties of the metals, and b is the width of the contact zone as computed from Hertz theory.

Kelley[38] has improved the Blok approach by including effects of reduction in load W due to multiple-pair contact and of surface finish. Experimental work by Kelley and by Dudley[42] show excellent correlation between the flash temperature of the lubricant and incipient scoring in spur gearing.

In applying the three criteria discussed above to a proposed gear design, one of the greatest difficulties that arises is the problem of determining the correct value of load W to use in the design equations. Attempts to employ the early semi-empirical equation of Buckingham (Eq. 1.4) often prove unsatisfactory for predicting dynamic loads, and in many cases large inaccuracies are present in current methods of predicting even static loads. In essentially all cases known to this author, dynamic loads are computed by industrial gear companies from various empirical formulas, which differ depending on the type of gearing manufactured, the past experience of the particular company, and also on the forms of failure criteria used. For example, some aircraft companies neglect dynamic loads entirely in their calculations, other companies employ the original Buckingham equation, while still others state that Buckingham's results give low estimates of dynamic load and that they employ empirical forms similar to the Barth equation (Eq. 1.3). In short, much confusion exists in the area of gear-tooth loads, particularly in connection with dynamic loads. The following paragraphs are concerned with the currently available information regarding gear-tooth loads.

2.22. Static-Load Distribution in Gear Teeth

Most spur gears are designed to have a contact-ratio between one and two under conditions of ideal geometry. That is, ideally, there is always at least one pair of teeth in contact, but never more than two pairs in contact. When only one pair of teeth is in contact, this pair necessarily must carry all the load transmitted through the mesh; however, when two or more pairs of teeth are in contact, there is a division of load between the pairs according to their respective flexibilities and geometrical errors. For example, one pair of teeth might have a large manufactured error relative to the adjacent pair, which would cause one pair to carry nearly all of the transmitted load. Since the maximum bending stress at the root of a tooth is approximately determined, for low-speed operation, by the maximum combination of static-load height and load magnitude (bending moment), it is important in applying the bending criterion to have

a complete knowledge of the load cycle or load history of any tooth as it passes through the mesh. This need is also apparent in connection with the scoring criterion.

The first input to any study of load distribution in gear teeth is a knowledge of tooth flexibility. Several investigations have been carried out in this area[9, 19, 22, 30 and 41]. Measurements have been made by Timoshenko and Baud[9], Walker[22], Buckingham[19], and Van Zandt[41]; and theoretical analyses have been carried out by Timoshenko and Baud, Walker, and Weber[30]. The best analytical treatment is that of Weber, who considered deformation due to bending, shearing, and direct compression of the tooth considered as a short beam; distortion of the rim material underneath the tooth; and local compression at the point of contact between mating teeth. Published measurements show differences of up to nearly a factor of two from theoretical calculations. This discrepancy appears to result from difficulties in establishing a reference point for zero deflection. Figure 2, adapted from a literature survey thesis by Brickman[51], shows representative tooth-flexibility curves according to various investigators, plotted as a function of the position of loading along the tooth profile. The apparently-best measured curve (Van Zandt) has essentially the same nonlinear shape as the best analytical curve (Weber), but the two curves appear to differ by the addition of a linear spring (constant amount of deformation per unit load).

Peterson, in 1930, presented an analysis and computed several representative curves showing the static load cycles for gears in the presence of elastic deformation and errors in tooth-to-tooth spacing[17]. Similar work has been done in England and Germany, and has been applied, in those countries and in the U. S., to computation of modified profile shapes for minimizing tooth loads over the whole engagement interval[22, 31, 32]. In all of these works known to the author, transfer of load from tooth to tooth has been assumed instantaneous, although in reality it must be a gradual process; and the effects of friction have not been considered.

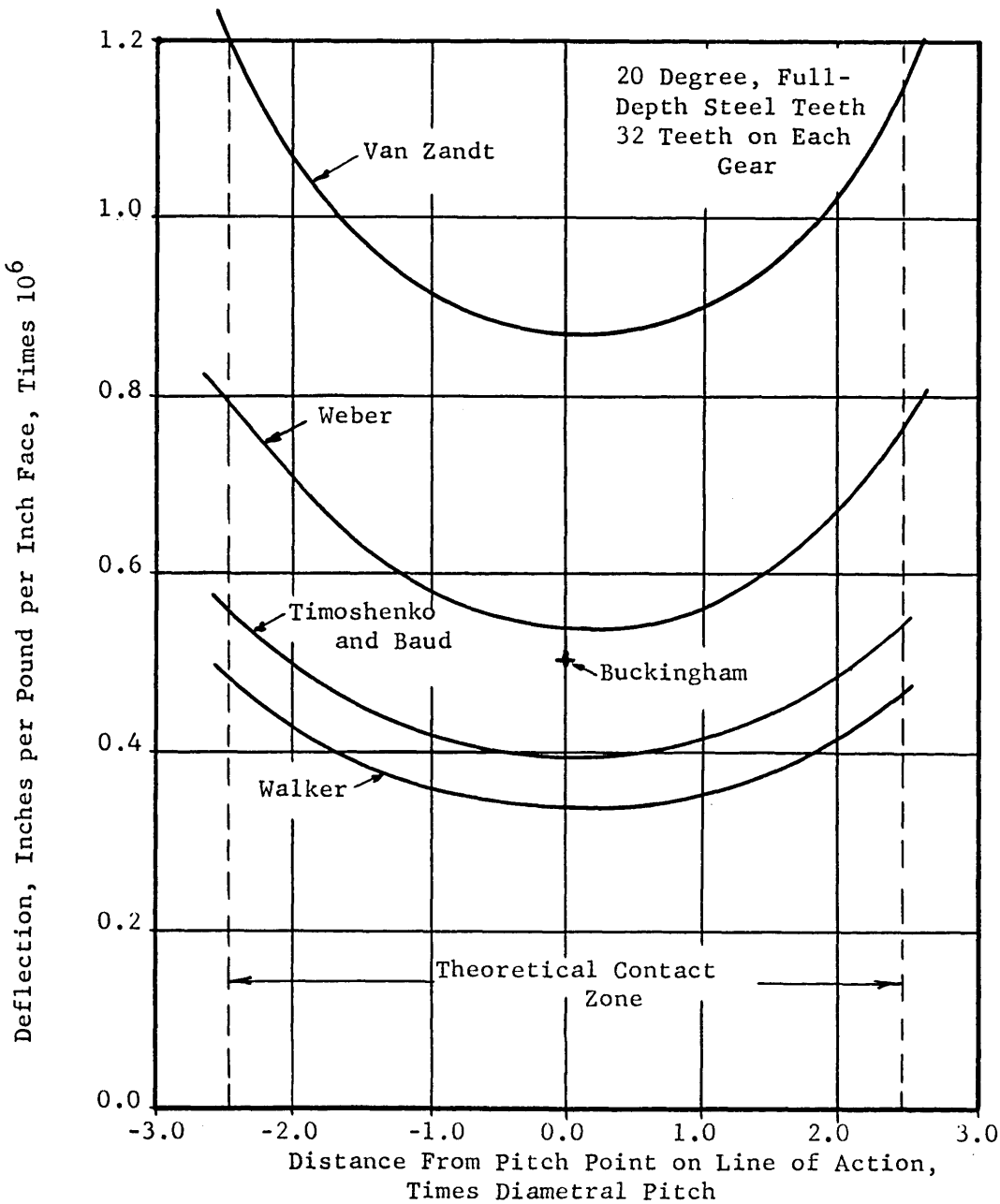

Fig. 2, Deformation of a Typical Pair of Teeth According to Various Investigators (Adapted from Fig. 6 of Ref. 51)

2.23. Dynamic Loads in Gear Teeth

All currently-available theoretical studies of dynamic loads are based on four general simplifications:

1. The torques applied to the gear pair are zero or constant.
2. The gear pair is reduced to a single-degree-of-freedom system consisting of the gear blanks considered as pure inertias coupled by the gear teeth considered as pure springs, and describable in terms of the relative motion of the pitch circles of the two gears.
3. The spring-stiffness of a tooth pair is assumed independent of the position of the contact point between teeth.
4. Errors between the ideal tooth geometry and the actual tooth geometry, whether due to manufacturing, wear or elastic deformation, are considered as disturbances which excite oscillations in the relative displacement of the gears and hence produce dynamic loads on the teeth.

Buckingham, in 1949, presented an analysis in which he considered the dynamic load to result from the engagement of a single pair of teeth containing an error. "Errors on gear-tooth profiles, caused by elastic deformation under load or by inaccuracies of production, or both, act to change the relative velocities of the mating members. This varying velocity---results in a varying load cycle on the teeth---(which) depends largely upon the extent of the effective errors, and the speed of the gears. --- If the materials were rigid, the acceleration load would vary as the square of the pitch-line velocity. As the materials are elastic, when the load required to deform the teeth the amount of the error is less than that required to accelerate the effective masses, the teeth will be deformed and the acceleration of the masses will be reduced accordingly."[29] From this reasoning, and a great deal of native intuition, Buckingham formulated the following expressions for the tangential component of the dynamic load, T_d.

$$T_d = T_t + \sqrt{f_a(2f_2 - f_a)}$$

$$f_a = \frac{f_1 f_2}{f_1 + f_2)} \tag{1.11}$$

$$f_1 = 2cmv^2; \quad f_2 = T_t + e_m k$$

where T_t is the average tangential load, f_1 is a so-called acceleration load, f_2 is the asymptotic or infinite-speed increment load, c is a derived constant, v is the pitch-line velocity, and m is the effective mass at the pitch-line of the two gears. Attempts to correlate the predictions of Eq. (1.11) with experimental results obtained with the Lewis machine were relatively unsuccessful, but this poor correlation was attributed in part to mechanical difficulties with the test machine.

Tuplin, in 1950, published an analysis of gear-tooth loads which considered dynamic loads to result from the insertion of a simple "resultant pitch error" wedge under an equivalent spring-mass system[34, 43]. This system is shown in Fig. 3a. The time of insertion or withdrawal of the wedge was assumed equal to the circular pitch divided by the average pitch-line velocity. The value of the dynamic increment load was found to vary from zero at low velocity to a value equal to the resultant error e times the tooth spring stiffness k at very high velocity. The dynamic analysis was not rigorous, since no oscillations of the spring-mass system were considered during the time the wedge was inserted or withdrawn. Effects of wedge shape were investigated and found to be relatively small. Tuplin's results were presented in the form of two equations:

$$T_d = T_t + \frac{ek}{1 + 6.6 \left(\frac{t_1}{T}\right)^2} \qquad t_1 < 0.3 \tag{1.12a}$$

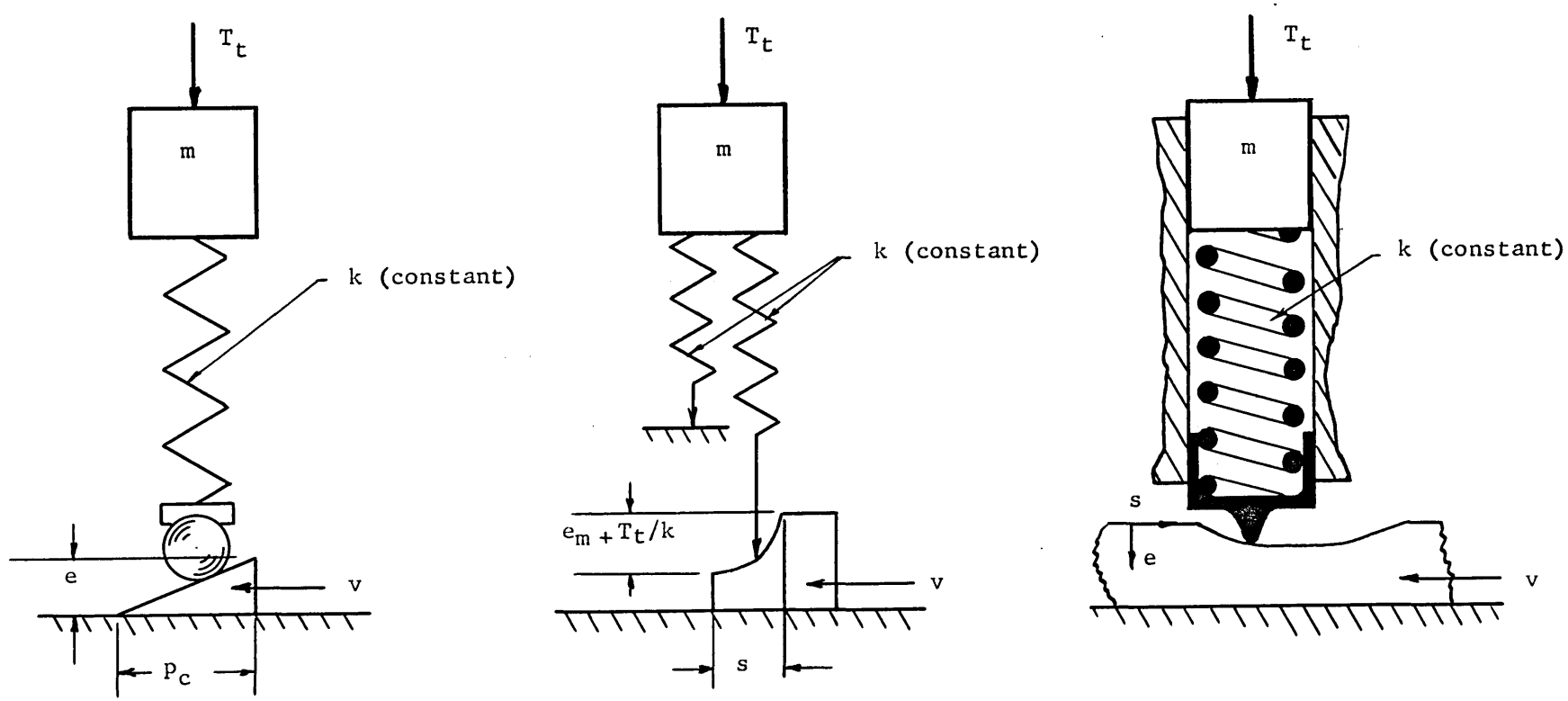

a) Tuplin Model (1950)
Ref. (43)

b) Reswick Model (1954)
Ref. (45)

c) Zeman Model (1957)
Ref. (50)

Fig. 3, Simple Models for Study of Dynamic Loads in Gearing, According to Various Investigators

$$T_d = T_t + \frac{0.815\ ek}{\sqrt{1 + 6.6\left(\frac{t_1}{T}\right)^2}} \qquad t_1 > 0.3 \qquad (1.12b)$$

where e is the "resultant pitch error," k is the tooth spring constant, T is the natural period of the spring-mass system, t_1 is the time to insert or withdraw the error, and T_d and T_t are the maximum dynamic load and average transmitted load, respectively.

Tuplin's results, modified slightly, have been employed successfully in at least one application to predict life and performance characteristics of high-speed, lightly-loaded computer gears[44].

In 1954, Reswick presented an independent analysis which was similar to Tuplin's analysis, but more rigorous[45]. An error wedge or "cam" of parabolic contour was assumed to represent load transfer, as shown in Fig. 3b, but the possibility of contact between more than one pair of teeth was considered. Reswick showed that for large manufactured and/or small transmitted loads, single tooth-pair action could be assumed. This mode of operation was termed "lightly-loaded." Analysis of this case predicted loads closely in agreement with Buckingham's theoretical results, Eq. (1.11). This agreement comes about in part because the time for the error cam to be inserted into the spring-mass system is computed from an equation derived by Buckingham in connection with the development of Eq. (1.11). A second mode of operation, "heavily-loaded" gears was distinguished where double-pair contact could not rationally be neglected. A detailed description and extension of the Reswick analysis is included in Chapter 3 of this thesis.

Zeman[50], in an extensive theoretical paper published in 1957, studied the dynamic model shown in Fig. 3c. This work is essentially the same as Tuplin's, except that the analysis is somewhat more rigorous; and continuous, periodic errors are studied in addition to single discrete errors. Two cases are discussed.

1. The oscillations resulting from the passage under the spring-mass system of various discrete error cams were studied. Curves, which appear to be in error in some regions, are presented for dynamic load versus the time for error to pass under the system divided by the natural period of the system.

2. The effects produced by the passage of a continuous and periodic cam under the system were studied, resulting in the well-known second-order-system resonance diagrams, and large dynamic loads were predicted when the period of the harmonic error cam becomes close to the natural period of the spring-mass system.

In both cases, Zeman assumes tooth-pair stiffness to be constant, and does not consider the possibility of multiple tooth-pair action.

Only one significant experimental work on gear-tooth loads has been published since the reporting of Buckingham's work (1931). In a recently completed doctoral thesis[46, 49], Rettig of Germany presented results of extensive measurements carried out on gears having various controlled errors. Measurements of dynamic load were made through direct observations of dynamic tooth-deflections under operational conditions. Deflections were indicated electrically by the change in reluctance of an air gap between one element attached to a gear tooth and another element rigidly connected to the main body of the gear wheel. Tests were run on gears of 90 mm pitch diameter at pitch-line velocities up to about 2000 ft/min. with pitch errors up to about 0.005 inches. Further discussion of Rettig's results is included in Chapters 2 and 4 of this thesis; however, two general observations will be made here.

1. For very lightly-loaded situations, where the manufactured errors were much greater than the deflection of the gear teeth due to load, the type of behavior predicted by the foregoing dynamic analyses was observed. That is, the dynamic increment load increases uniformly with pitch-line velocity (linearly for low speeds).

2. When transmitted loads become large, or manufactured errors small, the dynamic increment loads generally did not behave in a manner predictable from any of the theoretical analyses. In particular, there was a tendency for increment loads to disappear at large values of average transmitted load.

2.3. Summary

Three major criteria are in current usage today for predicting the strength and durability of gear teeth. These are concerned with the maximum bending stress at the root of the tooth, the compressive stress induced in the flank of the tooth at the point of contact with the mating tooth, and the ability of the lubricant to prevent metal-to-metal contact and scoring of the teeth. All of these criteria show excellent promise as design tools if the problem of predicting the static and dynamic loads which act on the teeth during operation of the gears can be solved.

At the present time no complete, rational method for computing these loads exists. Even static load cycles can only be estimated from currently available published information. In almost all cases, published analyses are unsupported by results of experimental studies, and in most instances are simplified to the point where many observed trends cannot be explained.

A need exists, if future progress is to be made in the gear design field, to find rational means of predicting, from parameters that are determinable during the design stage, the loads that will occur on the teeth of a proposed gear set during operation.

CHAPTER 2. STATIC LOAD, STRESS, AND DEFLECTION CYCLES IN SPUR GEARING

1. Objective

The objective of this chapter is to develop a rigorous analysis of the static or low-speed behavior of a gear system; to present curves, data, and equations which permit computation of the static load, stress, and deflection cycles for a gear tooth under operational conditions; and to verify the results of the analysis by comparison of predicted curves with measured stress cycles for actual gears.

The results presented in this chapter also are intended to provide a firm foundation for subsequent dynamic analysis of gear systems.

2. Ideal Kinematic Properties

The ideal kinematic requirement for gear action is constant speed ratio. That is, the angular velocity of the driven gear should be a constant multiple of the angular velocity of the driving gear. Two curves that possess the property of constant speed ratio when operated as contacting tooth surfaces are called conjugate curves.

2.1. Conjugate Curves.

Figure 4a shows two gear teeth in contact. Point L on gear 2 is in contact with point M on gear 1. At this point of contact, the two tooth surfaces must be tangent to each other and consequently must have a common normal W_1, W_2 passing through the point of contact. Since ideal gears are assumed rigid, the velocities of L and M along the normal W_1, W_2 must be equal. The velocities of L and M perpendicular to the normal are not generally equal, and the difference between these velocities is the sliding or relative velocity of the tooth surfaces.

From Fig. 4a

$$V_{t2} = \omega_2 \overline{C_2 W_2} \; ; \qquad V_{t1} = \omega_1 \overline{C_1 W_1} \tag{2.1}$$

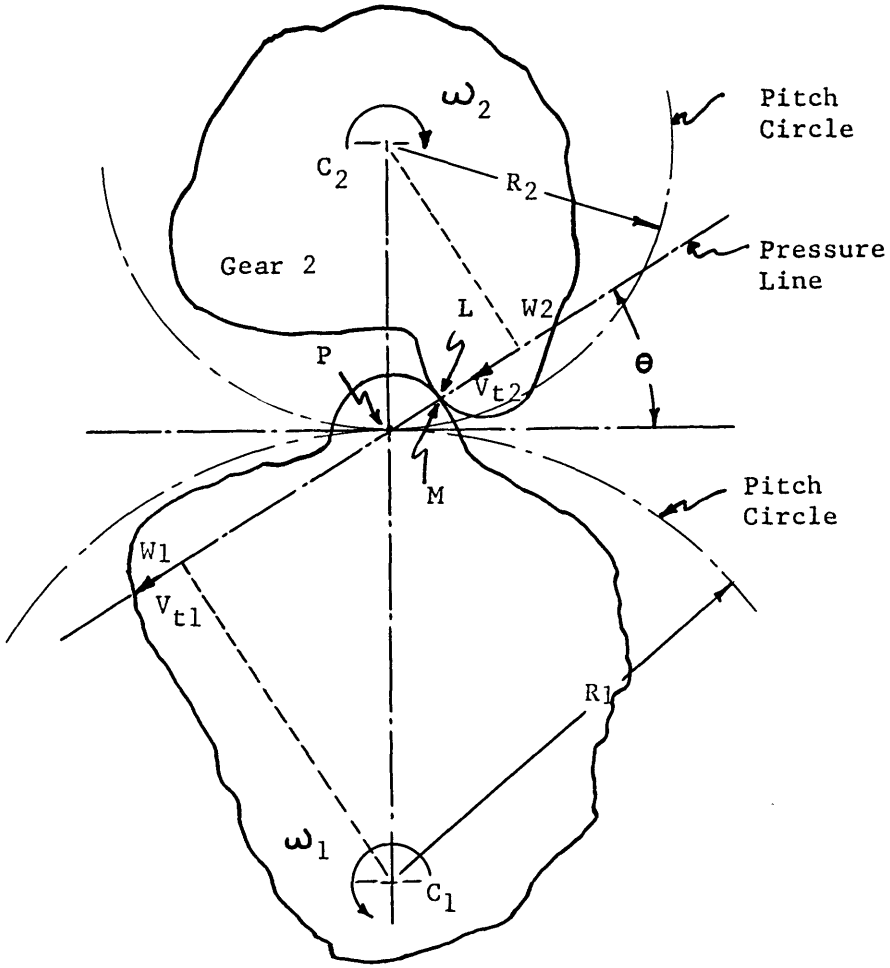

a) Conjugate Curves

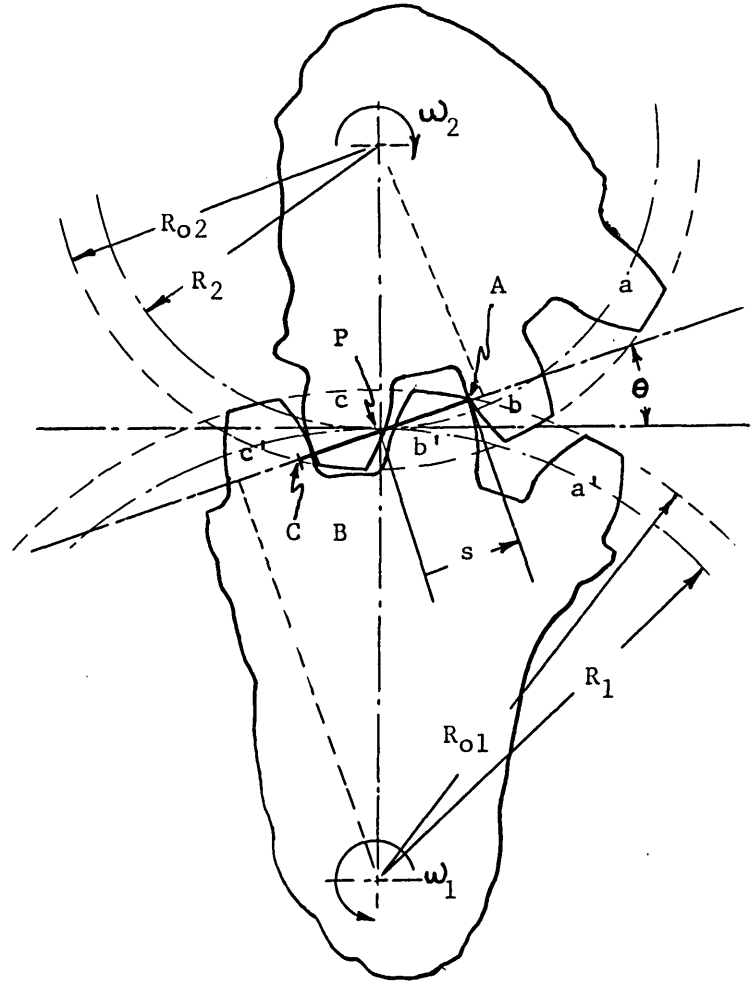

b) Involute Geometry

Fig. 4, a and b, Ideal Conjugate Curves and Involute Gear Geometry

where ω_1 and ω_2 are the angular velocities of gears 1 and 2, respectively. Hence, by similar triangles

$$\frac{\omega_1}{\omega_2} = \frac{R_2}{R_1} \tag{2.2}$$

Since the center distance $R_1 + R_2$ is fixed, R_1 and R_2 must be constant in order to achieve constant speed ratio. Thus the common normal must always pass through the same point P, called the pitch point, along the line of centers. Consequently, ideal gears can be represented kinematically by two imaginary cylinders of radii R_1 and R_2, called pitch cylinders, which roll on each other without slipping.

If no friction is present between the mating gear profiles, then the resultant force transmitted at the contact point L must lie along the common normal. For this reason the common normal is called the pressure line, and the angle between the normal and a line perpendicular to the line of centers C_1, C_2 is called the pressure angle (θ). The locus formed by all points of contact as the gears rotate is known as the path of contact.

In order to maintain continuous conjugate action, a series of conjugate curves are spaced uniformly around the circumference of a gear. The separation of these curves, measured along the pitch circle, is called the circular pitch

$$p_c = \frac{2\pi R}{i} \tag{2.3}$$

where i is the number of teeth, and R is the pitch-circle radius.

2.2. The Involute Gear

An involute curve is generated by the end of a line that is unwound from the circumference of a circle called the base circle. From the infinite variety of possible conjugate curves, the involute has been almost universally accepted for use in gearing. Among the reasons for this choice are:

1. Conjugate action is maintained regardless of changes in center distance.
2. The pressure angle is constant and the path of contact is a straight line.
3. Speed ratio is independent of changes in center distance.
4. Generation processes are simple, and interchangeability is possible.

In an involute gear, the spacing of successive involutes along the pressure line or line of action is known as the normal pitch, and is related to the circular pitch defined by Eq. (2.3) in the following way

$$p_n = p_c \cos \theta \tag{2.4}$$

In Fig. 4b, the involute teeth b and b' have moved into contact at point A on the line of action, while teeth c and c' are still in contact at point B (one normal pitch ahead of A on the line of action). The teeth b and b' will remain in contact until point A has moved down the line of action to point C at which time teeth b and b' will move out of contact. The path of contact for this gear pair is then the straight line segment AC. The contact-ratio is defined as the path of contact divided by the normal pitch, and is a measure of the average number of tooth-pairs in contact. To provide continuous action the contact ratio must be greater than one, and for most power transmission gearing, the value of this quantity lies between one and two.

The radial length of the teeth beyond the pitch circle is called the addendum distance, and the radial depth of the teeth below the pitch circle is called the dedendum distance. By trade association standards, these distances are specified as constant multiples of the circular pitch:

$$\text{Addendum} = R_o - R = \frac{a_a p_c}{\pi} \tag{2.5}$$

$$\text{Dedendum} = R - R_i = \frac{\alpha_d p_c}{\pi} \tag{2.6}$$

where R_i, R, and R_o are dedendum, pitch, and addendum radii, respectively. The most common standard gear proportions in use today are the 20° pressure-angle stub-tooth system and the 20° full-depth-tooth system. The values of α_a and α_d for these systems are listed in Table 1.

TABLE 1

System	20° Stub	20° Full-Depth
Addendum, α_a	0.8	1.0
Dedendum, α_d	1.0	1.157

2.3. Points of Load Transfer for Ideal Gears

The location in the gear mesh of the contact point between mating teeth can be specified conveniently by the distance, s, between the pitch point and the contact point, measured along the line of action. This convention is noted on Fig. 4b for the contact point A.

When load is being transmitted through the gear mesh, the load is carried either by one pair of teeth alone or jointly by two pairs of teeth. It is assumed here that the contact ratio is between one and two. As the gears rotate, the load is transferred from teeth that are in mesh to succeeding teeth that are moving into the mesh. Similarly, teeth moving out of the mesh relinquish load as they leave contact. The location (s) along the pressure line of the points of load transfer for ideal (rigid and geometrically-perfect) gear teeth will now be determined.

Figure 5 represents the condition when tooth-pair b shown in Fig. 4b is coming into contact. A study of the geometry gives the following equation for the distance (s_b) between the pitch point P and the engagement point A for tooth-pair b.

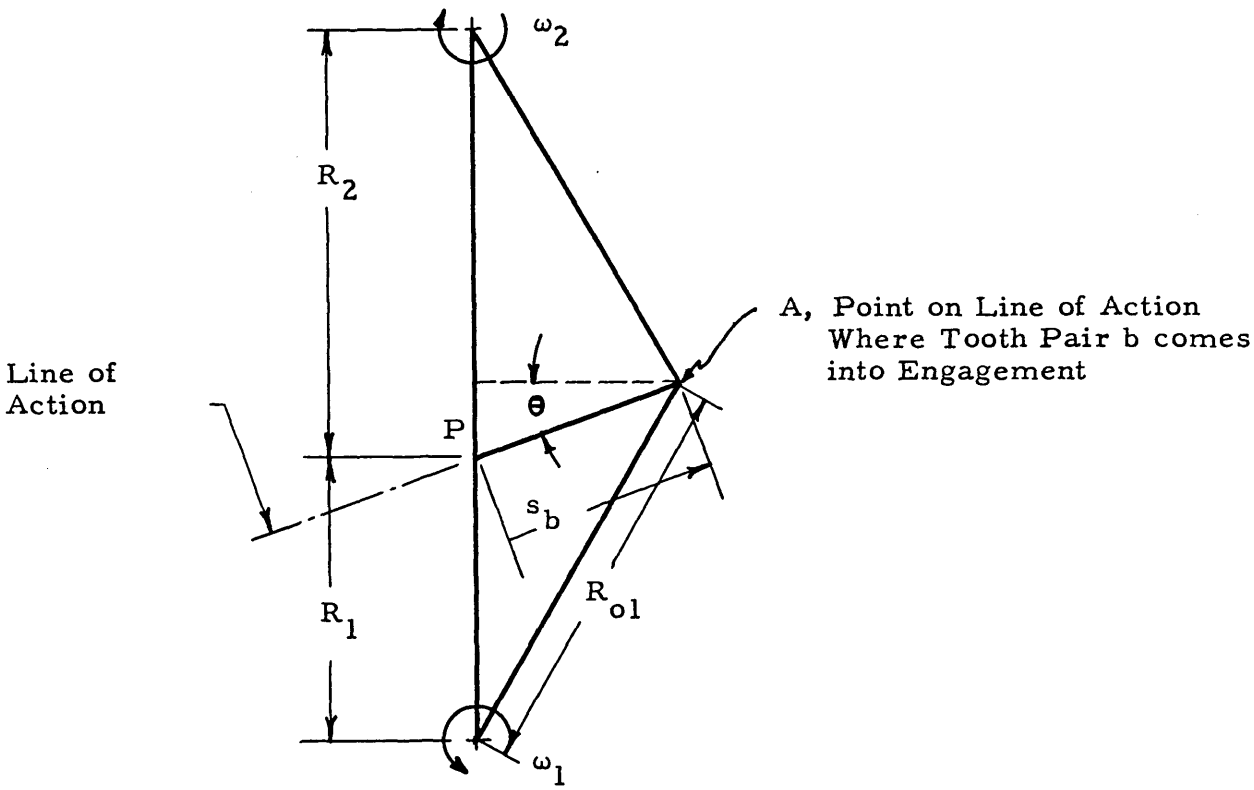

Fig. 5. Geometry for Point of Load Transfer in an Ideal Gear

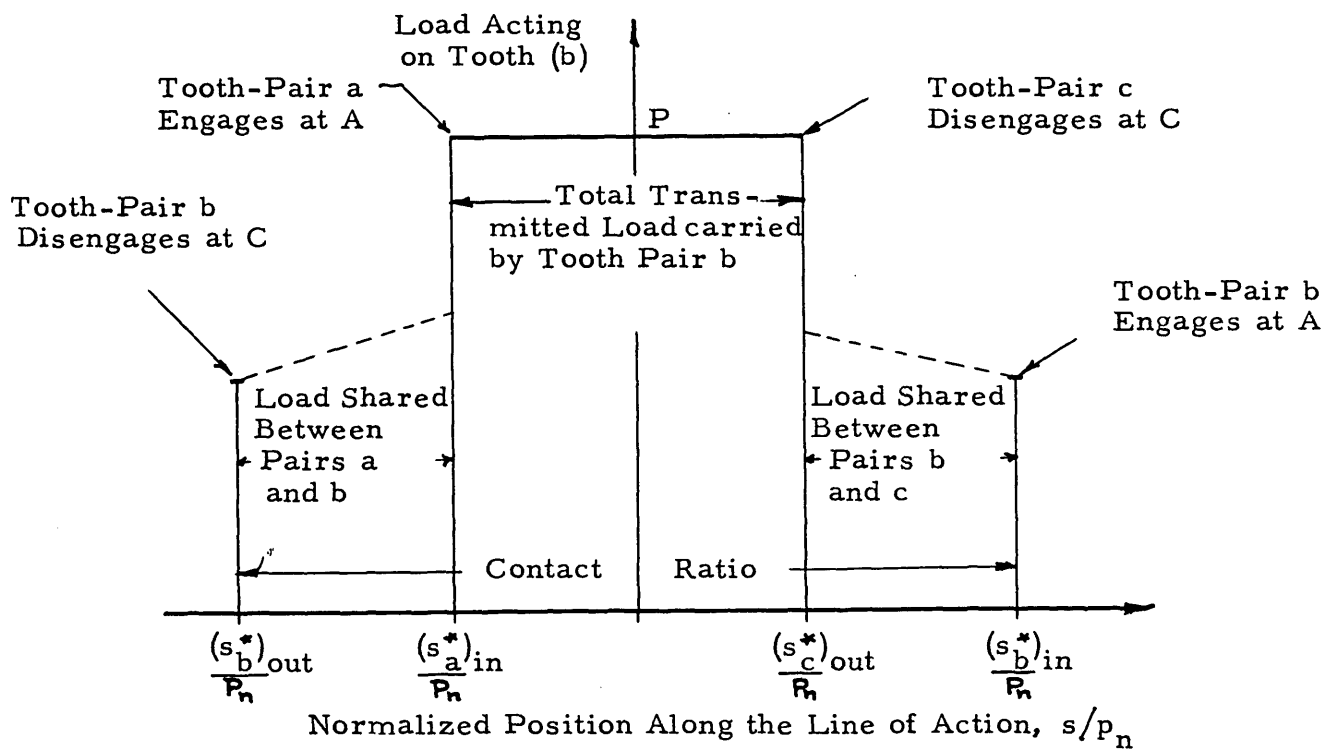

Fig. 6. Load-Transfer Locations for an Ideal Gear, Measured Along the Line of Action

$$s^* = \sqrt{R^2_{o1} - R^2_1 \cos^2 \theta} - \sin \theta \tag{2.7}$$

Equation (2.7) can be nondimensionalized by dividing the expression by the normal pitch, (p_n). Combining Eq. (2.7) with Eqs. (2.4) and (2.5) and substituting for R_{o1} from Eq. (2.5) gives

$$\frac{s^*}{p_n} = \frac{i_1}{2\pi \cos \theta} \left[\sqrt{\sin^2 \theta + \frac{4\alpha_a}{i_1} \left(1 + \frac{\alpha_a}{i_1}\right)} - \sin \theta \right] \tag{2.8}$$

where i_1 is the number of teeth on gear 1, θ is the pressure angle, and α_a is the constant, from Table 1, which determines the addendum distance $(R_{o1} - R_1)$.

The value of s^*/p_n that exists when the tooth-pair b disengages is negative, and is obtained from Eq. (2.8) by replacing i_1 by i_2, the number of teeth on the mating gear. If the addendum distance for gear 2 is different from the addendum distance for gear 1, α_a must be replaced in Eq. (2.8) by the corresponding value for gear 2.

The points of load transfer for an ideal gear pair can be completely determined from Eq. (2.8). In Fig. 6, tooth-pair b engages at $s/p_n = (s^* b/p_n)_{in}$ and disengages at $s/p_n = -(s^* b/p_n)_{out}$. Since the actual distance, s, between these two points is the total path of contact, the nondimensionalized distance between these points, as shown on Fig. 6, is numerically equal to the contact ratio. When tooth-pair b first engages at point A, it assumes only part of the load transmitted through the mesh and the remainder is carried by tooth-pair c. As the point of contact on tooth-pair b moves down the pressure line (Refer to Fig. 4b) tooth-pair c arrives at point C, and disengages, leaving tooth pair-b carrying the total transmitted load. Pair b continues to carry all the transmitted load until its contact point arrives at point B on the line of action; then tooth-pair a engages at point A and takes part of the load away from tooth pair b. The location of tooth-pair b when the engagement of tooth-pair a occurs, is along the pressure line, one normal pitch to the left of the engagement point of tooth-pair b. The location of

tooth-pair b when the disengagement of tooth-pair c occurs is one normal pitch to the right of the disengagement point of tooth-pair b. Thus computation from Eq. (2.8) of the distances between the pitch-point and the engagement and disengagement points, respectively for one tooth pair is sufficient to establish the four ideal load-transfer points, as depicted in Fig. 6. This calculation always will be the first step in computing the static load, stress, or deflection cycles for a given gear pair.

3. Load-Deflection Properties of a Gear Mesh

3.1. Definition of Spring-Stiffness of a Gear Mesh

The ideal curves that are used to form gear teeth are designed to produce a constant speed ratio. That is, so the gears behave like two imaginary pitch cylinders which roll without slipping.

In actual gears, the materials employed cannot be absolutely rigid; consequently, the gear-teeth will deflect due to the transmitted loads, and the ideal pitch circles will be caused to slip. Thus a deviation from ideal kinematic operation occurs.

Suppose, in Fig. 7, that gear 2 is held fixed, then by definition its pitch circle also is fixed. Now consider a torque τ_1 to be applied to the mating gear 1. This torque on gear 1 must be balanced, for static operation, by the moment of the resultant force W, which, in the absence of friction, acts along the pressure line.

$$\tau_1 = W \cos \theta \, R_1 \tag{2.9}$$

or in terms of T, the component of W which acts tangentially to the pitch circle,

$$\tau_1 = TR_1 \tag{2.10}$$

When friction is present, or contact between mating teeth lies off the pressure line, W and T in Eqs. (2.9) and (2.10) no longer represent tooth loads exactly, but are still convenient ways of expressing the input torque τ_1.

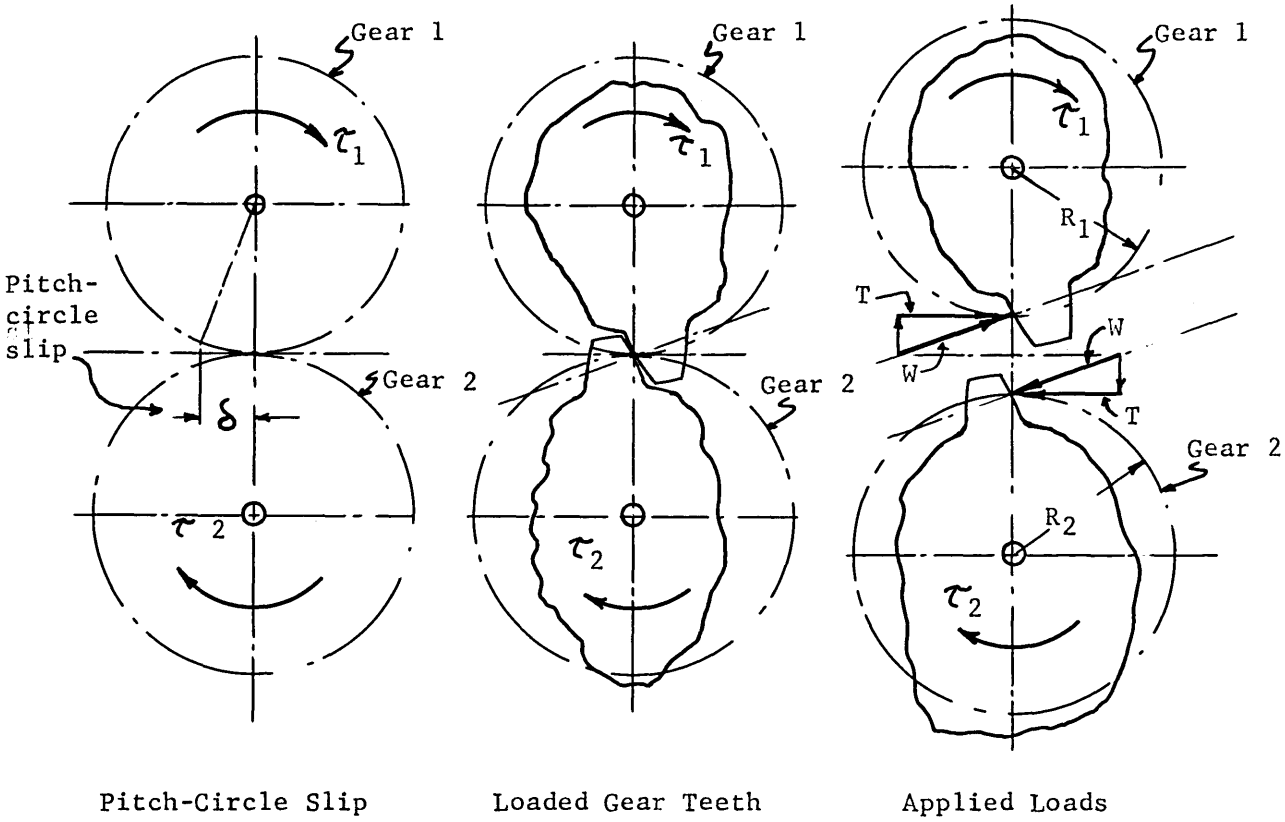

Fig. 7. Definition of Gear-Mesh Spring-Stiffness

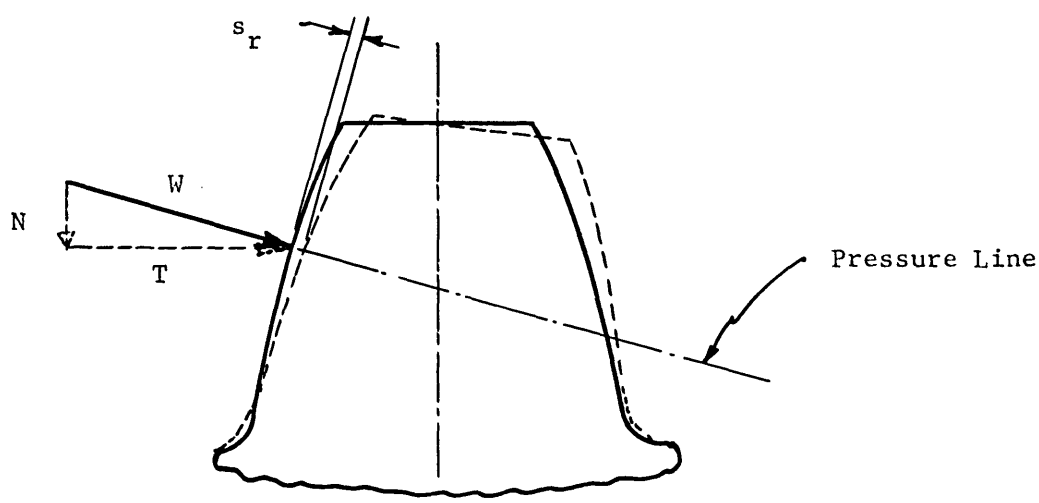

Fig. 8. Deformation of a Gear Tooth

The spring stiffness of the gear mesh is defined as the amount of tangential load T, computed from Eq. (2.10), to produce one unit of pitch-circle slip, δ, as shown in Fig. 7.

$$k_p = \frac{T}{\delta} \tag{2.11}$$

This definition can equally well be stated as the amount of load W acting along the pressure line, required to produce one unit of relative displacement (s_r) between gears, measured along the pressure line

$$k = \frac{W}{s_r} \tag{2.12}$$

where

$$W \cos \theta = T \tag{2.13}$$

and

$$s_r = \delta \cos \theta \tag{2.14}$$

These two spring stiffnesses are related by virtue of Eqs. (2.13) and (2.14)

$$k = \frac{T}{\delta (\cos^2 \theta)} = \frac{k_p}{\cos^2 \theta} \tag{2.15}$$

For convenience in subsequent calculations, a nondimensional compliance w is defined

$$w = \frac{s_r Ef}{W} \tag{2.16}$$

where E is Young's Modulus, and f is the gear-tooth face width. Let

$$W_o = \frac{W}{f}, \tag{2.17}$$

then

$$w = \frac{s_r E}{W_o} = \frac{fE}{k} \tag{2.18}$$

3.2. Load-Deflection Relationships for a Single Pair of Gear Teeth

3.21. Deformation Due to Gross Distortion

When a load W is applied to the surface of a gear tooth, as shown in Fig. 8, a deflection of the tooth occurs in the direction of the load. Suppose that the tooth is rigid near the point of loading. Then deflections of the tooth will still occur due to each of the following effects.

1. Bending of the tooth in the manner of a cantilever beam.
2. Direct compression of the tooth due to the radial component of the load (N).
3. Direct shearing of the tooth due to the tangential component of the load (T).
4. Bending, shearing, and direct compression of the rim material considered as an elastic foundation.

Weber has carried out a rigorous and rather complete analysis including all of the above effects. Energy methods, the two-dimensional theory of elasticity for simple shapes, and simple beam theory were employed to compute the various component deflections due to load.

Figure 9, adapted from Weber's results, gives curves of nondimensionalized compliance, w, due to gross deformation of a single gear tooth, as a function of the position of the contact point along the line of action. It is interesting to note that for given load position, this tooth compliance is a function only of the number of teeth in the gear and not of the size of the teeth. This fact has been demonstrated experimentally and can be rationalized by observing that the stiffnesses of two geometrically-similar cantilever beams are equal.

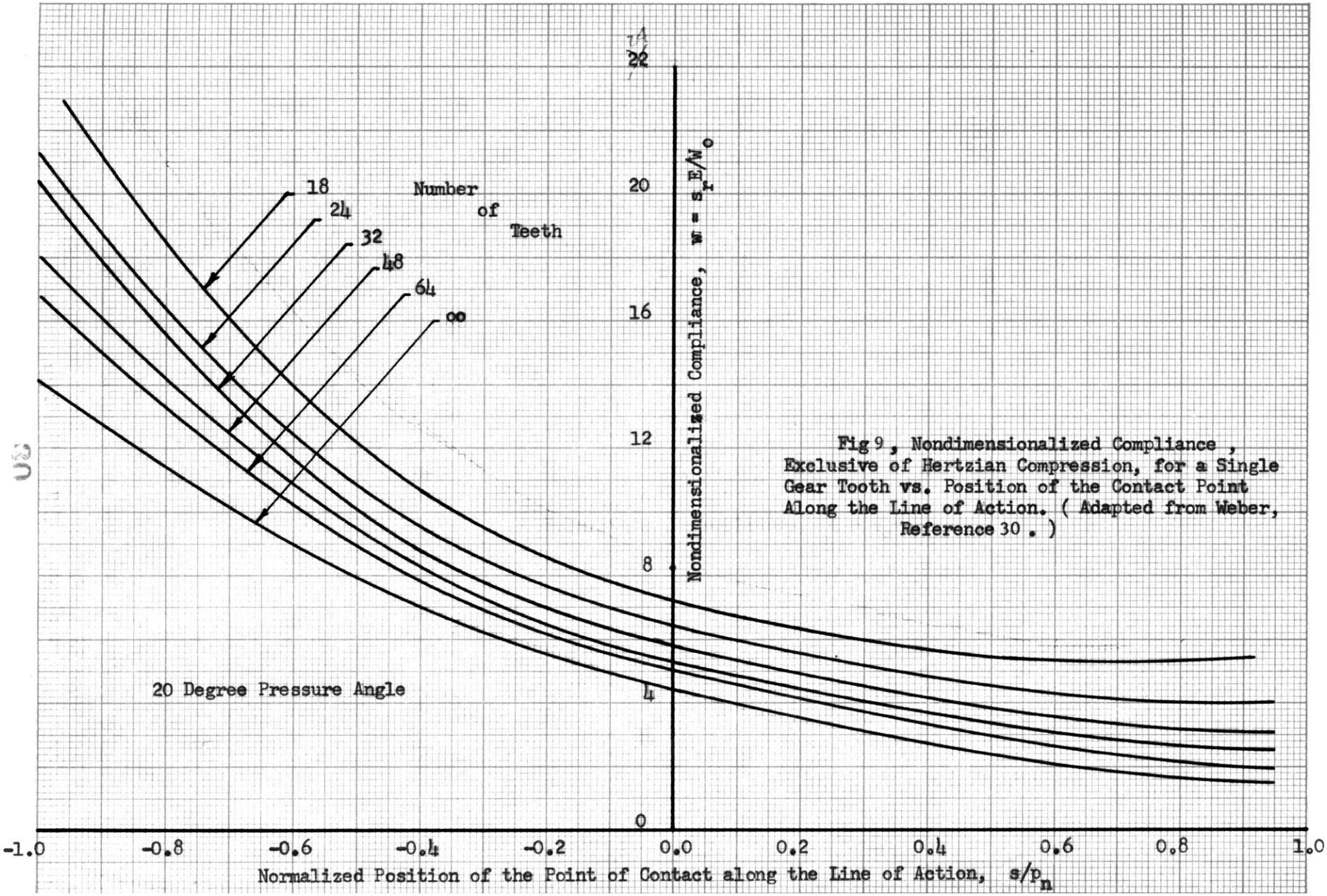

Fig 9, Nondimensionalized Compliance, Exclusive of Hertzian Compression, for a Single Gear Tooth vs. Position of the Contact Point Along the Line of Action. (Adapted from Weber, Reference 30 .)

When two gear teeth are in contact, the total gross deformation is obtained by adding the deflections given by Fig. 9 for each gear. However, in performing this addition, note must be taken that when the contact point moves toward the tip of one tooth, the contact point must move toward the base of the mating tooth. Thus, (See Fig. 4b) the compliance for tooth b' corresponding to contact-point A would be read from Fig. 9 at the proper negative s/p_n, while the compliance for tooth b at the same contact point would be read from Fig. 9 at the corresponding positive s/p_n.

3.22. Local Hertzian Compression of the Tooth Surfaces

In addition to the deformations mentioned above, a compression or flattening of the tooth profiles will occur in the region of contact. This local deformation will permit additional slippage of the pitch circles, and must be added to the previously determined gross deformations.

Weber has proposed an analysis of the local compression, based on Hertz's work on deformation between cylinders. The results of Weber are not employed in this work, but an independent development has been made.

Figure 10 represents an enlarged view of a gear tooth near the region of contact with a mating tooth. The origin of coordinates is located at the point where contact would exist in an ideal, rigid gear tooth.

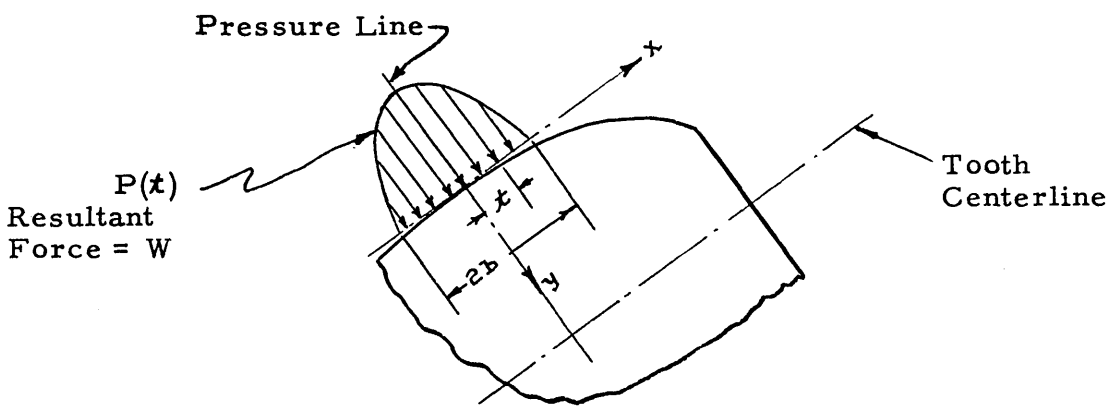

Fig. 10. Distribution of Transmitted Load Over the Local Contact Band Between Mating Gear Teeth.

Three assumptions are made initially:

1. The load distribution $P(t)$ is the same as the load distribution between cylinders that are forced together. This distribution was found by Hertz to have the following elliptic form

$$P(t) = \frac{2W_o}{\pi b^2} \sqrt{b^2 - t^2} \tag{2.19}$$

2. The width of the contact band also is the same as predicted by Hertz for contacting cylinders

$$b^2 = \frac{4W_o}{\pi} \left[\frac{r_1 r_2}{r_1 + r_2}\right] \left[\frac{1 - \eta_1^2}{E_1} + \frac{1 - \eta_2^2}{E_2}\right] \tag{2.20}$$

where η, E and r refer to Poisson's Ratio, Young's Modulus, and radii of curvature at the point of contact, respectively, of the mating gear teeth.

3. The tooth surface behaves near the contact region like a semi-infinite, slightly-curved plane.

4. Deformation effects are negligible beyond the tooth center-line.

With these assumptions, the problem is reduced to that of finding the deformation of an elastic semi-plane acted upon by a distributed loading $P(t)$. The generalized mathematical solution to this class of problems has been obtained by Muskhelishvili[52] in terms of complex potential functions. Two potential functions are defined in the following manner:

$$\Phi = \pm \frac{1}{2\pi j} \int_{-b}^{b} \frac{P(t)\, dt}{t \pm z} \tag{2.21}$$

and

$$\Psi = - z \frac{d\Phi}{dz} \tag{2.22}$$

where

$$z = x + jy, \tag{2.23}$$

and j is equal to $\sqrt{-1}$.

These potential functions are determined by substituting the pressure distribution $P(t)$ from Eq. (2.19) into Eq. (2.20) and performing the indicated integration.

The stresses inside the gear tooth are given in terms of the potential functions Φ and Ψ.

$$\sigma_x + \sigma_y = 4 \operatorname{Re} \left[\Phi \right] \tag{2.24}$$

$$- \sigma_x + \sigma_y - 2 \tau_{xy} j = 2 \left[\bar{z} \frac{d\Phi}{dz} + \Psi \right] \tag{2.25}$$

where σ_x and σ_y are normal stresses, τ_{xy} is shear stress, and Re indicates the real part.

In order to obtain the deformation of the surface in the direction of the load, the stresses must be related to the strains by means of Hooke's Law, and then the strains must be integrated. Only the strain ϵ_y in the direction of the load W is required here. If strain is assumed zero in the direction normal to the x-y plane---"plane strain," Hooke's law takes the form

$$\epsilon_y = \frac{1 + \eta}{E} \left[\sigma_y - \eta (\sigma_x + \sigma_y) \right] \tag{2.26}$$

Or, if stress is assumed zero normal to the x-y plane..."plane stress," Hooke's law becomes

$$\epsilon_y = \frac{1}{E}\left[\sigma_y - \eta\,\sigma_x\right] \tag{2.27}$$

In either case, the strain must be integrated along the y axis in order to evaluate the desired deformation s_r. In performing this integration, infinite deformations are predicted if the integration is permitted to extend to infinity. Consequently, the integration must be carried out over finite limits. In this investigation, the integration was extended into the tooth by one fourth of one normal pitch or approximately to the centerline of the tooth (see assumption 4 above). The total deformation, termed Hertzian Compression, is the sum of the integrated strains taken over each of the mating teeth.

$$(s_r)_H = \left[\int_0^{\frac{p_n}{4}} \epsilon_y\, dy\right]_{\text{tooth 1}} + \left[\int_0^{\frac{p_n}{4}} \epsilon_y\, dy\right]_{\text{tooth 2}} \tag{2.28}$$

The details of the calculations of Hertzian Compression are presented in Appendix A. Solutions have been worked out for both the plane-strain and plane-stress assumptions, and are plotted nondimensionally in Fig. 11, for conditions of contact at the pitch point and for the same materials in both mating teeth. The Hertzian deformation is not a linear function of the applied load, owing to the increase of contact area with load; however, over the practical loading range, the curves of Fig. 11 can be approximated by the constant factors, w_H, tabulated on Fig. 11. Then for pitch-point contact, the Hertzian deformation is expressed as

$$\left(\frac{s_r E}{W_o}\right)_H = w_H \tag{2.29}$$

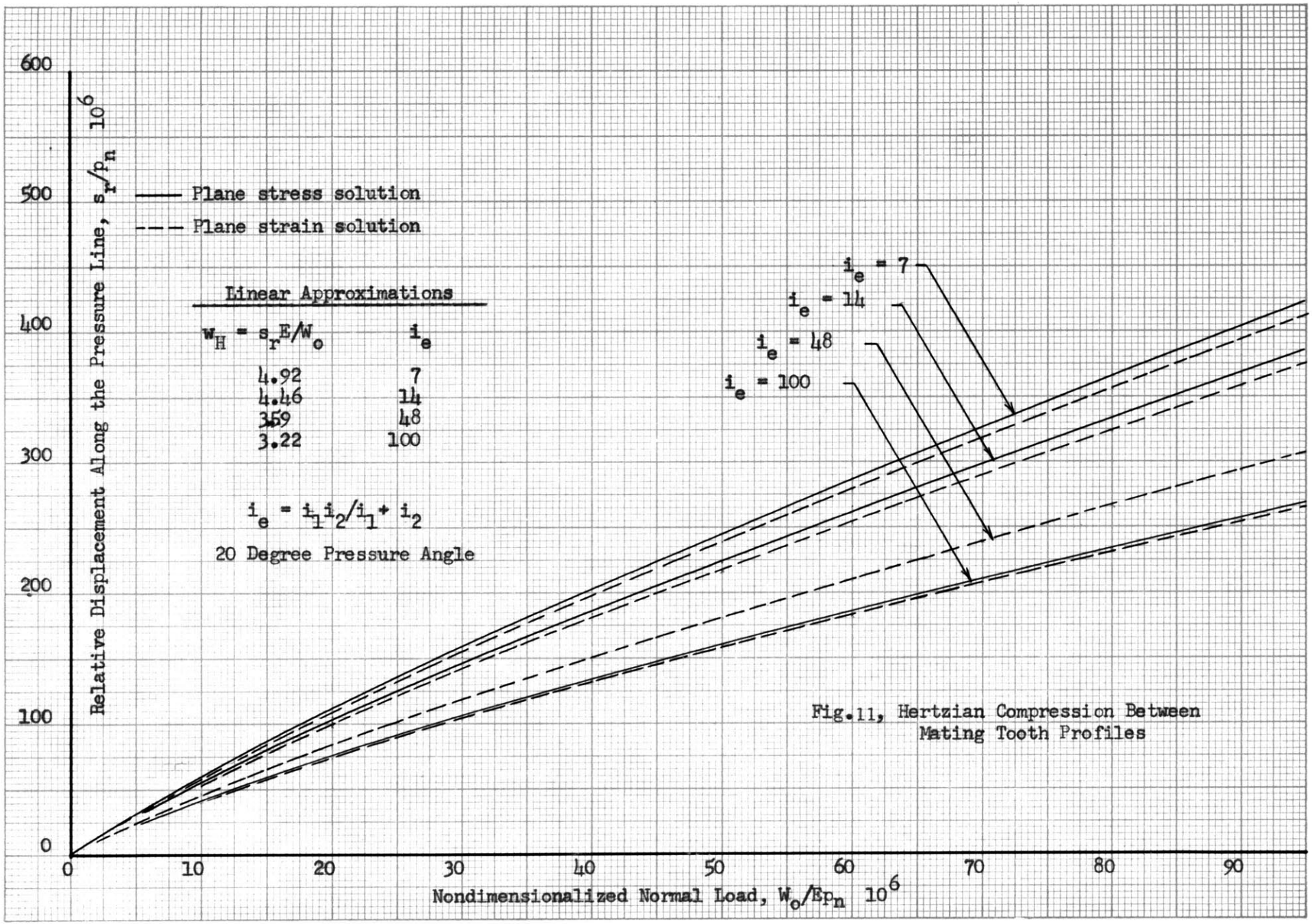

Fig. 11, Hertzian Compression Between Mating Tooth Profiles

When the point of contact between mating teeth moves away from the pitch point, the radius of curvature of each member changes, thus changing the contact width (2b) according to Eq. (2.20). This effect is accounted for by a linear (exactly) correction, Δw_H, which is added to the pitch-point deformation given by Fig. 11. Figure 12 gives this correction factor as a function of the position of contact along the line of action, (s/p_n), and the numbers of teeth in each of the mating gears. This correction normally is negligible except for very small numbers of teeth. The final expression for Hertzian compression then takes the form

$$\left(\frac{s_r E}{W_o}\right)_{\text{Hertz}} = w_H + \Delta w_H \left(\frac{s}{p_n}\right) \tag{2.30}$$

where the quantity w_H is found from Fig. 11 and Δw_H is found from Fig. 12.

3.23. Total Compliance for a Single Pair of Teeth

By means of Figs 9, 11, and 12, the total compliance that exists at any phase of engagement can easily be formulated for a single pair of teeth. As an example, the total compliance for a 27-tooth steel pinion mating with 34-tooth steel gear is constructed in Fig. 13. The compliance w_{27} is plotted directly from Fig. 9, and the compliance w_{34} is plotted by reversing the sign of the abscissa from that given in Fig. 9. Thus moving to the right in Fig. 13 corresponds to moving toward the base of the 27-tooth gear and toward the tip of the 34-tooth gear. The Hertzian compliance is then added to Fig. 13 from the table in Fig. 11. The correction Δw_H is small in this case and is omitted. The three component compliances or deformations-per-unit-load are then added to arrive at the total effective compliance for the given pair of teeth. This compliance curve is representative, and shows a characteristic stiffening of the tooth pair as the pitch point is approached from either direction.

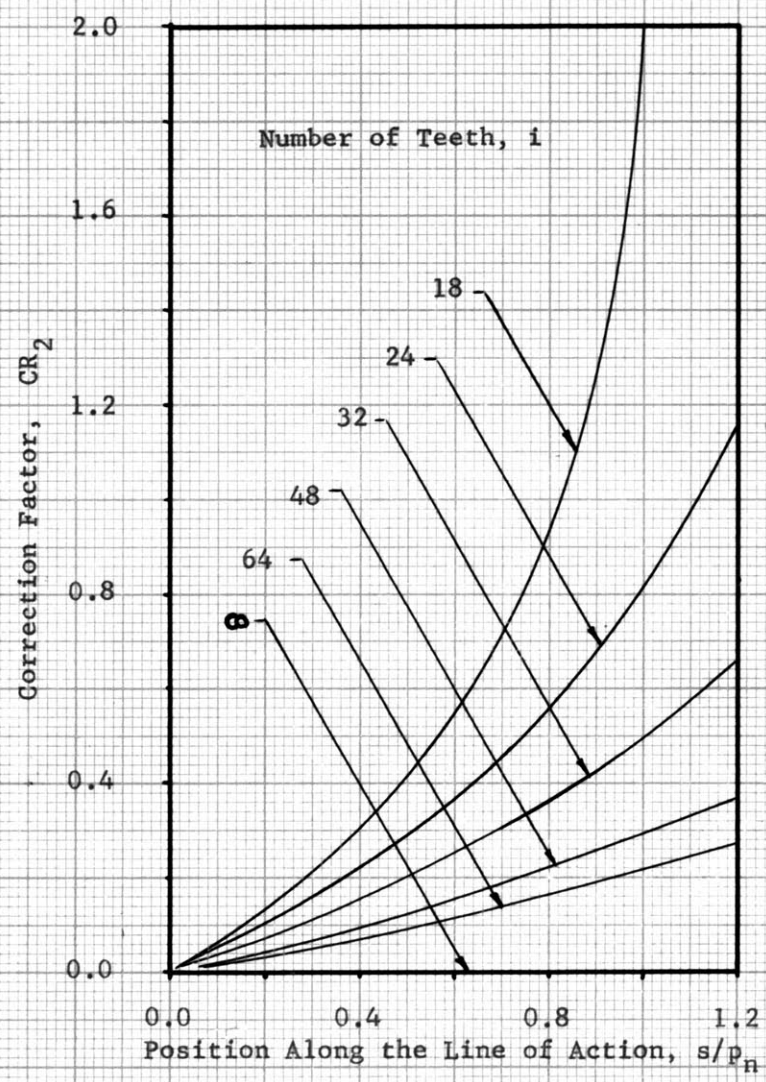

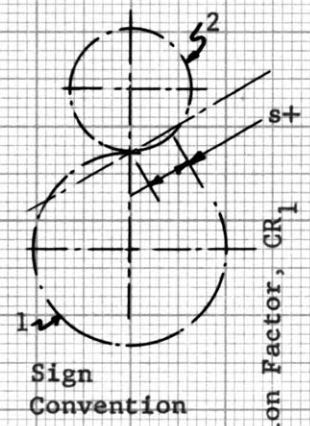

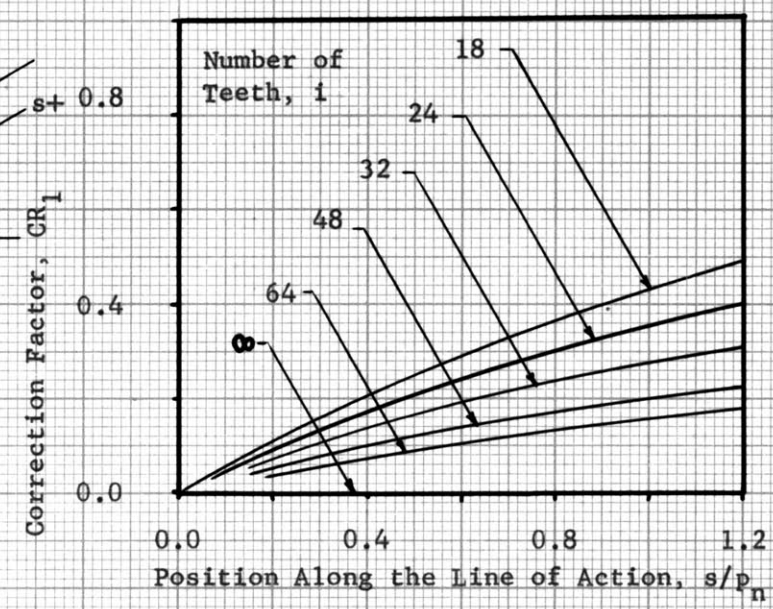

$$w_H = w_H \text{ (at pitch point) } + \Delta w_H$$

$$\Delta w_H = CR_2(i_2) - CR_1(i_1); \quad s/p_n > 0$$

$$\Delta w_H = CR_2(i_1) - CR_1(i_2); \quad s/p_n < 0$$

(Based on plane stress solution)

Fig. 12. Increment Hertzian Compliance Due to Change in Radii of Curvature Along the Line of Action

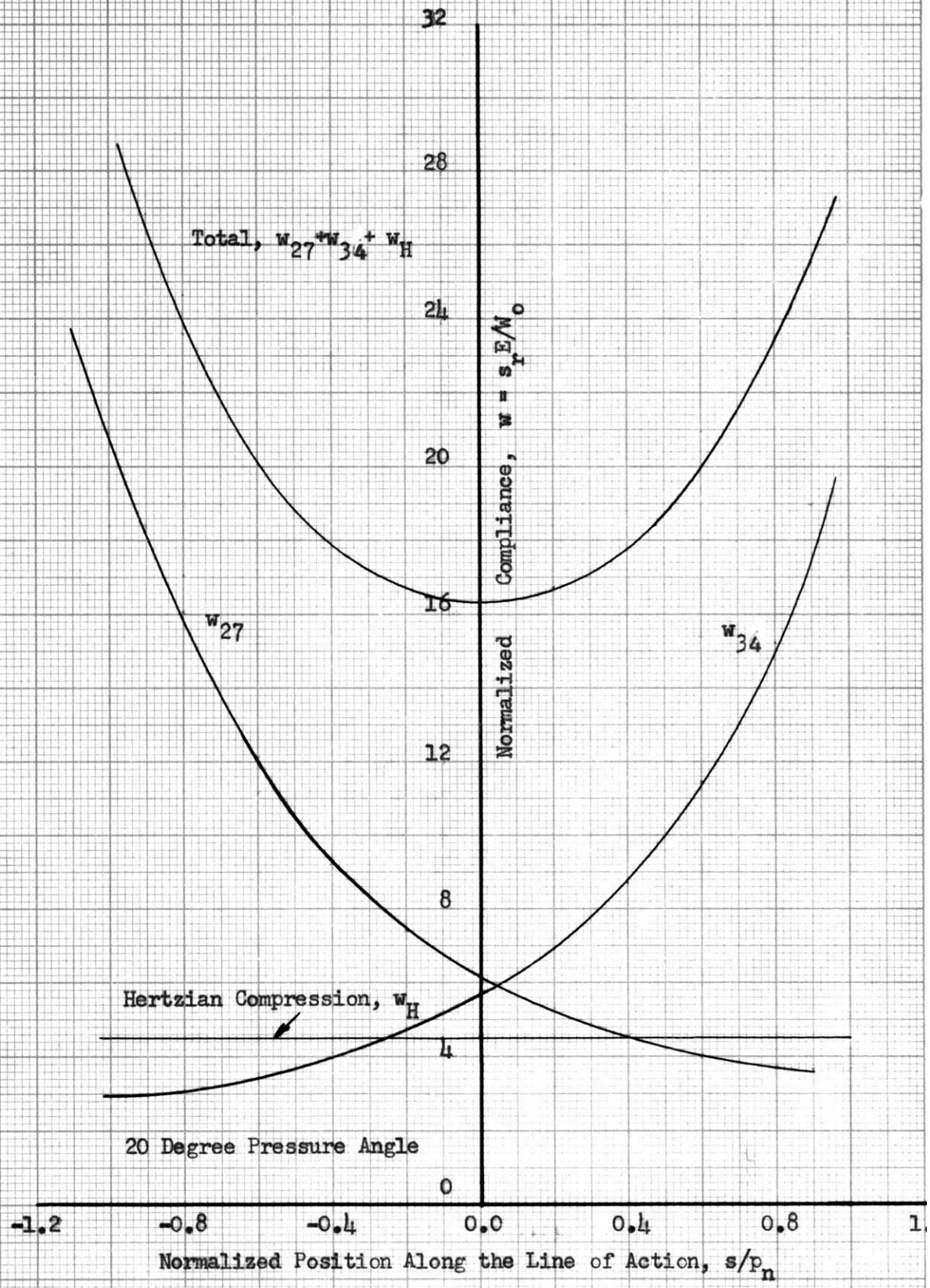

Fig.13, Component and Total Compliances for a 27 tooth Pinion Mating With a 34 Tooth Gear

3.3. Load-Deflection Relationships of a Gear Mesh

When the total compliance for a single pair of teeth is known for all points of contact along the pressure line, computation of the gear-mesh compliance can be carried out. Two cases are possible:

1. Only one pair of teeth is in contact; then the mesh compliance is equal to the single-tooth pair compliance. This is normally the case when contact is near the pitch point.
2. More than one pair of teeth is in contact. Successive pairs of teeth are spaced along the line of action by one normal pitch. Consequently, the compliance curves for successive tooth-pairs also can be spaced along the line of action by the same amount as indicated in Fig. 14a. It will be helpful to employ a schematic representation of the gear system in visualizing the load-deflection processes involved. Such a model is shown in Fig. 14b.

The load W is the total load transmitted through the mesh, and s_r is the relative motion between mating gears, measured along the pressure line. The relative motion is resisted by the tooth-pair stiffnesses, k_a, k_b, k_c, etc., depending on the number of teeth in contact.

Suppose, for example, that tooth-pairs a and b are in contact at the position shown in Fig. 14. Then the resultant compliance for the mesh at this position is given by the resultant compliance of tooth-springs a and b. Since the load W is shared between the two springs, the total compliance is the parallel-combination of the individual compliances.

$$\frac{1}{w_{total}} = \frac{1}{w_a} + \frac{1}{w_b}$$

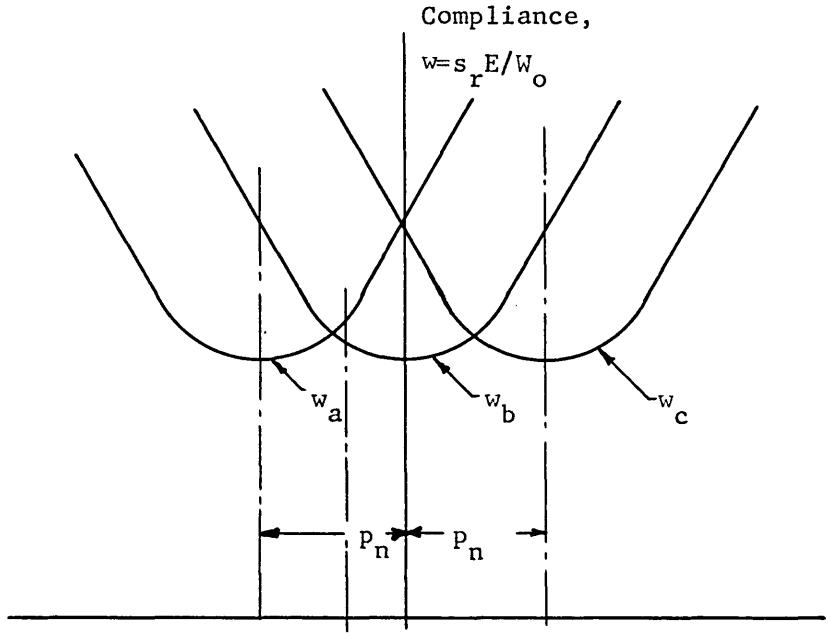

Distance Along the Line of Action, Measured from the Pitch-Point of Tooth-Pair b

a) Compliance

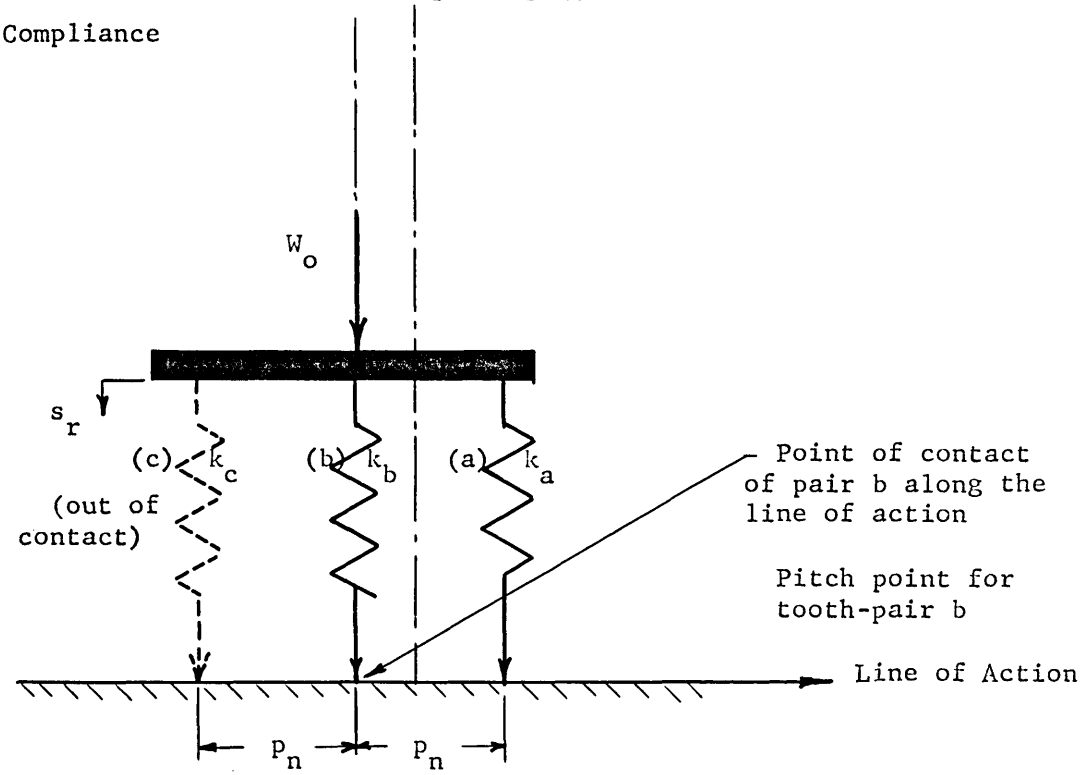

b) Model

Fig. 14, a and b. Model of Gear Action, Representing Multiple-Tooth-Pair Compliance.

or

$$w_{(a+b)} = \frac{w_a w_b}{w_a + w_b} \tag{2.31}$$

This result is easily generalized to the combined compliance for n pairs of teeth.

$$w_n = \frac{\prod_{1}^{n} w_i}{\sum_{r=1}^{n} \left[\prod_{k=1}^{r-1} w_k \prod_{m=r+1}^{n} w_m \right]} \tag{2.32}$$

where each w refers to the component compliance of a given tooth-pair at a certain location along the pressure line. For most practical gear designs a maximum of three pairs of teeth are ever in contact at the same time.

4. Ideal Geometry Under Conditions of No Load

Before the results of paragraph 3 above can be applied to determine the load distribution between various pairs of teeth, some additional information regarding the gear geometry must be available to aid in determining the number of teeth that will be in contact at any particular position of the gears. In this paragraph, the assumption is made that the gears are geometrically perfect as long as no load, or torque, is applied.

When a gear pair is rigid, in addition to being geometrically perfect, the points of load transfer are predictable from Eq. (2.8) and occur as shown in Fig. 6. However, when the gear teeth are flexible, engagement will not occur all at once, but deformation of the loaded teeth will permit premature contact of a tooth-pair which is approaching the theoretical engagement point. As a result the engagement process will be gradual rather than sudden. Similar effects occur at disengagement, and this process also will be gradual. The exact nature of the engagement or load-transfer process will depend on the manner in which engaging pairs of teeth approach each other.

In Fig. 15, a pair of teeth b and b' are shown just before engagement is to occur. Suppose that no load is being applied to the gears. Then the gears must be rotated through an additional small angle before contact between b and b' occurs at point s^* on the line of action. But now if gear 2 is fixed at the position shown, thus fixing its pitch circle, and a torque is applied to gear 1, the pitch-circle of gear 1 will rotate slightly and slip on the pitch circle of gear 2 by an amount that is predictable from the compliance of the teeth already in engagement. This relative motion of gear 1 will be sufficient, at some time during the approach of b and b', to cause contact between these teeth. Therefore, the first step in a study of the mechanics of gear-tooth engagement is a determination of the amount of pitch-circle slippage necessary to cause contact between a pair of teeth that are almost touching. This distance, expressed as relative motion along the pressure line, rather than in terms of pitch-circle slip, will be termed the "no-load separation" of the profiles (Δs).

In a determination of the no-load separation, the following difficulty arises. It is evident from Fig. 15 that a single quantity is not sufficient to describe the approach of the gear teeth to each other. If gear 2 is held fixed and gear 1 is loaded, contact will occur between teeth b and b' after the distance Δ_1 shown in Fig. 15b is closed up. However, if gear 1 is held fixed and gear 2 is loaded, the larger distance Δ_2 must be closed up before contact can occur. Hence, the no-load separation is not unique for a given position of the approaching tooth-pair, but depends on the conditions placed upon the absolute displacements of the pitch circles. Therefore, strictly speaking, any model of gear action that deals only with the relative motion between two gears is incorrect. However, if the two displacements Δ_1 and Δ_2 differ only slightly, then a relative motion model can be justified.

Exact computation of the distances Δ_1 and Δ_2 shown in Fig. 15b, is a straight-forward although somewhat involved geometry problem. The exact analyses and the suggested step-by-step calculation procedures are given in Appendix B. In presenting the results of no-load separation calculations, the following conventions have been employed.

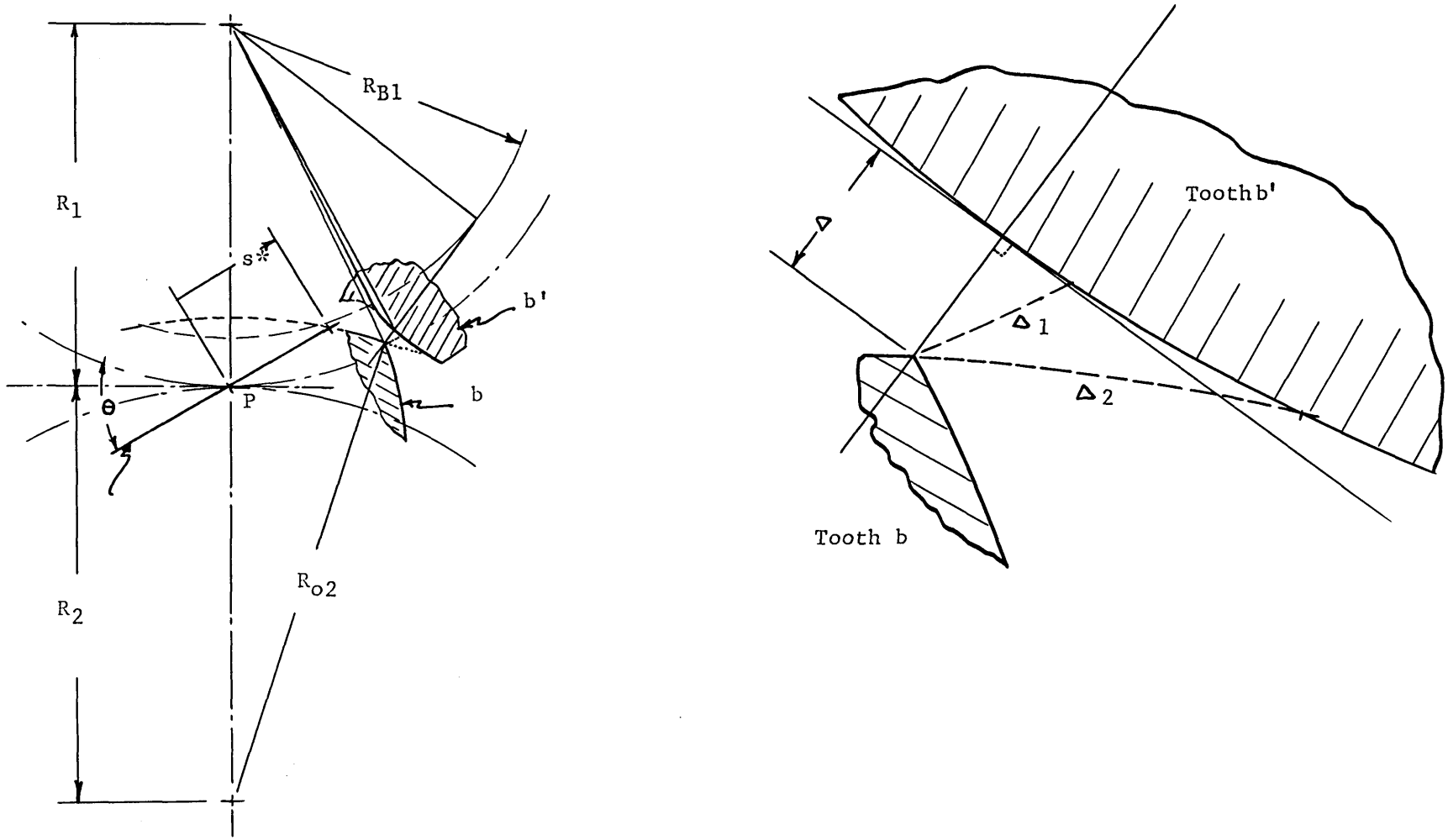

a) Approach of Teeth to Contact Zone

b) Enlarged View of the Region of Imminemt Contact

Fig. 15, Separation of Involute Gear Teeth that are Approaching Contact.

1. No-load separation is given by the amount of rotation $\Delta\psi$ of one gear, necessary to cause contact with an approaching tooth on the other gear. This angle is expressed conveniently as a relative motion along the pressure line, by virtue of the relation

$$(\Delta s) = \Delta\psi \, R \cos\theta \tag{2.33}$$

or, nondimensionalizing with respect to the normal pitch,

$$\frac{\Delta s}{p_n} = \frac{\Delta\psi R \cos\theta}{p_n} \tag{2.34}$$

2. The absolute position of the fixed gear corresponding to a particular value of no-load separation is stated in terms of displacement, along the pressure line, measured from the point where the no-load separation is zero.

Thus for a given gear pair, the no-load separation is presented in the following functional form

$$\frac{\Delta s}{p_n} = f\left(\frac{s - s^*}{p_n}\right) \tag{2.35}$$

The particular function in Eq. (2.35) depends on the numbers of teeth in each gear and on which gear is assumed to be fixed in computing the no-load separation.

Figure 16 shows exact solutions for no-load separations in a pair of gears having 24 and 36 teeth. The two solutions were found to differ only slightly over the anticipated ranges of separation. It is readily apparent from Fig. 16 that the approach of a pair of teeth is extremely gradual. For example, if the normal pitch is one inch, the approaching pair of teeth will be separated by only 0.003 inches when the displacement $(s - s^*)$ is still 0.10 inches.

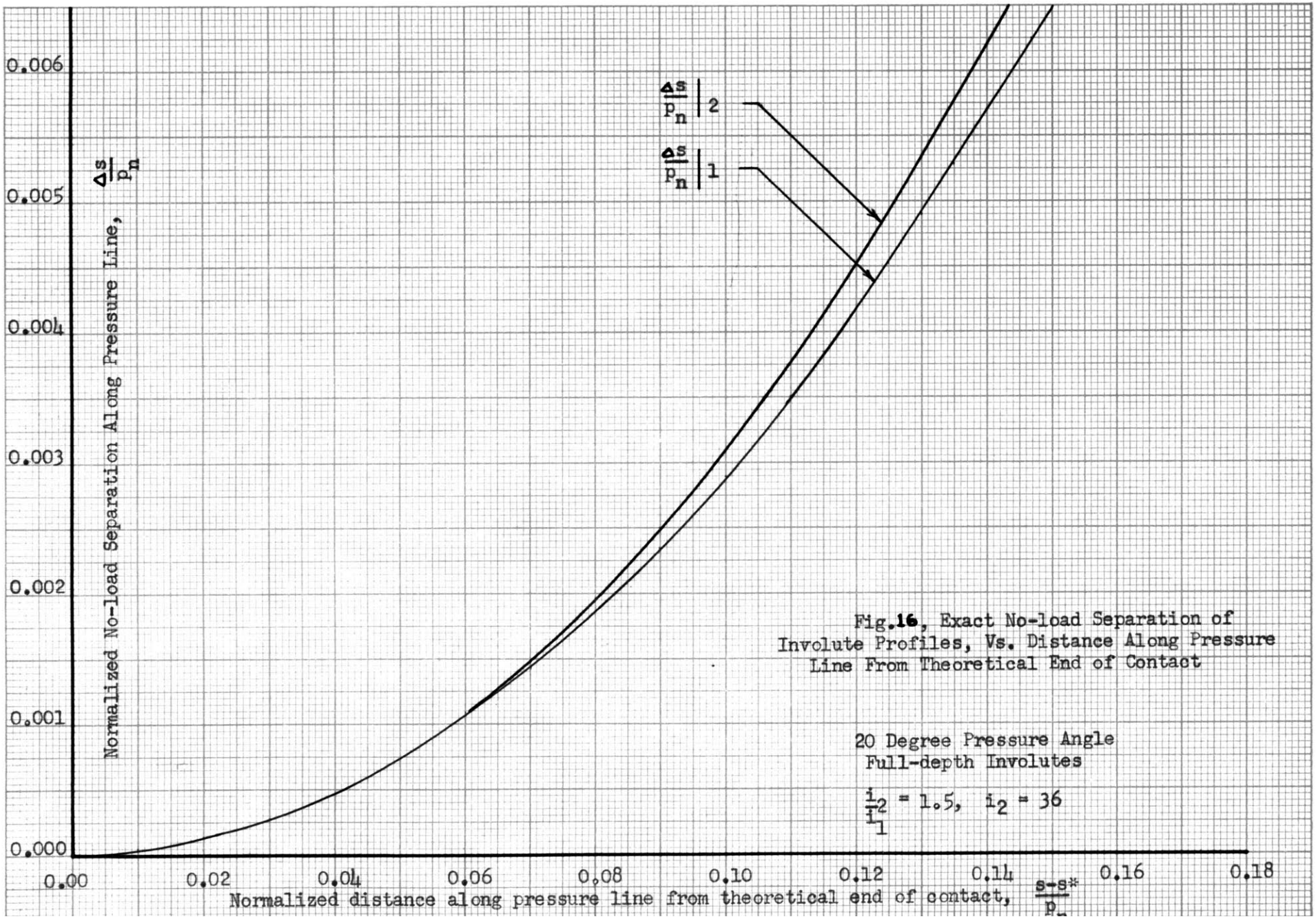

Fig.16, Exact No-load Separation of Involute Profiles, Vs. Distance Along Pressure Line From Theoretical End of Contact

Since the two solutions for no-load separation are nearly the same, it is justified to continue the gear-system analysis on the basis of a relative-motion model. For future computations of no-load separation, the simpler equations denoted as Case II in Appendix B are recommended.

The curves of Fig. 16 are plotted on logarithmic paper in Fig. 17. A parabola was found to be an excellent approximation for the no-load separation curves. Figure 18 gives a series of approximate no-load separation curves calculated for various numbers of teeth (i_1, i_2). In this figure, the subscript 2 refers to the gear which engages or disengages at its tip. The no-load separation can be represented by an equation of the form

$$\frac{\Delta s}{p_n} = cp_n \left(\frac{s - s^*}{p_n} \right)^2 \tag{2.36}$$

where the quantity (cp_n) is determined from Fig. 18 as a function of the numbers of teeth in the mating gears.

For negative values of ($s - s^*$) the teeth are in contact under no-load conditions, and Δs is zero.

5. External Input-Output Load Relationships in the Absence of Friction

When one or more pairs of teeth are in full contact along the pressure line, i.e., engagement or disengagement is not occurring, and friction is negligible, the force transmitted through the mesh must be a vector that lies along the line of action. Under these conditions the torques applied to the gears are simply related to the total transmitted load W according to Eq. (2.9). If R_B is the base circle radius, Eq. (2.9) can be written

$$\tau_1 = R_{B1} W \tag{2.37}$$

and a similar equation can be written for gear 2

$$\tau_2 = R_{B2} W \tag{2.38}$$

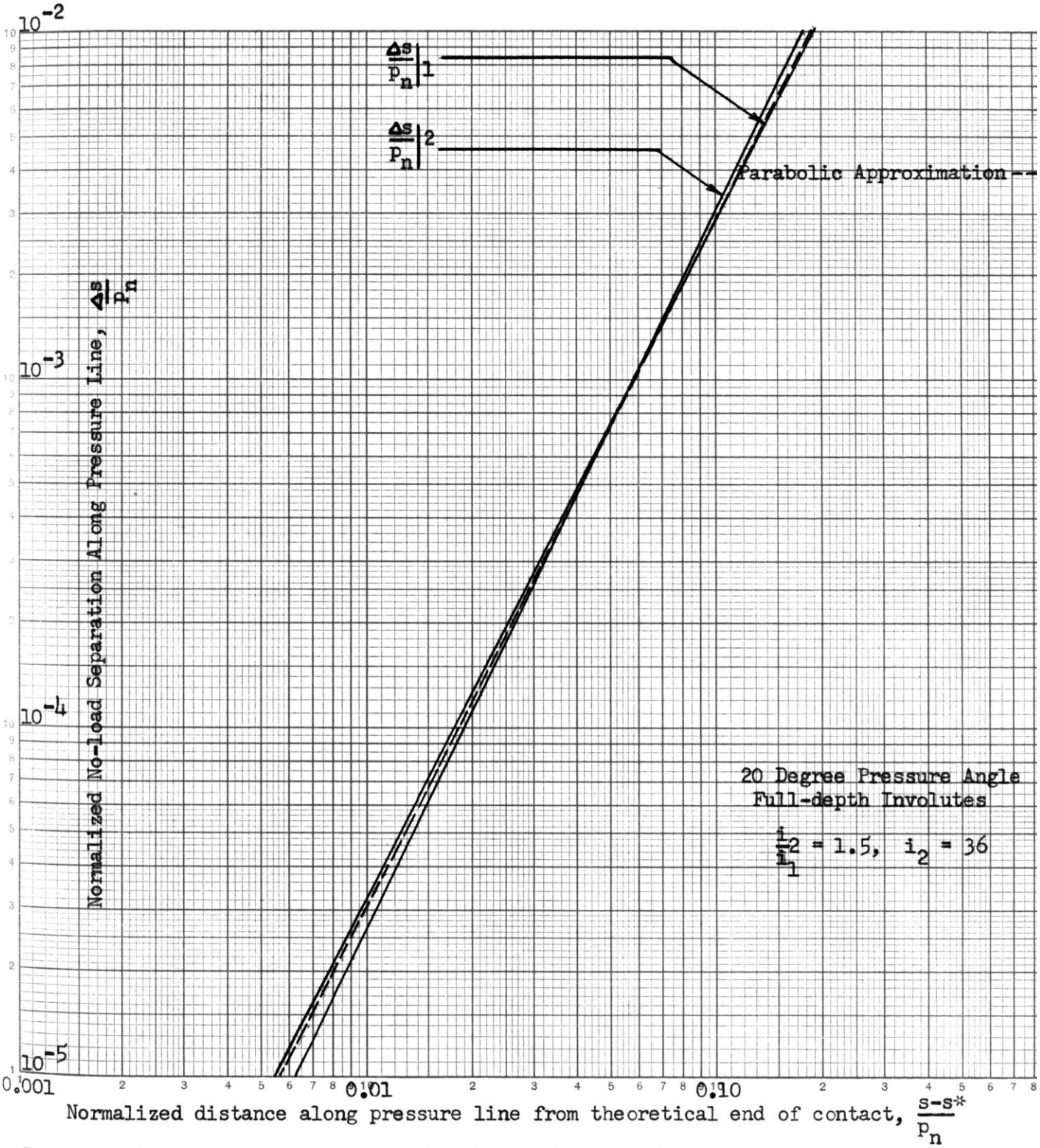

Fig. 17 EXACT AND APPROXIMATE NO-LOAD SEPARATION OF INVOLUTE PROFILES, VS. DISTANCE ALONG PRESSURE LINE FROM THEORETICAL END OF CONTACT

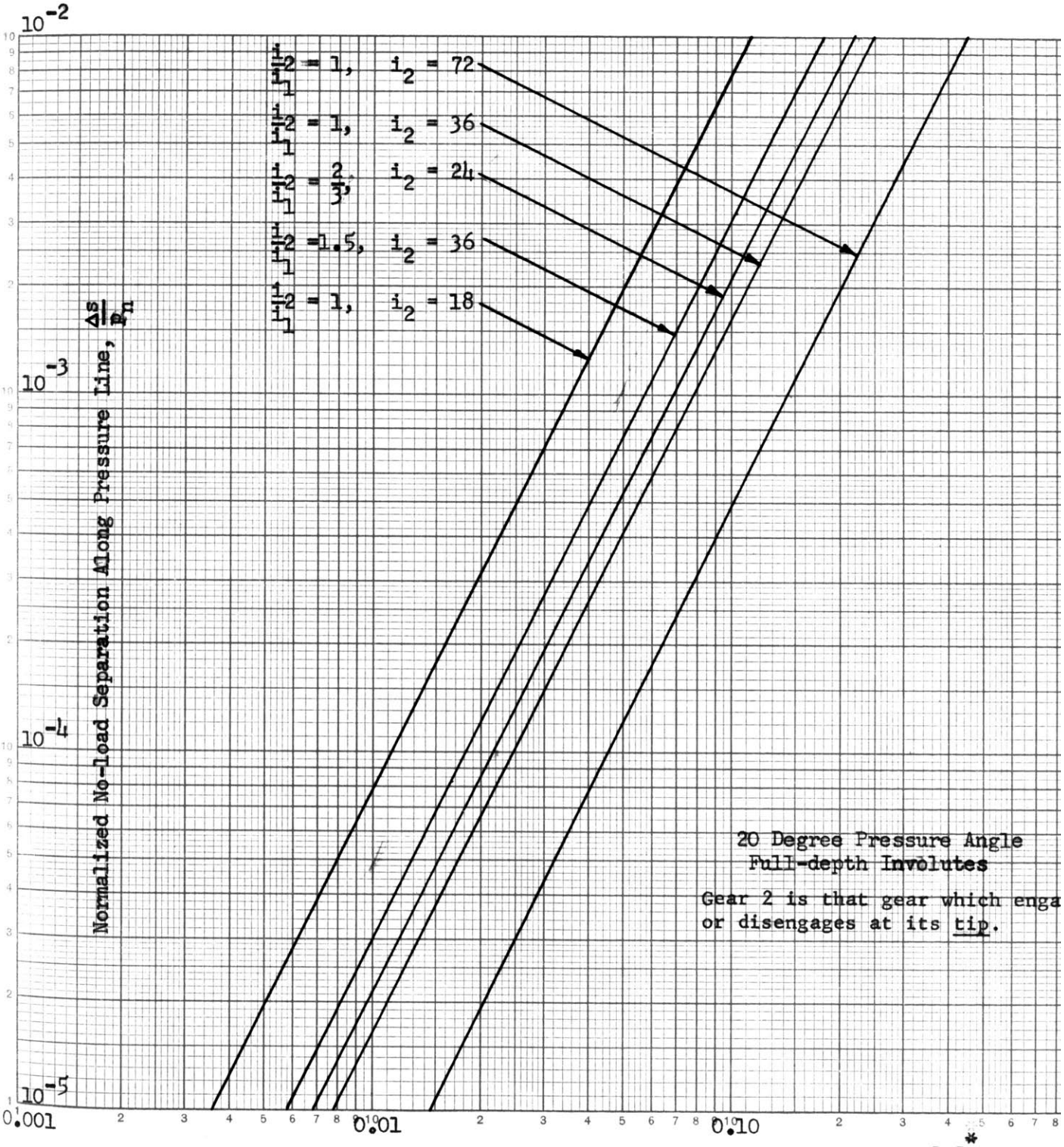

Normalized distance along pressure line from theoretical end of contact, $\frac{s-s^*}{p_n}$

Fig.18, APPROXIMATE NO-LOAD SEPARATION OF INVOLUTE PROFILES, VS. DISTANCE ALONG PRESSURE LINE FROM THEORETICAL END OF CONTACT

Since gear teeth have very high stiffness, of the order of 10^6 lbs/in. for a one inch face width gear, the shafts that couple a pair of gears to the other elements of a machine usually are very flexible in comparison to the gear-pair itself. Under these conditions it seems reasonable to assume that the input and output torques to the gear pair are constant. Then, according to Eqs. (2.37) and (2.38) the load W also is constant. However, when the point of contact between a pair of teeth occurs off the pressure line, as it does during engagement or disengagement, Eqs. (2.37) and (2.38) cannot both be valid. As a pair of teeth is brought into engagement, that pair of teeth must be deformed according to its flexibility and according to the load it must eventually carry. This deformation of an engaging tooth-pair requires a certain amount of energy which can only come from an increase in the input torque or a decrease in the output torque, or both. If the input and output torques are absolutely constant tooth engagement cannot occur and the gears will cease to rotate as soon as the engagement of a pair of teeth starts. Therefore, the input and output torques cannot always be constant.

An analysis of the mechanics of gear-tooth engagement has been made to determine the variations of input and/or output torque.necessary to force an approaching tooth into engagement. This analysis is presented in Appendix C. The results of the analysis show that the required torque variations are second-order small compared with the average torques. The reason for the smallness of the torque variation is that the gears rotate a very large distance during engagement, compared with the necessary deformation of the engaging tooth pair.

The conclusion is reached, as a consequence of the analysis given in Appendix C, that the input and output torques on a gear system can be assumed nearly constant, even during tooth engagement or disengagement, as long as friction is neglected. Then the equilibrium equations for the gear system are given by Eqs. (2.37) and (2.38) and the total force W must be the sum of the forces acting on each tooth-pair in contact. For two-pair contact

$$W = W_a + W_b \tag{2.39}$$

where W_a and W_b refer to the loads acting on tooth-pairs a and b, respectively. In the case of n pairs in contact

$$W = \sum_{m=1}^{n} W_m \tag{2.40}$$

When friction is present, the average output torque must be decreased by an amount determined by the frictional losses in the mesh. The effects of friction on the static behavior of gears is discussed in Sec. 10 of this chapter.

6. Static Load and Deflection Cycles; Zero Friction and Zero Manufactured Errors.

6.1. Model of Gear-Tooth Action

The model shown in Fig. 14b now can be extended to represent engagement and disengagement of the various pairs of teeth, as indicated in Fig. 19. As long as the gear teeth are geometrically perfect under conditions of zero transmitted load, the gear action can be represented by the movement of a cam underneath successive pairs of teeth. This cam is shown in Fig. 19 during its passage underneath tooth-pairs a, b, and c; however, after leaving these pairs, it will continue on, bringing other tooth pairs into contact in succession. Point P on the cam surface corresponds to pitch-point contact, and when any tooth-spring is contacting the cam at P, that tooth-pair is in contact at the pitch-point in the real gear system. Tooth-springs in the model are spaced by an interval of one normal pitch, just as the actual tooth-pairs are spaced in the gear system. The distance AC on the cam is flat, and is equal to the ideal path of contact. Note that under no-load conditions, any tooth-pair engages at point A and remains in contact until point C is reached, then disengages. When a load W (or Torque τ) is applied to the gears, the pitch-circles of the gears will slip and a finite value of s_r will be established. Figure 19 is drawn for the condition when tooth-pair b is carrying all of the load W, but tooth pair a is just about to start engagement. At this point, the deflection of tooth-pair b is just equal

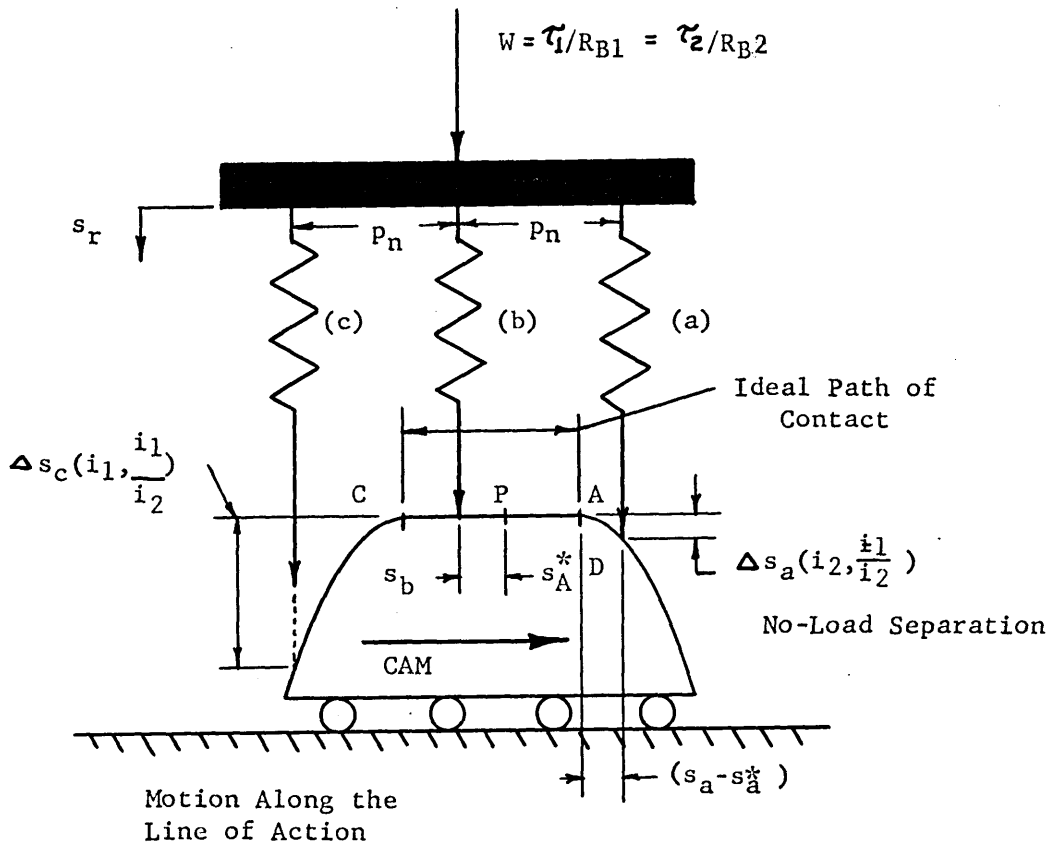

a) Model

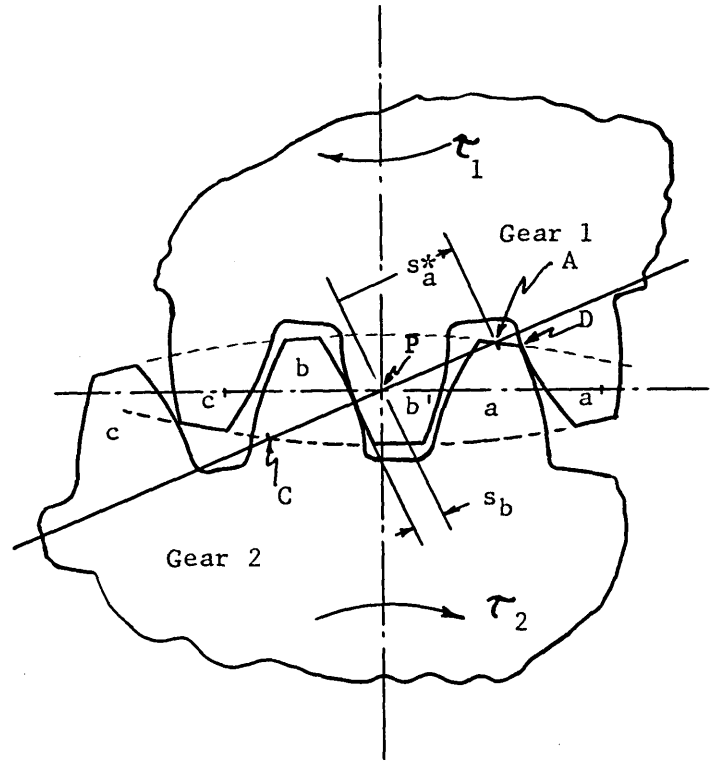

b) Physical System

Fig. 19, a and b, Model of Gear-Action; Static Operation Without Manufactured Errors or Friction

to the no-load separation for tooth-pair a and tooth- pair a is just contacting the cam surface. Tooth a is shown in Fig. 19b, just touching tooth a' at point D. Reference to the diagram of the actual gears in Fig. 19 shows that the no-load separation curve for the right side of the cam corresponds to engagement at the tip of a tooth on gear 2. Hence the no-load separation curve is obtained using the number of teeth on gear 2 as the i_2 value in Fig. 18. Similarly, the no-load separation curve for the left side of the cam is obtained using the number of teeth on gear 1 as the i_2 value in Fig. 18.

6.2. Computation of Static Load and Deflection Cycles

The model of Fig. 19, the no-load separation data from Fig. 18, and the tooth-pair compliance curve computed from Figs. 9, 11, and 12, are sufficient to permit computation of the static load or deflection cycles for a given pair of friction-free, errorless gears.

At the position shown in Fig. 19, the forces in tooth-springs a and b are

$$W_b = k_b s_r = \frac{Ef}{w_b} \quad s_r \tag{2.41}$$

$$W_a = k_a(s_r - \Delta s_a) = \frac{Ef}{w_a} \quad (s_r - \Delta s_a) \tag{2.42}$$

When Eqs. (2.41), (2.42), and (2.39) are combined, the deflection is found to be

$$\frac{s_r E}{W_o} = \frac{w_a w_b}{w_a + w_b} + \frac{Ep_n}{W_o} \left(\frac{\Delta s_a}{p_n}\right) \frac{w_b}{w_a + w_b} \tag{2.43}$$

Combination of Eqs. (2.43) and (2.41) yields an expression for the load on tooth-pair b

$$\frac{W_b}{W} = \frac{w_a}{w_a + w_b} + \frac{Ep_n}{W_o} \left(\frac{\Delta s_a}{p_n}\right) \frac{1}{w_a + w_b} \tag{2.44}$$

where W_o is load-per-unit of face-width, and w_a and w_b are tooth-pair compliances at the given position of the cam (s_b). As the cam moves to the left, in Fig. 19, tooth-pair a moves out of contact, and Eqs. (2.43) and (2.44) do not hold. When tooth-pair b is the only tooth pair in contact,

$$\frac{s_r E}{W_o} = w_b \tag{2.45}$$

and

$$\frac{W_b}{W} = 1 \tag{2.46}$$

For all other positions of the cam, while tooth-pair b is in contact, Eqs. (2.43) and (2.44) can be applied by changing subscripts and signs as dictated by inspection of the model. For example, as the cam moves to the right in Fig. 19, tooth-pair a becomes fully engaged and Δs_a goes to zero. As tooth-pair b crosses point C on the cam, Δs_c assumes finite values and the load on pair b is reduced accordingly. For this situation the quantity $(\Delta s_a)w_b$ in Eq. (2.43) is replaced by $-(\Delta s_c)$wa, and (Δs_a)in Eq. (2.44) is replaced by $-(\Delta s_c)$.

In some cases three or more pairs of teeth may be in contact at the same time. Equations for calculating deflections or tooth-load cycles under these conditions are easily derived by referring to the geometry of the model. Relations are written for each tooth load, taking into account no-load separation Δs and deflection s_r; these loads are summed according to Eq. (2.40), and the resulting equation is solved for s_r or for any individual tooth load that is of interest.

Figure 20 shows static load cycles computed for a tooth in a gear pair which has the following dimensions:

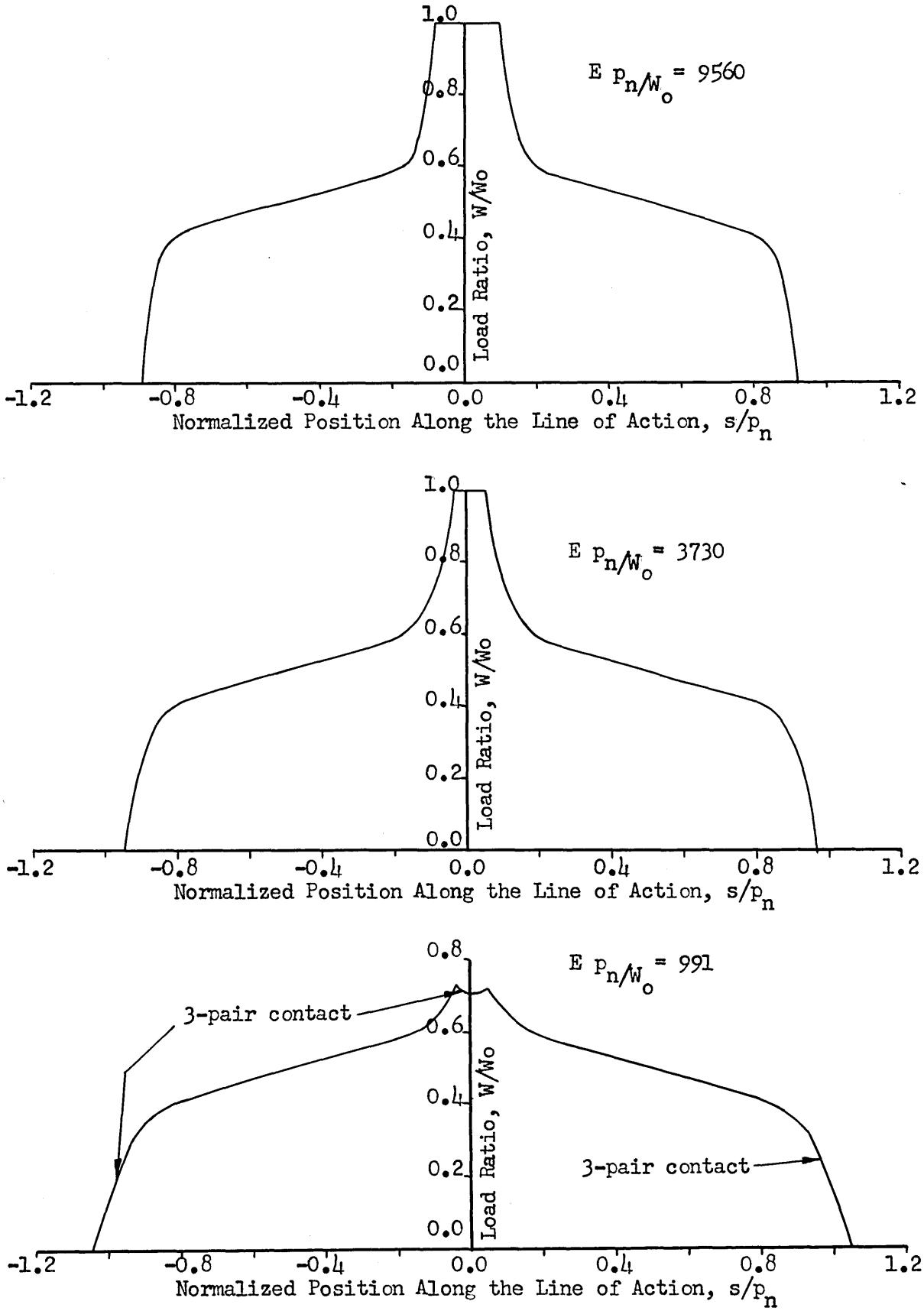

Fig.20, Static Load Cycles for Various Transmitted Loads and Negligible Manufacturer's Errors. For a 27 Tooth Pinion Mating With a 34 Tooth Gear. 20 Degree Pressure Angle.

Normal Pitch (p_n) = 0.35 in.
Face Width (f) = 0.394 in.
Teeth on Pinion (i_p) = 27
Teeth on Gear (i_g) = 34
Materials: Hardened steel
20°, Full-Depth Involutes

Tooth-pair compliance was taken from Fig. 13, and values of cp_n defining no-load separations were found by interpolation in Fig. 18. The model of Fig. 19 was used as the basis for making computations of tooth load at various phases of engagement.

Movement along the line of action in the positive sense ($+s/p_n$) in Fig. 20 corresponds to movement toward the tip of the pinion. Three load cycles are plotted for three different values of load. The analysis predicts different load cycles for different values of the dimensionless parameter (Ep_n/W_o). In this case, contact between three pairs of teeth is achieved at the highest value of load ($Ep_n/W_o = 991$). Thus the operating contact ratio for this pair of gears is increased from 1.65 at zero load to about 2.1 at the highest load, as a result of elastic deformation! It is also significant that the maximum tooth load is approximately 30 per cent less than the transmitted load W, when $Ep_n/W_o = 991$. Therefore, calculations of strength made on the basis of the whole transmitted load would be in considerable error for this situation. The errors involved will tend to increase as the size of the gears decreases or as the load increases.

The results obtained here show the importance of including a detailed study of the processes of tooth engagement and disengagement in any analysis of static loads or deflections in gear teeth.

7. Relationships Between Tooth Load and Significant Stresses

As discussed in Chapter 1, failure of gear teeth due to excessive stress has been found to be related to two localized stresses: The compressive stress induced in the region of contact between mating teeth, and the bending stress induced in the root section of the tooth considered as a cantilever beam.

The first of these stresses is directly related to the contact load, but the bending stress at the tooth base will vary considerably with the position of loading along the tooth.

In evaluating the stress cycle that the material near the root of a gear tooth will experience as the gear tooth passes through a loaded gear mesh, it is convenient to work with nominal stresses. That is, to define a nominal stress as that stress which would be present at the root of a tooth if the tooth were truly a simple cantilever beam. When this nominal stress has been evaluated, for a given gear tooth, the more refined techniques described in Sec. 2.211 of Chapter 1 can be employed in critical regions of the nominal stress cycle to obtain highly accurate calculations of the actual maximum stresses at the tooth root.

The variation of nominal bending stress in the root section of a gear tooth due to variation of the position of load along the tooth profile can be expressed by the simple-beam formula. In terms of the quantities defined in Fig. 21.

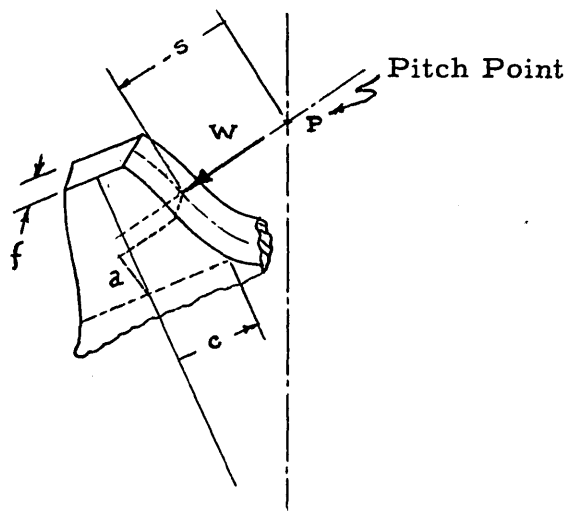

Fig. 21. Geometrical Relationships for a Loaded Gear Tooth.

$$\sigma_B = \frac{a\,W}{\frac{8}{12}\,f\,c^2} \tag{2.47}$$

The Lewis form factor Y is defined by Eq. (1.1).

$$W \cos\theta = \frac{fY\,\sigma}{p_d} \tag{1.1}$$

It is convenient to express the nominal stress σ_B in nondimensional terms by utilizing the Y Factor. When diametral pitch is replaced by normal pitch, Eq. (1.1) becomes

$$\frac{\sigma_B p_n}{W_o} = \pi \cos^2\theta \, \frac{1}{Y} \tag{2.48}$$

Comparison of Eq. (2.48) with Eq. (2.47) gives a relationship for the reciprocal Y factor.

$$\frac{1}{Y} = \frac{3}{2}\left(\frac{1}{\pi \cos^2\theta}\right)\left(\frac{a\,p_n}{c^2}\right) \tag{2.49}$$

For any given position of the load W, the distances "a" and "c" in Fig. 21 and Eq. (2.49) are directly proportional to the size of the tooth or the normal pitch. Hence, the reciprocal Y factor is independent of the tooth size and is only a function of the number of teeth in the gear, the position of load along the tooth, and the tooth system or dedendum distance employed.

Figure 22 gives plots of Eq. (2.49) for 20° pressure-angle, full-depth involute gears as functions of the number of teeth (i) and of load position, (s/p_n). The equations upon which these curves are based are given in Appendix D.

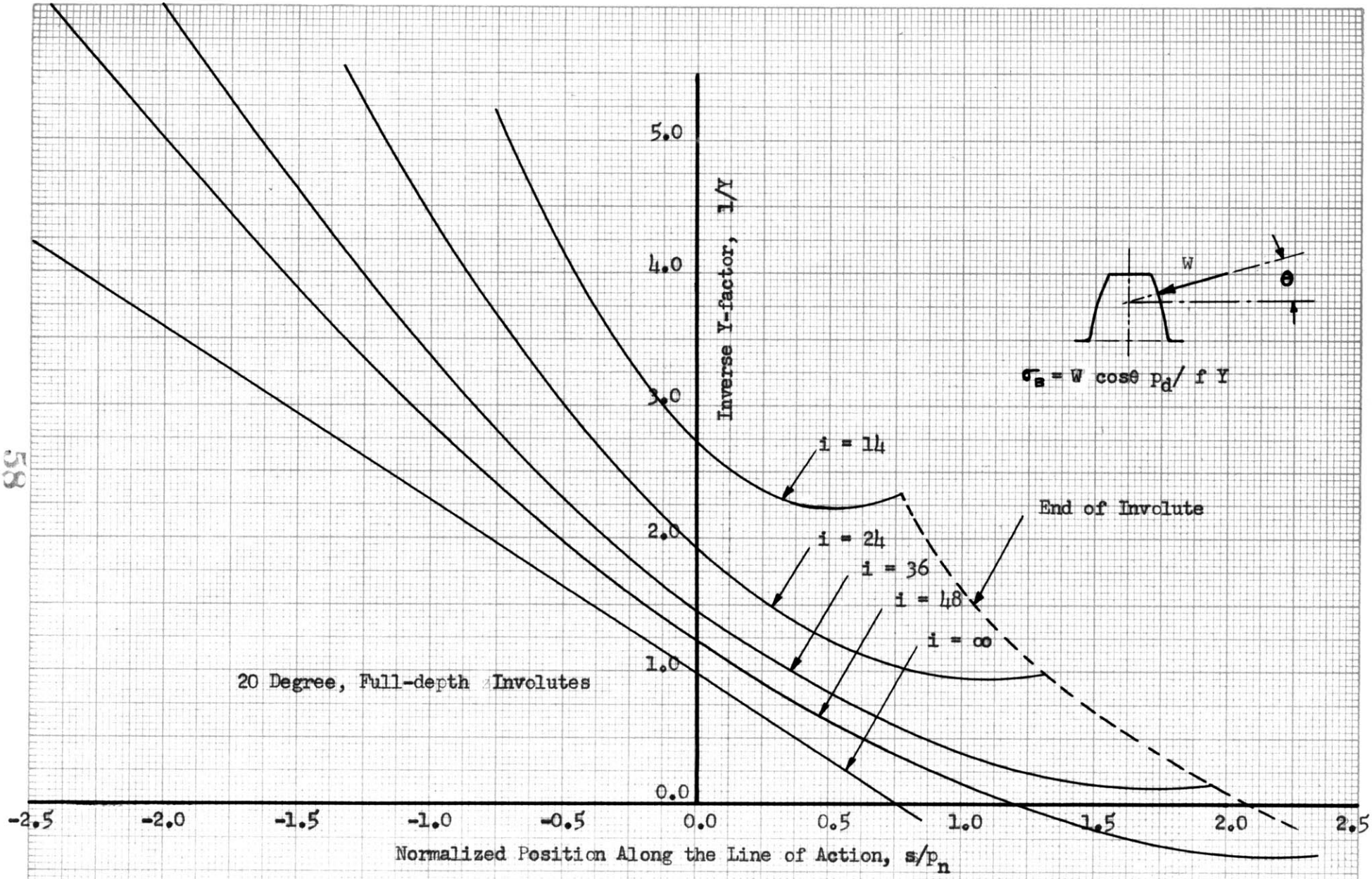

Fig.22, Inverse Y-factor vs. Position Along the Line of Action

8. Static Bending Stress Cycles: No Friction and No Manufactured Error

Plots of static bending stress can be computed directly from static load cycles, by multiplying the load at any phase of engagement by the corresponding factor, Eq. (2.48), obtained from Fig. 22. The static load cycles presented in Fig. 20 have been transformed in this manner to obtain the bending-stress cycles shown in Fig. 23. These stress cycles are plotted for the 27-tooth gear.

Figure 24 is an overlay showing measured curves of static bending stress as taken from data of Rettig, (Ref. 49 p. 92). These measurements were made on very accurate, ground gears having manufactured errors less than 2×10^{-4} inches; the nominal stress was derived from observed values of the deflection of a given point on an instrumented gear tooth relative to the main body of the gear wheel.

At the largest value of load, the measured curve of Rettig shows the highest degree of agreement with the calculated curve of Fig. 23. This is to be expected, since at small values of load the small manufactured errors present can have appreciable influence on the measured stress and load cycles. For these gears, the assumption of negligible friction, which was made in computing the theoretical results, seems to be justified.

9. Manufactured Errors: Influence of Errors on Static Load and Stress Cycles

Gear teeth can never be manufactured with exactly the desired shape and orientation. The machining processes will always introduce some finite amount of error between the ideal geometry and the actual manufactured geometry. Such errors may, and in fact usually do, interfere with the conjugate action (constant speed ratio) of the gears, and will affect the nature of the static load and stress cycles.

Manufactured error for a single gear is defined as the amount by which an ideal rack would advance beyond its theoretical position when driven under no load by the gear. Manufactured error for a gear pair is then defined as the amount of pitch-circle slip that occurs at any position as the gears are rotated together.

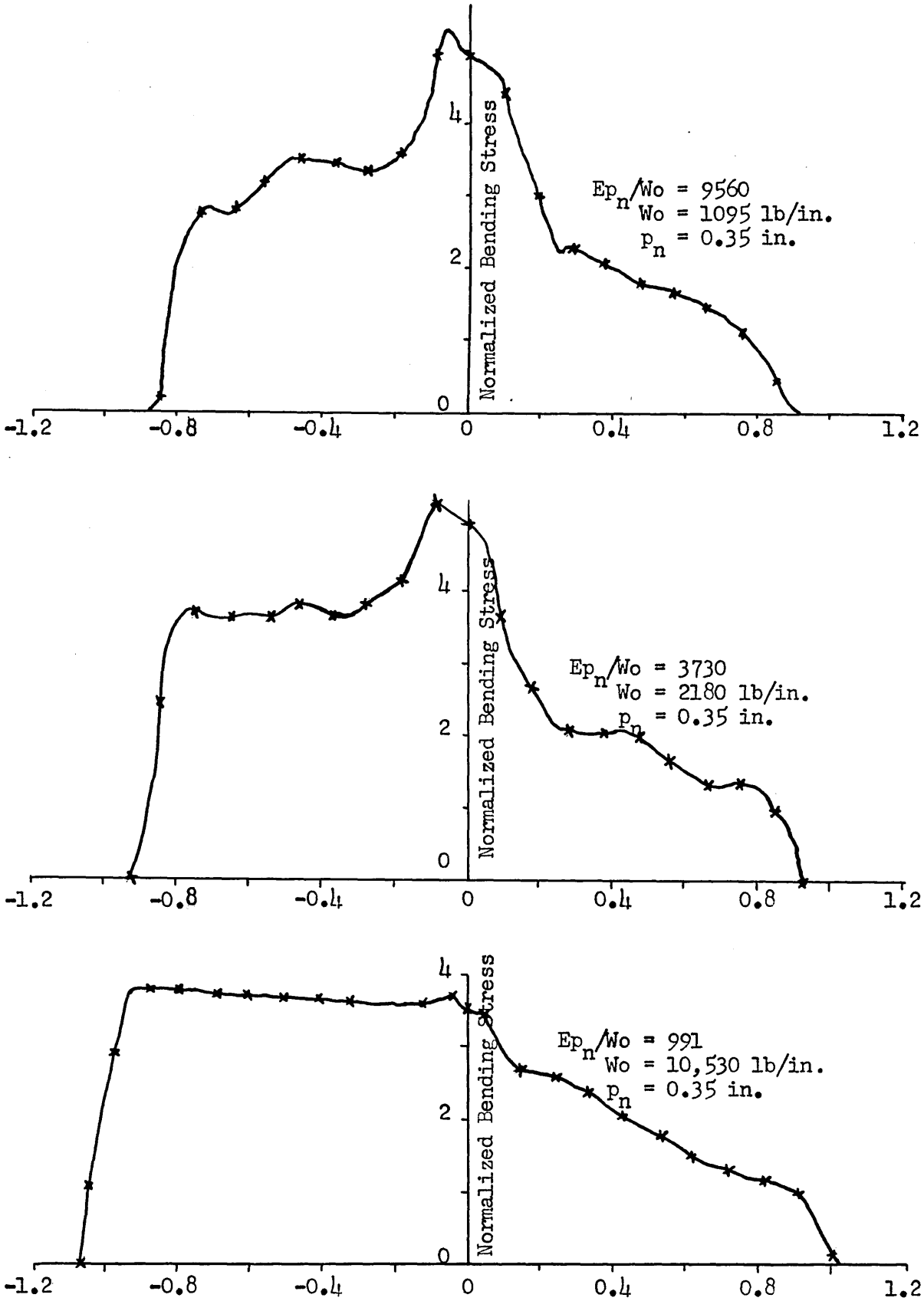

Fig.24, Overlay. Experimental Static Stress Cycles from Niemann and Rettig, Reference **49**, p.92. For a 27 Tooth Pinion Mating With a 34 Tooth Gear. 20 Degree Pressure Angle.

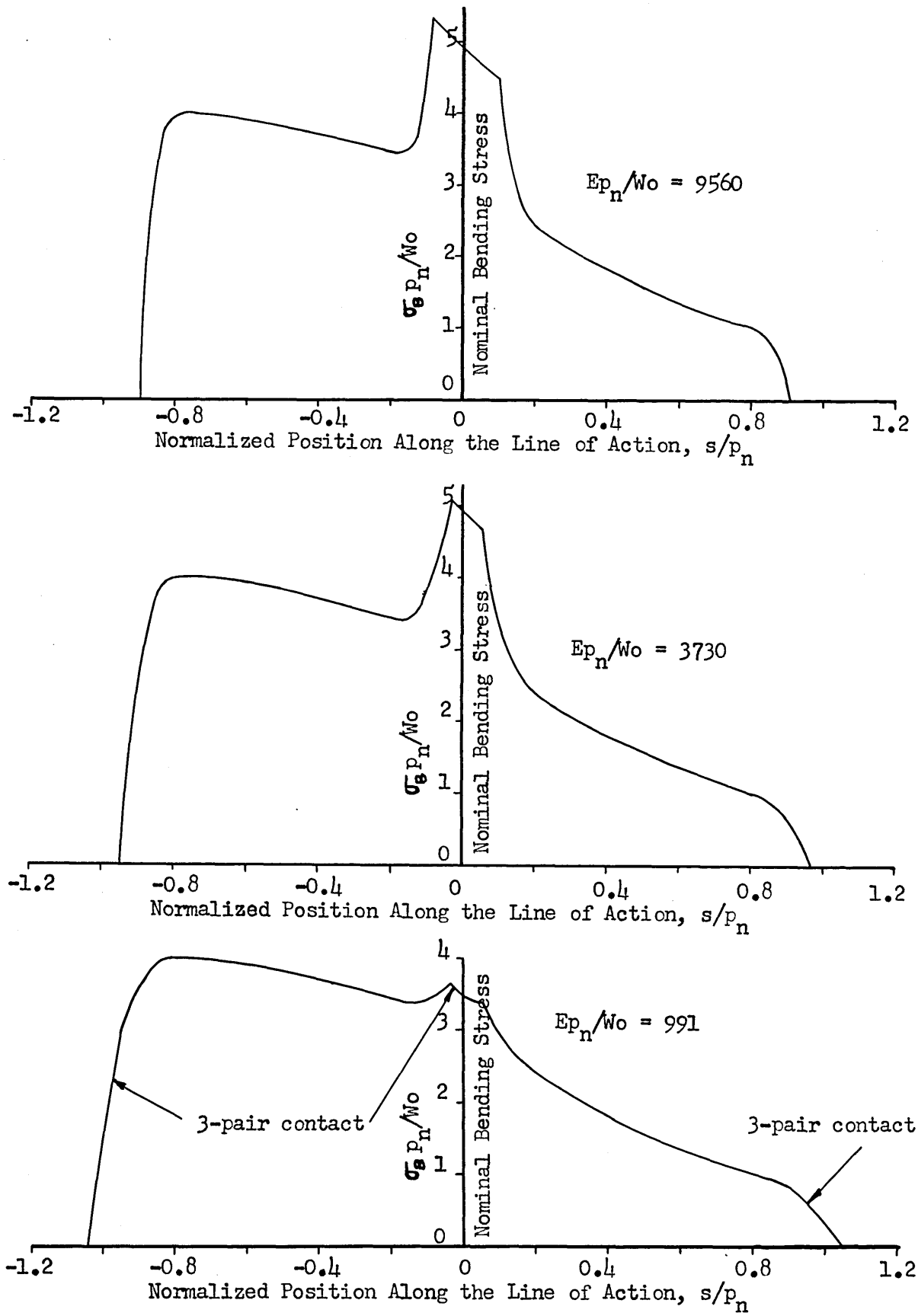

Fig.23, Nominal Static Bending Stress Cycles for Various Transmitted Loads and Negligible Manufacturer's Errors. For a 27 Tooth Pinion Mating with a 34 Tooth Gear. 20 Degree Pressure Angle.

9.1. Types of Manufactured Errors

Manufactured errors or errors due to wearing of gear-tooth profiles usually are classified in the following manner:

1. Profile Error - the deviation, measured normal to the ideal-involute surface, between the actual and ideal or theoretical tooth form. Profile error is designated here by the quantity e_p, and is defined to be positive when the actual profile lies outside of the theoretical tooth contour. Profile error is slways defined to be zero at the pitch point.

2. Pitch Error or Spacing Error. Pitch error usually is defined as the deviation of the distance between two neighboring teeth, measured along the pitch circle, from the specified circular pitch. For use in load-cycle calculations, it is more convenient to express the pitch error in terms of the normal pitch rather than the circular pitch. In order to do this, the following procedure must be followed.

   (i) The perpendicular distance from the pitch point of one tooth (a) to the surface of the adjacent tooth (b) is measured, and deviation of this distance from the specified normal pitch is computed. The deviation is considered positive if the measured distance exceeds the specified normal pitch.

   (ii) The profile error is determined for the point on the adjacent tooth (b) at the point where measurement (i) was made.

   (iii) The difference between the deviation measured in (i) and the profile error measured in (ii) is the spacing error e_s for the tooth pair. These conventions are illustrated graphically for a rack in Fig. 25.

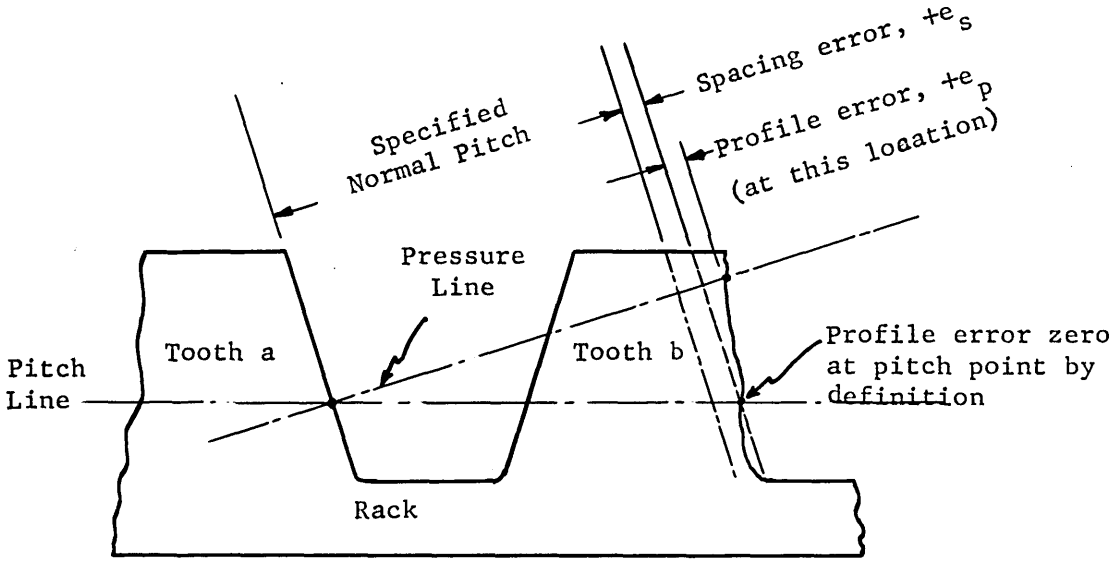

Fig. 25. Definitions and Conventions for Tooth Errors.

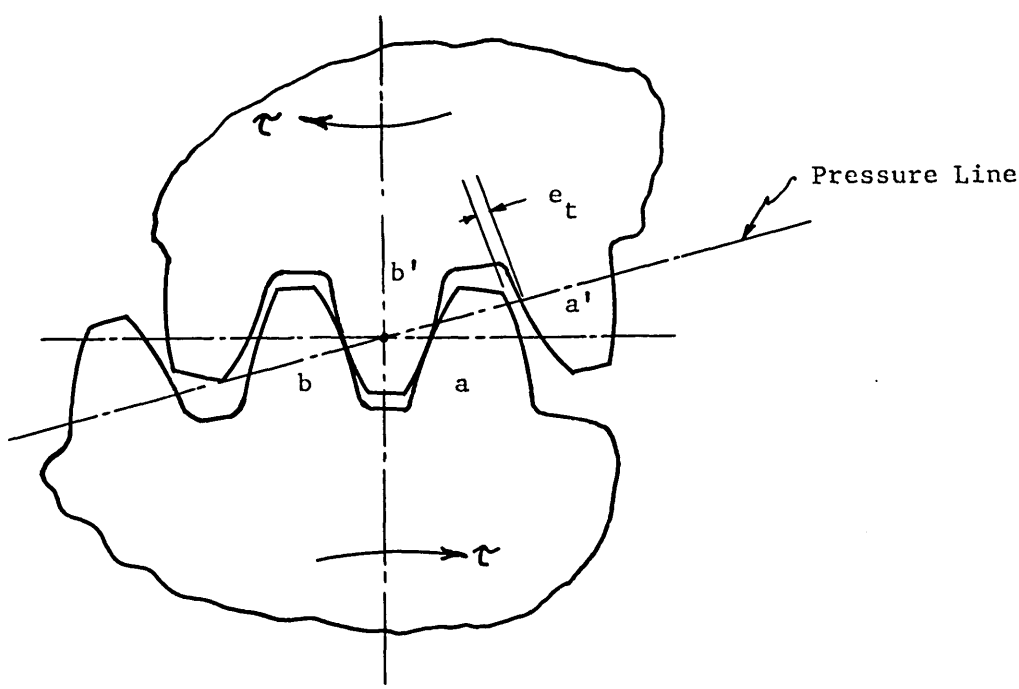

Fig. 26. No-Load Geometry for Adjacent Tooth Pairs That Have Manufactured Errors.

3. Pitch-Line Runout - the variation in pitch-circle radius around the gear. This type of error produces a slight variation in speed-ratio as a function of angular position of the gear when the gear is operated with a mating gear. Errors of this type, unless extraordinarily large, will not influence the static load or stress cycles for individual gear teeth.

4. Lead Error - failure of the tooth surface to be parallel to the axis of rotation of the spur gear. This error may affect the tooth flexibility slightly, and causes non-uniform stress distribution across the face of the tooth. The effects of this type of error can be minimized by crowning of the tooth face during manufacture of the gear.

9.2. Effect of Manufactured Errors on Static Load and Stress Cycles

With the definitions of and conventions for manufactured errors established in Sec. 9.1 the model of gear-tooth action shown in Fig. 19 can be extended to include the effects of manufactured errors on gear-tooth loads and stresses.

If only one pair of teeth is in contact in the gear mesh, manufactured error obviously cannot affect the load or stress in that pair of teeth. The deflection s_r will be changed by an amount equal to the combined spacing and profile errors for both teeth which are in contact. However, when two or more pairs of teeth are in contact in the mesh, errors in spacing or profile act to change the distribution of load between various pairs of teeth. For example, suppose that tooth-pair b in Fig. 26 is geometrically perfect under conditions of no load. At the position shown, there is, however, a negative error $(e_s + e_p)_a$ in the distance from tooth b to tooth a, and a positive error $(e_s + e_p)_{a'}$ in the distance from tooth b' to tooth a'. Therefore, under conditions of no load, tooth-pair a will be separated along the line of action by the algebraic difference of the positive and negative error. This total separation will be called the effective error e_t for tooth-pair a relative to tooth pair b; or for brevity, the error for

tooth-pair a. When load is transmitted through the gear mesh in Fig. 26, tooth pair b will now carry all of the transmitted load up to the point where the deflection (s_r) of tooth-pair b becomes equal to the total error (e_t) of tooth-pair a relative to tooth-pair b. Then tooth-pair a will start to assume part of the transmitted load as the load is increased further. The total error e_t will be defined as positive if it tends to increase the load on the tooth-pair being studied.

To illustrate how this total error e_t is incorporated into the model of gear-tooth action, the load equations will be written for the position of the model shown in Fig. 19a. Tooth-pair b has no error, but tooth-pair a is assumed to have a positive error e_{ta} relative to b. By definition of positive error, this error is such as to make tooth-spring a shorter than tooth-spring b under conditions of no load. Hence, the tooth-load equations are:

$$W_b = k_b s_r = \frac{Efs_r}{w_b} \tag{2.50}$$

$$W_a = k_a (s_r - \Delta s_a - e_{ta}) = \frac{Ef}{w_a} (s_r - \Delta s_a - e_{ta}) \tag{2.51}$$

When the tooth loads are summed according to Eq. (2.39) and the resulting equation is solved for W_b, the following expression is obtained.

$$\frac{W_b}{W} = \frac{w_a}{w_a + w_b} + \frac{Ep_n}{W_o} \left(\frac{\Delta s_a}{p_n}\right) \frac{1}{w_a + w_b} + \frac{Ee_{ta}}{w_o W_o} \frac{w_o}{w_a + w_b} \tag{2.52}$$

where w_a, w_b are tooth compliances for pairs a and b, respectively, at the value of s/p_n being examined, Δs_a is the no-load separation, e_{ta} is the total error of pair a relative to pair b and w_o is the tooth-pair compliance for pitch-point contact of a single pair of teeth. The quantity $Ee_{ta}/w_o W_o$ has the physical significance of being the total error that exists at the given contact point (s/p_n), divided by the deflection under load W of a single pair of teeth which is in contact at the pitch point. If δ_s is defined in the following way,

$$\delta_s = \left(\frac{E}{w_o W_o}\right)^{-1} \tag{2.53}$$

then

$$\frac{E e_{ta}}{w_o W_o} = \frac{e_{ta}}{\delta_s} \tag{2.54}$$

In the case of spacing error, e_t would be independent of s/p_n, but generally e_t is a function of position along the line of action.

For positions of the "cam" other than that shown in Fig. 19, and when more than one tooth-pair is in contact, the equations for the load acting on any tooth pair assume the same form as Eq. (2.52). The signs of each term, and the subscripts for compliance, no-load separation, and error are readily determined, for any specific situation, by examination of the model, Fig. 19.

Figure 27 shows the effects of positive and negative spacing errors $e_t = e_s$ on the static load and stress cycles. The gears employed in computing the curves shown in Fig. 27 are the same as those used in constructing Figs. 20 and 23. A constant load, given by $Ep_n/W_o = 9560$, was assumed in all cases shown on Fig. 27. Inspection of the stress cycles presented in Fig. 27 seems to indicate that negative spacing errors produce a decrease in maximum stress, while positive errors produce an increase. However, as shown in Fig. 28, the presence of a negative spacing error on one tooth-pair will increase the stress in the following tooth-pair. Thus the first part of the stress cycle for a perfect tooth which follows a tooth that has a negative error looks like the first part of the stress cycle for a tooth that has a positive error. Figure 29 shows stress cycles for teeth preceding and following a tooth-pair that has a positive spacing error.

10. Effects of Static Friction on Static Load and Stress Cycles

When friction is present between mating gear teeth, the input and output torques no longer are related according to Eqs. (2.28) and (2.29). The equilibrium equations for a pair of gears which have friction can be derived with the aid of Fig. 30.

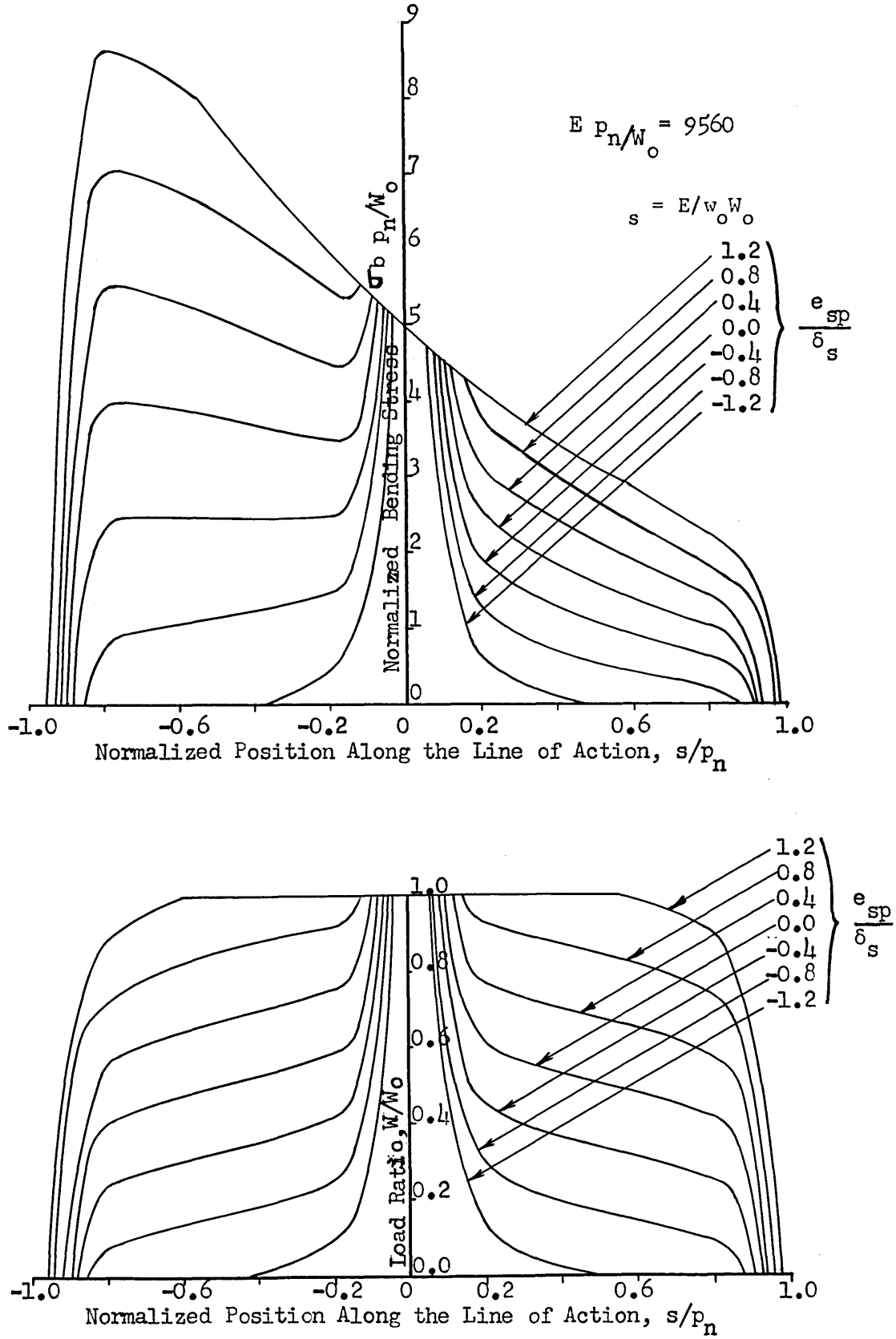

Fig27, Static Load and Bending Stress Cycles for Various Spacing Errors, at Constant Transmitted Load. For a 27 Tooth Pinion Mating With a 34 Tooth Gear. 20 Degree Pressure Angle.

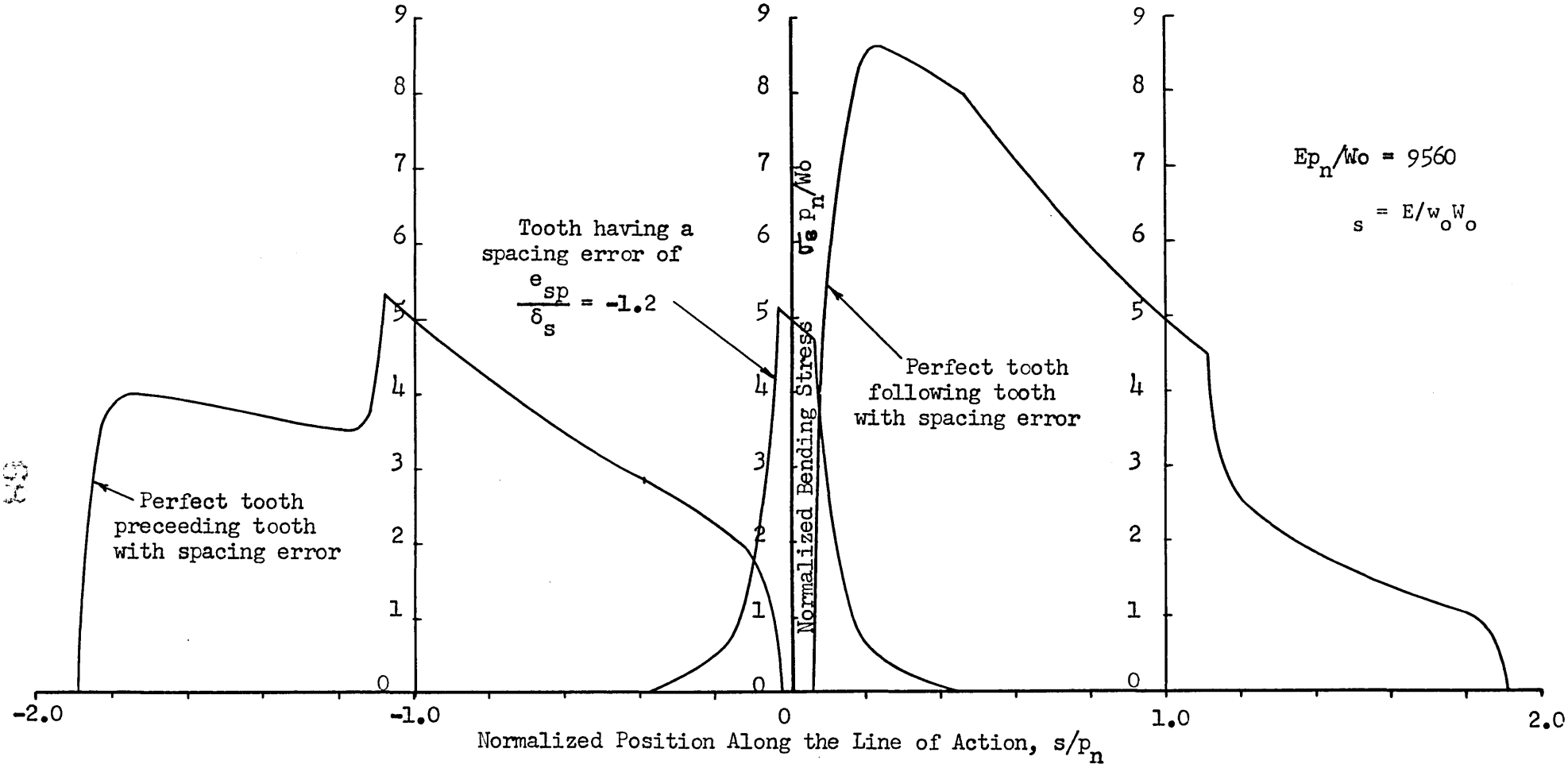

Fig.28, Effect of a Tooth Having a Negative Spacing Error on the Stress Cycles of the Adjacent Perfect Teeth. For a 27 Tooth Pinion Mating With a 34 Tooth Gear. 20 Degree Pressure Angle.

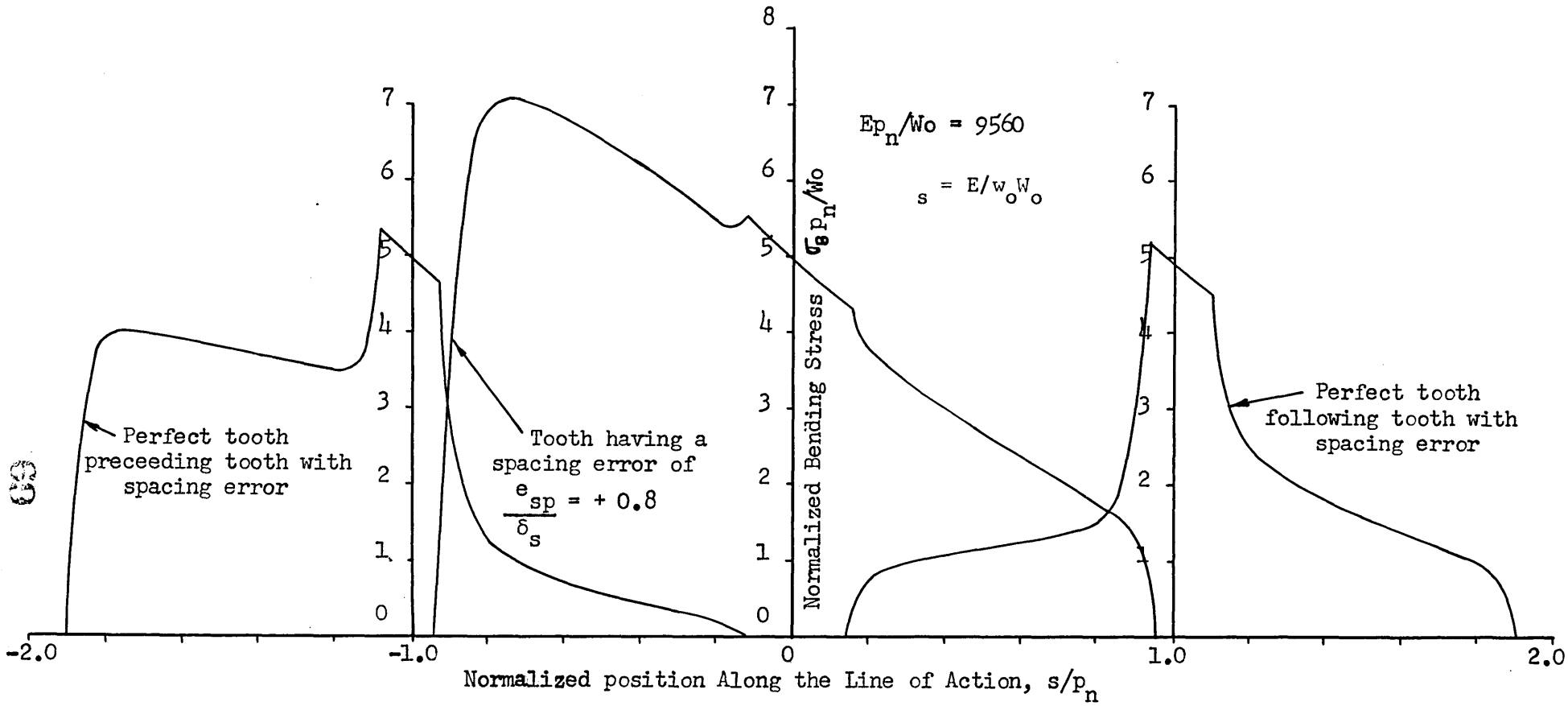

Fig.29, Effect of a Tooth Having a Positive Spacing Error on the Stress Cycles of the Adjacent Perfect Teeth. For a 27 Tooth Pinion Mating With a 34 Tooth Gear. 20 Degree Pressure Angle.

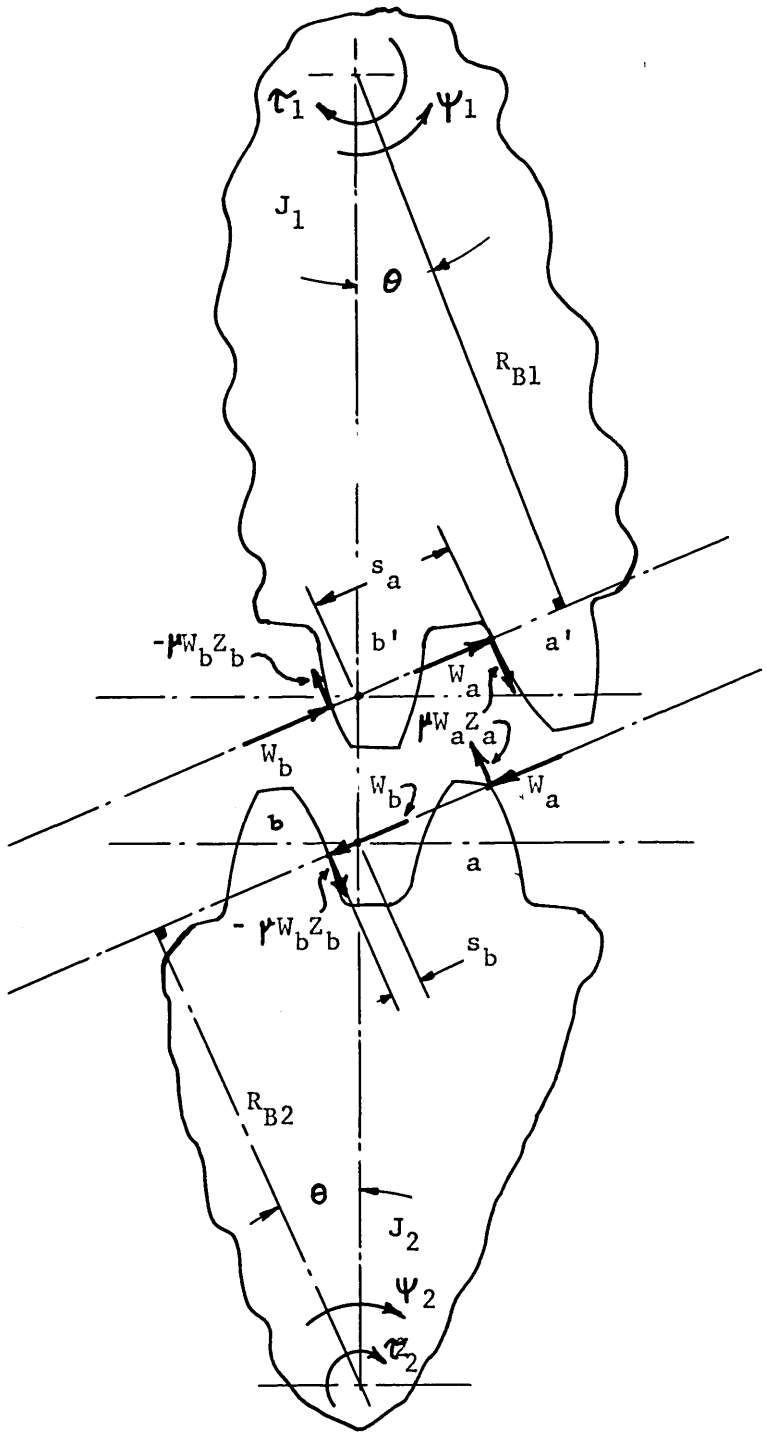

Fig. 30. Forces and Moments Acting on a Pair of Gears, Including Static Friction.

For gear 1

$$\frac{\tau_1}{R_{B1}} = W_a + W_b + W_a \mu Z_a \left[\tan\theta - \frac{s_a}{R_{B1}}\right] + W_b \mu Z_b \left[\tan\theta - \frac{s_b}{R_{B1}}\right] \tag{2.55}$$

and for gear 2

$$\frac{\tau_2}{R_{B2}} = W_a + W_b + W_a \mu Z_a \left[\tan\theta + \frac{s_a}{R_{B2}}\right] + W_b \mu Z_b \left[\tan\theta + \frac{s_b}{R_{B2}}\right] \tag{2.56}$$

where μ is the coefficient of friction, and θ is the pressure angle. The quantities Z_a and Z_b have magnitude unity, and the same sign as s_a and s_b, respectively. (In Fig. 30, s is positive measured to the right of the pitch point). These factors are necessary since the direction of sliding, and therefore of the friction force, reverses direction at the pitch point. Assume now that the input torque τ_1 is constant. Then according to Eqs. (2.55) and (2.56), the output torque τ_2 cannot also be constant. Since only the influence of friction on the loads, W_a and W_b, is of interest here, Eq. (2.56) is unnecessary and can be discarded. If the input torque τ_1 is expressed in terms of a constant load W, according to Eq. (2.37) and R_{B1} is expressed in terms of normal pitch p_n and number of teeth i, Eq. (2.55) can be written

$$W = W_a \left[1 + \mu Z_a \left(\tan\theta - \frac{2\pi}{i_1} \frac{s_a}{p_n}\right)\right] + W_b \left[1 + \mu Z_b \left(\tan\theta - \frac{2\pi}{i_1} \frac{s_b}{p_n}\right)\right] \tag{2.57}$$

The values of s_a and s_b in this result must of course differ by one normal pitch.

$$s_a - s_b = p_n \tag{2.58}$$

In the presence of friction, therefore, the simple equilibrium equation, Eq. (2.39), must be replaced by the more complicated Eq. (2.57). If the assumption is made that the small frictional component of force does not appreciably affect the tooth-pair spring stiffness or the nominal stress in the tooth, all other steps in computing load and stress cycles are the same as when friction is absent. The forces W_a and W_b are expressed from the model of Fig. 19, taking into account elastic deformation s_r, no-load separation Δs, and manufactured error, e_t. The two equations obtained in this way, together with Eq. (2.57), can be solved for s_r, W_a, or W_b at any position s along the pressure line.

Figure 31 is a representative calculated load cycle showing the effects of friction on the static tooth load for a coefficient of friction of 0.1. The zero-friction load cycle, shown as a dashed line in Fig. 31, is taken from Fig. 20. Inspection of Fig. 31 shows that the main effect of the friction is to cause a sudden jump in the tooth load as contact passes through the pitch point. To the left of the pitch point, in the region of single-pair contact, the tooth load is greater than the input load W; to the right of the pitch point, also in the region of single-pair contact, the tooth load is less than the input value. In all other regions of the load cycle, the frictional effects appear to be of minor importance. As the gears are rotated at finite speeds, it is expected that sliding velocities, which become large as contact moves away from the pitch point, will further reduce the effects of static friction in regions of double-pair contact.

On the basis of calculated curves, such as the one shown in Fig. 31, the following approximations are suggested for including frictional effects in computations of static load and stress cycles.

1. Friction is neglected except in the vicinity of the pitch point or when only one pair of teeth is in contact.

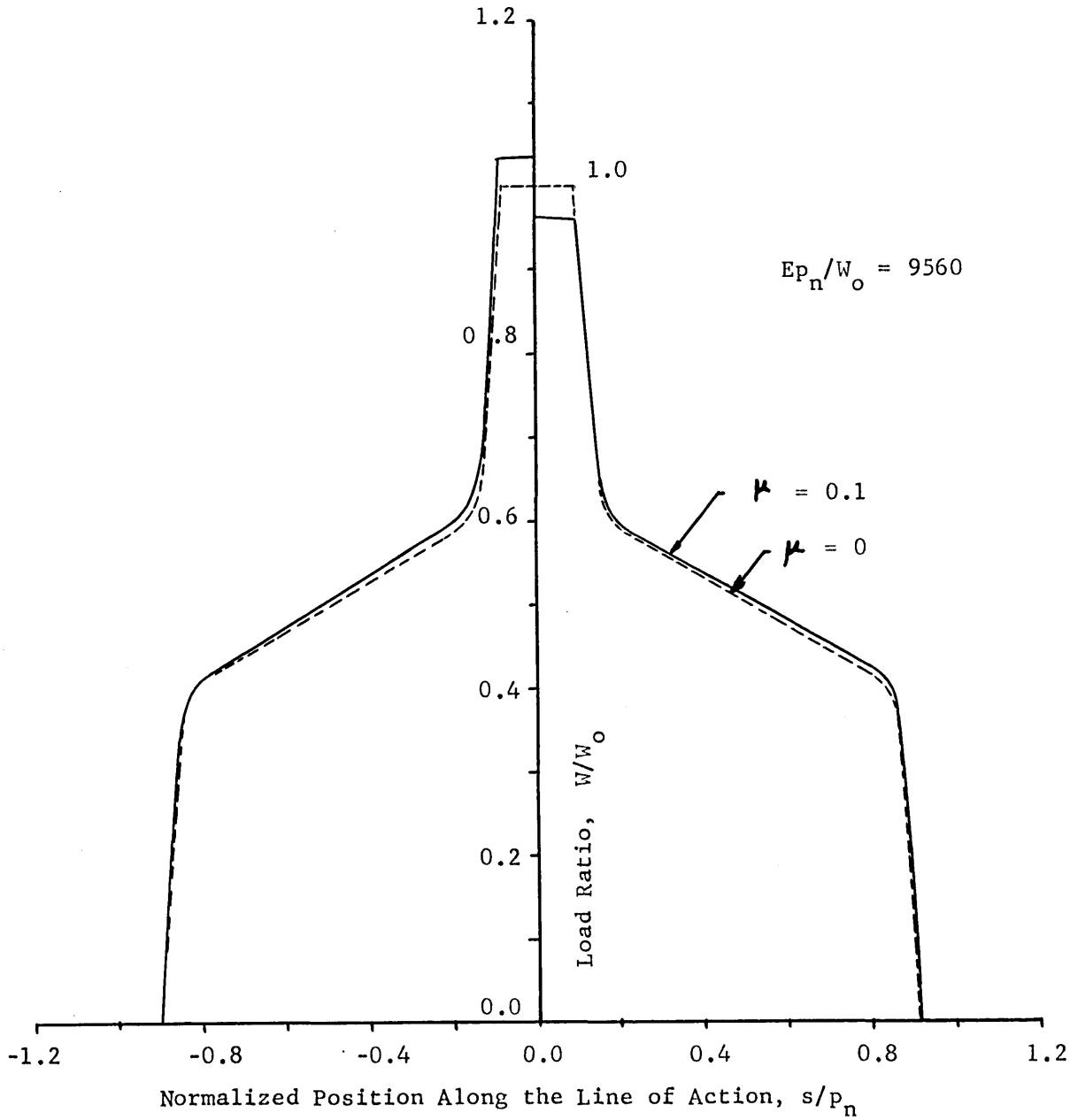

Fig. 31. The Effect of Static Friction on the Static Load Cycle.

2. When one pair of teeth is in contact, the following simplified version of Eq. (2.57) is employed.

$$\frac{W}{W_b} = 1 + \mu Z_b \tan \theta \tag{2.59}$$

11. Generalized Model for Gear Action Under Static Conditions

The developments made in the preceding paragraphs can be incorporated into the generalized model shown in Fig. 32. This model refers to the gear system defined in Fig. 19b, and includes manufactured errors and friction. The manufactured errors generally are functions of position along the line of action, and consequently e_a, e_b, and e_c shown in the model must be varied as the "cam" moves along the line of action. The tooth-pair compliances also are varied as a function of cam position (s/p_n) to correspond with the proper tooth-pair compliance curves as was shown in Fig. 14a and b. Frictional effects are accounted for by summing tooth-spring forces according to Eq. (2.57) rather than Eq. (2.39). However, the effects of static friction can be approximated sufficiently well for most practical purposes by neglecting the friction forces except when only one pair of teeth is in contact. During single-tooth-pair contact, the load on that tooth-pair is given by Eq. (2.59), and during multiple-tooth-pair contact, all tooth-spring forces are summed according to Eq. (2.39).

In all cases, the no-load separation curves for the cam surface are determined from Fig. 18 and the tooth-pair compliances are determined from Figs. 9, 11, and 12.

12. Static Stress Cycles for Test Gears

During the investigation reported in this thesis, measurements were made of nominal stress in two different pairs of test gears. The details of these measurements, including the methods employed to read nominal stress, the experimental technique, and the test set-up are discussed in Chapter 4.

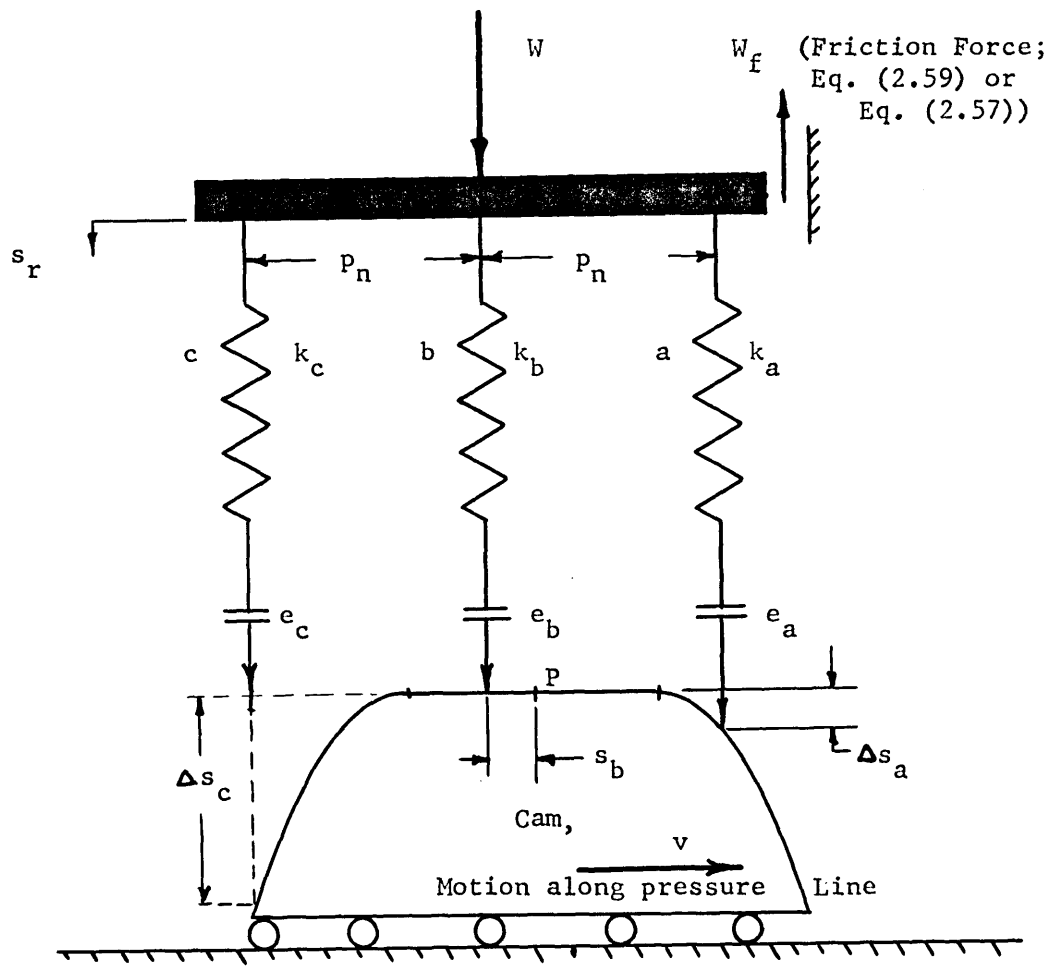

Fig. 32. Generalized Model of Gear Action; Static Conditions.

Theoretical stress cycles have been computed for each of the two sets of test gears employed. These predicted stress cycles are presented in this section, together with the corresponding measured curves.

12.1. Precision Test Gears

One pair of test gears was precision ground to an accuracy such that manufactured errors were less than about 2×10^{-4} inches. These gears were provided for use in this investigation through the cooperation of the Caterpillar Tractor Company and the Pratt and Whitney Tool Company. The characteristics of the gears are

Pinion pitch diameter	6.00 inches
Gear pitch diameter	9.00 inches
Diametral pitch	3 $(\text{inches})^{-1}$
Face width	0.75 inches
20° full-depth involutes	
S.A.E. 8622 steel, carburized and hardened to R_c 58-60.	

Figure 33 shows component and total compliances for three adjacent pairs of teeth (a, b, and c). Compliances for gross deformation, w_{27} and w_{18}, were obtained from Fig. 9. Because of the small numbers of teeth in these gears, the corrections Δw_H from Fig. 12, as well as the normal Hertzian compliance w_H from Fig. 11, were used in plotting the curve of total Hertzian compression shown in Fig. 33. Compliance curves for different tooth pairs are identical, but are separated along the line of action by one normal pitch to correspond with the physical spacing along the pressure line of the actual tooth-pair. The no-load separations were determined from Fig. 18. By referring to the model shown in Fig. 32 and applying Eqs. (2.39), (2.48), (2.52), and (2.59), the stress cycles for a tooth on the 27-tooth gear were calculated and are shown in Fig. 34. The load-parameter Ep_n/W_o was given the value 8190. The two stress cycles shown in Fig. 34 differ only by direction of rotation of the gears; that is, the directions of the friction forces are opposite in these two stress cycles.

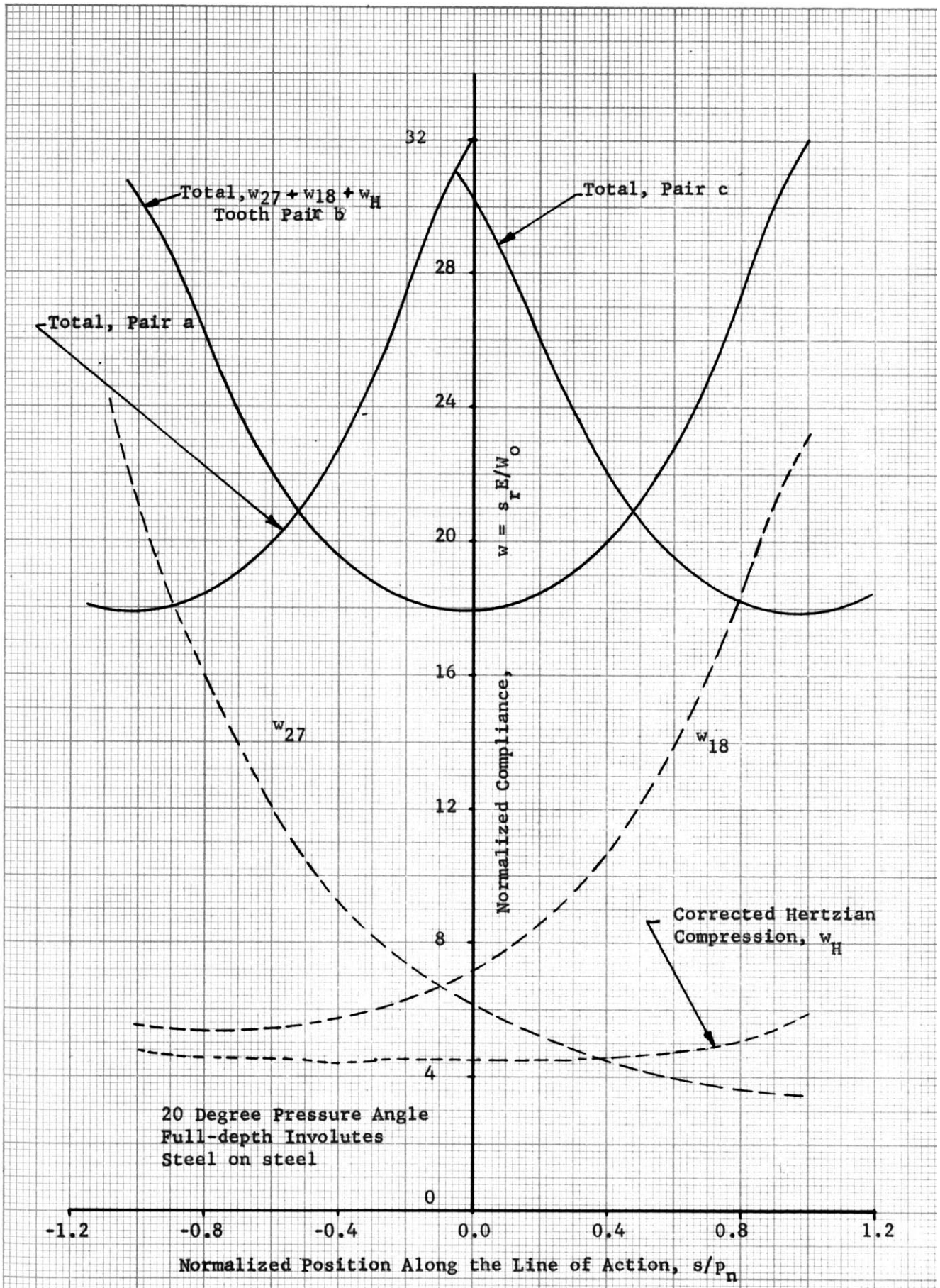

Fig. 33. Component and Total Compliances for a 27 Tooth Gear Mating With an 18 Tooth Pinion.

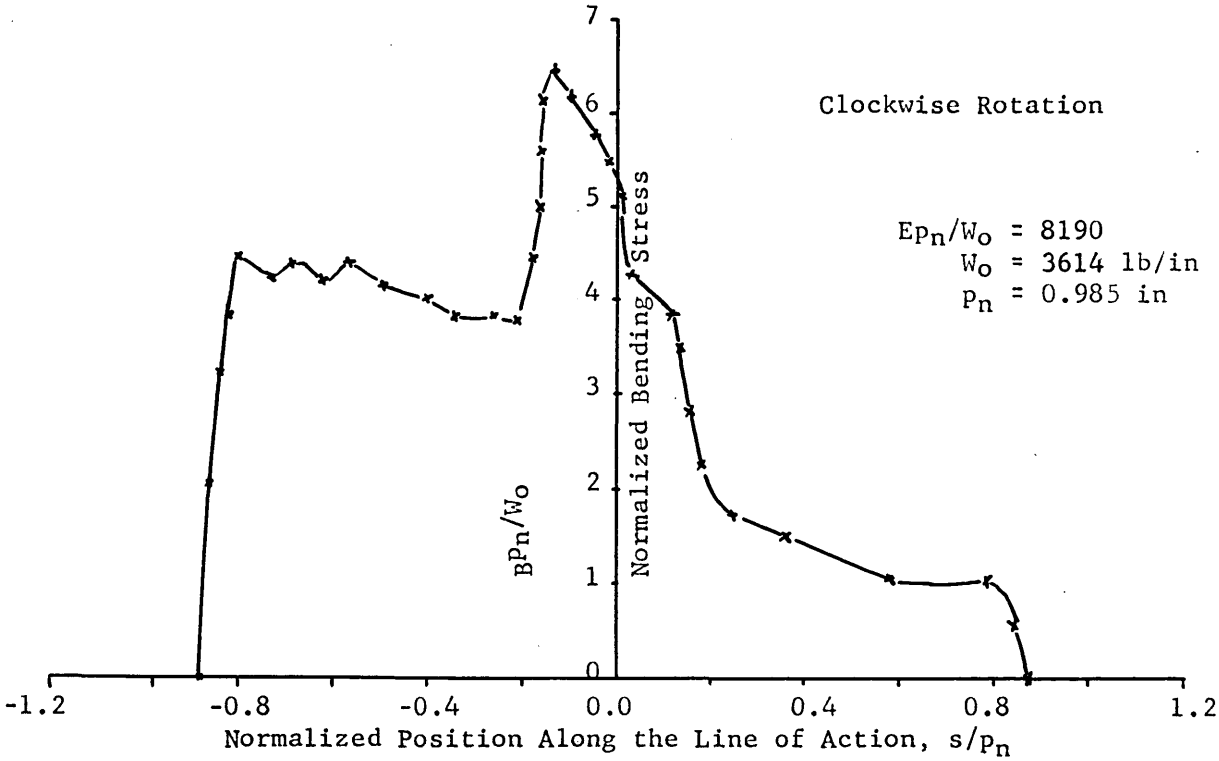

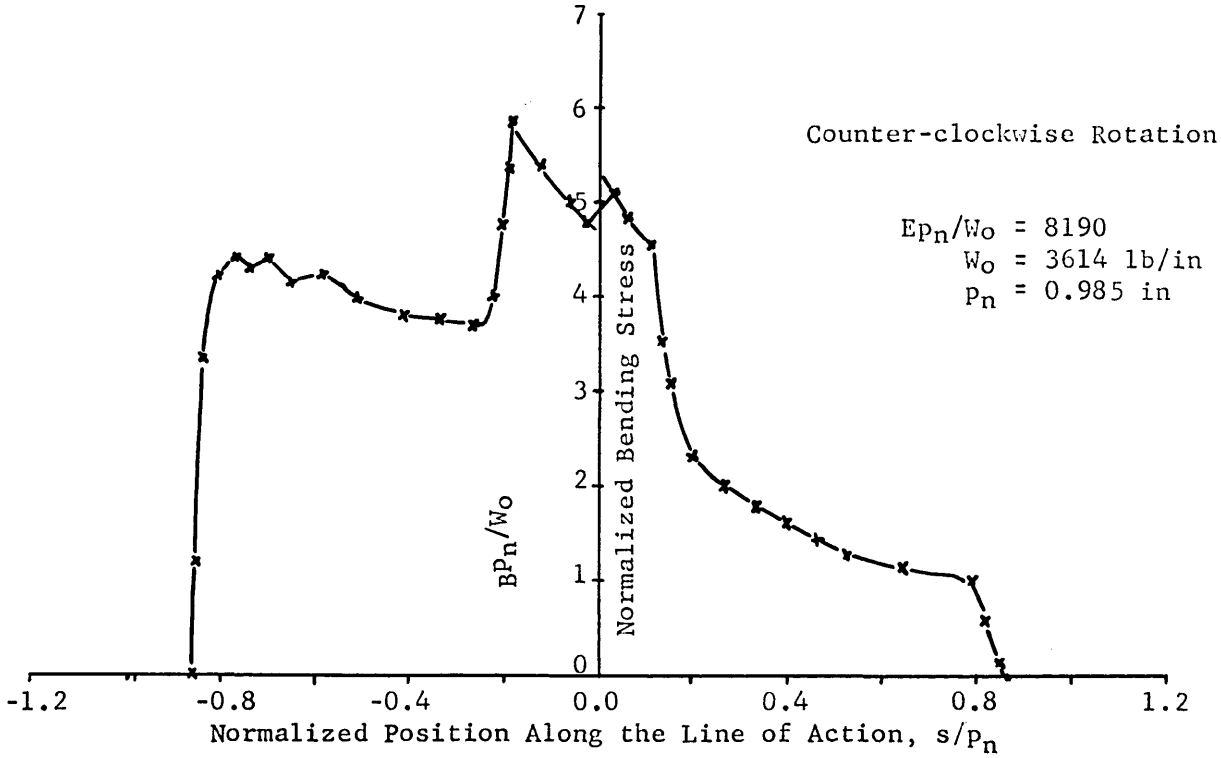

Fig.35, Overlay. Measured Nominal Static Bending Stress Cycles for Precision Test Gears. Measurements Taken Prior to Continuous Operation Under Load. For an 18 Tooth Pinion Mating With a 27 Tooth Gear. 20 Degree Pressure Angle, Full-depth Involutes.

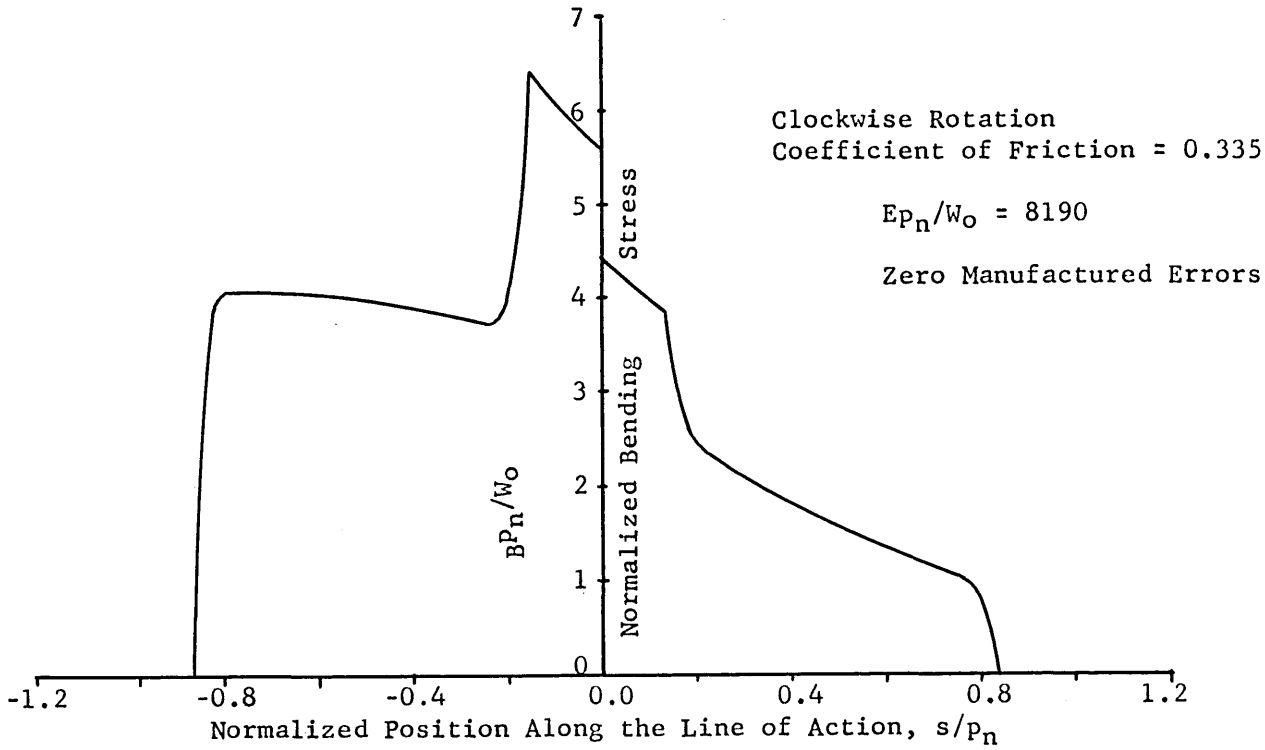

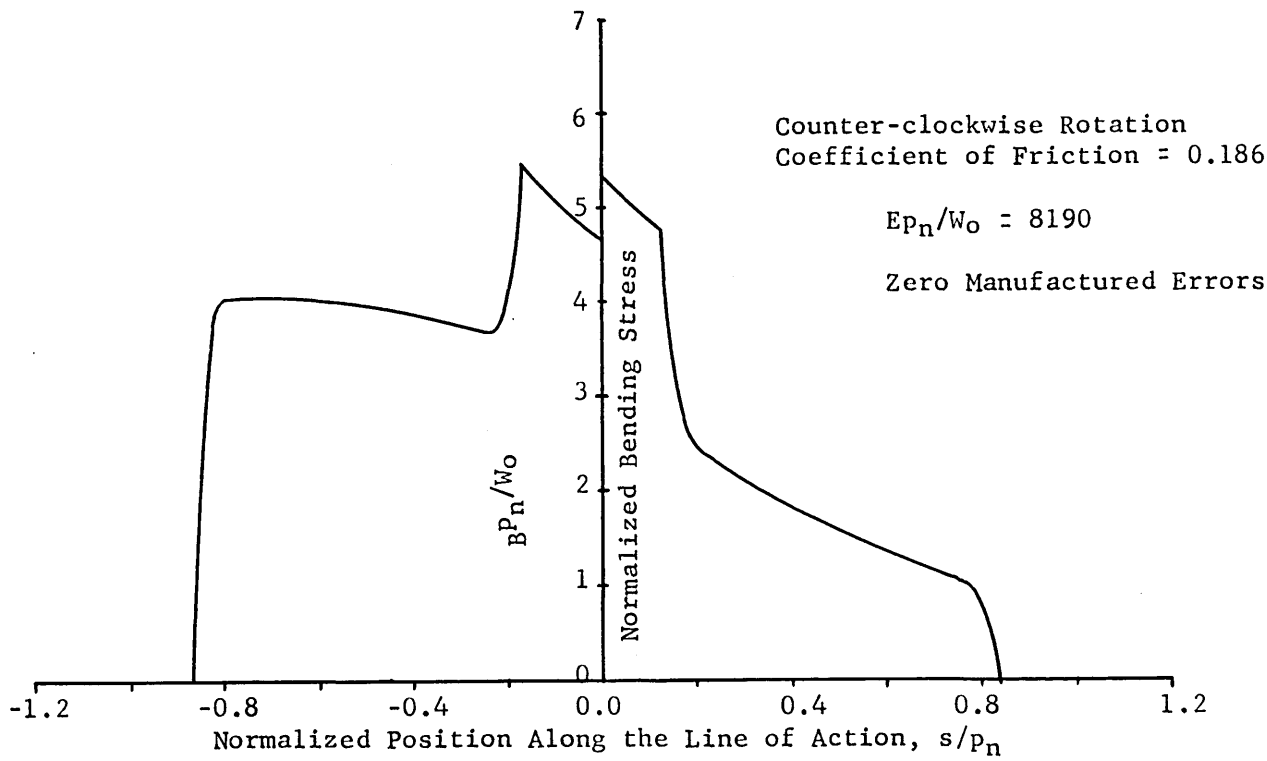

Fig.34, Calculated Nominal Static Bending Stress Cycles, Including Measured Static Friction. For an 18 Tooth Pinion Mating With a 27 Tooth Gear. 20 Degree Pressure Angle, Full-depth Involutes.

The coefficients of friction used in computing the stress cycles were obtained experimentally, according to Eq. (2.59), by measuring the magnitude of the observed change in load which occurs as the contact point between teeth passes through the pitch point. The manufactured errors were small enough to be neglected in these stress calculations.

Figure 35 is an overlay showing measured nominal stress cycles for the conditions assumed in computing the theoretical cycles of Fig. 34. The actual record from which Fig. 35 is taken is reproduced in Fig. 36a. Figure 36b shows the static stress cycles for a lower value of transmitted load. When the stress cycles for clockwise and for counter-clockwise rotation are superimposed, very little difference exists between the two curves except in the region of single-tooth-pair contact. This fact tends to substantiate the assumption made in connection with Eq. (2.59) that frictional effects are confined to the vicinity of the pitch point.

12.2. Production-Grade Gears

Static stress cycles also were measured for a pair of high-quality production-grade gears supplied by the Caterpillar Tractor Company. These gears were shaved; then carburized and hardened to R_c 58-60. The other characteristics of these test gears are:

Pinion pitch diameter	3.00 inches
Gear pitch diameter	9.00 inches
Diametral pitch	4 $(\text{inches})^{-1}$
Face width	0.50 inches
Pinion addendum	0.288 inches
Gear addendum	0.213 inches

Figure 37 shows records for four measured static stress cycles for the gears just described. Figure 38 shows theoretical stress cycles for the same gears, with a transmitted load of 4420 lbs/in. or a load-variable Ep_n/W_o of 5000. The solid curves in Fig. 38 give stress cycles computed without considering manufactured errors. The dash-dot curves include the influence of errors measured in the test gears before the gears were operated under load. Figure 39 is an overlay

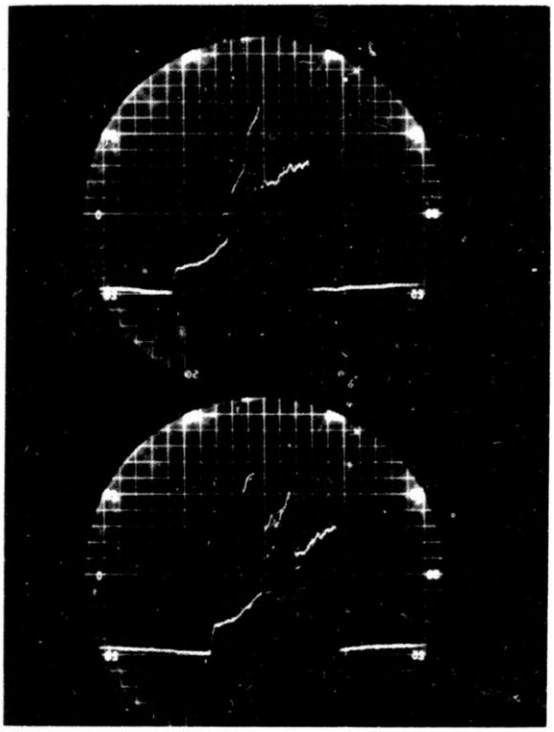

Counter-clockwise Rot.; Clockwise Rotation

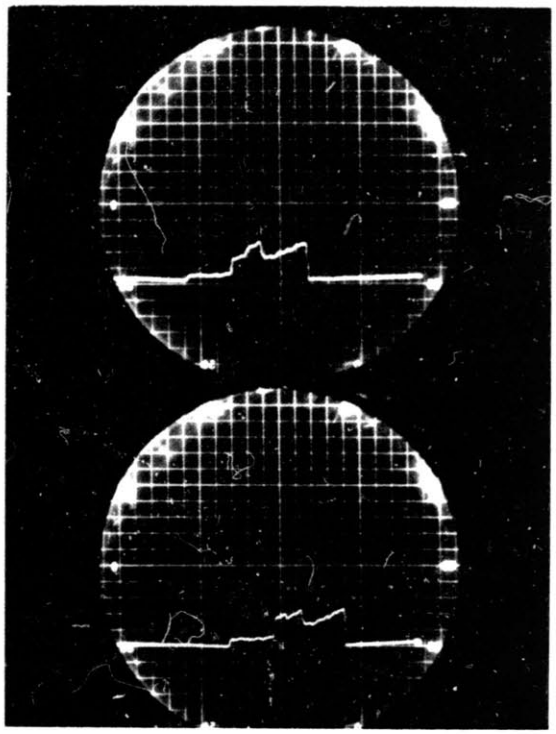

a) Transmitted Load = 3614 lbs./in. b) Transmitted Load = 809 lbs./in.

Fig. 36, a and b. Experimental Static Stress Cycles for Master Test Gears; for Two Values of Transmitted Load, and Clockwise and Counter-clockwise Directions of Rotation.

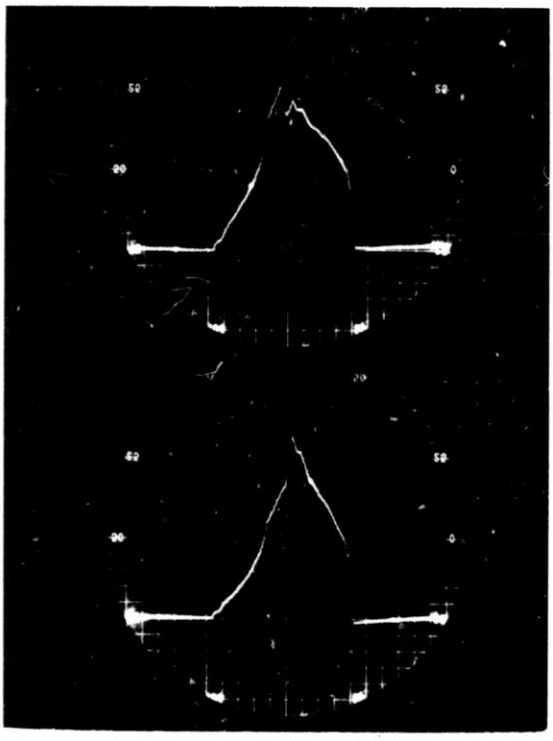

Clockwise Rotation; Counter-clockwise Rot.

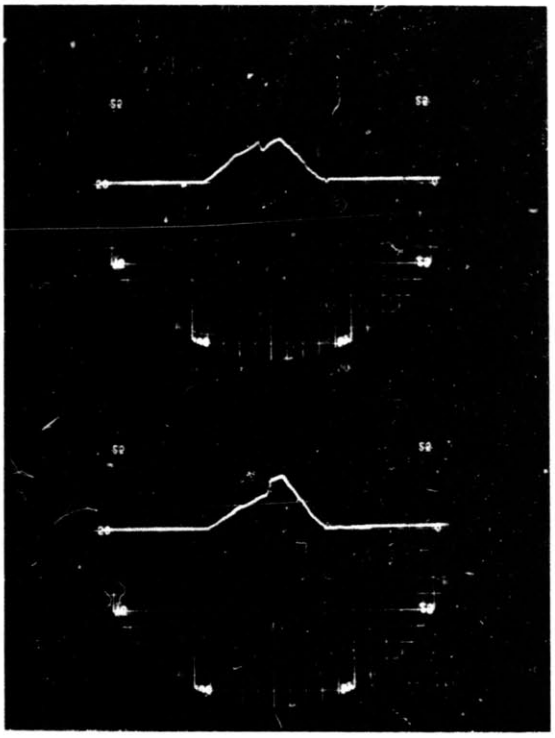

a) Trandmitted Load = 4420 lbs./in. b) Transmitted Load = 1380 lbs./in.

Fig. 37, a and b. Experimental Static Stress Cycles for Production-Grade Test Gears.

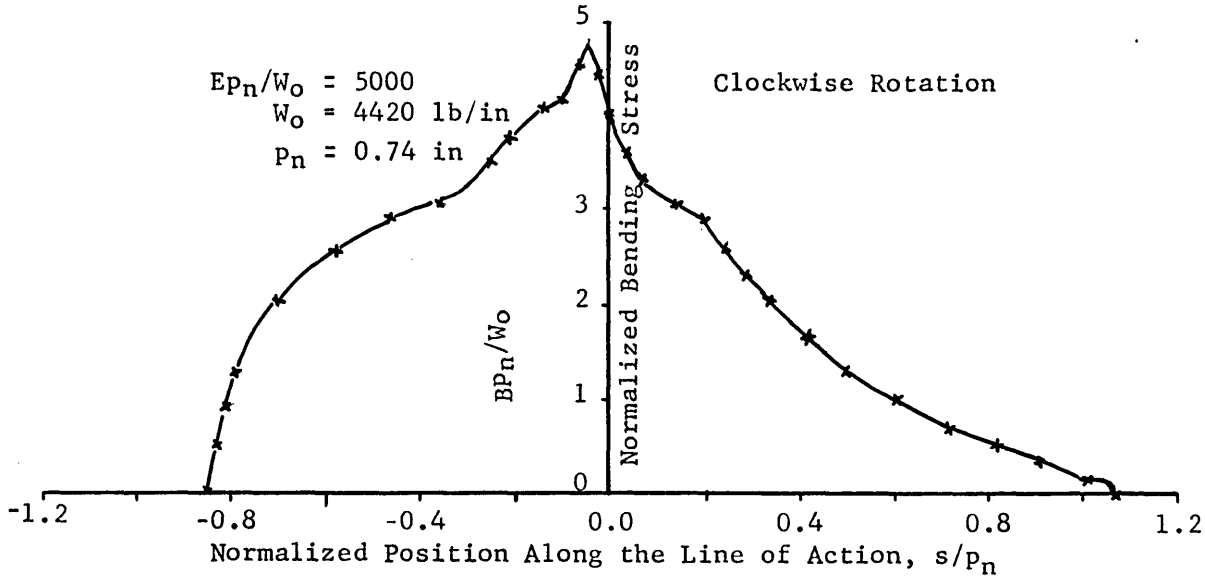

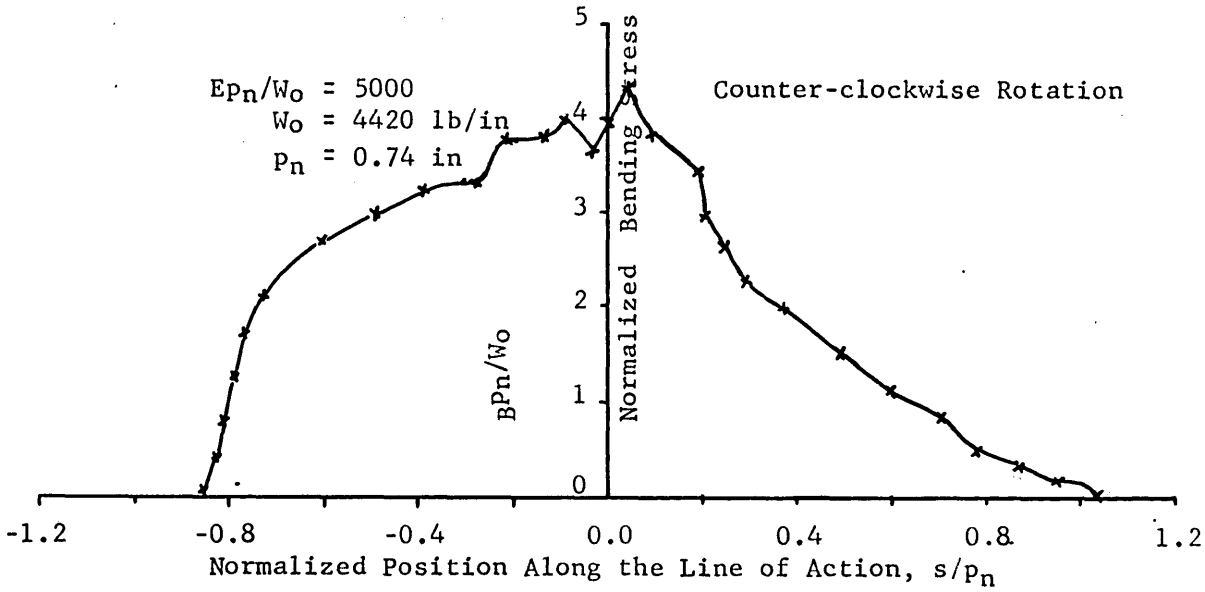

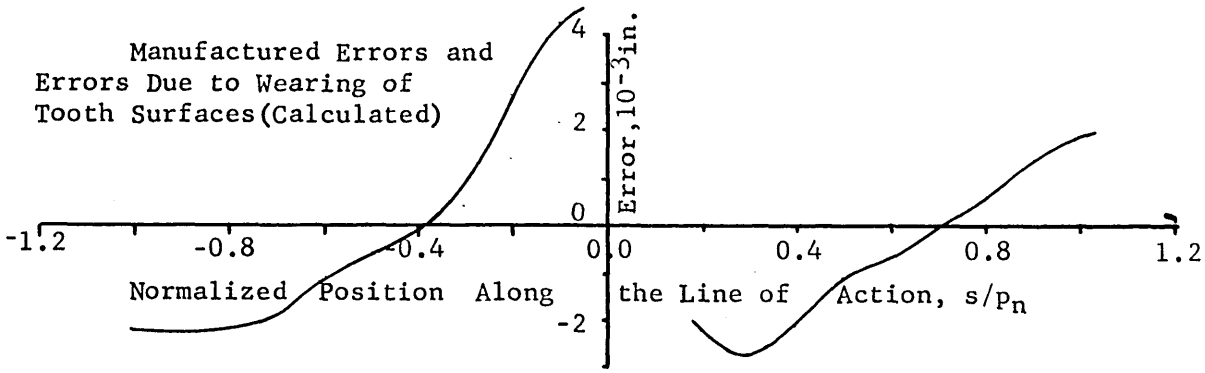

Fig.39, Overlay, Measured Nominal Static Bending Stress Cycles for Caterpillar Tractor Company 4X5422, 4X5421 Test Gears. Stress Measurements Taken After Five Hours Operation Under Load. For a 24 Tooth Pinion Mating With a 36 Tooth Gear.

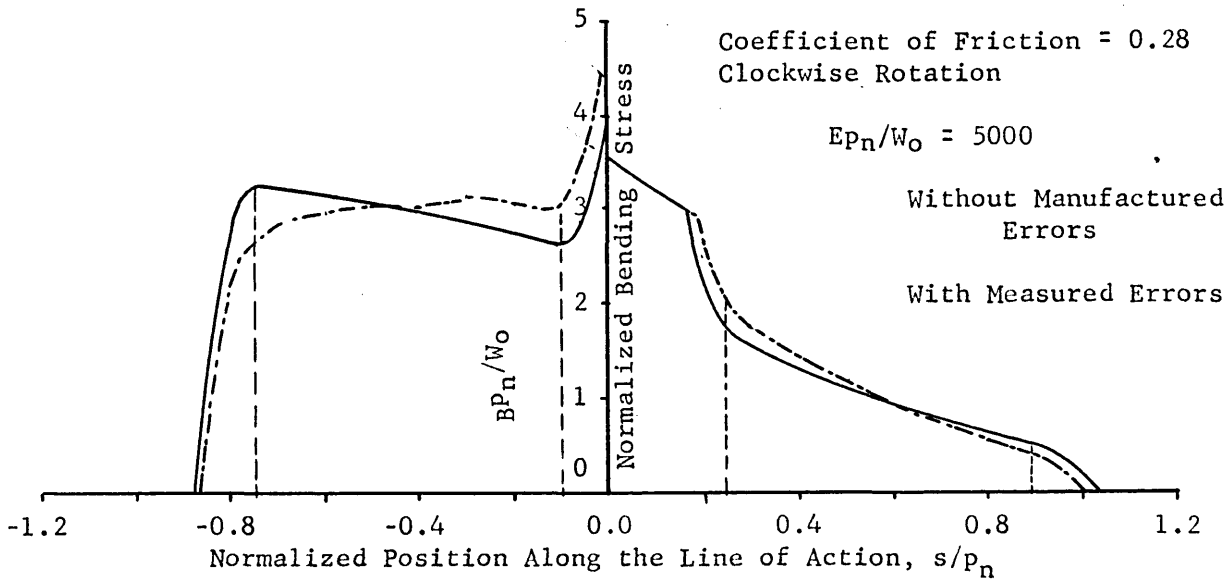

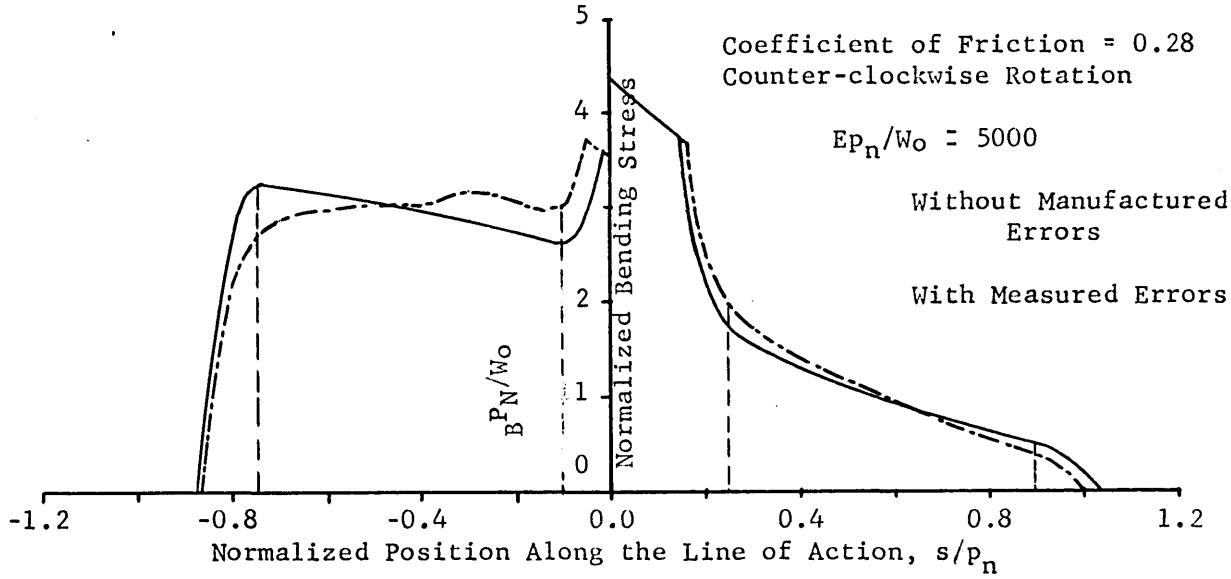

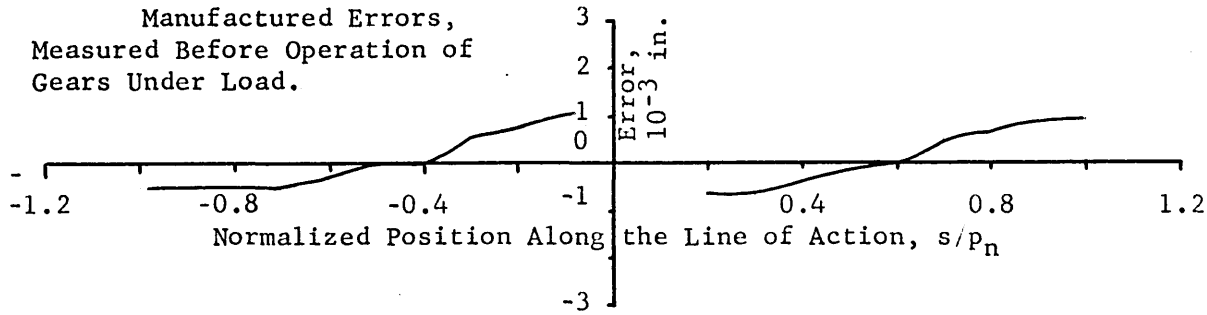

Fig.38, Calculated Nominal Static Bending Stress Cycles, Including Friction and Manufactured Errors. Manufactured Errors Measured in Caterpillar Tractor Company 4X5422,4X5421 Test Gears Before Operation of Gears Under Load. For a 24 Tooth Pinion Mating With a 36 Tooth Gear.

showing the measured static stress cycles corresponding to the calculated curves of Fig. 38. Also shown in Fig. 39 are the calculated errors that would cause the theoretical load cycles to coincide substantially with the measured load cycles. The measured load cycles were obtained after the test gears had been run for several hours under load. No stress measurements for the gears prior to running under load are available. Wear of the gear teeth in the direction indicated by Fig. 39 is observable, but no quantitative measurements of these errors are available at the time of writing of this thesis. Attempts to obtain approximate measurements with a dial indicator were quite unsuccessful, and are considered unreliable; however, they indicated increases of error of about 2×10^{-3} inches near the tip of gear and of about $x \times 10^{-3}$ inches near the root of the gear. No wear was evident on the pinion. These errors are of the order of magnitude necessary to account for the discrepancy between the curves of Fig. 38 and Fig. 39.

13. Summary

A method has been developed in this chapter for predicting the load, stress, and deflection cycles that the teeth of a given gear, real or proposed, will experience during static or low-speed operation. All the factors that appear to influence the nature of these cycles have been included in the analysis and are incorporated in the suggested calculation procedures. Many important quantities which involve tedious calculation have been tabulated or presented in the form of curves to facilitate construction of load, stress, or deflection cycles in connection with future gear designs.

Predicted stress cycles were found to show excellent agreement with measured stress cycles obtained by this author and by Rettig of Germany (Ref. 49).

A conceptual model (Fig. 32) is presented to aid in visualizing the load transfer processes involved, and to aid in setting up the load and deflection equations for a particular gear system.

CHAPTER 3. ANALYSIS OF DYNAMIC LOAD, STRESS, AND DEFLECTION CYCLES IN SPUR-GEAR SYSTEMS

1. Objective

In Chapter 2, a comprehensive study of the load, stress, and deflections that occur in gear systems during static or low-speed operation was made. Chapter 3 is concerned with the behavior of gear-tooth loads and stresses under conditions of dynamic or high-speed operation in the presence of appreciable rotating inertia.

The objectives of this chapter are to present general equations for gear-system dynamics, and to work out useful solutions to simplified versions of these equations which can be used in connection with gear design. However, the results presented in this chapter do not, and are not intended to constitute a complete solution of the gear dynamics problem. The intent is to point out and study, in at least a qualitative way, all of the physical phenomena that can affect dynamic loads in gearing. Simplified solutions presented here then can be compared with experimental results to determine the relative importance of the various system parameters and to suggest the most fruitful avenues for further investigations.

2. General Equations for Gear-System Dynamics

Figure 30 shows free-body diagrams for a pair of spur gears. The steady-state or statics equations already have been written for this system (Eqs. (2.55) and (2.56). These equations can be modified to include the inertias J_1 and J_2 of the two gears, and any viscous-damping effects B_1 and B_2 which may be present due to the action of a lubricant film between mating teeth or in the main support bearings for the gears. When Eqs. (2.55) and (2.56) are rewritten, Newton's law of motion for each gear shown in Fig. 30 can be expressed in the following way:

$$\frac{\tau_1}{R_{B1}} = W_a + W_b + \mu z_a W_a \left[\tan\theta - \frac{s_a}{R_{B1}}\right] + \mu z_b W_b \left[\tan\theta - \frac{s_b}{R_{B1}}\right] - \frac{J_1}{R_{B1}}\ddot{\psi}_1 - \frac{B_1}{R_{B1}}\dot{\psi} \tag{3.1}$$

$$\frac{\tau_2}{R_{B2}} = W_a + W_b + \mu z_a W_a \left[\tan\theta + \frac{s_a}{R_{B2}}\right] + \mu z_b W_b \left[\tan\theta + \frac{s_b}{R_{B2}}\right] + \frac{J_2}{R_{B2}}\ddot{\psi}_2 + \frac{B_2}{R_{B2}}\dot{\psi}_2 \tag{3.2}$$

where $\dot{\psi}$ and $\ddot{\psi}$ refer to angular velocity and angular acceleration, respectively, and other symbols are as defined in Chapter 2.

If the following quantities are defined,

$$W = \frac{\tau}{R_B} \quad \text{(effective load at the pressure line)} \tag{3.3}$$

$$m = \frac{J}{R_B^{\,2}} \quad \text{(effective mass at the pressure line)} \tag{3.4}$$

$$b = \frac{B}{R_B^{\,2}} \quad \text{(effective damping at the pressure line)} \tag{3.5}$$

and the relation $s = R_B\psi$ is recalled, Eqs. (3.1) and (3.2) can be written in the form

$$W_1 = W_a + W_b + \mu z_a W_a \left[\tan\theta - \frac{s_a}{R_{B1}}\right] + \mu z_b W_b \left[\tan\theta - \frac{s_b}{R_{B1}}\right] - m_1\ddot{s}_1 - b_1\dot{s}_1 \tag{3.6}$$

$$W_2 = W_a + W_b + \mu z_a W_a \left[\tan\theta + \frac{s_b}{R_{B2}}\right] + \mu z_b W_b \left[\tan\theta + \frac{s_b}{R_{B2}}\right] + m_2\ddot{s}_2 + b_2\dot{s}_2 \tag{3.7}$$

where s_a and s_b differ by one normal pitch.

The tooth loads W_a and W_b can be expressed in terms of known manufactured errors, tooth-pair compliances, and no-load separations, as described in Chapter 2. These equations assume several different forms similar to Eqs. (2.50) and (2.51), depending upon the phase of engagement (s/p_n), and can be established from the generalized model shown in Fig. 32. Therefore

$$W_a = f_1\left(w_a, w_b, \frac{s}{p_n}, e_t, \Delta s, s_r \text{ or } (s_2 - s_1)\right) \tag{3.8}$$

$$W_b = f_2\left(w_a, w_b, \frac{s}{p_n}, e_t, \Delta s, s_r \text{ or } (s_2 - s_1)\right) \tag{3.9}$$

For any known or assumed variation of the input and output torques, given by W_1 and W_2, Eqs. (3.6) to (3.9) can be solved for the unknown quantities W_a, W_b, s_1 and s_2, subject to prescribed initial conditions. It is apparent from the form of Eqs. (3.6) and (3.7) that these two equations cannot be combined in any simple way that will eliminate altogether the absolute displacements s_1 and s_2. Therefore, no simple, relative-motion model can describe the gear-dynamics problem completely.

The numerical, step-by-step solution of Eqs. (3.6) to (3.9), although possible, would be very time consuming and the results obtained would be complicated functions of a large number of variables. Such information would be difficult to interpret and probably would be useless for practical design purposes. As a result, a simplified approach to the problem is almost mandatory.

3. Simplified Equations for Gear-System Dynamics

In order to simplify the general dynamic equations presented in the preceding paragraph, the following assumptions are made:

1. Static friction is negligible during dynamic or high-speed operation.
2. The input and output torques τ_1 and τ_2 are constant and equal to their respective average values, that is,

$$W_1 = W_2 = W \tag{3.10}$$

3. The viscous damping effect can be represented by a force proportional to the relative velocities of the two gears along the pressure line.

$$W_f = b(\dot{s}_2 - \dot{s}_1) = b\,\dot{s}_r \tag{3.11}$$

Then Eqs. (3.6) and (3.7) take the form

$$W = W_a + W_b - m_1\ddot{s}_1 + W_f \tag{3.12}$$

$$W = W_a + W_b + m_2\ddot{s}_2 + W_f \tag{3.13}$$

When Eq. (3.12) is divided by m_1 and Eq. (3.13) is divided by m_2 and the results are added, the following equation for the relative displacement s_r is obtained

$$W\left[\frac{1}{m_1} + \frac{1}{m_2}\right] = (W_a + W_b + W_f)\left[\frac{1}{m_1} + \frac{1}{m_2}\right] + \ddot{s}_r \tag{3.14}$$

A total effective mass at the pressure line can be defined as

$$m = \frac{m_1\,m_2}{m_1 + m_2} = \frac{1}{\dfrac{R_{B1}^{\;2}}{J_1} + \dfrac{R_{B2}^{\;2}}{J_2}} \tag{3.15}$$

When Eqs. (3.11), (3.14) and (3.15) are combined, the final dynamic equation takes the simple form

$$m\ddot{s}_r + b\dot{s}_r + W_a + W_b = W \tag{3.16}$$

The relationship given by Eq. (3.16) can be visualized by a dynamic model similar to the model shown in Fig. 32. It is easily verified that the model given in Fig. 40 leads to the equation of motion expressed by Eq. (3.16)

4. Single-Engagement Model of Dynamic Gear Action

In many cases the influence of gear error is most predominant during transfer of load from one tooth pair to another. When a pair of teeth enters or leaves the gear mesh, the current error and the no-load separation combine to produce a disturbance in the equivalent spring-mass system of Fig. 40. The oscillations in relative displacement resulting from this disturbance will produce dynamic loads in the tooth-pair springs which will exceed the average or static loads that exist under low-speed conditions. If the oscillations thus induced die out, owing to the action of viscous or static friction, before the next disturbance or load transfer occurrs, then the maximum dynamic tooth load can be determined by investigating the behavior of the spring-mass system only in the neighborhood of the points of load transfer. As mentioned in Chapter 1, essentially all published analyses of dynamic loads in gearing have approached the problem in this manner.

The analysis presented in this paragraph is essentially an extension of the work of Reswick[45].

The simplified dynamic equation, Eq. (3.16) is employed in the following development, and in addition, the following assumptions are made.

1. Viscous and static friction are negligible during and immediately after load transfer.
2. Oscillations induced by one load transfer die out before another load transfer occurs.
3. The tooth-pair flexibilities are essentially constant during the load-transfer process.

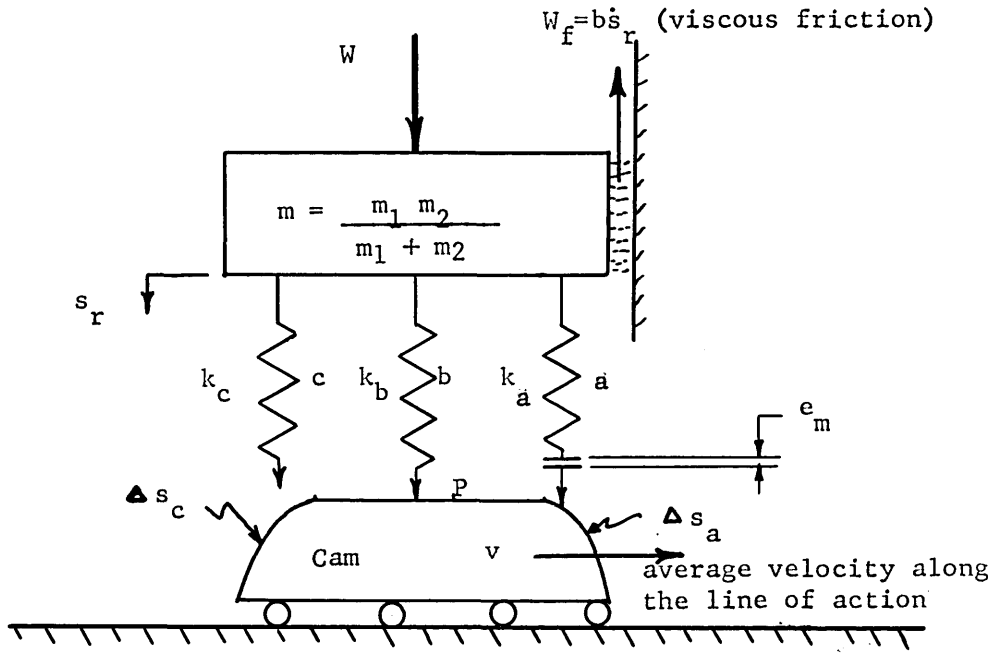

Fig. 40. Simplified Model for Study of Gear-System Dynamics.

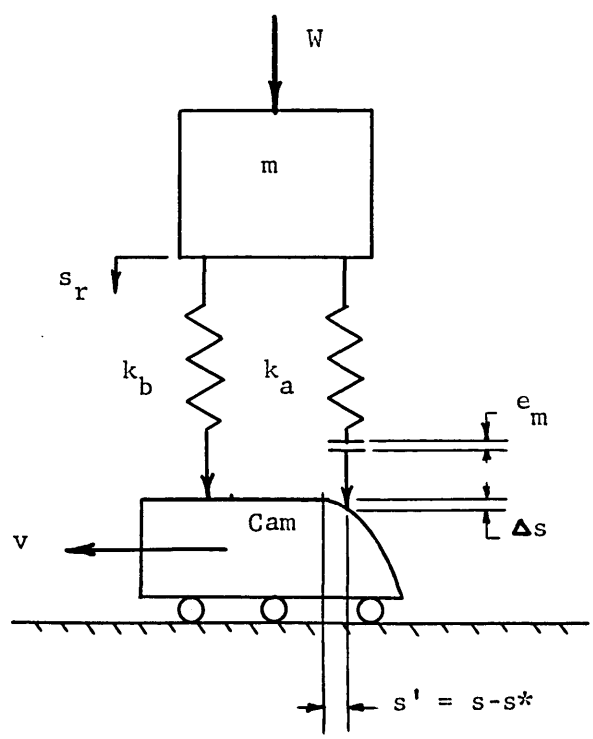

Fig. 41. Simplified Model for Load Transfer from Two Pairs of Teeth to One Pair of Teeth in Heavily-Loaded Gears.

4. The total effective error is essentially constant during the load transfer.
5. The motion of the no-load separation "cam" along the line of action occurs at the average velocity of the gears, referred to the line of action. That is, if ω is the average angular velocity, and v is the average linear velocity along the pressure-line,

$$v = \omega R_B \tag{3.17}$$

In setting up the dynamic model for a single load transfer, two situations must be distinguished, as pointed out by Reswick. Figure 40 shows the dynamic model for the conditions when tooth-pair a is engaging. Suppose for the moment that this engagement is taking place very slowly, and that tooth-pair a has a manufactured error which makes this tooth-pair longer than tooth-pair b by an amount e_m. If the deflection of tooth pair a due to the load W is less than e_m, then tooth-pair a will carry all of the load after engagement has occurred and pair b will be entirely out of contact. Conversely, if e_m is less than the deflection of tooth-pair a due to the transmitted load, pairs a and b both will be in contact after engagement has occurred and the transmitted load will be shared between them. On this basis, Reswick has postulated two modes of dynamic operation according to the following criteria.

1. Heavily-loaded Gears: if s_{rt} is defined as the static deflection of the engaging pair of teeth due to the transmitted load, a pair of gears is considered to be "heavily-loaded" if

$$e_m \leqq s_{rt} \tag{3.18}$$

2. Lightly-loaded Gears: if the manufactured error is large for the engaging tooth, single tooth-pair action will predominate during load transfer. Thus a pair of gears is said to be lightly-loaded if

$$e_m >> s_{rt} \tag{3.19}$$

These two regimes of operation will now be investigated.

4.1. Heavily-Loaded Gears

Reswick has analyzed the heavily-loaded gear behavior for the case when load is transferred from one pair of teeth to two pairs of teeth; that is, for the situation shown in Fig. 40. The reverse process, that of load transfer from two pairs of teeth to one pair of teeth was not investigated. Since this case is the most severe one, as far as dynamic loads are concerned, it will be analyzed in this section.

Figure 41 shows the dynamic model for load transfer from two pairs of teeth to one pair of teeth. The gears are heavily-loaded, so Eq. (3.18) applies.

The tooth-spring loads W_a and W_b can be expressed by inspection of Fig. 41.

$$W_b = k_b s_r \tag{3.20}$$

$$W_a = k_a (s_r - \Delta s + e_m) \tag{3.21}$$

For simplicity, it is assumed now that the spring constants k_a and k_b are equal.

$$k_a \approx k_b = k \tag{3.22}$$

Combination of Eqs. (3.22), (3.21), (3.20), and (3.16) gives

$$m\ddot{s}_r + 2ks_r = k(\Delta s - e_m) + W \tag{3.23}$$

According to Eq. (3.20), the static deflection s_{rt} of a single pair of teeth can be expressed as

$$s_{rt} = \frac{W}{k} \tag{3.24}$$

If the substitution

$$s' = s - s^* \tag{3.25}$$

is made, the no-load separation from Eq. (2.36) can be written

$$\Delta s = c s'^2 \tag{3.26}$$

Since, according to Eqs. (3.17) and (3.25),

$$v = \omega R_B = \dot{s} = \dot{s}' = \text{constant} \tag{3.27}$$

equation (3.26) can be written

$$\Delta s = c\, v^2\, t^2 \tag{3.28}$$

where t is time in seconds, v is the average circumferential velocity of the base circle in in./sec., c is a so-called "cam-constant", in in.$^{-1}$, and Δs is the no-load separation, in inches.

Define the quantity

$$\omega_n = \sqrt{\frac{k}{m}} \tag{3.29}$$

This quantity is the frequency of free vibration of the effective mass on one tooth-pair spring. When Eqs. (3.29), (3.28), (3.24), and (3.23) are combined, the differential equation for relative deflection s_r becomes

$$\frac{\ddot{s}_r}{\omega_n^2} + 2\, s_r = c\, v^2\, t^2 - e_m + s_{rt} \tag{3.30}$$

Let

$$e = e_m + s_{rt} \tag{3.31}$$

The magnitude of e determines the value of Δs at which the disengaging tooth-pair a would leave the cam surface if the cam were withdrawn very slowly. It is a measure of the amount of disturbance caused by the disengagment, and is termed the "combined error"; the manufactured error plus the static deflection due to load of a single pair of teeth.

Let

$$\beta = \frac{v}{\omega_n} \sqrt{\frac{c}{e}} \tag{3.32}$$

The quantity β is proportional to the ratio of the natural period of the spring-mass system to the time required to withdraw the cam if no oscillations took place during withdrawal. Thus e measured the magnitude, and β the rate of the load-transfer disturbance. When Eqs. (3.32), (3.31), (3.30), and (3.29) are combined,

$$\frac{\ddot{s}_r}{s_{rt}} \frac{1}{\omega_n^2} + 2 \frac{s_r}{s_{rt}} = \frac{e(\beta^2 \omega_n^2 t^2)}{s_{rt}} - \frac{e_m}{s_{rt}} + 1; \qquad t < t_1 \tag{3.33}$$

Equation (3.33) is valid as long as two pairs of teeth are in engagement. The time when double-tooth-pair contact ceases is designated by $t = t_1$. Since only compressive forces can occur between gear tooth surfaces, the force in the disengaging tooth a cannot become negative. Thus, from Eq. (3.21) disengagement occurs when

$$s_r = \Delta s - e_m, \qquad t = t_1 \tag{3.34}$$

or, from Eqs. (3.34), (3.29), and (3.28)

$$\frac{\ddot{s}_r}{s_{rt}} = \frac{cv^2}{\omega_n^2} \frac{(\omega_n^2 t_1^2)}{s_{rt}} - \frac{e_m}{s_{rt}} \tag{3.35}$$

When Eqs. (3.35) and (3.32) are combined, the criterion for disengagement becomes

$$\frac{s_r}{s_{rt}} = \frac{e\beta^2 \omega_n^2 t_1^2}{s_{rt}} - \frac{e_m}{s_{rt}} \tag{3.36}$$

After disengagement has occurred, $t > t_1$, Eq. (3.33) no longer describes the motion, and must be replaced by the equation for the vibration of the mass on one tooth spring

$$\frac{\ddot{s}_r}{s_{rt}} \frac{1}{\omega_n^2} + \frac{s_r}{s_{rt}} = 1; \qquad t > t_1 \tag{3.37}$$

The solution of Eqs. (3.33) and (3.37) for the static or zero-mass case ($\beta = 0$) is obtained by setting $\ddot{s}_r = 0$ in these equations. This solution is shown in Fig. 42 as a dashed line. In this case the disengagement of the cam occurs at point D, where the deflection s_r becomes equal to the static deflection s_{rt} of one pair of teeth. Also shown on Fig. 42 is the curve of $(\Delta s/s_{rt} - e_m/s_{rt})$ defined by Eq. (3.34). According to Eq. (3.34), disengagement occurs when this curve crosses the curve of s_r/s_{rt}. This situation occurs, for static operation, at point D in Fig. 42.

When the mass (m) is finite and $\beta > 0$, the detailed solutions of Eqs. (3.33) and (3.37) are required. According to assumption 2 of paragraph 4, the initial conditions for $t = 0$ to be used in Eq. (3.33) are

$$t = 0 \qquad s_r = \frac{s_{rt} - e_m}{2} \tag{3.38a}$$

$$\dot{s}_r = 0 \tag{3.38b}$$

The general solution of Eq. (3.33) consists of the homogeneous solution (with the right-hand side of the equation set equal to zero), plus any particular solution which satisfies the complete equation. This solution, subject to the prescribed initial conditions, Eq. (3.38), is

$$\frac{s_r}{s_{rt}} = \frac{1}{2} + \frac{1}{2} \frac{e}{s_{rt}} \left[\beta^2(\omega_n^2 t^2 + \cos\sqrt{2}\, \omega_n t - 1) - \frac{e_m}{e}\right]; \qquad t < t_1 \tag{3.39}$$

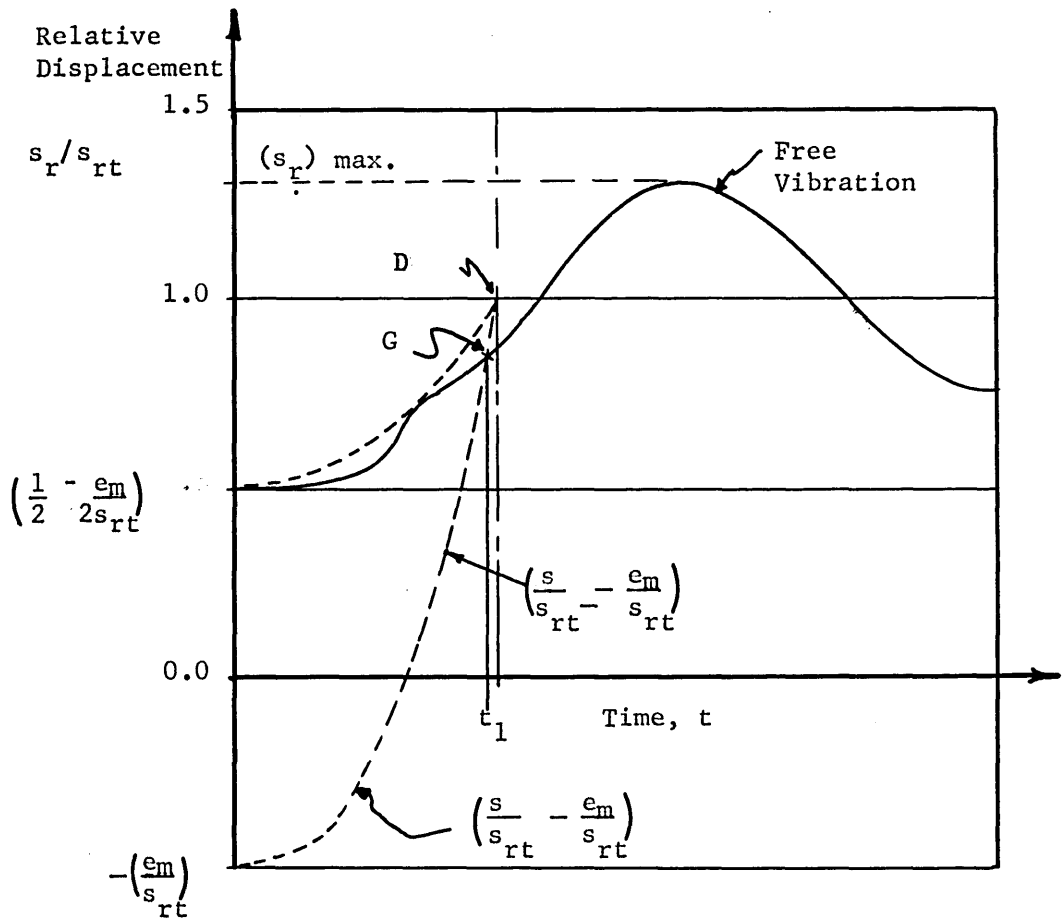

Fig. 42. Dynamic Relative Displacement in Heavily-Loaded Gears.

Equation (3.39) represents a forced oscillation of frequency $\sqrt{2}\,\omega_n = \sqrt{2k/m}$ which has the general shape shown in Fig. 42. This motion persists until $t = t_1$ when the curve of (s_r/s_{rt}) crosses the curve of $(\Delta s/s_{rt} - e_m/s_{rt})$; that is, point G in Fig. 42. The condition at $t = t_1$ can be expressed analytically be combining Eqs. (3.39) and (3.36)

$$\omega_n^2 t_1^2 - \cos\sqrt{2}\,\omega_n t_1 + 1 = \frac{1}{\beta^2} \tag{3.40}$$

For any value of β, Eq. (3.40) determines the value of $\omega_n t_1$ at which single tooth-pair action commences.

In order to determine the motion for $t > t_1$, Eq. (3.37) must be solved for the initial conditions prescribed by the solution for $t < t_1$, Eq. (3.39), at $t = t_1$; that is, the displacement s_r and the velocity $\dot{s}_r$ must be continuous functions of time at $t = t_1$.

According to Eq. (3.39), the conditions at $t = t_1$ are

$$\left(\frac{s_r}{s_{rt}}\right)_{t_1} = \frac{1}{2} + \frac{e}{2s_{rt}}\left[\beta^2(\omega_n^2 t_1^2 + \cos\sqrt{2}\,\omega_n t_1 - 1) - \frac{e_m}{e}\right]$$

$$\left(\frac{\dot{s}_r}{s_{rt}}\right)_{t_1} = \frac{\omega_n e}{2\,s_{rt}}\left[\beta^2\,(2\omega_n t_1 - \sqrt{2}\,\sin\sqrt{2}\,\omega_n t_1)\right] \tag{3.41}$$

The solution of Eq. (3.37) for $t > t_1$ can be expressed in the form

$$\frac{s_r}{s_{rt}} = 1 + C_1 \sin\omega_n(t - t_1) + C_2 \cos\omega_n(t - t_1)\ ; \qquad t > t_1 \tag{3.42}$$

From Eq. (3.42) the displacement and velocity at $t = t_1$ are

$$\left(\frac{s_r}{s_{rt}}\right)_{t=t_1} = 1 + C_1$$

$$\left(\frac{\dot{s}_r}{s_{rt}}\right)_{t=t_1} = \omega_n C_2 \tag{3.43}$$

Equation (3.42) describes a free vibration of the system about $s_r/s_{rt} = 1$ as an average value, as shown on Fig. 42. Since only one pair of teeth is in contact for $t > t_1$, the maximum tooth load or dynamic load is determined directly from the maximum value of s_r according to Eq. (3.20). If W_d is the maximum dynamic load, a dynamic increment load W_i can be defined by the equation

$$W_d = W + W_i = k(s_r)_{max} \tag{3.44}$$

The maximum value of s_r for $t > t_1$ is obtained in terms of C_1 and C_2 from Eq. (3.42)

$$(s_r)_{max} = s_{rt}\left[1 + \sqrt{C_1^2 + C_2^2}\right] \tag{3.45}$$

When Eq. (3.45) is multiplied by the spring stiffness k and the result is compared with Eq. (3.44) the dynamic increment load is found to be

$$W_i = k\, s_{rt} \sqrt{C_1^2 + C_2^2} \tag{3.46}$$

The constants C_1 and C_2 are obtained by combining Eqs. (3.43), (3.41) and (3.31).

$$C_1 = \frac{e}{2s_{rt}} \left[\beta^2 (\omega_n{}^2 t_1{}^2 + \cos \sqrt{2}\, \omega_n t_1 - 1) - 1 \right]$$

$$C_2 = \frac{e}{2s_{rt}} \left[\beta^2 (2\omega_n t_1 - \sqrt{2}\, \sin\sqrt{2}\,\omega_n t_1) \right] \tag{3.47}$$

When Eqs. (3.47) and (3.46) are combined, the dynamic increment load is found to be

$$\frac{W_i}{ek} = f_1(\omega_n t_1, \beta) \tag{3.48}$$

Equations (3.48) and (3.40) are sufficient to determine the increment load W_i, for any given values of β and ek. However, owing to the transcendental nature of Eq. (3.40), this solution cannot be obtained in closed analytical form. Therefore, the increment load relationship is presented in the form of a chart, described by the functional relationship

$$\frac{W_i}{ek} = f_2(\beta) \tag{3.49}$$

The procedure for computing the curve of increment load is the following

1, Assume a value of $\omega_n t_1$

2. Compute β from Eq. (3.40)

3. Substitute these values of β and $\omega_n t_1$ into Eq. (3.47) and compute the values of $C_1 s_{rt}/e$ and $C_2 s_{rt}/e$

4. Compute W_i/ek from Eq. (3.46)

The increment load curve defined by Eq. (3.49) is given in graphical form in Fig. 43. The maximum dynamic load for transfer from two pairs of teeth to one pair of teeth can be computed from the curve given in Fig. 43 and the equation

$$W_d = W + \left(\frac{W_i}{ek}\right)\left(e_m + \frac{W}{k}\right)\kappa \tag{3.50}$$

where W is the average or static load, W_i/ek is the increment-load ratio from Fig. 43, e_m is the total manufactured error, and k is an average single-tooth-pair spring constant. These results apply as long as the manufactured error e_m is less than the static tooth deflection $s_{rt} = W/k$. The maximum dynamic load, as $\beta \to \infty$, according to these results, is

$$(W_d)_{max} = \frac{3}{2} W + \frac{e_m k}{2} \tag{3.51}$$

Values of tooth-pair spring stiffness can be obtained from Figs. 9, 11, and 12 of Chapter 2. For approximate calculations, Table 2 gives useful values of spring constant per unit of face width, as published by Buckingham[19].

TABLE 2

Approximate Values of Tooth-Pair Stiffness, Per Unit of Face Width, k/f, lbs./in.^{2}

Materials	20° Stub	20° Full Depth
Steel and steel	1.95×10^6	1.88×10^6
Steel and gray iron	1.34×10^6	1.29×10^6
Gray iron and gray iron	0.97×10^6	0.94×10^6

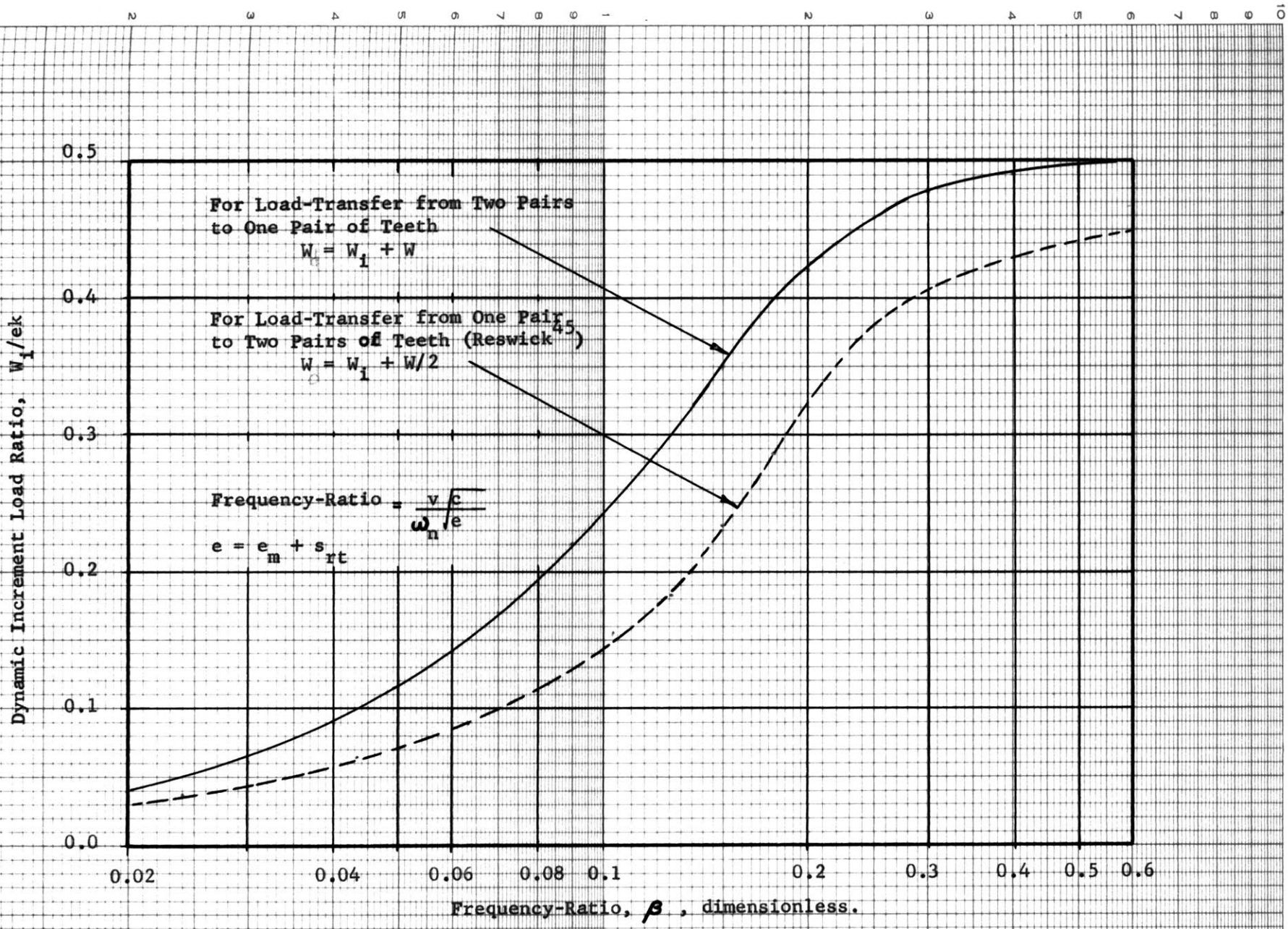

Fig. 43. Dynamic Increment-Load Ratio Versus Frequency Ratio, for Heavily-Loaded Gears. Single Load-Transfer Theory.

Reswick[45] has analyzed the load transfer from one pair of teeth to two pairs of teeth for heavily-loaded gears. For that case the dynamic load was found to be

$$W_d = \frac{W}{2} + \left(\frac{W_i'}{ek}\right) ek \tag{3.52}$$

where W_i'/ek is given by the dashed line in Fig. 43. For all values of β, the load given by Eq. (3.52) is less than the load given by Eq. (3.50). However, in the case of bending stress, the most severe condition sometimes occurs at load transfer from one to two pairs of teeth, because the load then acts at the tip of the tooth. The maximum dynamic bending stress therefore must be determined by considering both engagement and disengagement. The maximum dynamic load is evaluated for both conditions, then the stress for each case is computed by applying the appropriate Lewis form factor from Fig. 22 or from published tables[29].

In studying the transfer of load from two pairs of teeth to one pair of teeth, in this paragraph, the load transfer was represented by the parabolic "cam" defined in Chapter 2. As an actual pair of gears is operated under load, a certain amount of wear will occur, particularly at the tips of the teeth, and the actual "cam" will tend to become more gradual than the one defined by the no-load separation of perfect involutes. Consequently, use of the no-load separation data of Chapter 2 in computing the cam constant "c" probably will lead to conservative estimates of dynamic load. Buckingham has developed a relationship for such a cam constant, in connection with his theoretical dynamic load equations, Eq. (1.11). For 20° involutes,

$$c = 0.183\left(\frac{1}{R_{B1}} + \frac{1}{R_{B2}}\right) \text{ in}^{-1} \tag{3.53}$$

Essentially, if wear is important, the cam constant must be considered to be an empirical constant which is determinable from representative measurements of dynamic loads in actual gear systems. If wear does occur, however, the shape of the effective cam may no longer be parabloic. In order to evaluate the importance of cam shape, curves of dynamic increment load, similar to those shown in Fig. 43 were computed for the following cam shapes.

1. Cubic $\Delta s = e(\beta^3 \omega_n^3 t^3)$ (3.54)

2. Linear $\Delta s = e(\beta \omega_n t)$ (3.55)

3. Harmonic $\Delta s = e(1 - \cos \frac{\pi}{2} \beta \omega_n t)$ (3.56)

The increment load curves for all of these cam shapes are shown in Fig. 44. The parabolic cam shape results in predicted dynamic loads that lie near or above the loads predicted by all other cam shapes which were studied.

Figure 45 shows a qualitative picture of the dynamic load cycle that is predicted for a heavily-loaded gear. Oscillations induced by particular load transfers die out completely during the intervals between successive load transfers.

Dynamic deflection cycles are proportional to the dynamic load cycles, since the spring constants of the teeth have been assumed constant. Dynamic stress cycles are obtained by applying the Y factor given in Fig. 22. to the dynamic load cycles.

4.2. Lightly-Loaded Gears

Reswick has analyzed the lightly-loaded-gear case, $e_m \gg s_{rt}$, using the model shown in Fig. 46. The effect of transmitted load on the dynamic increment load is assumed negligible, and the cam is assumed to have the parabolic shape shown in Fig. 46. This shape is reversed from that given by the no-load separation cam shown in Fig. 40.

During operation of lightly-loaded gears, the gear teeth inevitably will separate, move through the backlash space, and come into contact on their backs. A conservative estimate of the dynamic load is obtained by assuming that all the energy present in the spring-mass system when the free vibration commences (after the cam has been inserted) is completely stored in a single tooth-pair spring at some time during the ensuing motion.

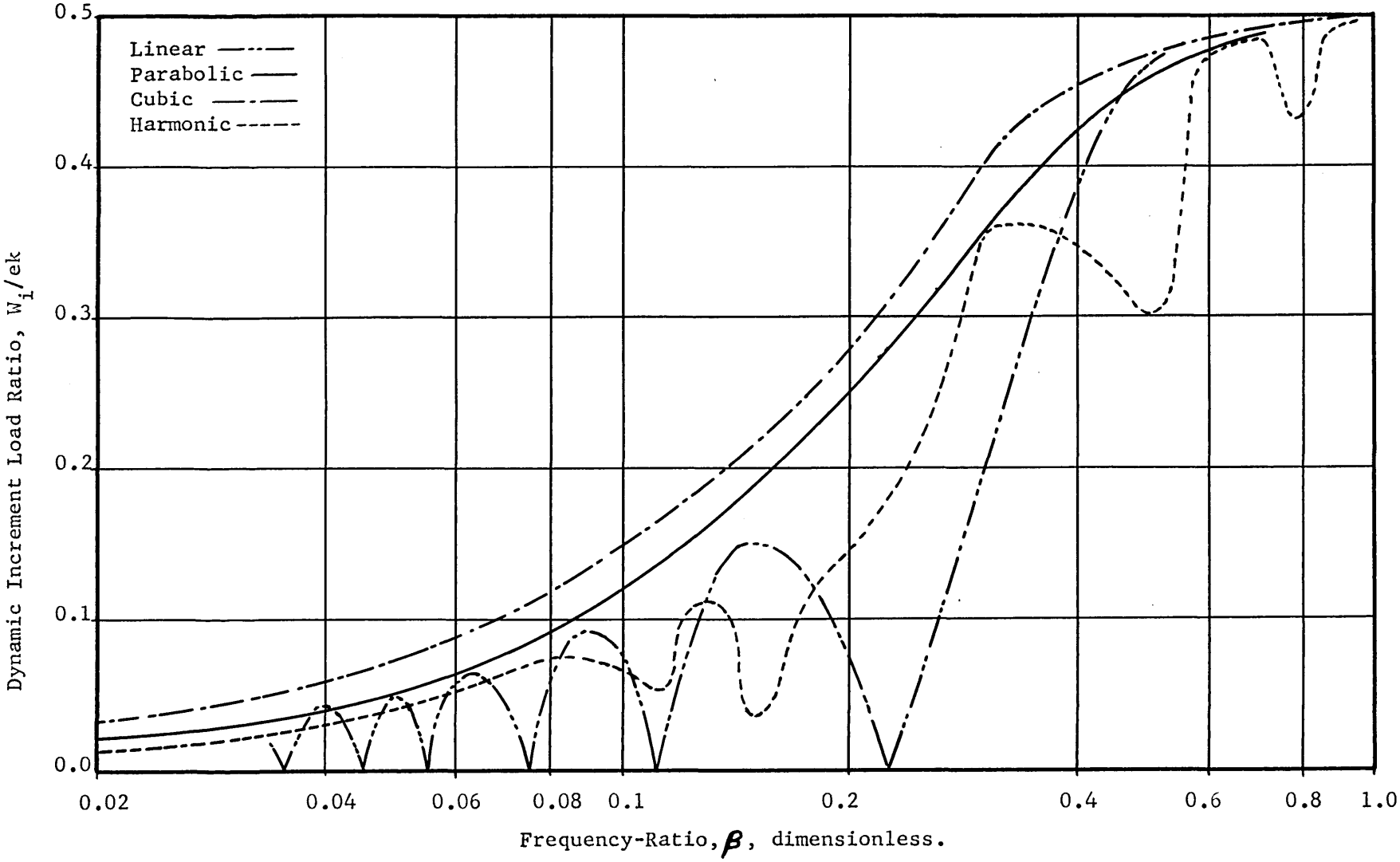

Fig. 44. Effect of Error-Cam Shape on the Dynamic Increment Load in Heavily-Loaded Gears

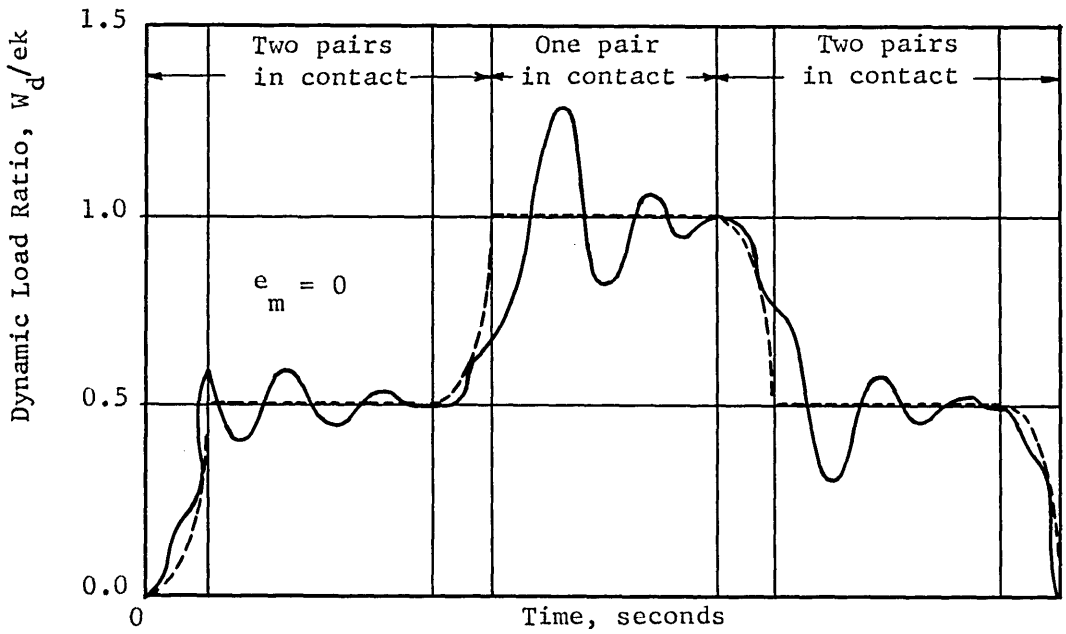

Fig. 45. Load History for a Tooth that Passes Through a Loaded Gear Mesh. Computed from the Single-Load-Transfer Model. For Heavily-Loaded Gears with Zero Manufactured Error.

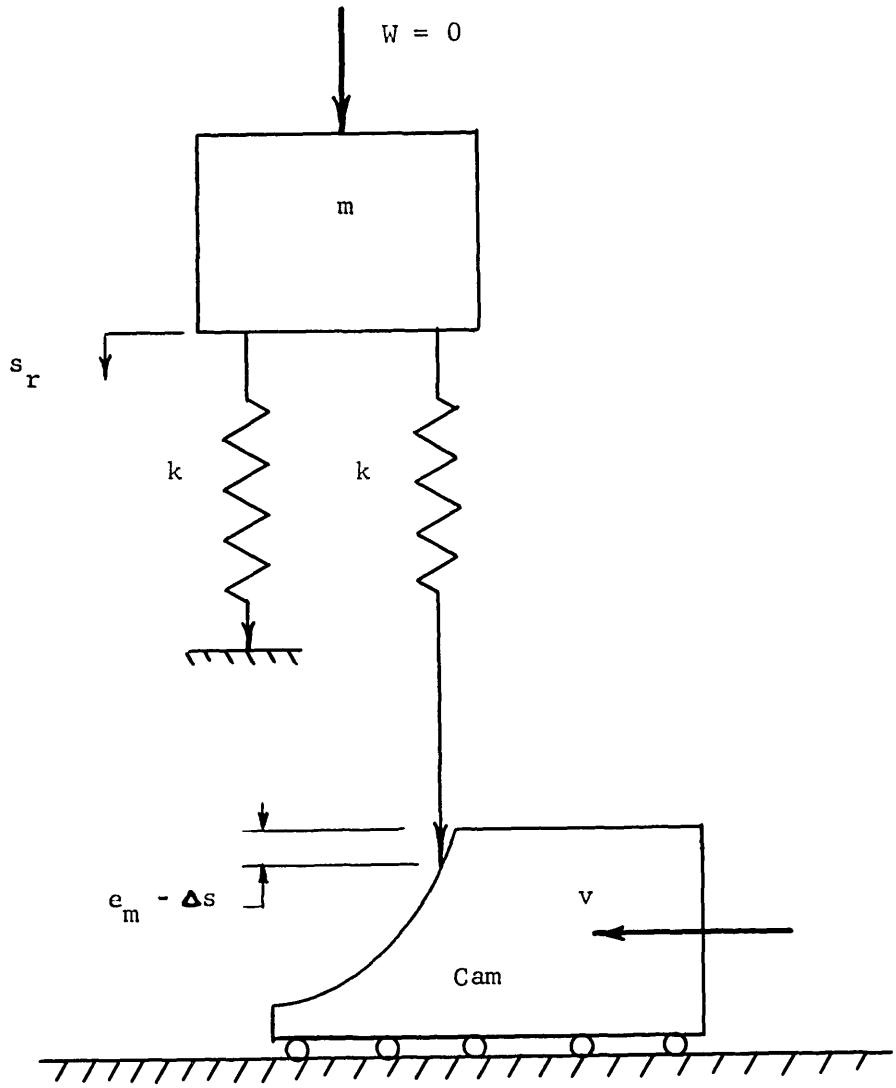

Fig. 46. Simplified Model for Load-Transfer in Lightly-Loaded Gears. Single-Load-Transfer Theory.

Reswick's results for lightly-loaded gears can be put in the form[+]

$$\frac{W_i}{ek} = f_3(\beta) \tag{3.57}$$

$$W_d = W + \left(\frac{W_i}{ek}\right) (ek) \tag{3.58}$$

where the function W_i/ek is plotted as a solid curve in Fig. 47.

Approximations have been suggested by Reswick[45] which facilitate the use of the results given in Fig. 47 and Eq. (3.58) for design of lightly-loaded gears.

The dashed line in Fig. 47 shows the dynamic increment load, as computed by this author, for the cam shape given by the no-load separation curve, i.e., a parabola, but concave downward. The major difference in these two solutions occurs at low values of β. The physical reason for this difference is that in the case of the dashed curve, the spring-mass system leaves the camsurface before the cam has been completely inserted, while in the case of the solid curve, the system remains in contact with the cam until after the cam is completely inserted.

The maximum dynamic increment load for the lightly-loaded case occurs at large values of β, which corresponds to instantaneous introduction of the error-cam. Under these conditions, the mass moves a negligible amount during introduction of the cam, and the tooth spring is deformed by the total error e_m, thus causing a maximum dynamic load $e_m k$. Therefore for lightly-loaded gears,

$$(W_d)_{max} = W + e_m k \tag{3.59}$$

[+]The reader is cautioned in reading Reference 45, that Reswick employs the pitch circle as the basis for defining v, c, s_1, etc., whereas this author employs the base circle.

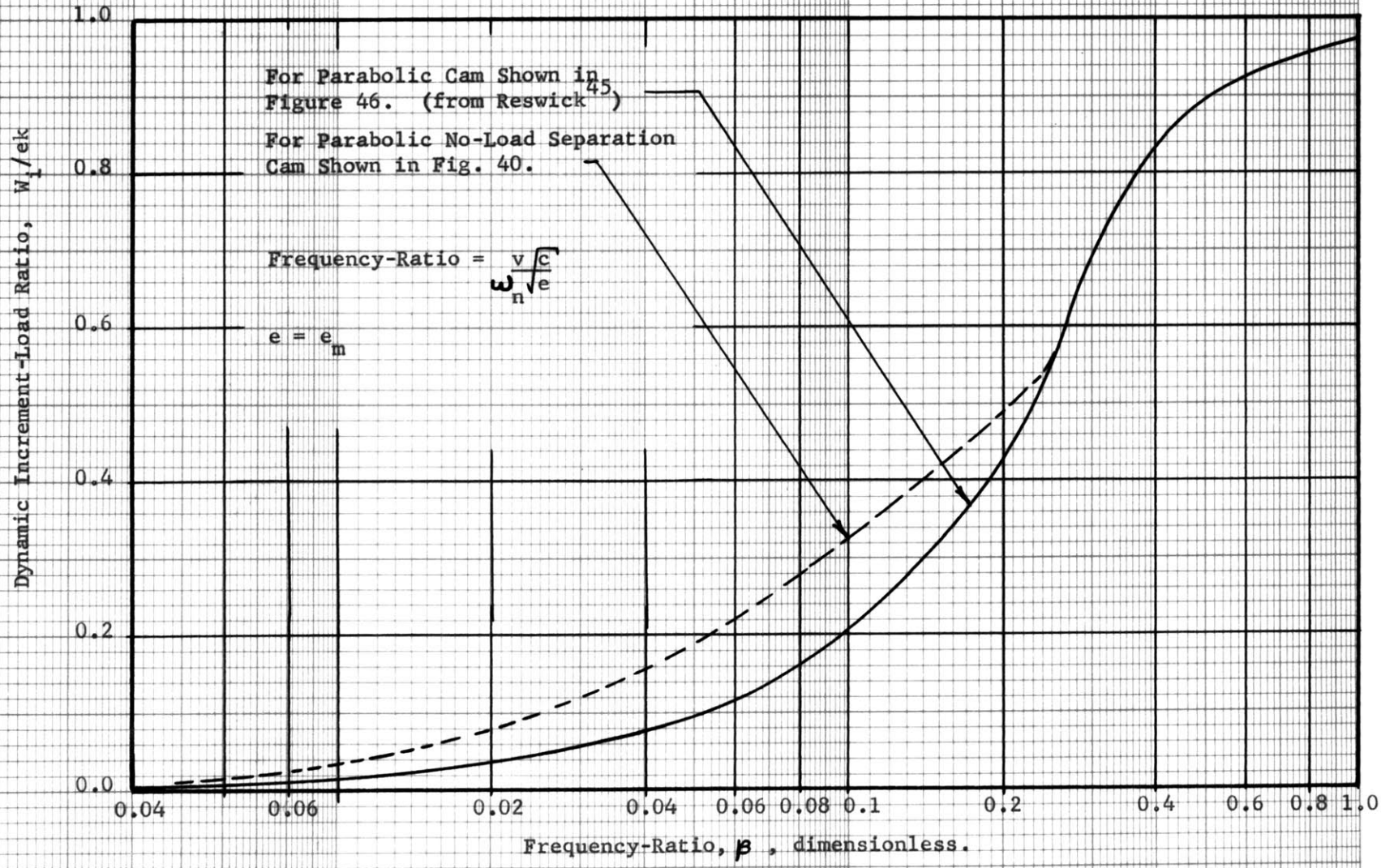

Fig. 47. Dynamic Increment-Load Ratio Versus Frequency Ratio, for Lightly-Loaded Gears. Single Load-Transfer Theory.

For smaller values of β, Eq. (3.58) and the plots given in Fig. 47 must be employed in computing the dynamic load.

5. Variable-Elasticity Model of Dynamic Gear Action: High-Speed, Accurate Gearing

When a gear system is operated at high pitch-line velocity ($v/\cos\theta$), the time required for load transfer from one tooth to another to occur becomes very small compared with the natural period of the spring-mass system. Then the effects of errors due to manufacturing or elastic deformation depend only on the magnitude and not on the nature of the errors. This condition is apparent in Figs. 43 and 47 when $\beta > 2$. At the same time, increase of pitch-line velocity tends to make untenable the assumption, made in the single load-transfer analyses, that system oscillations damp out during the intervals between successive load transfers.

The following analysis is intended to study in a semi-quantitative way the behavior of a gear system operated at very high pitch-line velocities relative to the system natural frequency.

The assumptions of constant input load W, and constant tooth-pair stiffness k are retained in the following analysis, and the following additional assumptions are made.

1. The error is introduced rapidly compared with the natural period of the spring-mass system, i.e., $\beta > 2$.
2. Manufactured errors are very small compared with the elastic tooth deflection

$$e_m \ll s_{rt} \tag{3.60}$$

3. Viscous and static friction can be treated as an equivalent viscous damping which depends on the relative velocity s_r of the two gears.
4. The viscous damping when two pairs of teeth are in contact is twice as great as when one pair of teeth is in contact.

Under the conditions established by the foregoing assumptions, the gear system model exhibits effectively a time-varying spring-stiffness as shown in Fig. 48. When two pairs of teeth are in contact, the stiffness is 2k, while when one pair of teeth is in contact the stiffness is only k. The spring-stiffness variation is shown in Fig. 48b, as a function of time and contact-ratio. The total cycle time for the stiffness variation is the time for one tooth to move through the mesh.

$$T_c = \frac{p_n}{v} \tag{3.61}$$

Of this total time T_c, the stiffness is equal to k (one tooth-pair in contact) for a time

$$T_1 = \frac{p_n}{v} \quad (2 - CR) \tag{3.62}$$

where p_n is normal pitch, v is the average velocity along the line of action, and CR is the contact ratio. In this preliminary study, the contact ratio was taken to be 1.5.

For the model of Fig. 48a, the dynamic equation, Eq. (3.16) can be written

$$m\ddot{s}_r + b(I)\,\dot{s}_r + k(I)\,s_r = W \tag{3.63}$$

where I is defined to be an operator which is equal to the number of tooth pairs in contact. According to Fig. 48, the quantity I varies periodically between 1 and 2. When a damping-ratio is defined,

$$\zeta_a = \frac{b}{2\sqrt{mk}} \tag{3.64}$$

Equation (3.63) can be written

$$\frac{1}{\omega_n^2}\,\ddot{s}_r + \frac{2\,\zeta_a}{\omega_n}\,(I)\dot{s}_r + (I)\,s_r = s_{rt} \tag{3.65}$$

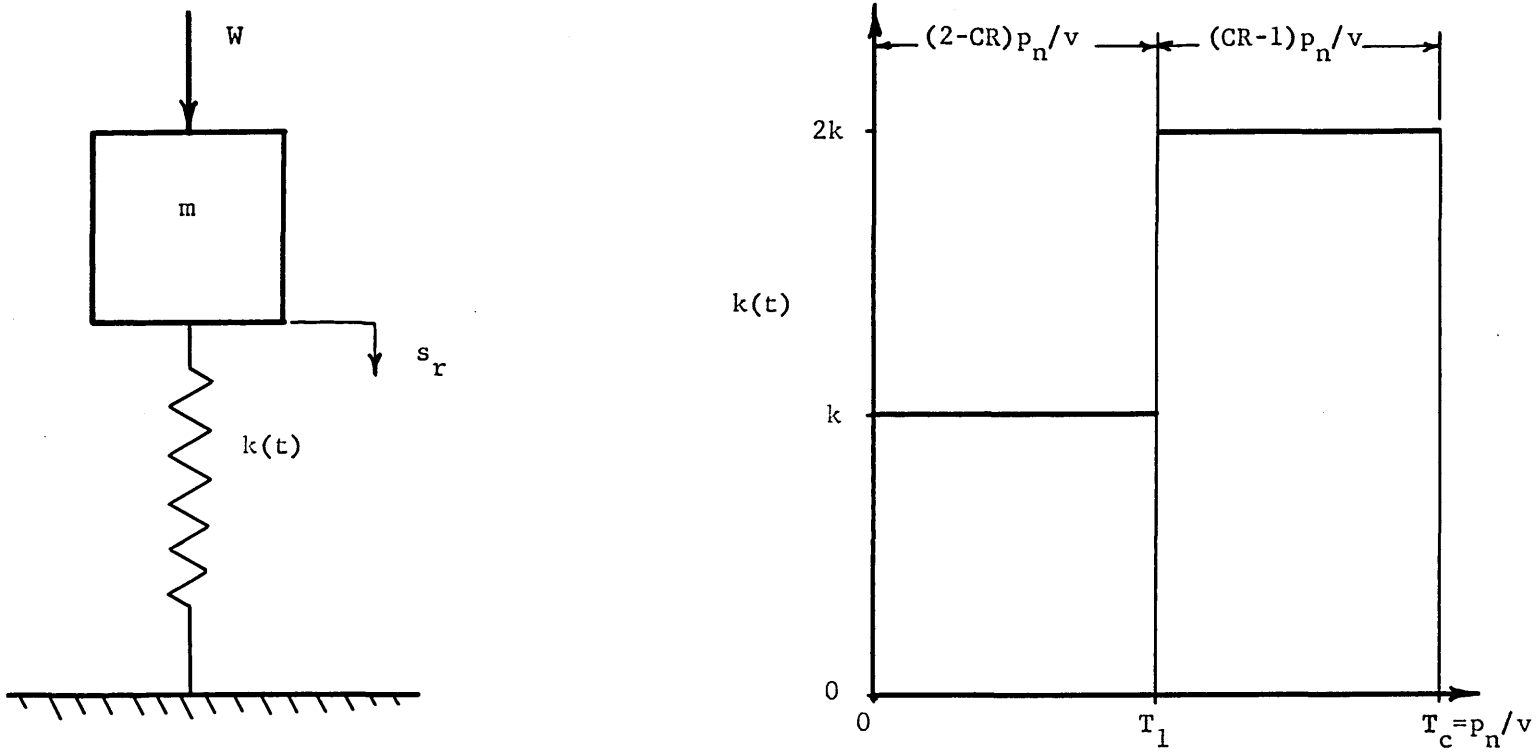

a) Model

b) Spring-Constant Variation

Fig. 48. Variable-Elasticity Model for Gear Dynamics; Heavily-Loaded, High-Speed Gears.

The complete solution to Eq. (3.65), which is really two equations, depends both on the initial conditions and on the nature of the spring-constant variation. However, during steady-state operation, solutions of Eq. (3.65) will exist which are periodic with the same period as that of the spring-constant variation. These periodic solutions are determined by the conditions that the displacement and velocity at $t = 0$ are equal to the displacement and velocity at $t = T_c$ (one period later), and that the displacements and velocities match at $t = T_1$.

These four conditions, expressed mathematically, are

$$\begin{aligned} s_r(0) &= s_r(T_c) \\ \dot{s}_r(0) &= \dot{s}_r(T_c) \\ s_r(T_1 - \epsilon) &= s_r(T_1 + \epsilon) \\ \dot{s}_r(T_1 - \epsilon) &= \dot{s}_r(T_1 + \epsilon) \end{aligned} \tag{3.66}$$

where ϵ is a vanishingly small quantity.

If the damping b is assumed to be zero, the two solutions of Eq. (3.65) are of the form

$$t < T_1 \qquad s_r = c_1 \sin \omega_n t + c_2 \cos \omega_n t + s_{rt} \tag{3.67}$$

$$t > T_1 \qquad s_r = c_3 \sin \sqrt{2}\, \omega_n t + c_4 \cos \sqrt{2}\, \omega_n t + \frac{1}{2} s_{rt} \tag{3.68}$$

When Eqs. (3.67) and (3.68) are substituted into Eq. (3.66), the following result is obtained

$$
\begin{aligned}
&0 + c_2 - c_3 \sin\sqrt{2}\,\omega_n T_c - c_4 \cos\sqrt{2}\,\omega_n T_c = -s_{rt} \\
&c_1 - 0 - c_3\sqrt{2}\cos\sqrt{2}\,\omega_n T_c + c_4\sqrt{2}\sin\sqrt{2}\,\omega_n T_c = 0 \\
&c_1 \sin\omega_n T_1 + c_2 \cos\omega_n T_1 - c_3 \sin\sqrt{2}\,\omega_n T_1 - c_4 \cos\sqrt{2}\,\omega_n T_1 = -\frac{1}{2}\, s_{rt} \\
&c_1 \cos\omega_n T_1 - c_2 \sin\omega_n T_1 - c_3\sqrt{2}\cos\sqrt{2}\,\omega_n T_1 + c_4\sqrt{2}\sin\sqrt{2}\,\omega_n T_1 = 0
\end{aligned}
\tag{3.66}
$$

Equations (3.66) are four simultaneous linear algebraic equations for the unknown constants c_1, c_2, c_3, and c_4. Since T_1 is a given fraction of T_c, for fixed contact-ratio, the solution can be described in terms of the quantity $\omega_n T_1$. Let

$$q_a = \sqrt{2}\,\omega_n T_1 = \frac{1}{\sqrt{2}} \frac{\omega_n p_n}{v} \tag{3.70}$$

Because q_a is the argument of the harmonic functions given in Eqs. (3.69), it is convenient to express q_a in degrees, instead of radians. When the solution for displacement s_r is obtained, the dynamic load is determined by multiplying the displacement by the spring-constant k.

The solid curves in Figs. 49 and 50 give the maximum dynamic load for any value of q_a when ζ_a is zero, as computed from Eqs. (3.69). Figure 51 shows the calculated load cycle for one pair of teeth for $q_a = 950^\circ$ and $\zeta_a = 0$. The general appearance of the load cycles for other values of q_a are sketched on Figs. 48 and 49.

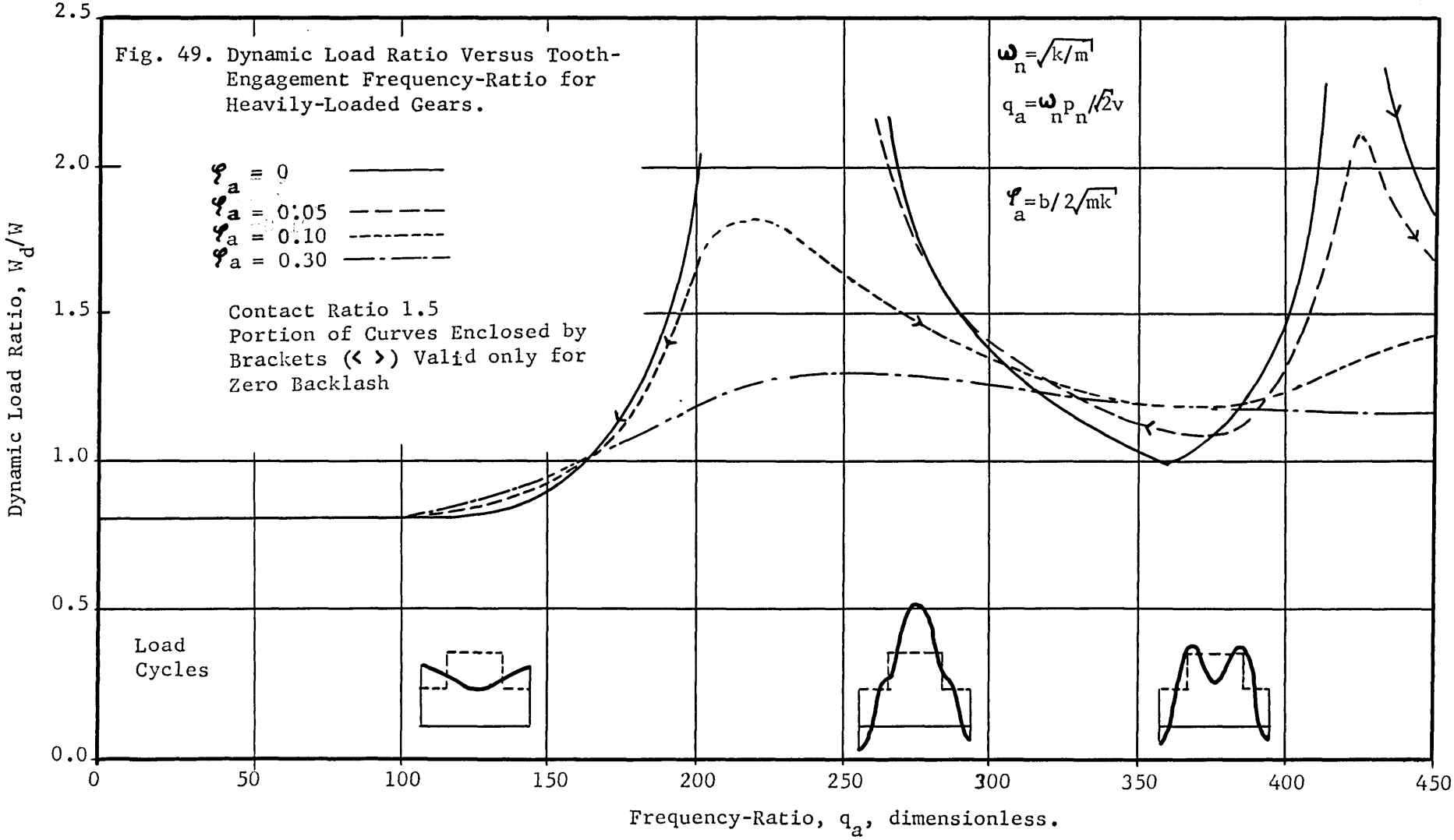

Fig. 49. Dynamic Load Ratio Versus Tooth-Engagement Frequency-Ratio for Heavily-Loaded Gears.

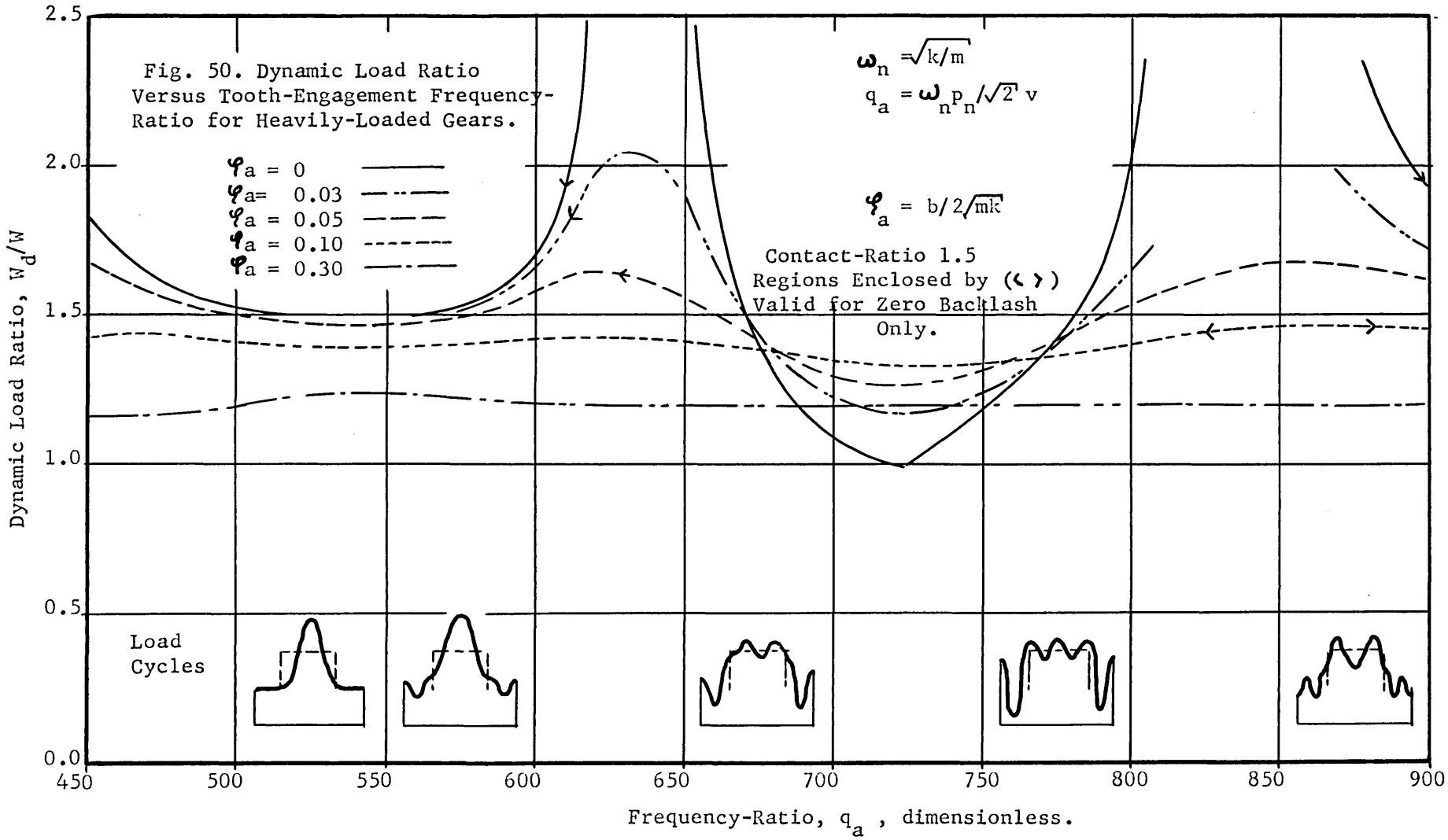
Fig. 50. Dynamic Load Ratio Versus Tooth-Engagement Frequency-Ratio for Heavily-Loaded Gears.
φa = 0
φa= 0.03
φa = 0.05
φa = 0.10
φa = 0.30
ωn = √k/m
qa = ωn pn/√2 v
φa = b/2√mk
Contact-Ratio 1.5
Regions Enclosed by (< >)
Valid for Zero Backlash Only.
Load Cycles
Dynamic Load Ratio, Wd/W
Frequency-Ratio, qa , dimensionless.
2.5
2.0
1.5
1.0
0.5
0.0
450
500
550
600
650
700
750
800
850
900

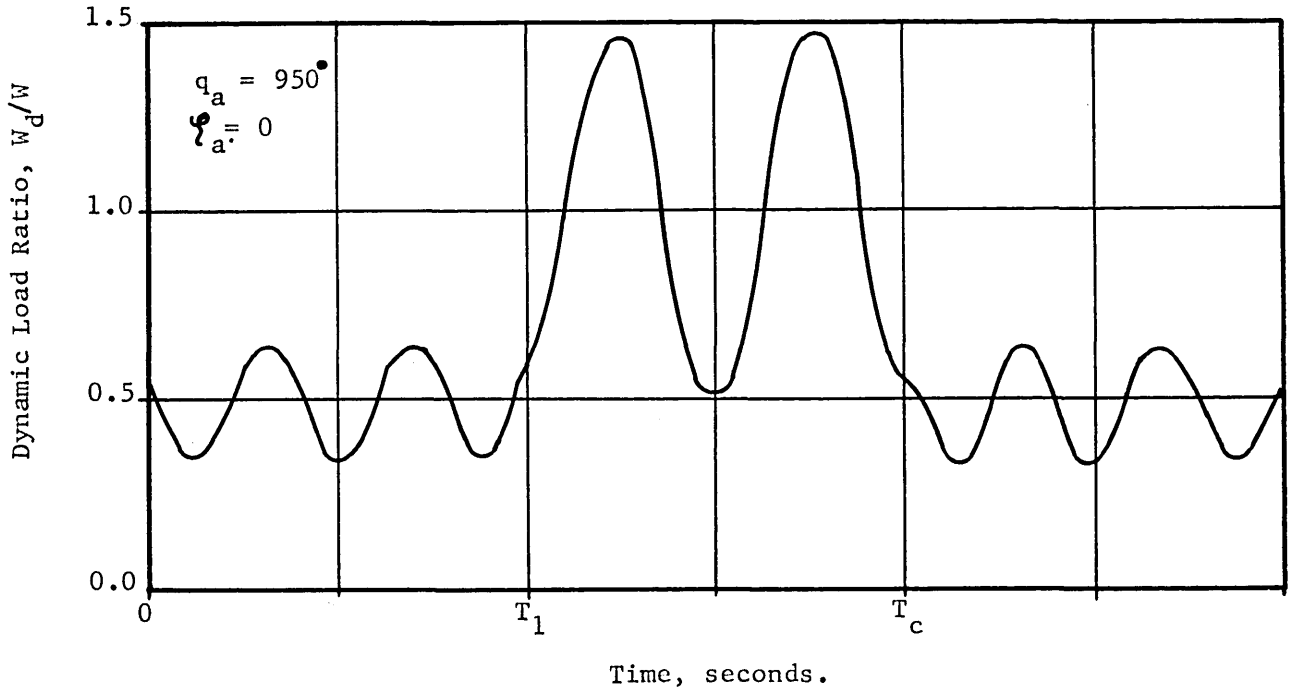

Fig. 51. Dynamic Load Cycle , Predicted From the Variable-Elasticity Model of Gear Dynamics. For q_a = 950 degrees, and φ_a = 0.

When the damping ratio, ζ_a, is not zero, the analytical solution of Eq. (3.63) becomes extremely difficult. In order to obtain solutions for finite ζ_a, an electronic analog computer was utilized. Figure 52 shows the functional block diagram which describes the set up of a Philbrick analog computer for solving Eq. (3.63). In order to achieve the time-variable coefficients involved, two multipliers were used in conjunction with a square-wave generator. The calculated curve for zero damping was used in checking the computer circuit, and the computed results for this case were found to correspond with the calculated results within 5 per cent. Figures 49 and 50 show the computed results for various damping ratios ζ_a and frequency ratios q_a.

When a finite amount of damping is present, the amplitudes of the peaks in maximum dynamic load become limited. For a fixed damping ratio, the magnitudes of the peaks become less as the value of frequency ratio q_a becomes larger.

At low pitch-line velocities ($q_a \rightarrow \infty$) many oscillations of the spring-mass system occur between load transfers, and even a small amount of damping will produce substantial integrated effects over the whole interval between load transfers. For damping ratios of 0.30 or larger, the peaks in dynamic load almost disappear except for the final peak near $q_a = 250^\circ$. One significant observation that can be made from the results presented in Fig. 49 is that for pitch-line velocities which cause q_a to be less than 150°, the dynamic load <u>decreases</u> slightly with increasing velocity. When q_a is less than 80° an asympotic dynamic load is reached which is less than the static load and which then is maintained at a constant value as pitch-line velocity ($v/\cos\theta$) goes to infinity and q_a goes to zero. This asymptotic dynamic load is a weighted mean between having the static load carried by one pair of teeth and by two pairs of teeth.

A difficulty arises in connection with the dynamic load predictions given in Figs. 49 and 50. In certain regions of these curves, enclosed by angle brackets (‹ ›), the tooth loads become negative during part of the dynamic-load cycle. Therefore, in these regions, the predictions are valid

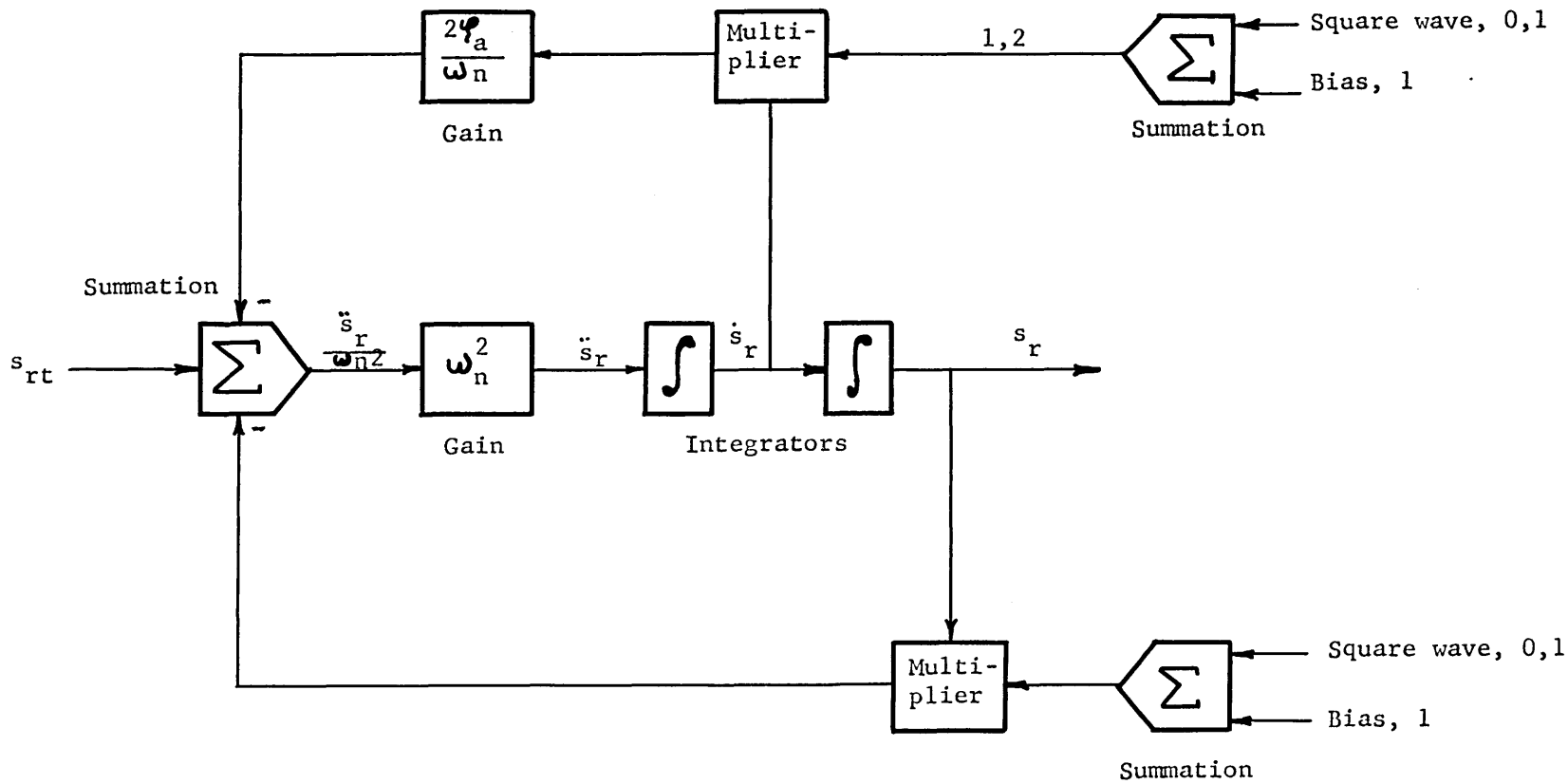

Fig. 52. Block Diagram for Philbrick Analog Computer Set-Up; Variable-Elasticity Model for Heavily-Loaded Gears.

only for zero backlash. In any real gear system, some backlash will exist, and the teeth will separate when tooth-load tends to become negative. Since the tooth deflections in dynamic operation are very small, a real gear system would behave essentially as though it had an infinite amount of backlash. That is, the teeth will remain separated until the action of the applied torque brings them back into contact. The assumption of negligible manufactured error is necessary to justify the preceding statement.

In order to make a qualitative study of the nature of dynamic loads induced by the variable gear-mesh elasticity when backlash is not zero, one section of the Dynamic Analysis and Control Laboratory Generalized Computer was employed. The functional diagram for the computer set-up is shown in Fig. 53. The summation No. 1 in Fig. 53 performs the operation indicated by Eq. (3.65) which can be expressed in the form

$$s_{rt} - (I)\left[\frac{2\zeta_a}{\omega_n}\dot{s}_r + s_r\right] = \frac{1}{\omega_n^2}\ddot{s}_r \tag{3.71}$$

The output of summation No. 1 ismultiplied by $1/\omega_n^2$ and is integrated once to obtain $\dot{s}_r$, then once more to obtain s_r. The quantity $\dot{s}_r$ is multiplied by $2\zeta_a/\omega_n$ and is added to s_r in summation No. 2. The output of summation No. 2 is the total force transmitted from the gear teeth to the equivalent mass m. From summation No. 2, the force signal is led through a relay R_1 and into the summation No. 1. Whenever the relative motion s_r becomes negative, the relay R_1 is opened, thus causing the force transmitted to the mass from the tooth-spring to be zero. The time variable I is obtained by leading the output of relay R_1 into summation No. 1 through two channels. The first channel is direct and corresponds to I = 1. The second channel passes through relay R_2, which is opened and closed periodically by the action of a sinusoidal voltage impressed on the relay actuator. Consequently the total transmitted force $2\zeta_a/\omega_n \dot{s}_r + s_r$ effectively is multiplied by 1 or 2, periodically, corresponding to the desired periodic change of the number of tooth-pairs in contact.

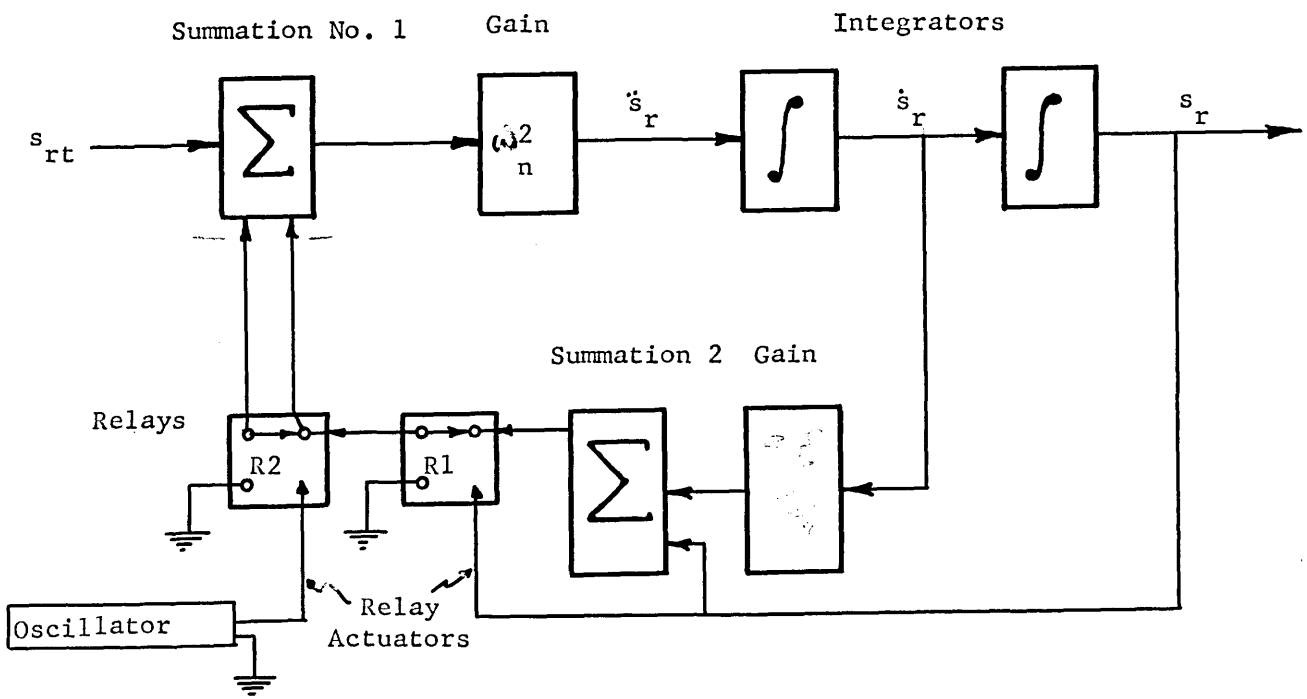

Fig. 53. Block Diagram for Flight-Simulator Set-Up; Variable-Elasticity Model for Heavily-Loaded Gears. Effects of Backlash.

Figures 54 to 62 are computer solutions for relative displacement, and therefore dynamic load, for various values of q_a and ζ_a. In the regions where the transmitted force would go negative in the case of zero backlash, solutions are shown for both the zero and infinite backlash situations. The infinite backlash solutions are identified by the term "limited" in Figs. 54 to 62, since the tooth forces in this case are limited to positive values. Figure 54 is a check solution which can be compared with the calculated load cycle given in Fig. 51.

The following qualitative conclusions are drawn from the computer study just discussed.

1. When the damping ratio ζ_a is greater than about 0.05, the presence of backlash has essentially no effect on the dynamic load.

2. For damping-ratios less than 0.05, the presence of backlash has pronounced effects.

   a. In most cases, the dynamic loads are <u>increased</u> above the values predicted for zero backlash, e.g. Figs. 56 and 57.

   b. In some cases a periodic solution cannot be established and an apparently unpredictable wandering of the relative displacement amplitudes occurs, e.g., Fig. 55.

   c. For some values of q_a and ζ_a, two periodic solutions were observed, one with period equal to the period of the spring-constant variation, and one with twice this period. See for example, Fig. 55, $\zeta_a = 0.02$, where the period is twice the spring-constant-variation period.

   d. For low damping ratios ($\zeta_a < 0.02$), the transient dynamic loads that occur before the periodic solutions are established often are several times as large as the final steady-state loads.

Fig. 54. Dynamic Load Cycles

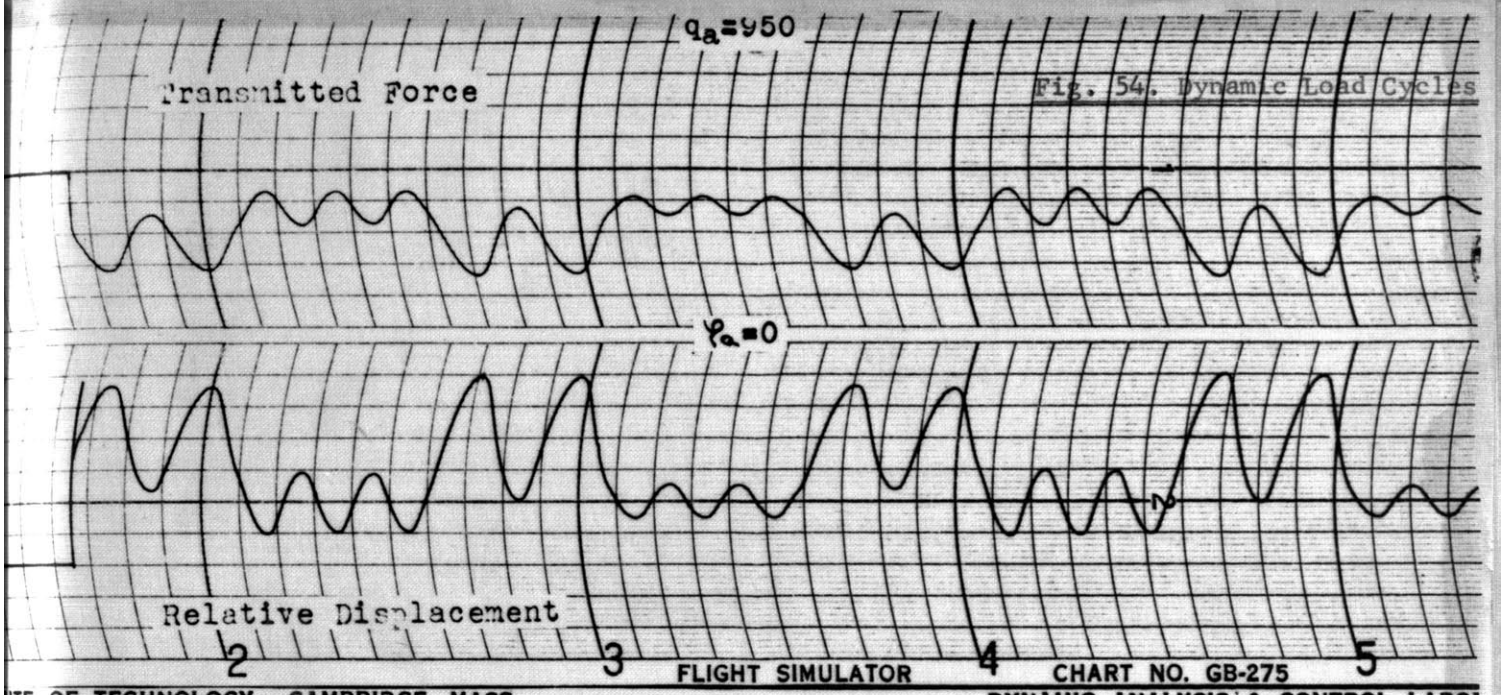

FLIGHT SIMULATOR CHART NO. GB-275

UTE OF TECHNOLOGY — CAMBRIDGE, MASS. DYNAMIC ANALYSIS & CONTROL LABOR

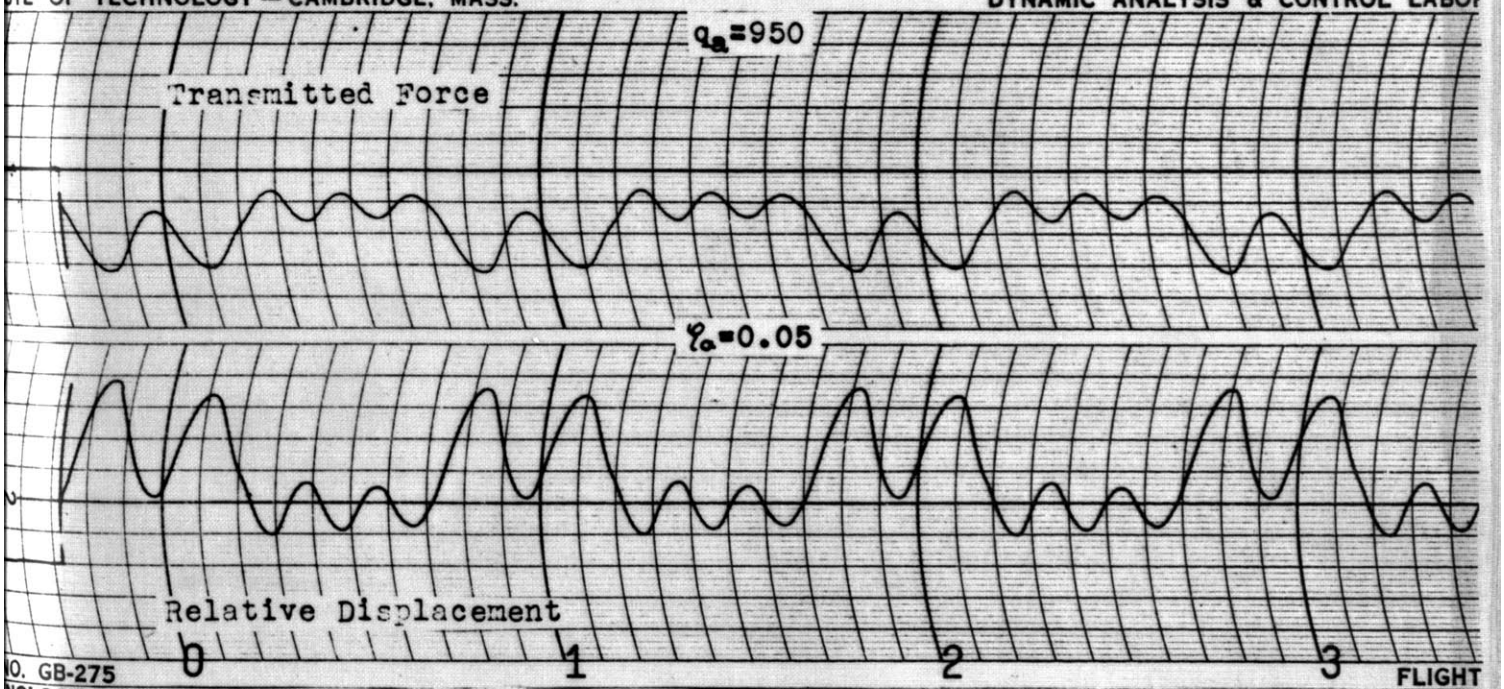

NO. GB-275 FLIGHT

NOLOGY — CAMBRIDGE, MASS. DYNAMIC ANALYSIS & CONTROL LABORATORY-MASSA

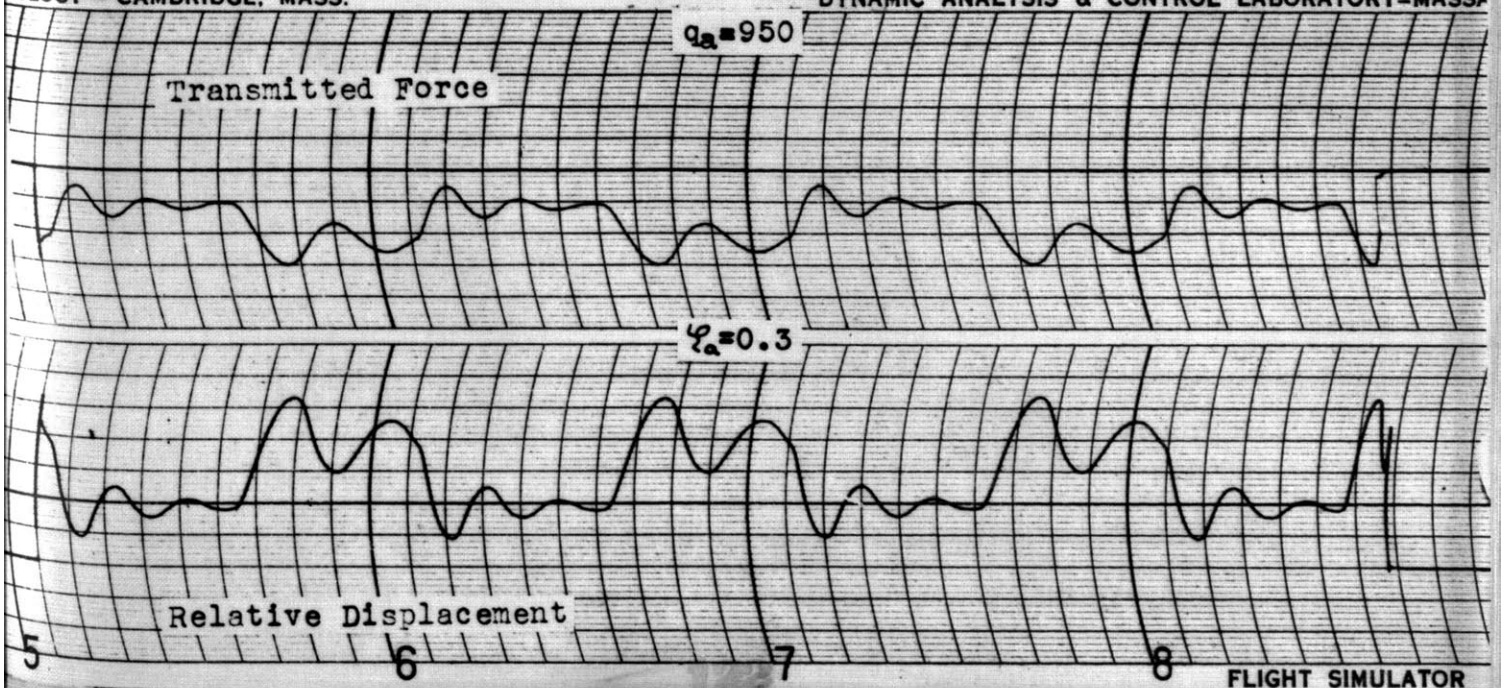

FLIGHT SIMULATOR

Fig. 55. Dynamic Load Cycles

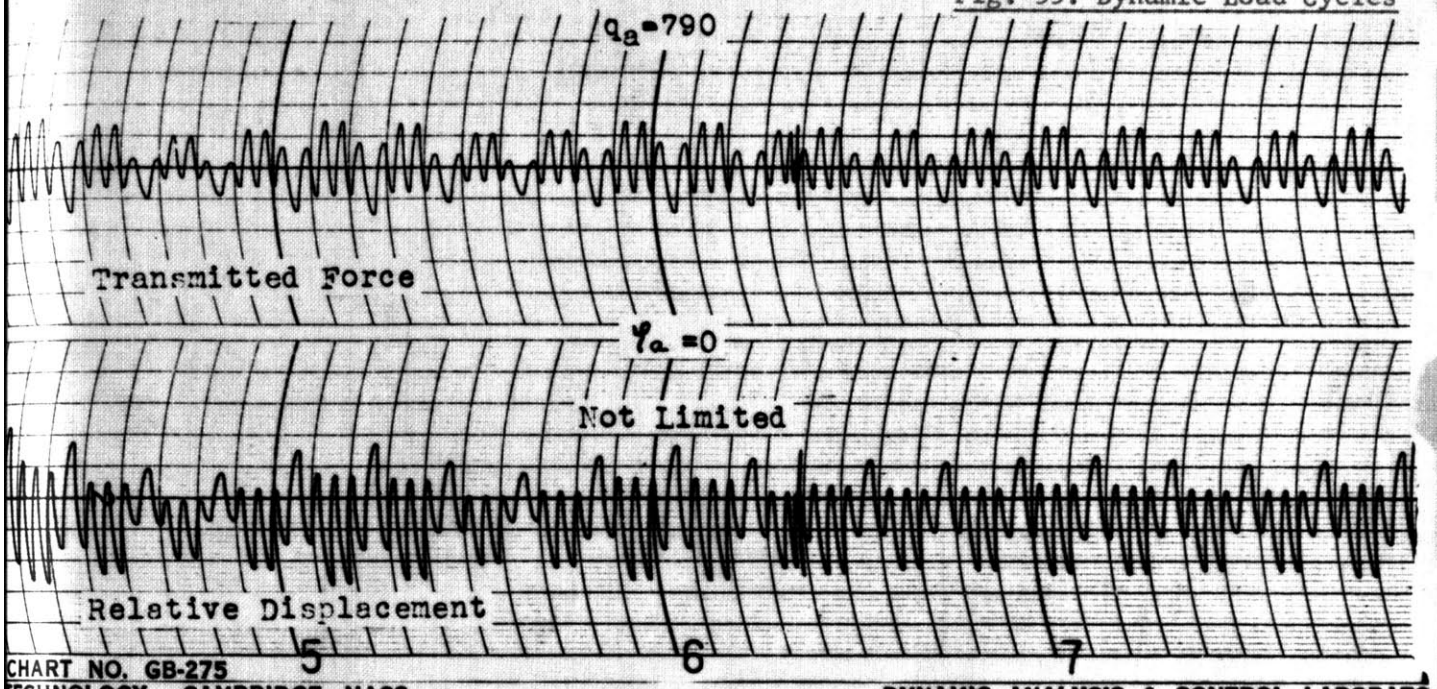

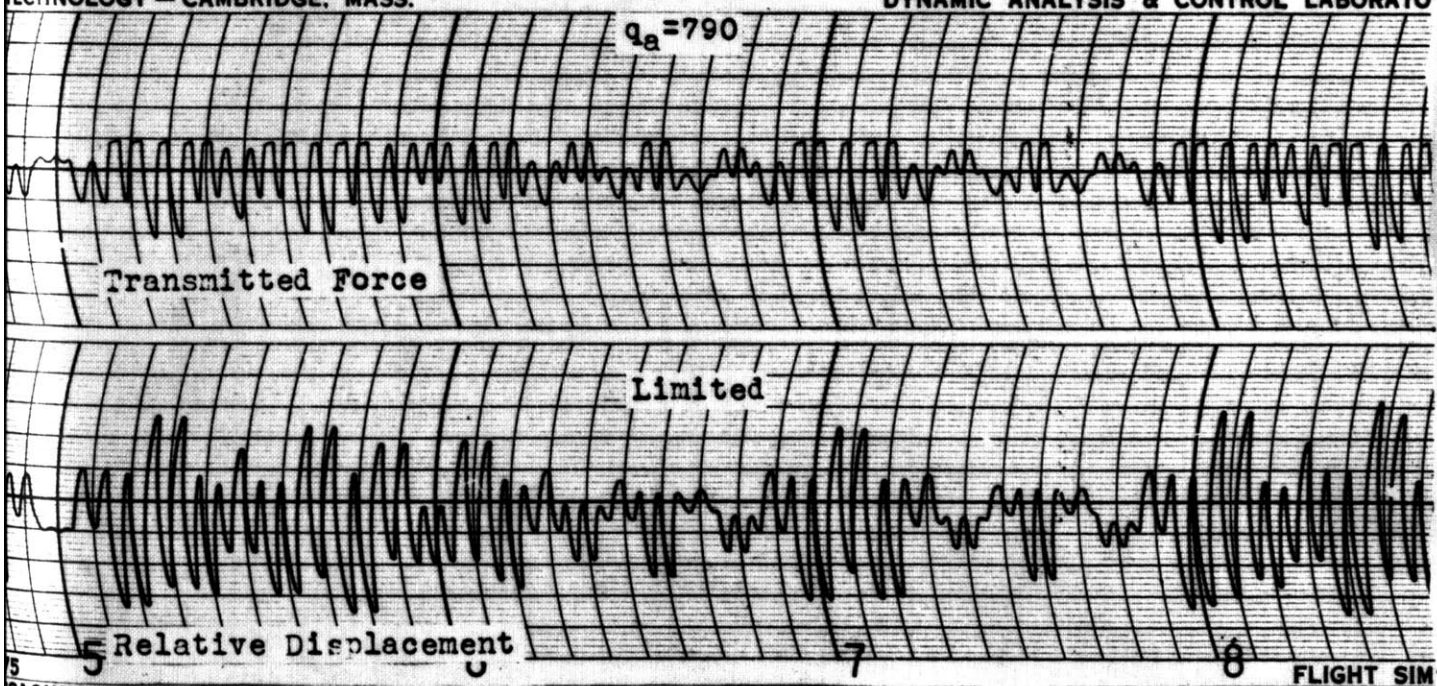

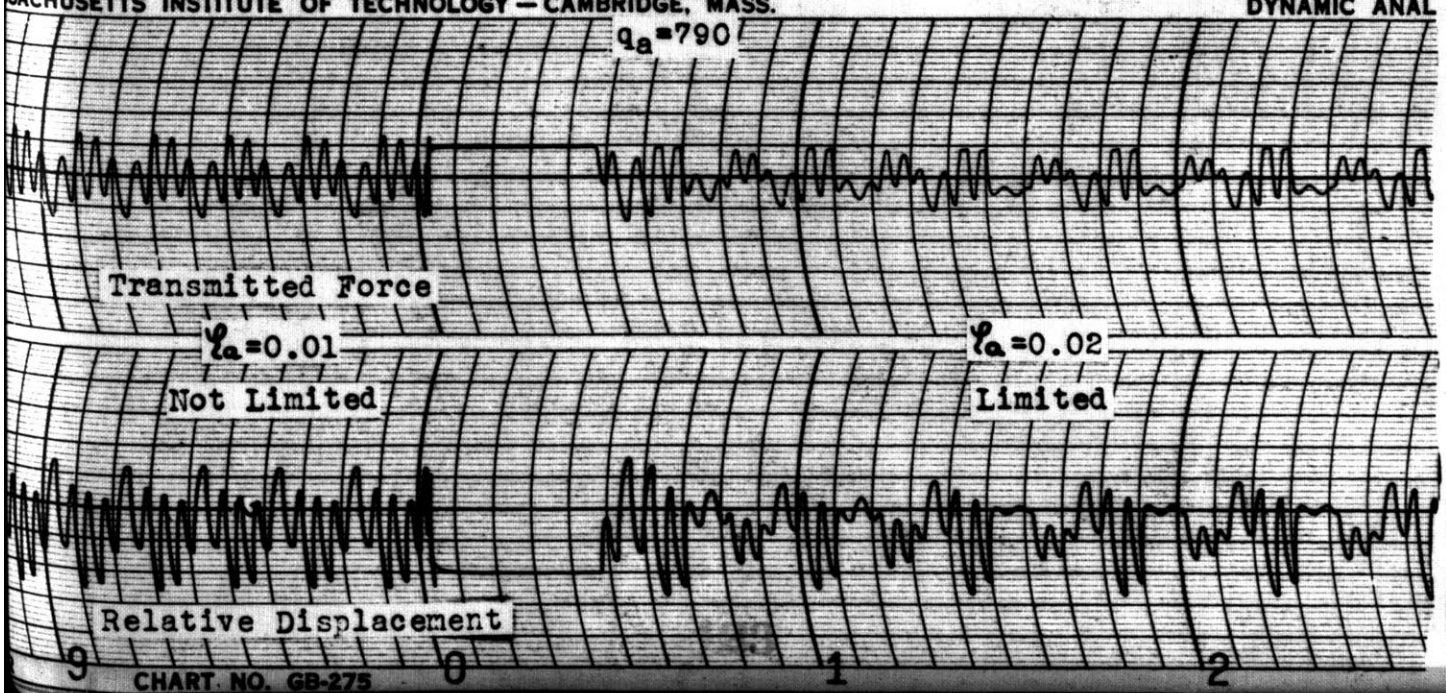

Fig. 56. Dynamic Load Cycles

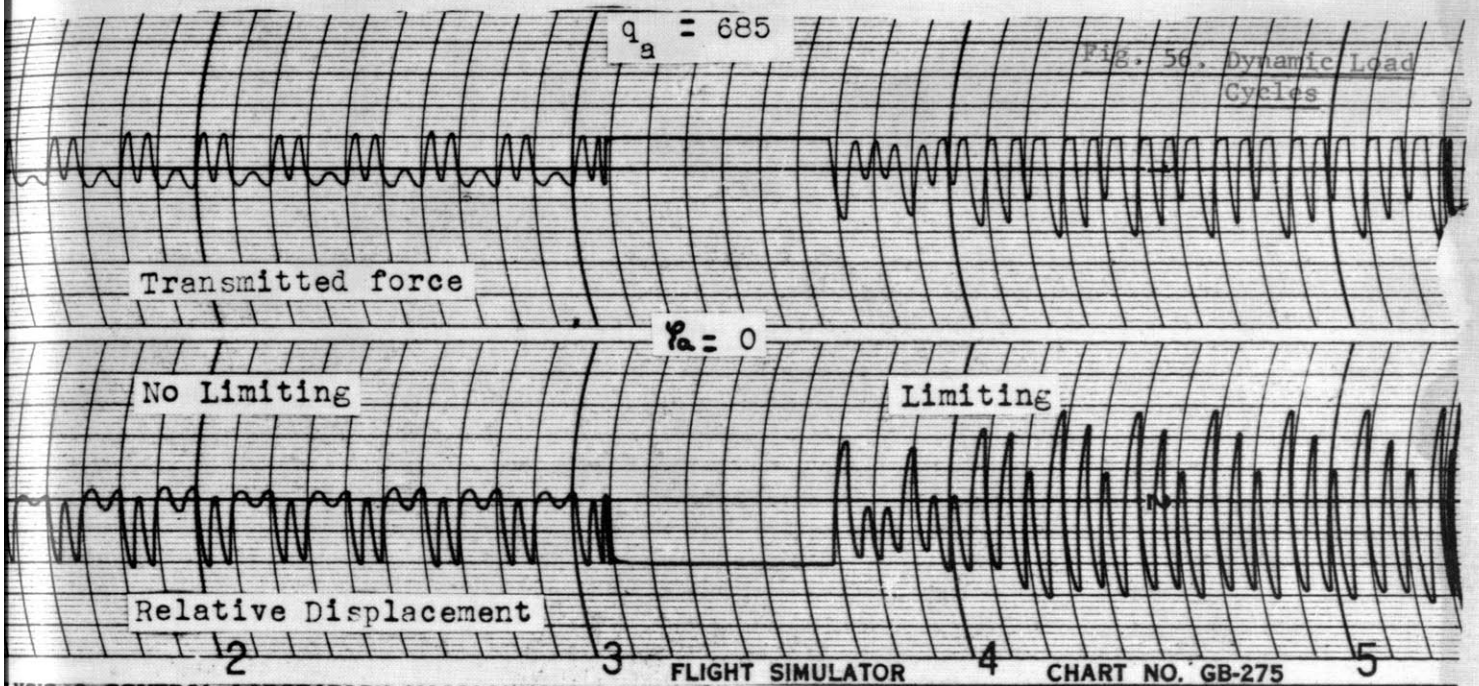

FLIGHT SIMULATOR CHART NO. GB-275

LYSIS & CONTROL LABORATORY-MASSACHUSETTS INSTITUTE OF TECHNOLOGY — CAMBRIDGE, MASS.

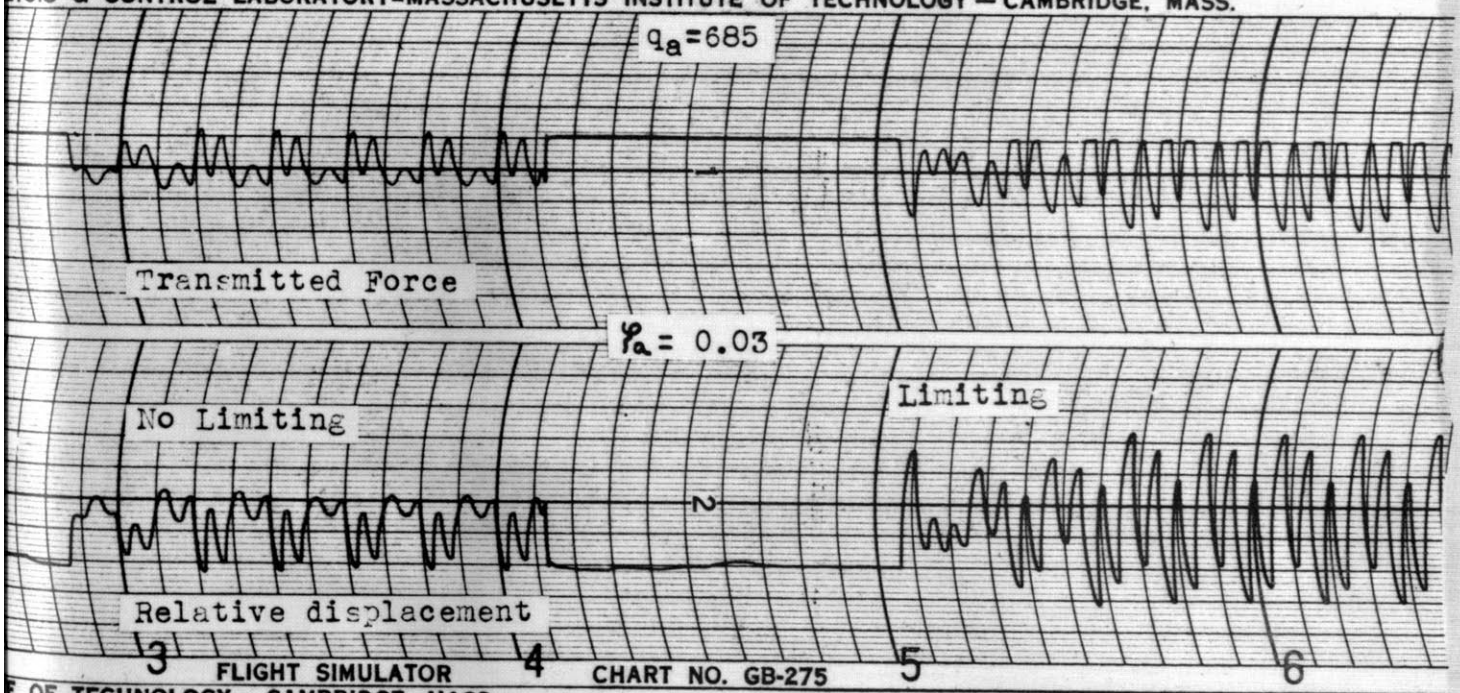

FLIGHT SIMULATOR CHART NO. GB-275

E OF TECHNOLOGY — CAMBRIDGE, MASS.

DYNAMIC ANALYSIS & CONTROL LABO

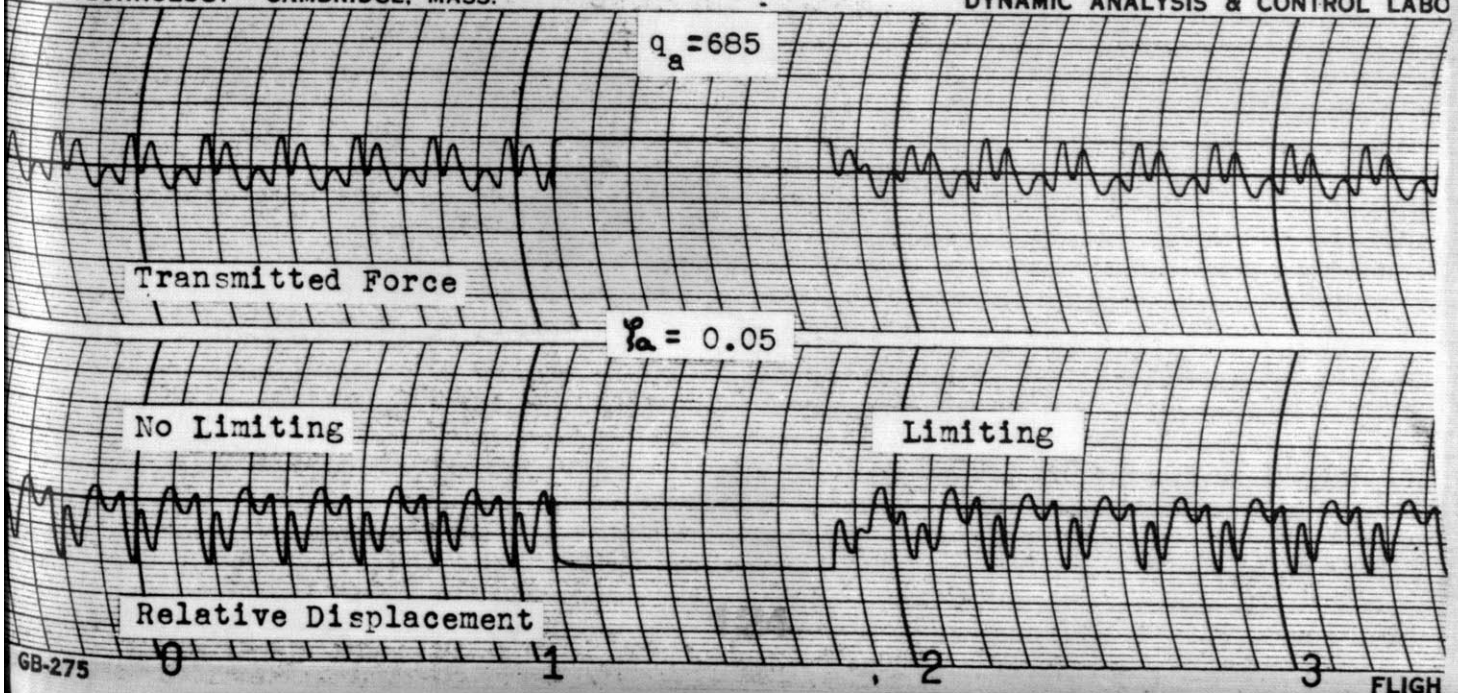

GB-275

FLIGH

Fig. 57. Dynamic Load Cycles

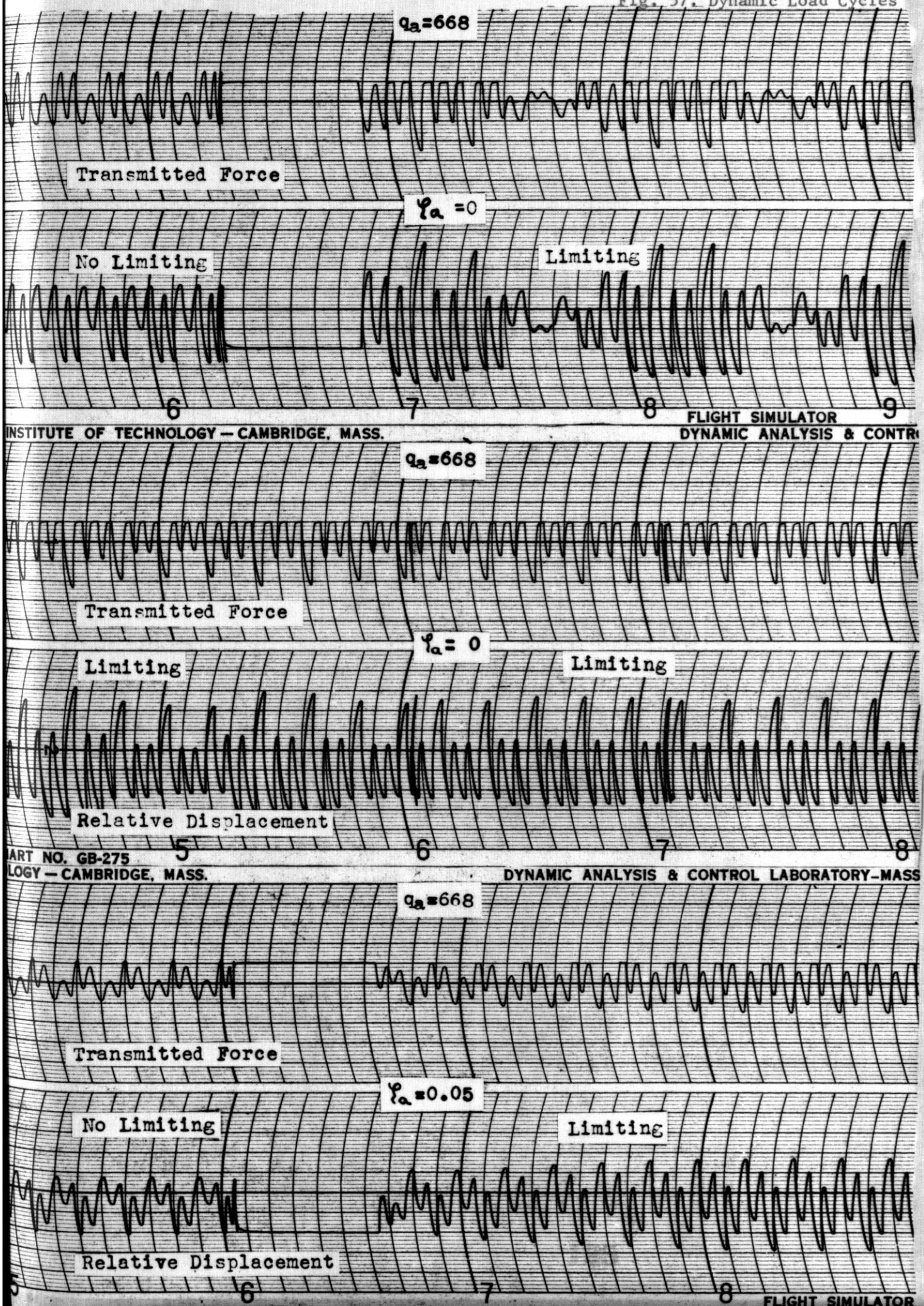

Fig. 58. Dynamic Load Cycles

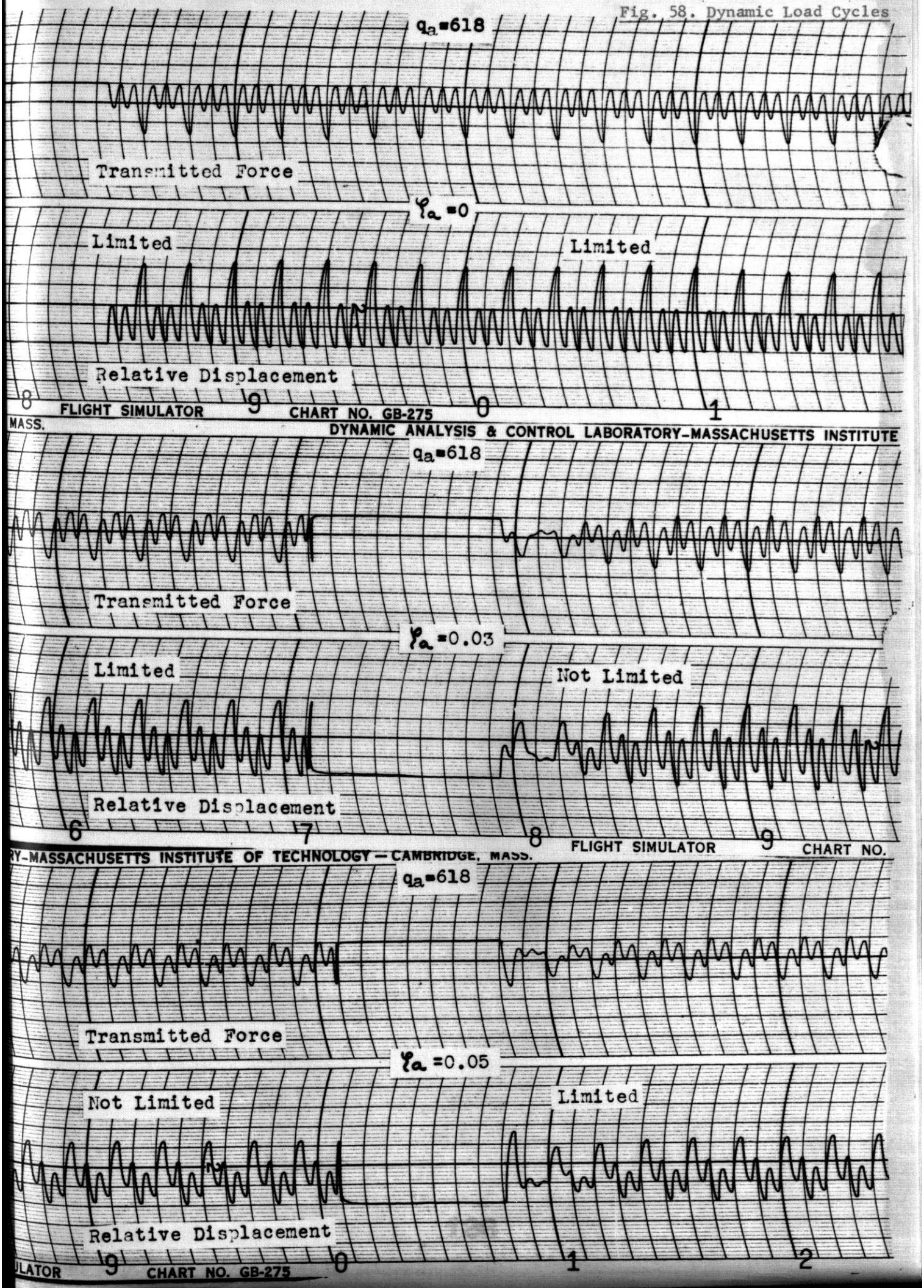

Fig. 59. Dynamic Load Cycles

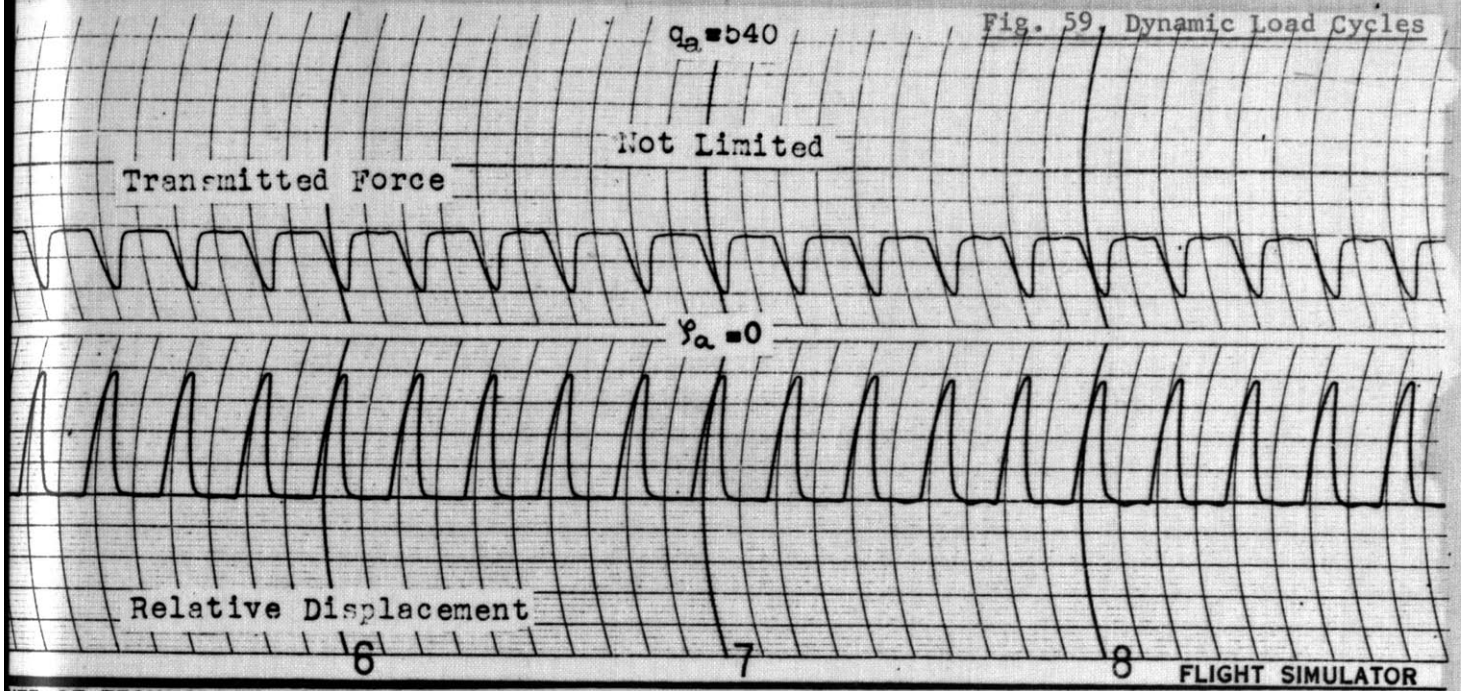

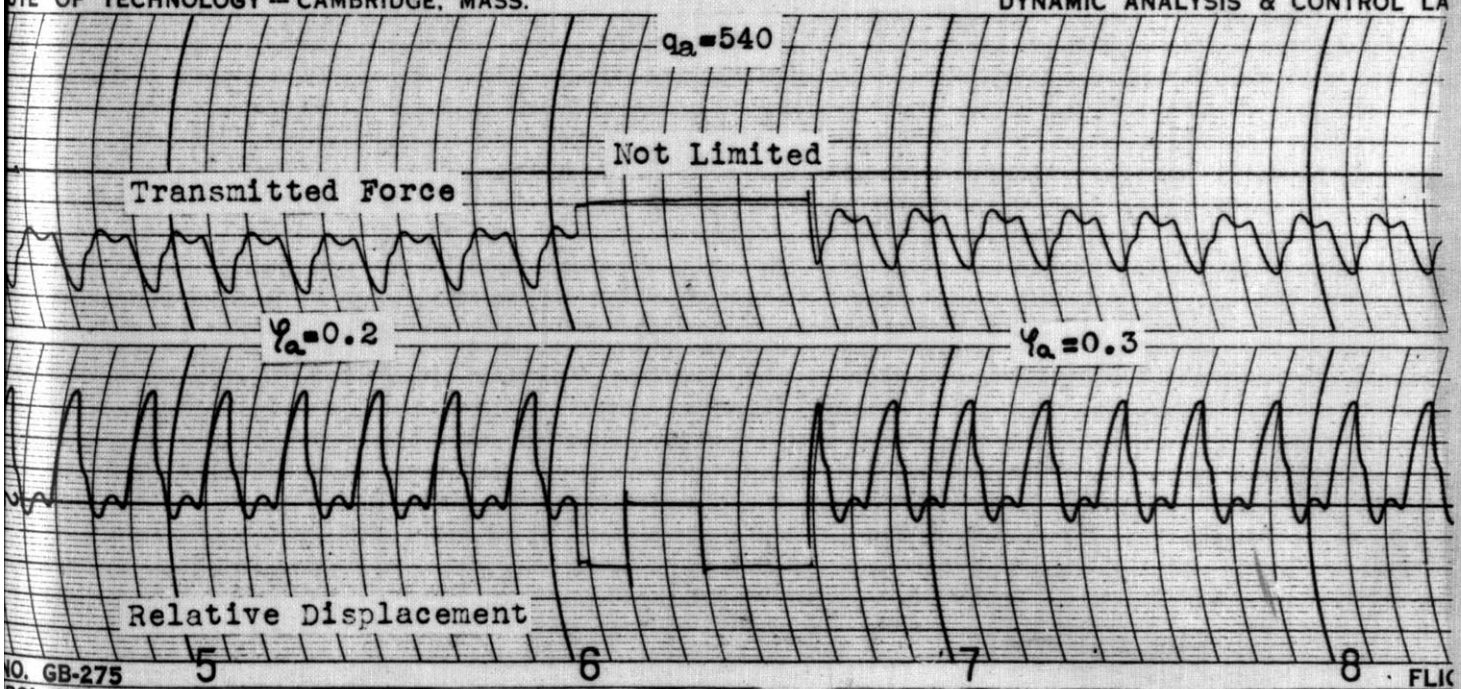

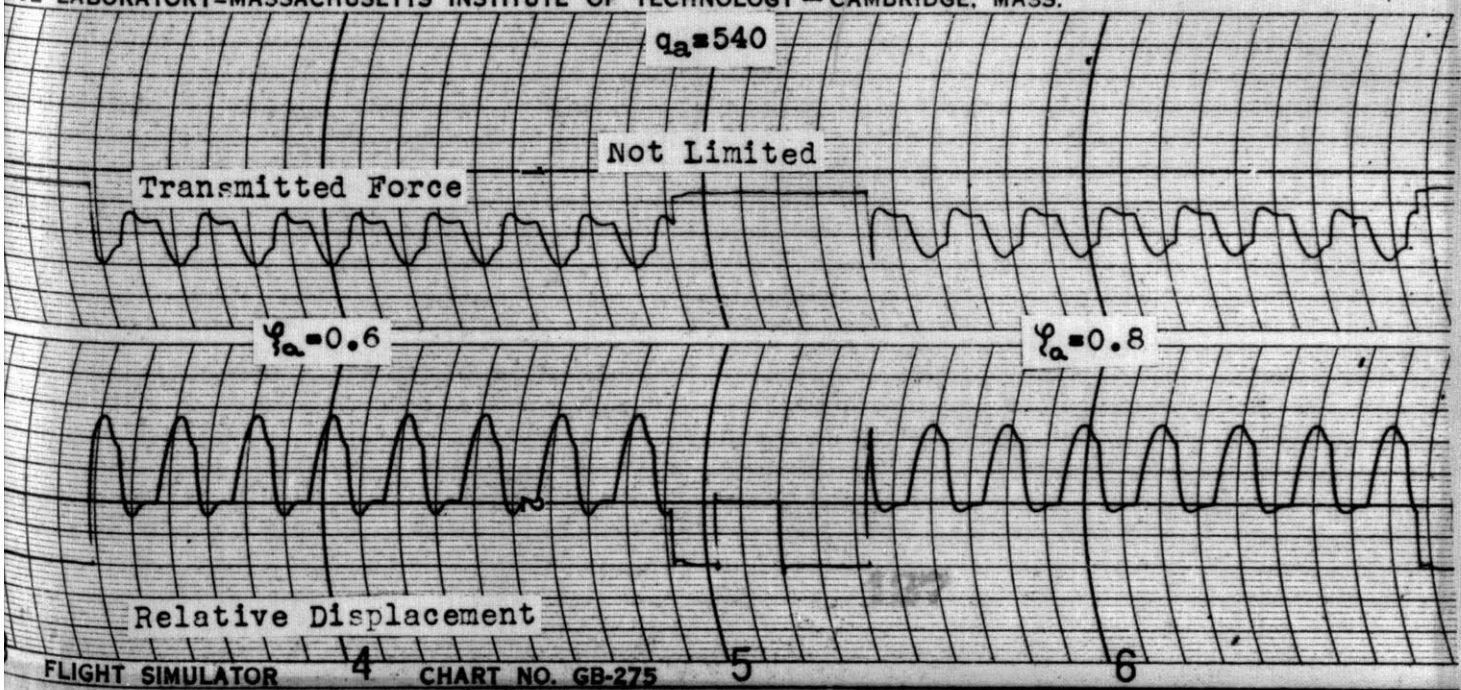

Fig. 60. Dynamic Load Cycles

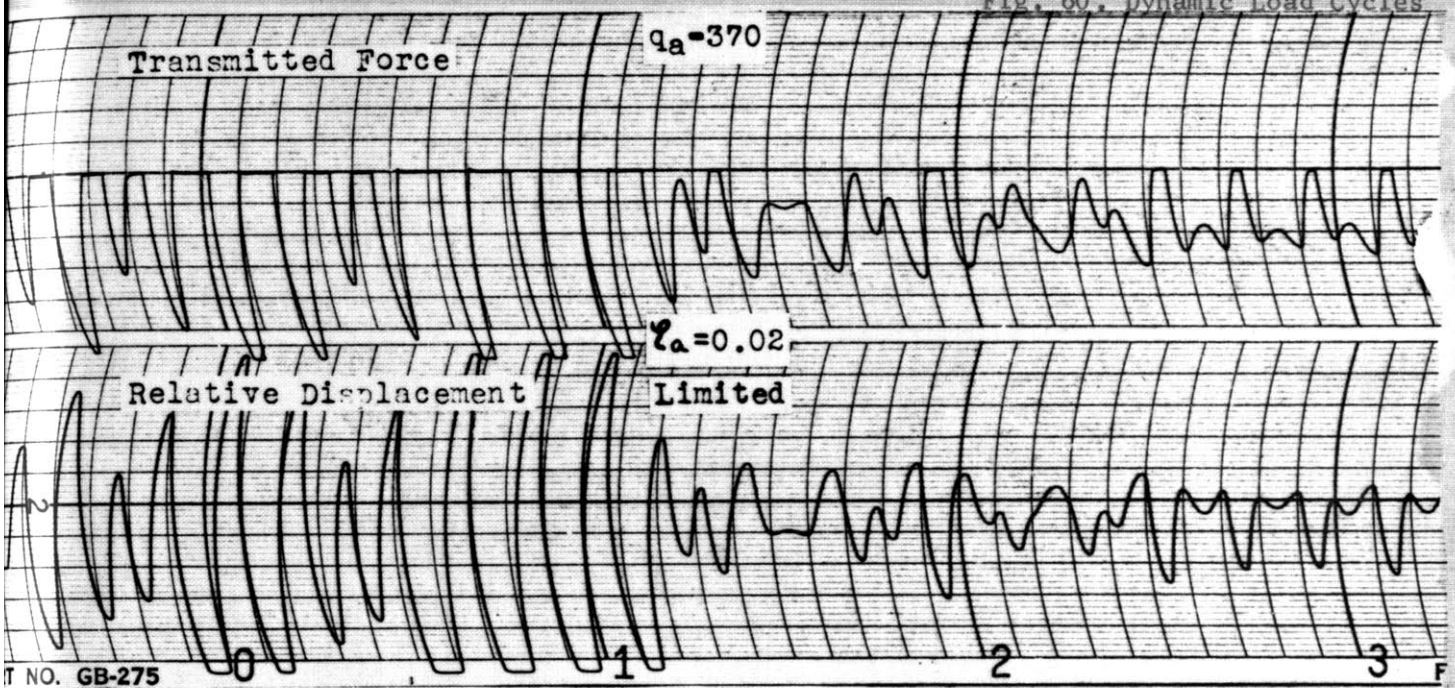

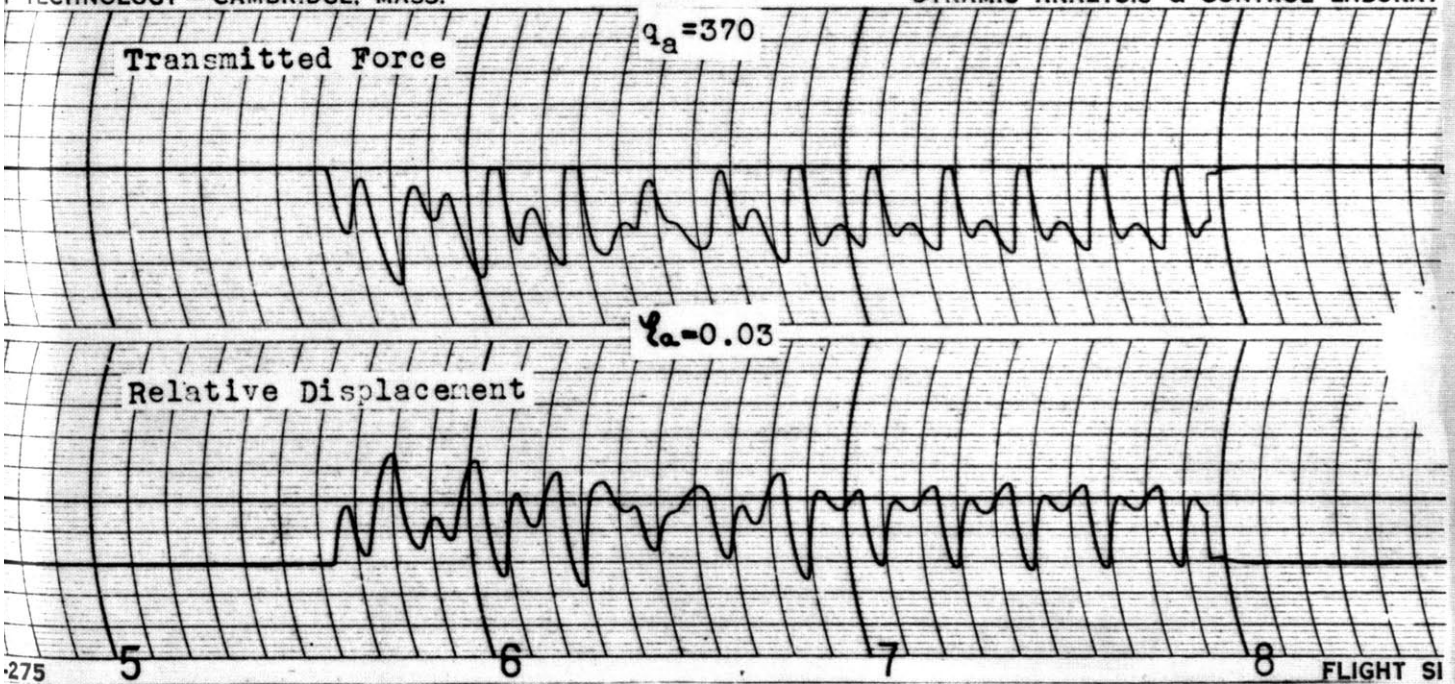

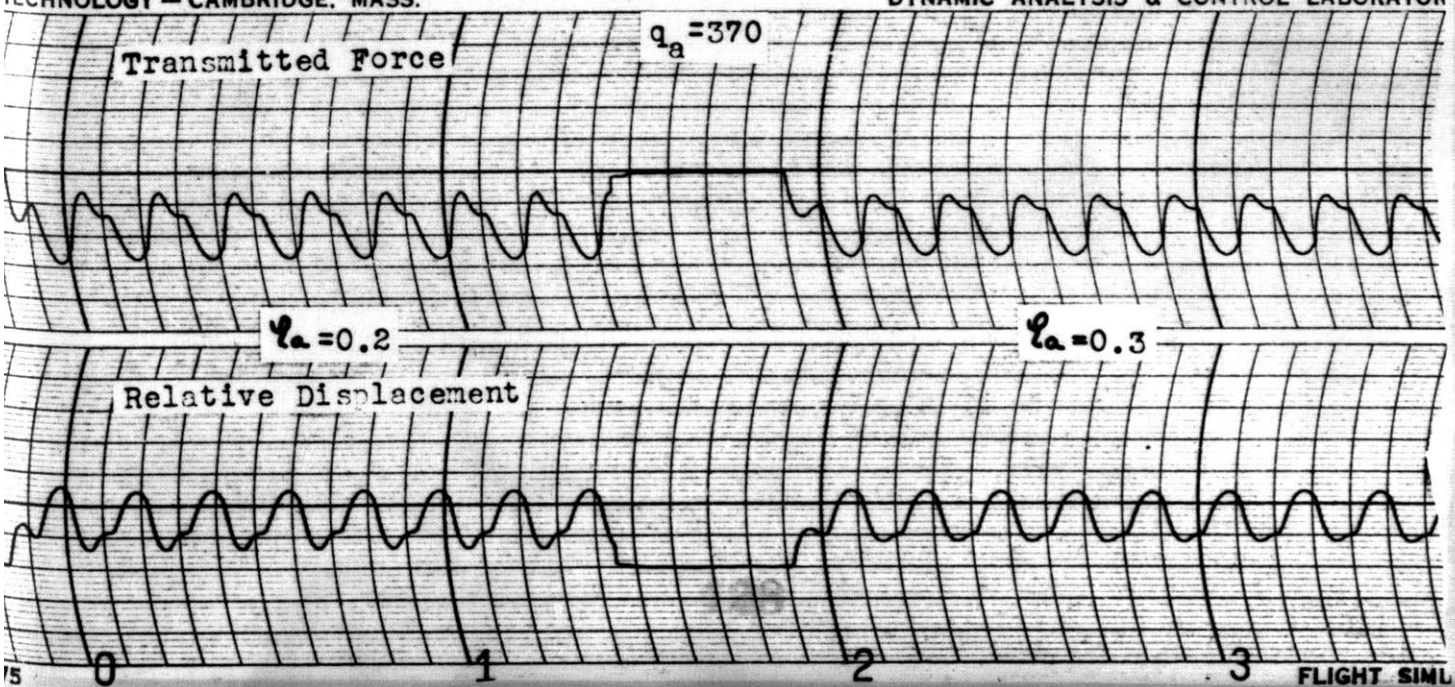

Fig. 61. Dynamic Load Cycles

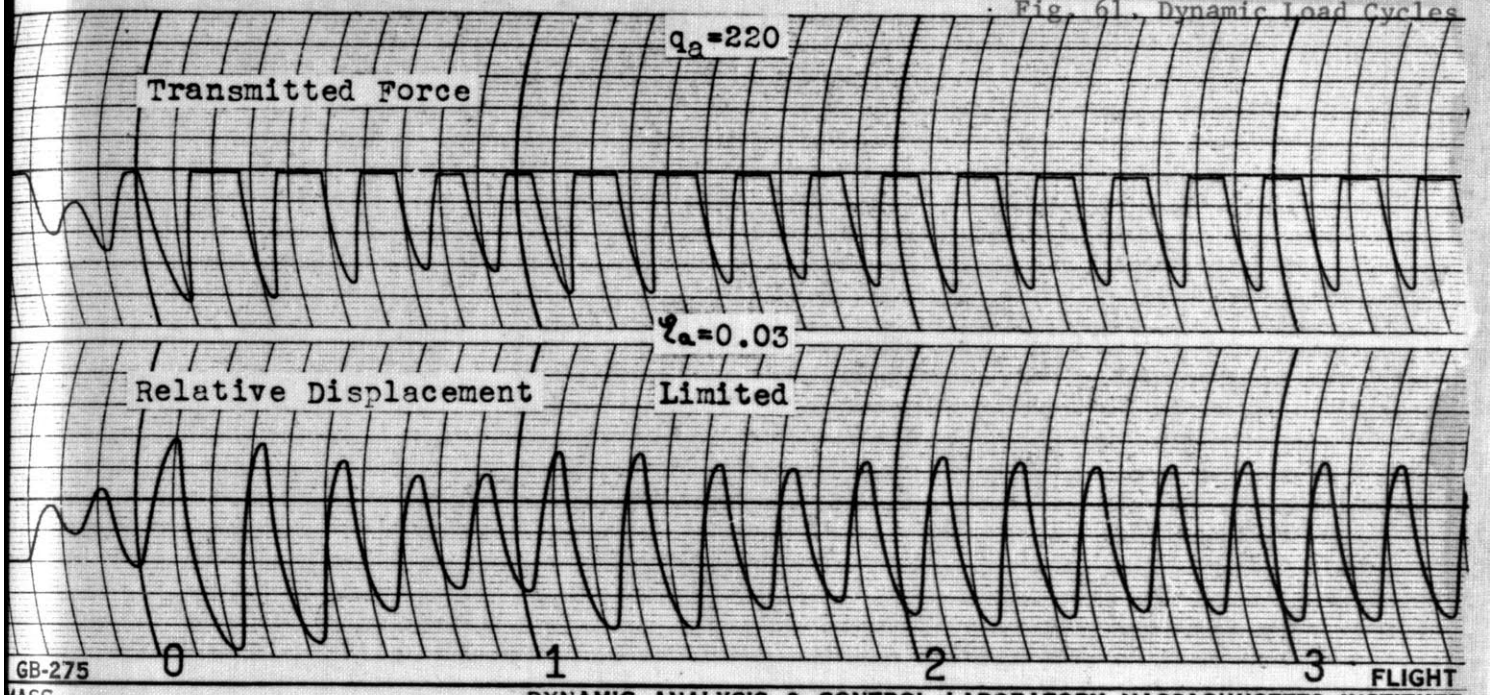

GB-275 FLIGHT
MASS. DYNAMIC ANALYSIS & CONTROL LABORATORY-MASSACHUSETTS INSTITUTE

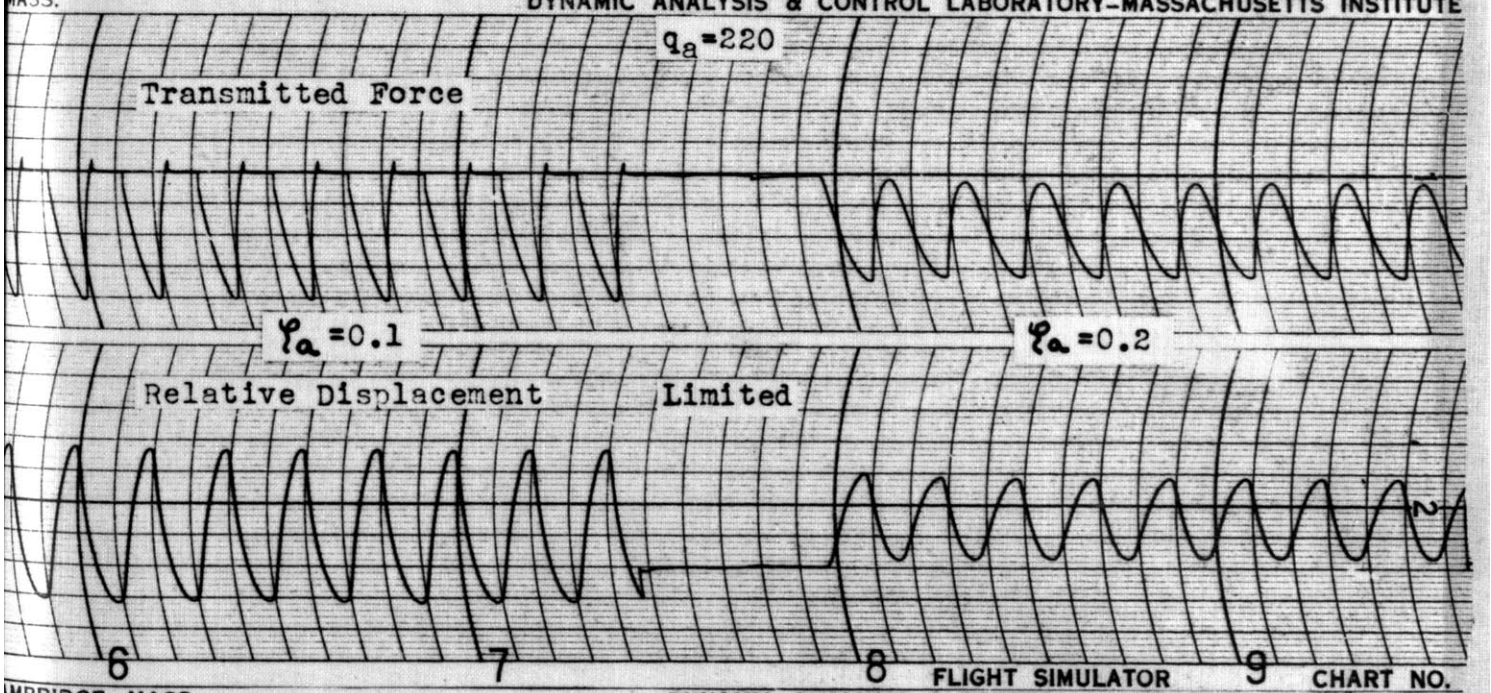

FLIGHT SIMULATOR CHART NO.
AMBRIDGE, MASS. DYNAMIC ANALYSIS & CONTROL LABORATORY-MASSACHUSETTS

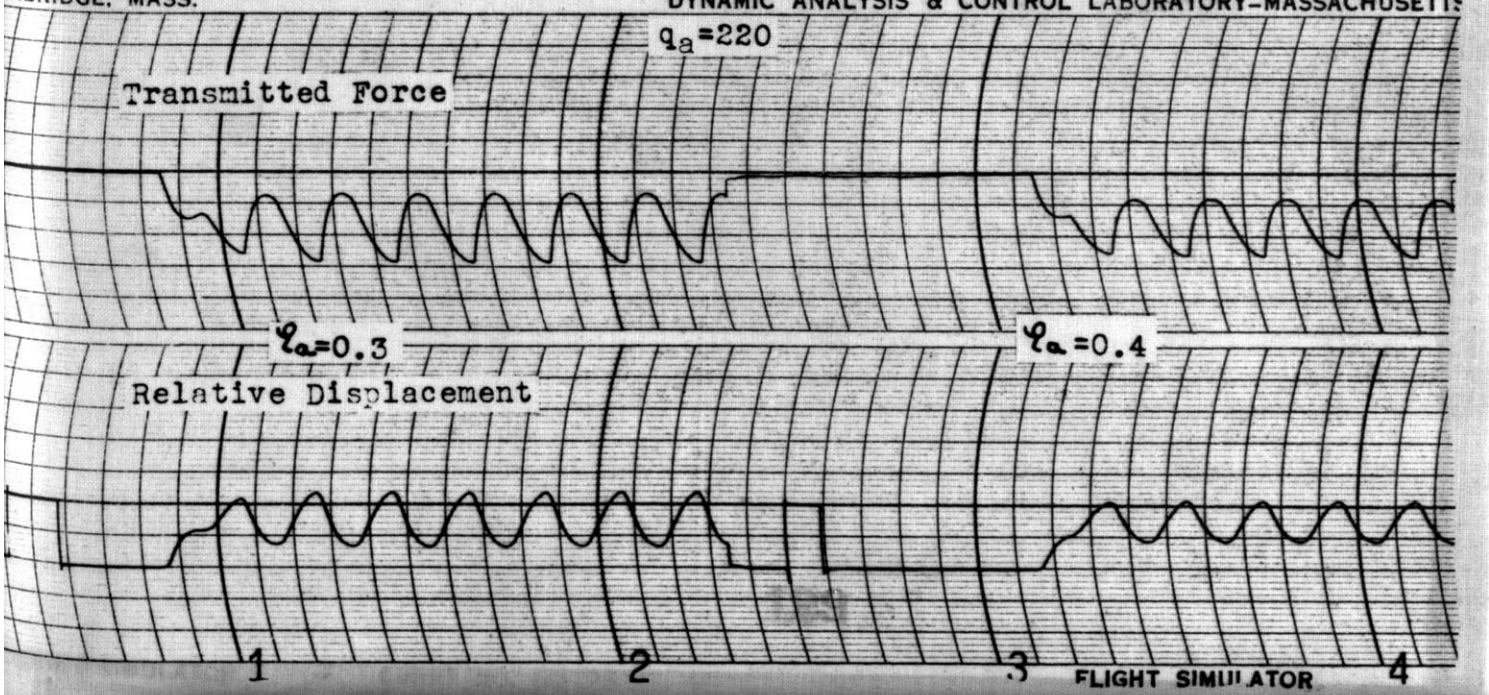

FLIGHT SIMULATOR

Fig. 62. Dynamic Load Cycles

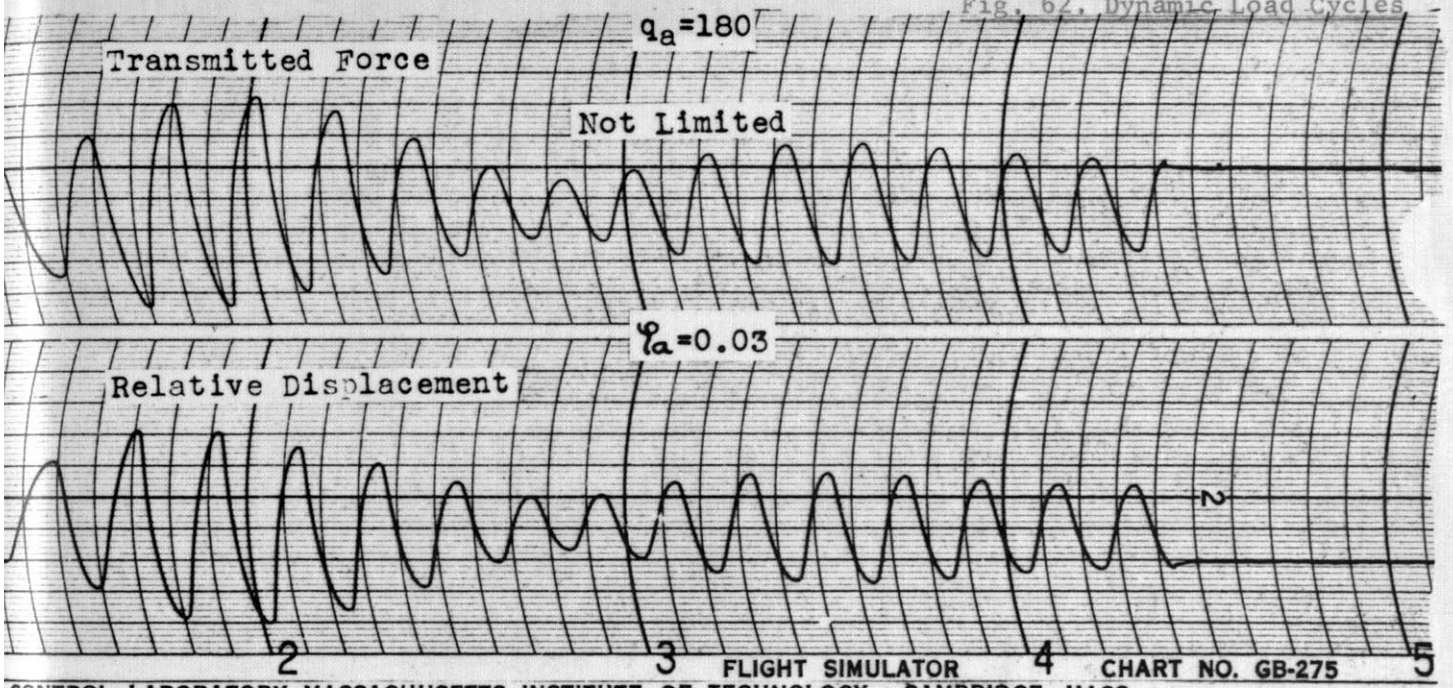

FLIGHT SIMULATOR CHART NO. GB-275

CONTROL LABORATORY-MASSACHUSETTS INSTITUTE OF TECHNOLOGY — CAMBRIDGE, MASS.

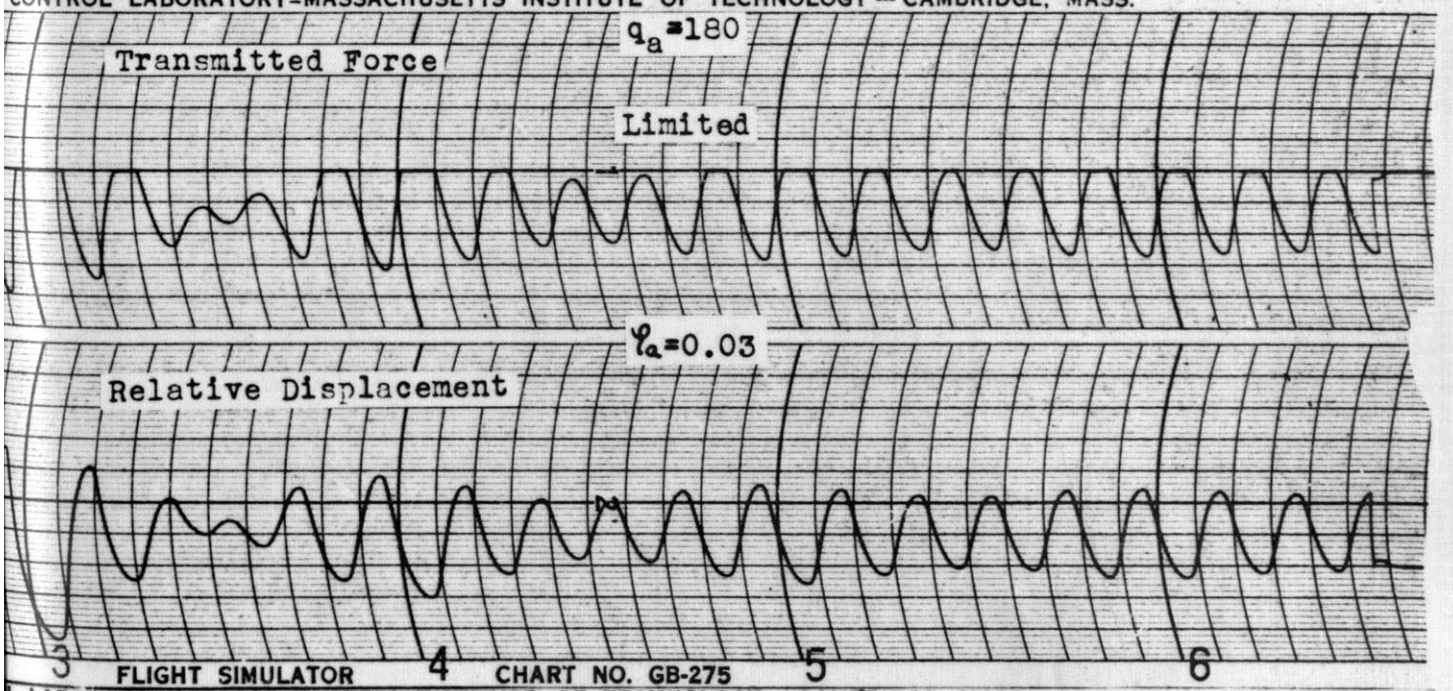

FLIGHT SIMULATOR CHART NO. GB-275

L LABORATORY-MASSACHUSETTS INSTITUTE OF TECHNOLOGY — CAMBRIDGE, MASS.

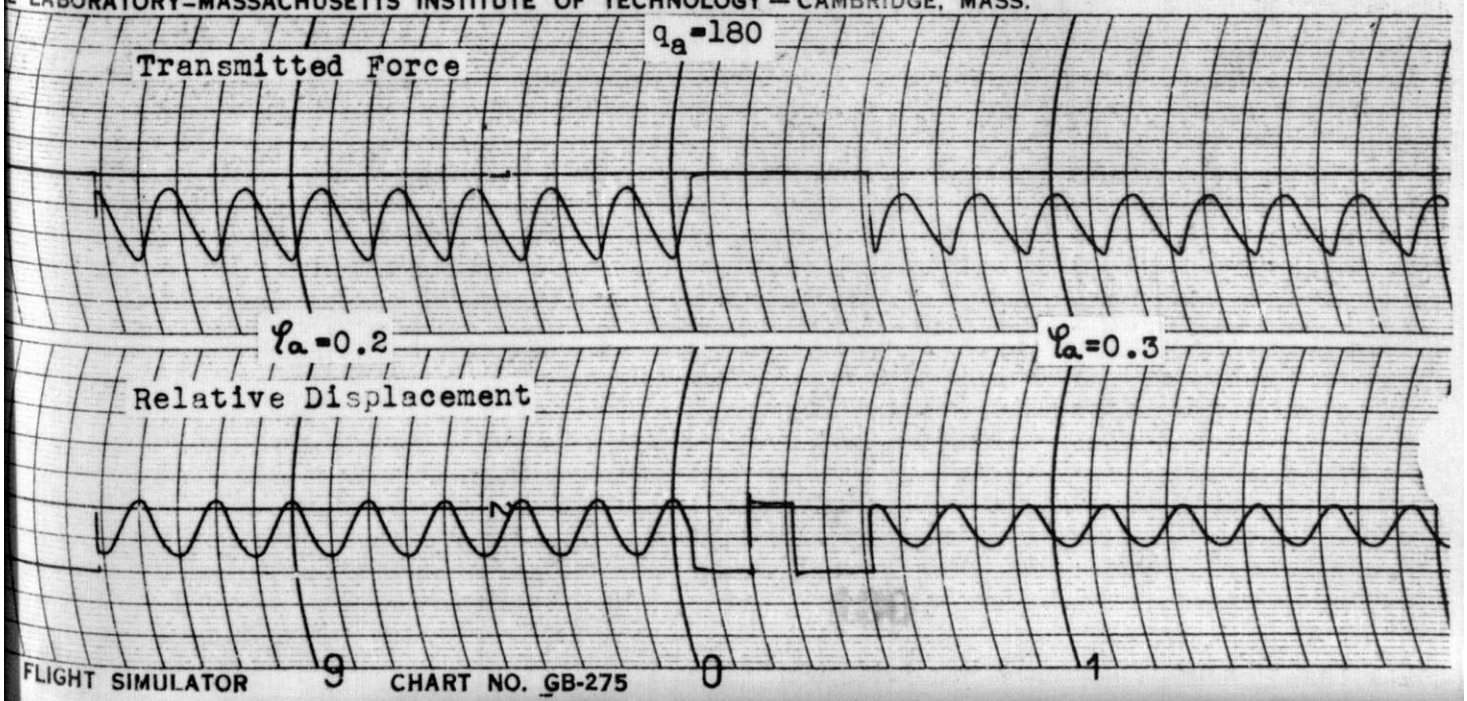

FLIGHT SIMULATOR CHART NO. GB-275

These qualitative conclusions emphasize the desirability of maintaining a certain degree of friction or effective damping in high-speed gears, both from the standpoint of minimizing dynamic loads and from the standpoint of insuring reproducible results in operation. To a certain extent this conclusion is obvious; however, the foregoing analysis serves to show qualitatively the exact consequences of inadequate damping and defines, at least to a degree, the meaning of "sufficient" damping.

6. Summary

General and simplified equations describing gear-tooth action under conditions of dynamic operation have been derived.

Two physical phenomena have been studied as causes of dynamic loads in gearing, these are

1. The oscillation of the gear spring-mass system induced by the engagement or disengagement of an isolated pair of teeth which contains an error due to manufacturing or elastic deformation. The magnitude of the dynamic increment loads produced by this single-engagement effect is limited to one half the tooth-pair spring-constant times the effective error in the case of heavily-loaded gears, and to the tooth-pair spring stiffness times the manufactured error in the case of lightly-loaded gears. The relative magnitude of the increment load is determined by β, the ratio of system period to tooth-engagement time, according to the curves given in Figs. 43 and 47.

2. The oscillation of the spring-mass system excited by the effective time-varying spring-stiffness of the gear mesh. The magnitude of the dynamic increment loads produced by the stiffness-variation effect is limited only by the effective damping that is present in the gear system. However, a relatively minute amount of damping ($\zeta_a > 0.3$) will serve to limit the dynamic increment loads to less than 20 per cent

of the average transmitted load, as shown in Figs. 49 and 50. In all cases, when pitch-line velocity becomes very large ($q_a < 150^\circ$), the dynamic load becomes <u>less</u> than the average transmitted load and <u>decreases</u> monotonically with increasing pitch-line velocity.

With the exception of occassional dynamic loads produced by peculiar combinations of profile error, it is believed that the effects studied in this chapter are the major factors that influence dynamic loads in spur gearing. The analysis presented is considered in part to be qualitative and is intended for use in interpreting the preliminary measurements of dynamic loads presented in Chapter 4. This interpretation then can be used as the basis for further and more rigorous analytical and experimental study of the most important or controlling factors in dynamic gear-tooth loads.

CHAPTER 4. EXPERIMENTAL INVESTIGATION OF GEAR TOOTH LOADS AND STRESSES

1. Experimental Apparatus

A dynamic gear-test machine was provided on a loan basis by the Caterpillar Tractor Company for use in this investigation. This machine is one of a series of test machines designed and built by the Caterpillar Tractor Company for use in various gear-research programs at the company's research laboratory. Figures 63 and 64 are photographs which show the test machine and the associated instrumentation. Figure 65 is a schematic diagram of the apparatus. Two pairs of gears (1.5 to 1 ratio) are mounted rigidly on parallel shafts and are connected in a back-to-back arrangement by gear couplings. One pair of gears is the test set and the other pair, which is precision-lapped helical, transmits torque back to the test set. By sliding one of the helical gears axially through a lever arrangement (loading linkage), the two transmission shafts are twisted and a mean torque level is established in the tandem circuit. An axial force is exerted on the sliding helical gear by means of a moment applied to the loading linkage. This axial force, together with the helix angle of the loading gears, determines the torque in the system. By this type of arrangement it is possible to apply high loads to the test-set at high rotational speeds without supplying or absorbing large amounts of power outside the test machine. A variable-speed D.C. motor is used to rotate the gear sets and to supply frictional losses which occur in the system. Continuous lubrication of the test gears is assured by spraying oil directly onto the gear teeth. Oil is circulated by a small hydraulic pump, and a filter in the lubrication system removes foreign particles from the oil. A heat exchanger also in the lubrication circuit, is used to maintain constant lubricant temperature. The oil temperatures in both gear boxes are monitored by thermocouple temperature gages. The rotational inertia of the test gears can be changed by adding disks directly to the gear blanks. In order to prevent slippage between the disks and the gears during dynamic operation, the inertia disks are coupled to the gear blanks by means of wedged, low-angle cup and cone arrangements.

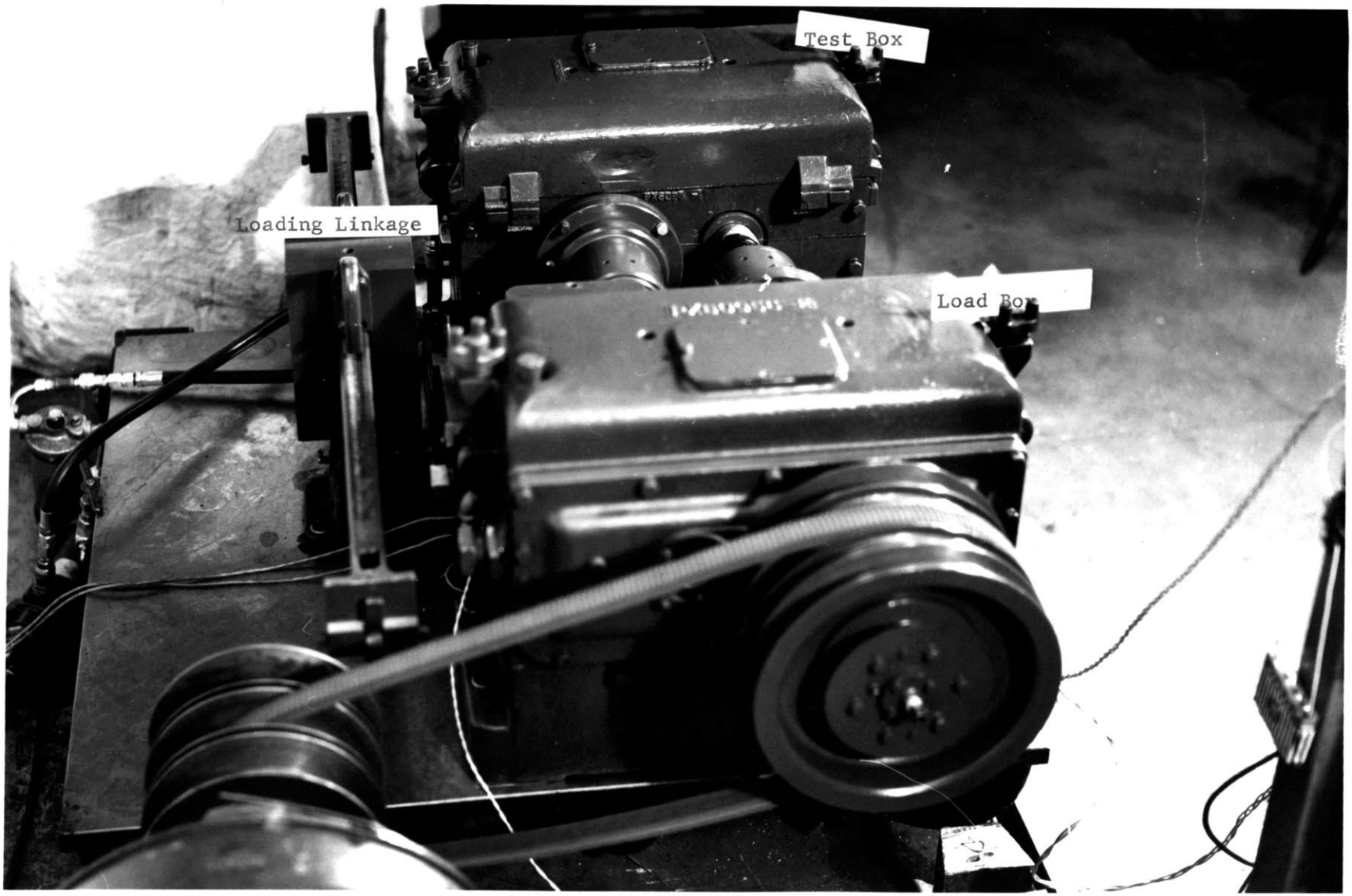

Fig. 63. Gear-Test Machine

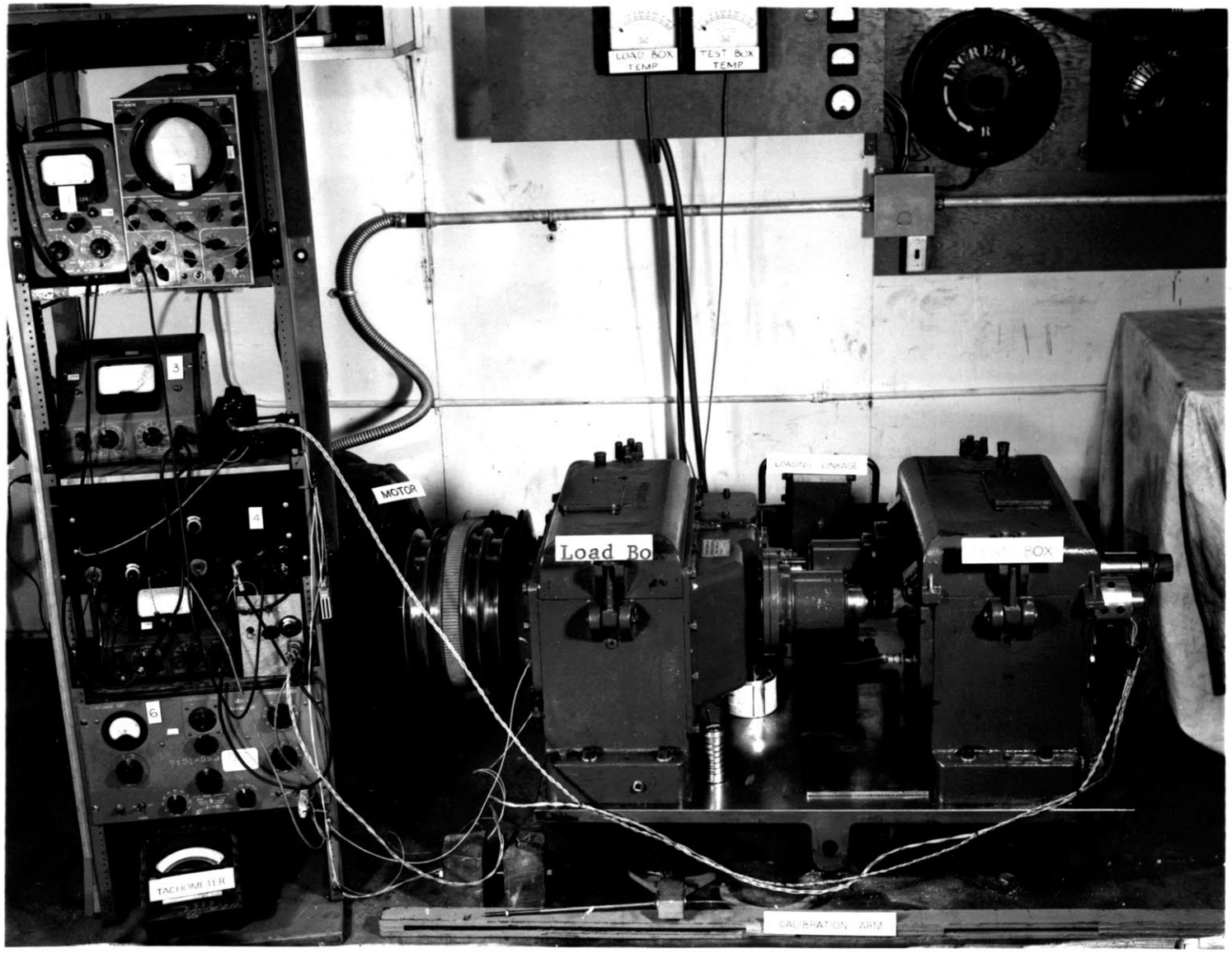

Fig. 64. Gear-Test Machine and Associated Instrumentation

The stress cycle for an individual tooth on the large gear was measured by means of 1/16 inch constantan-wire strain gages (A-19) which were bonded to the root sections of the teeth. These gages were attached to a gear tooth as shown in Fig. 65. The gages were connected so that stress caused by the radial or direct-compressive component of the tooth load would be cancelled out, and were placed some distance away from the root fillet and from the surface of the tooth in order to avoid stress concentrations and proximity effects due to the Hertzian contact stresses. Thus the gages were connected in such a location that they would indicate approximately the nominal or cantilever-beam stress in the tooth. Figure 66 shows the circuit arrangement and electronic equipment used in reading the strain gages. This equipment is shown in Fig. 64 and is identified by numbers attached to various components. A carrier frequency of 20 kc at 2.5 volts rms., supplied by a Hewlett-Packard Oscillator (6), was used to excite the strain-gage bridge. The output of the bridge was fed into an A.C. amplifier and demodulator (4) through a 10:1 ratio shielded input transformer. The filtered output of the demodulator was measured with a D.C. vacuum-tube voltmeter (1) and was observed on an oscilloscope (2). The A.C. output of the bridge circuit was monitored with an Instrument Electronics vacuum-tube voltmeter (3).

The torque level in the tandem gear circuit was indicated by other strain gages of 3/4 inch gage length bonded to one transmission shaft at 45° angles with the shaft axis. The electronic circuit for the torque strain gages is identical to that used for the tooth-stress gages. However, to minimize interference between the two strain-gage circuits, a carrier frequency of 5 kc (at 6 volts, rms.) was used to excite the torque strain gages.

The strain signals were transmitted from the rotating system to the measuring equipment through collector assemblies. A mercury-pool collector was designed and built for use in the tooth-stress circuit. This collector made use of a mercury contact between a moving and a stationary copper element in order to transmit the desired signals. The noise introduced by this collector was found to be very slight even at the maximum

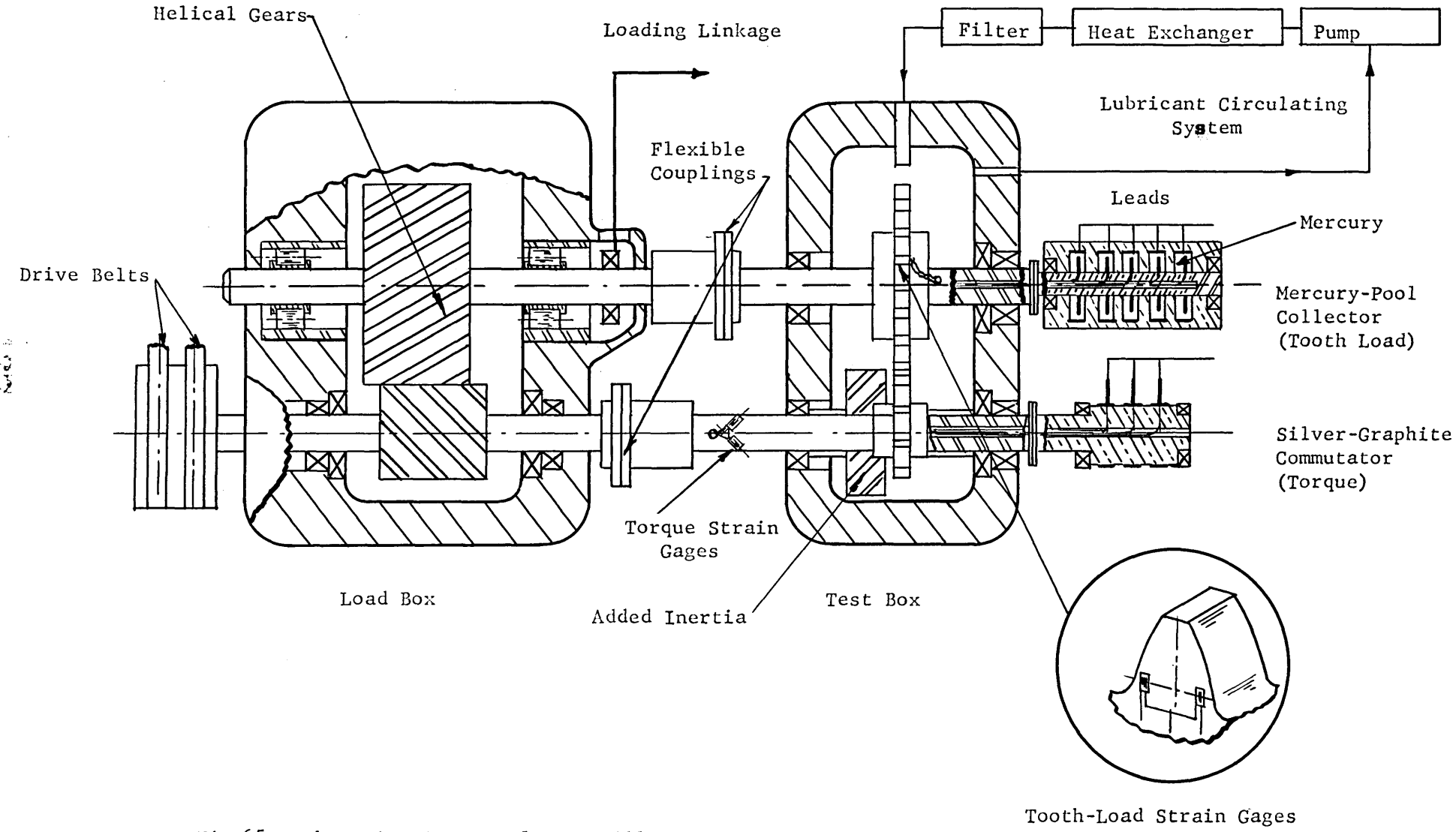

Fig.65, Schematic Diagram of Caterpillar Tractor Company Gear Testing Machine, Showing Instrumentation for Measuring Dynamic Loads in Gear Teeth.

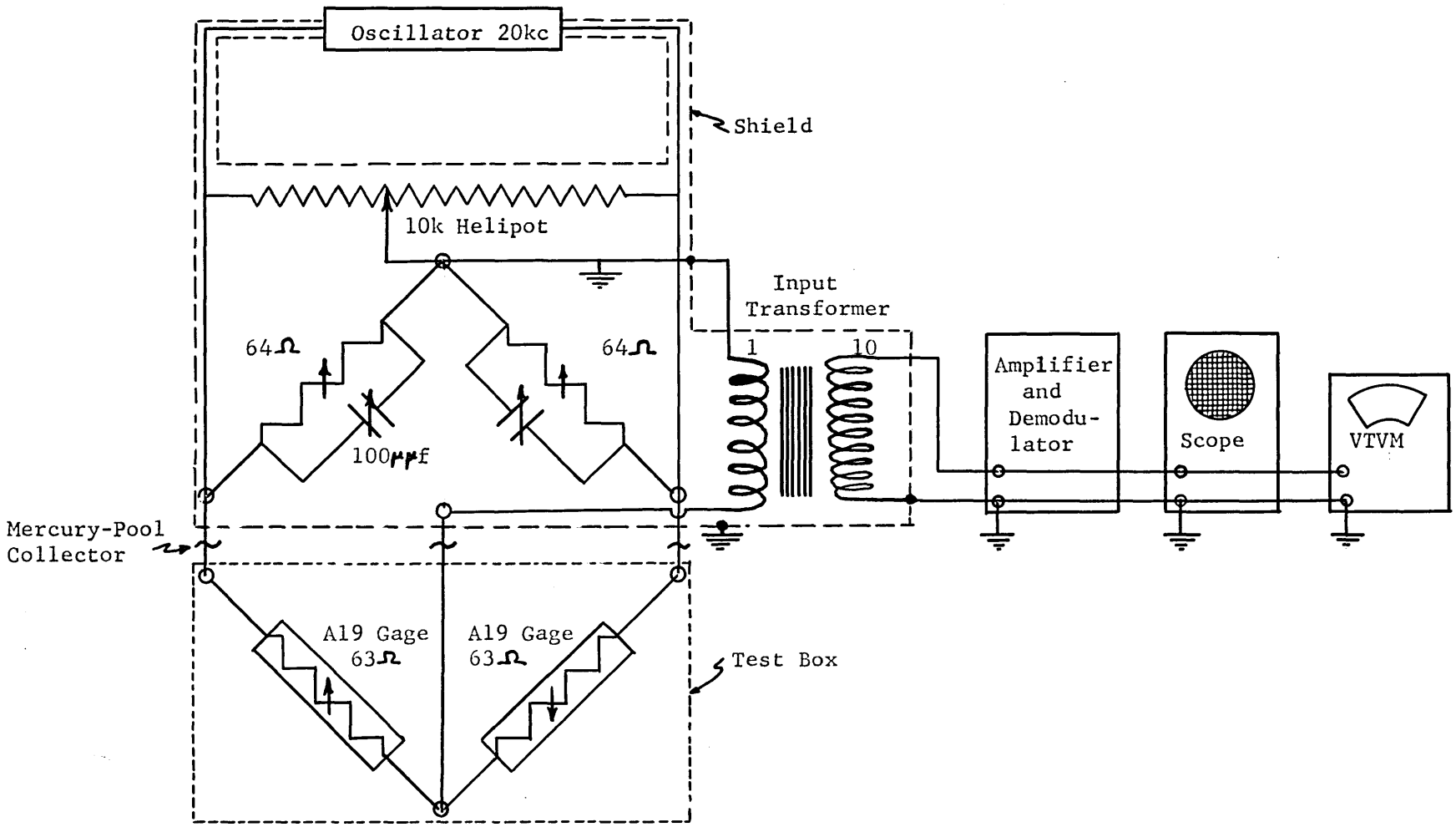

Fig. 66. Circuit for Measuring and Recording Dynamic Stress in a Gear Tooth

speed of about 1000 rpm. The noise level under operational conditions due to all causes corresponded to less than 10 lbs. of tooth load. Some difficulty was encountered with the mercury collector due to the active chemical nature of the mercury. Oxidation of the mercury is relatively rapid, and the collector must be disassembled and cleaned, and fresh mercury must be added about once a month. The mercury also reacts with soldered connections and causes the solder to become semi-liquid. Therefore, great care must be taken to protect from the mercury any soldered connections that rotate. In the collector used in this investigation, the rotor assembly was encased or potted in a plastic material which left exposed only the outer edges of 1/8 inch thick copper disks. Deterioration of contacts and wires on the stationary part of the collector is not as much of a problem as on the rotor, since the connections on the stator are not stressed and can be replaced in a relatively easy manner. The torque strain signals, which were considered less critical, were transmitted through a standard silver-graphite brush assembly. This arrangement was far less satisfactory than the mercury collector as far as noise was concerned, but it gave acceptable results. The maintenance problems are, of course, less severe in the mechanical collector than in the mercury device. The collector assemblies are shown in the schematic diagram, Fig. 65, and are visible in the photograph of the test machine, Fig. 64.

A generator-tachometer was used to measure speed of the gear system in rpm, and the electrical inputs to the drive motor were monitored with ammeters and voltmeters.

Calibration of the strain gages was accomplished by means of a calibration arm, shown in Fig. 64, that was attached to one of the test-gear shafts while the other shaft was held fixed. The load box was disconnected from the test box during calibration. The torque system was calibrated by sliding a known weight along the calibration arm and recording the corresponding output of the torque strain gage system. A sample torque-gage calibration is given in Fig. 67. The calibration of the tooth-load strain gages varies as a function of the position of the contact point between mating teeth and of load inclination. Therefore, calibrations were made for various

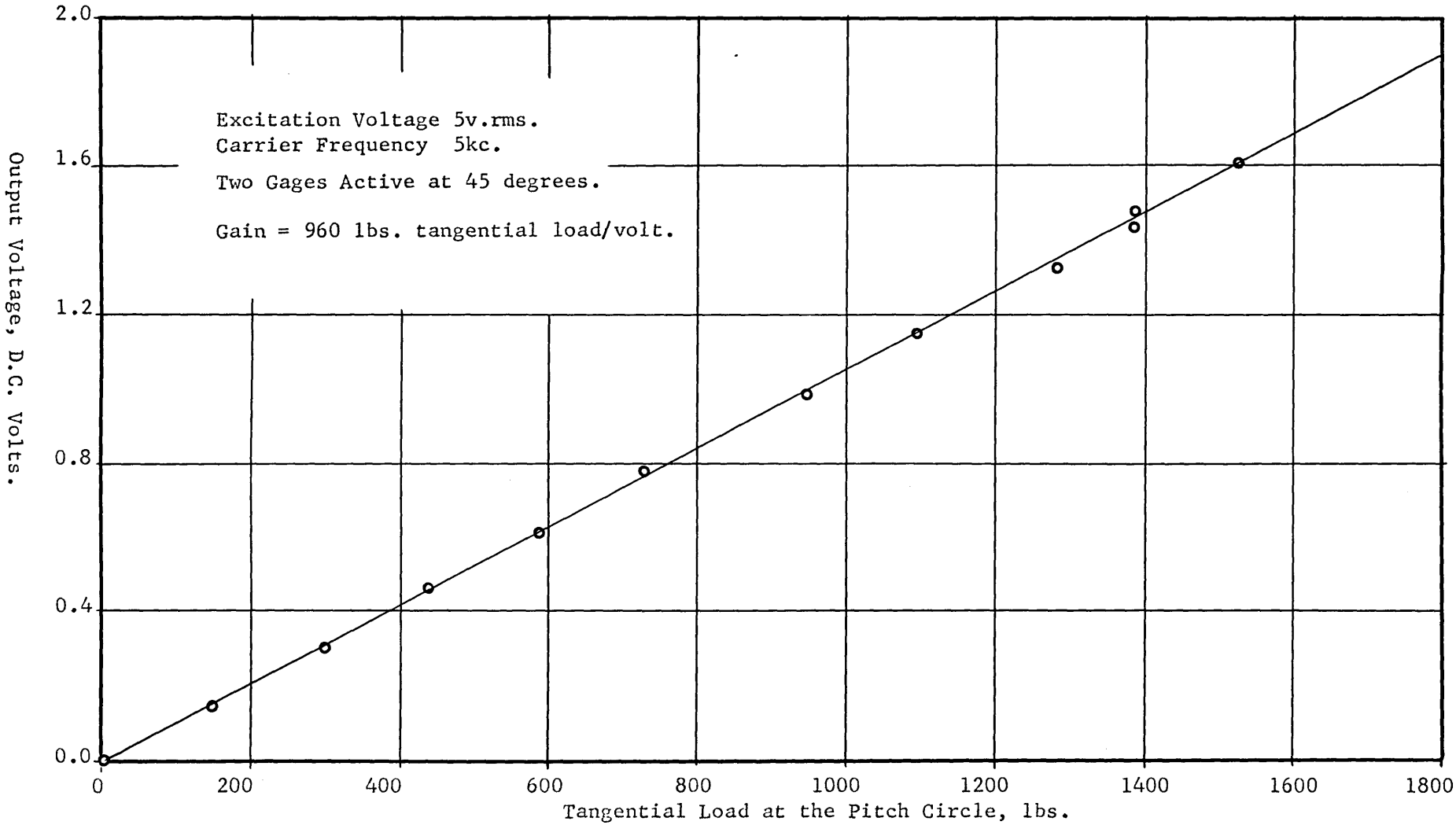

Fig. 67. Torque Strain-Gage Calibration

points of contact along the tooth surface. During a given calibration run, the point of contact between mating teeth was maintained always at the same location by indicating gear position with a dial gage. Figure 68 shows a sample calibration for tooth-load for conditions of contact at the pitch point.

2. Tests of Precision Gears

A set of precision-ground gears were supplied for use in this study by the Caterpillar Tractor Company and the Pratt and Whitney Tool Company. The characteristics of these test gears are listed in Chapter 2, Paragraph 12.1. These gears were instrumented with strain gages and were installed in the test machine. Calibration of the gages was carried out as described in paragraph 1 of this chapter.

2.1. Static-Stress Measurements

The static stress cycles shown in Fig. 36a were obtained by rotating the instrumented tooth through the loaded gear mesh by hand. The horizontal sweep was obtained by means of a rotary potentiometer attached to the test-gear shaft. The stress cycles maintained the same general shape as the transmitted-load was varied but the engagement and disengagement regions broadened out at high loads. The effects of friction on the static stress cycles were quite pronounced near the pitch-point but were small in other regions of the stress cycles. Comparison between these measured cycles and theoretical predictions was made in Figs. 34 and 35 of Chapter 3.

2.2. Dynamic-Stress Measurements

Figures 69 to 71 show representative records of dynamic stress measured in the precision test gears under operational conditions. The transmitted load W_o employed in these tests was 2830 lbs./in. However, there was very little difference in the shape of the stress cycles as the transmitted load was varied. Pitch-line velocity was varied from 0 to 2360 ft/min.

The effective mass at the base circle for the gear blanks and one added inertia disk (see Fig. 65) was computed to be 5.41 lbs. From Chapter 2, the spring constant for pitch-point contact is found to be

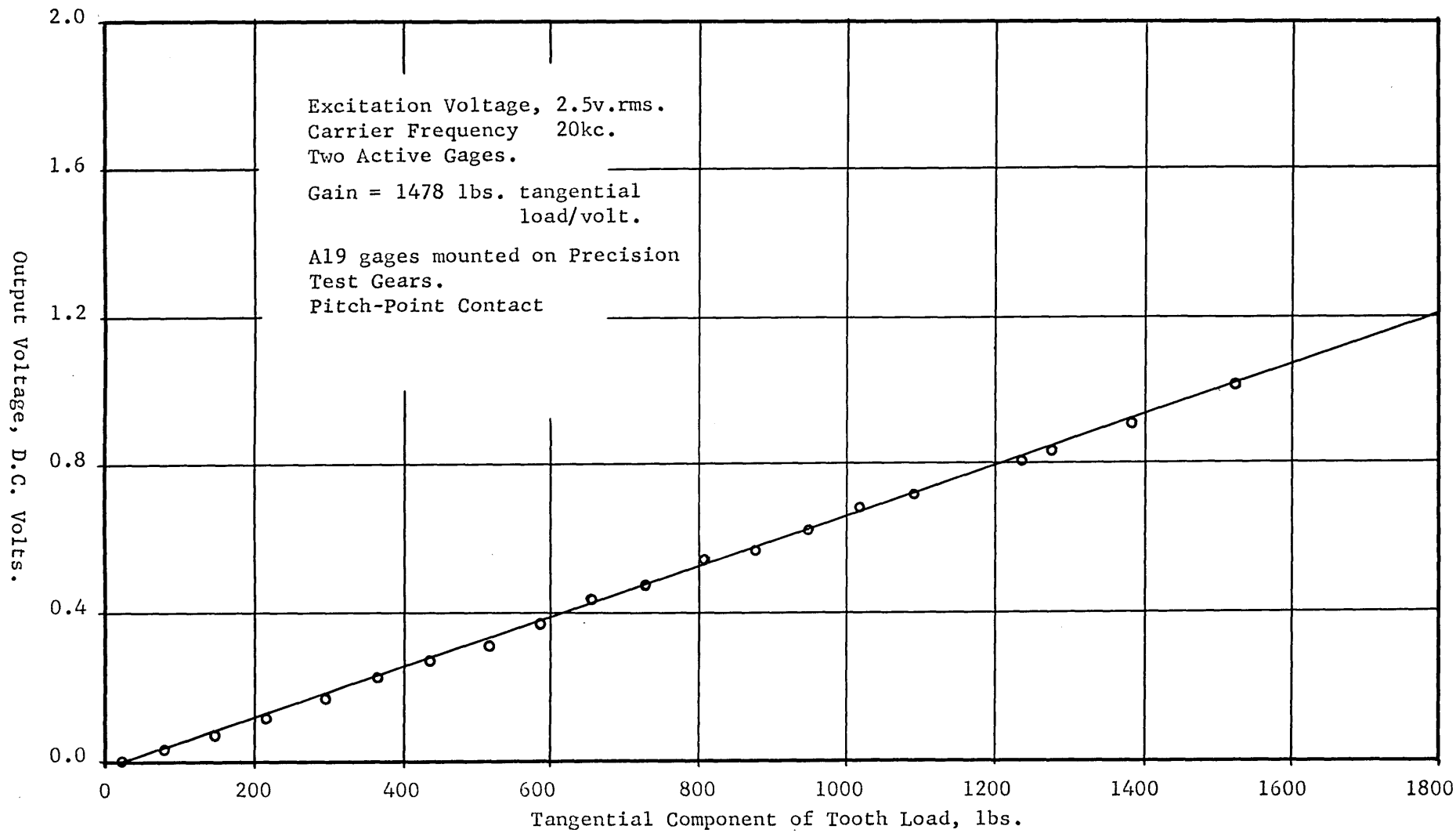

Fig. 68. Tooth-Stress Strain-Gage Calibration Curve for Contact at the Pitch Point.

a) 400 rpm. 60 cps.timing Wave

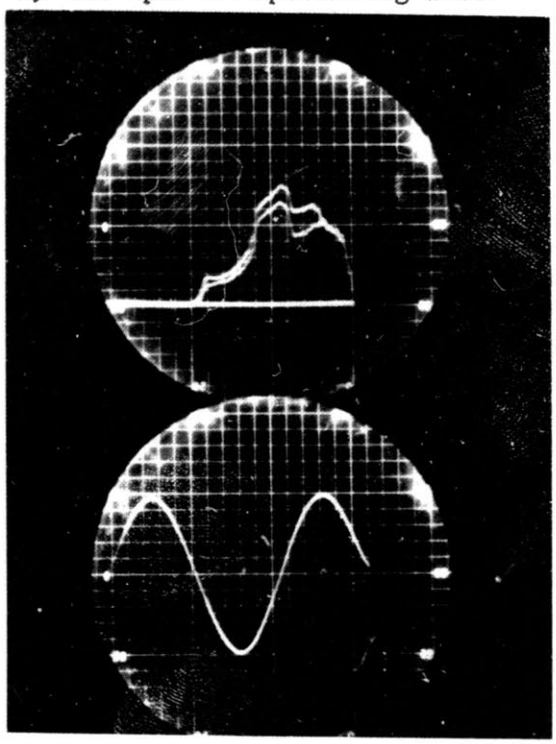

b) 435 rpm. 60 cps.timing wave

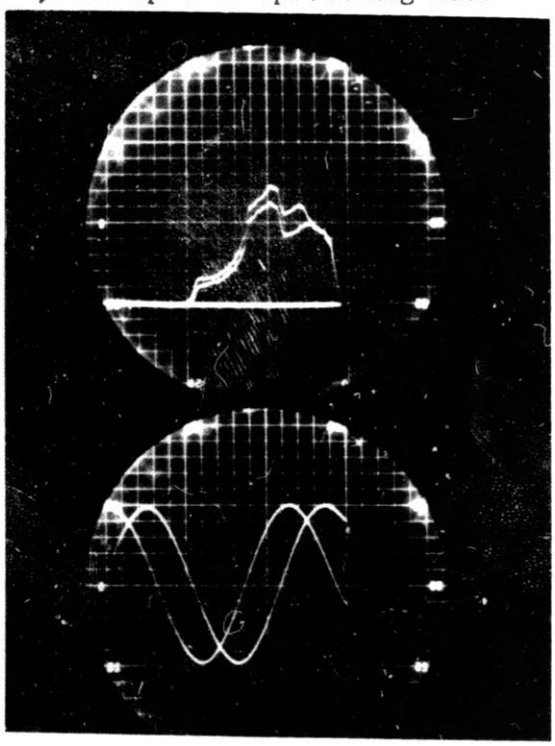

c) 650 rpm. 60 cps.timing wave

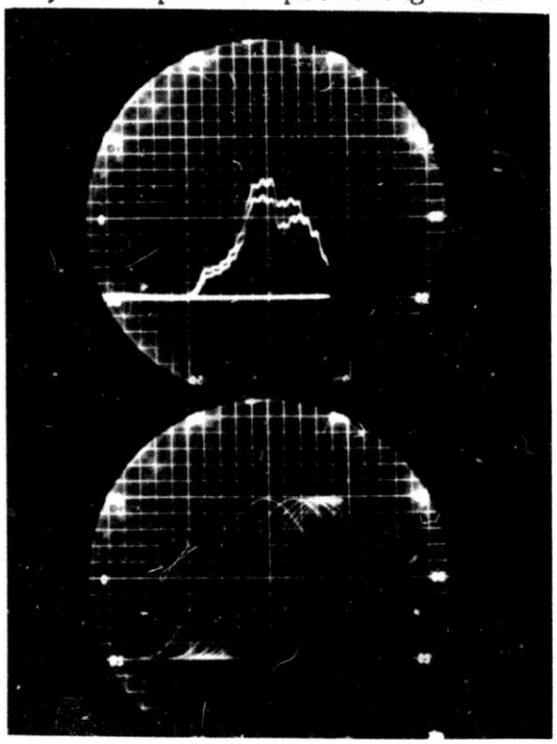

d) 710 rpm. 3600 cps.timing wave

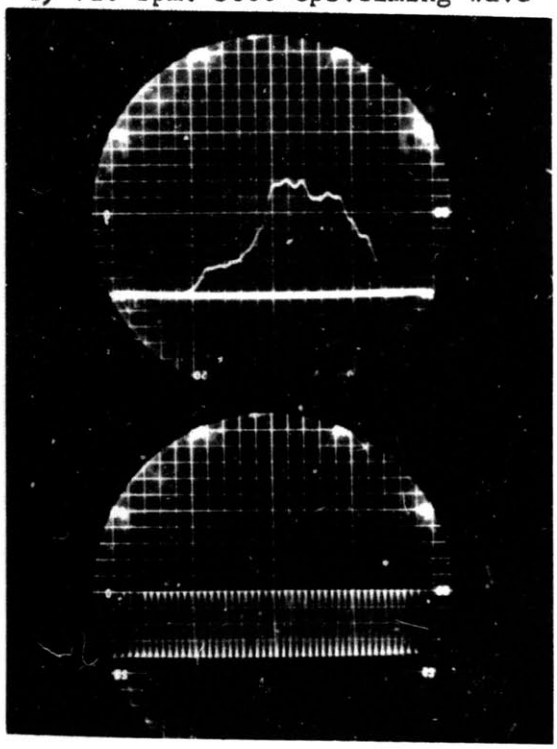

Fig. 69. Dynamic Stress Cycles for Precision Test Gears, at a Transmitted Load of 2830 lbs/inch.

a) 813 rpm. 3600 cps.timing wave

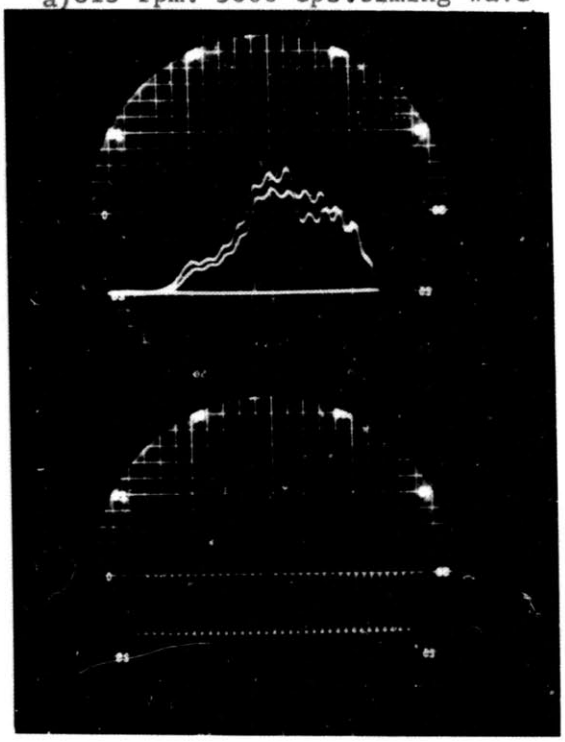

b) 830 rpm. 60 cps.timing wave

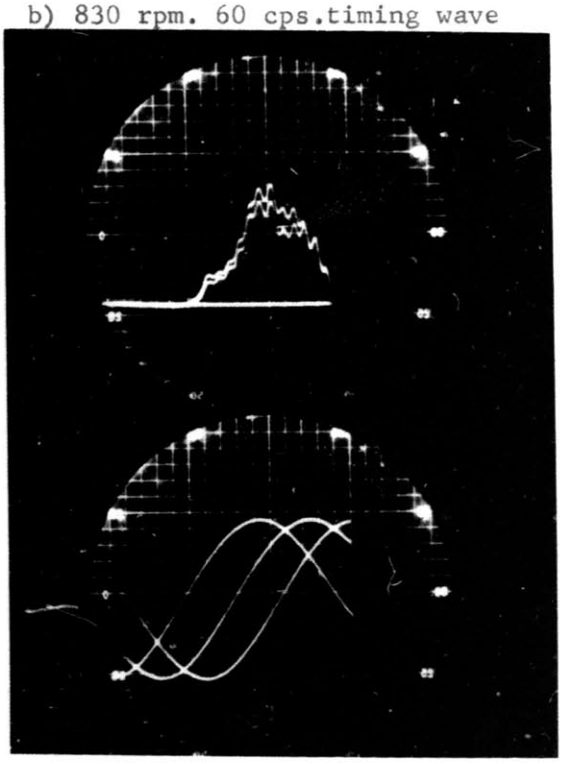

c) 1100 rpm. 3600 cps.timing wave

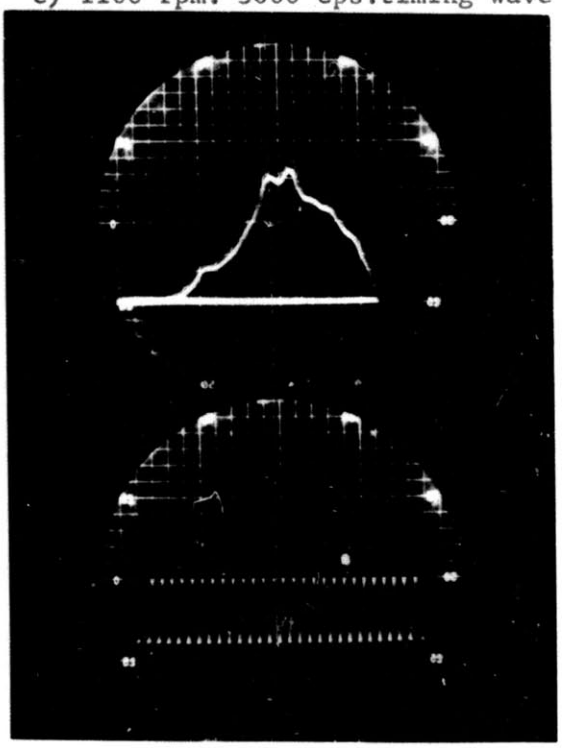

d) 1180 rpm. 3600 cps.timing wave

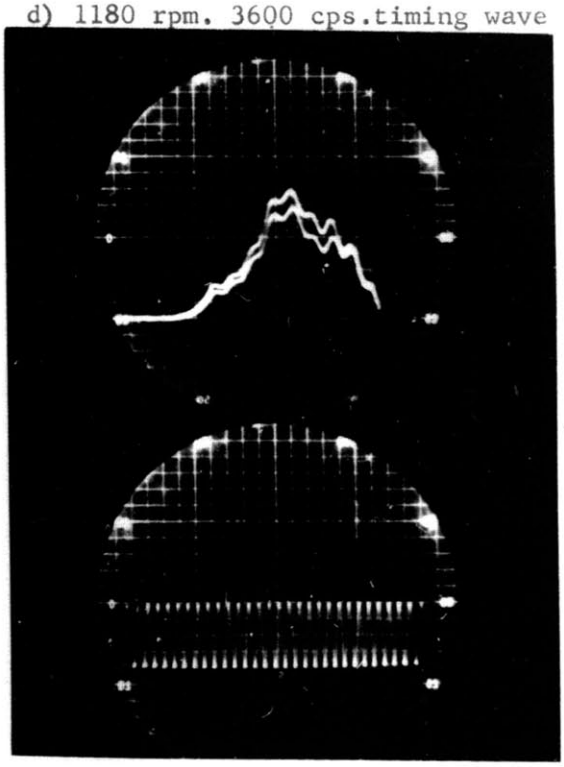

Fig. 70. Dynamic Stress Cycles for Precision Test Gears, at a Transmitted Load of 2830 lbs/inch.

a) 1270 rpm. 3600 cps.timing wave

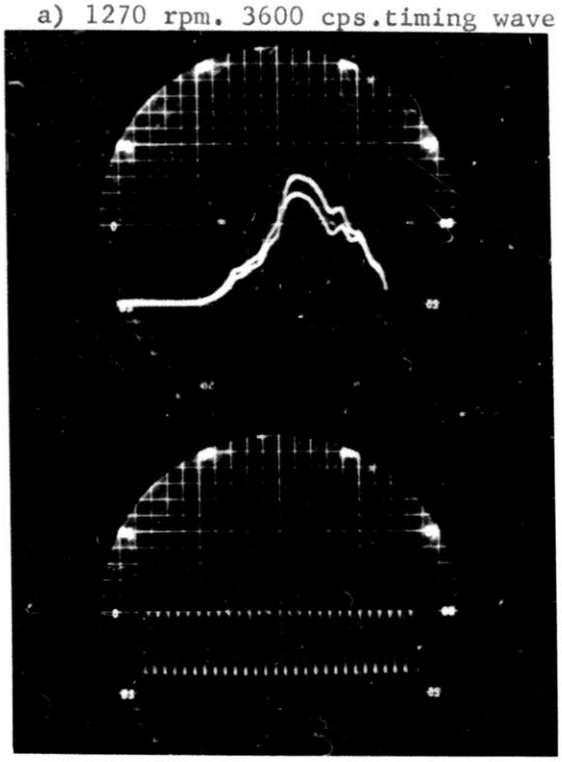

b) 1400 rpm. 3600 cps.timing wave

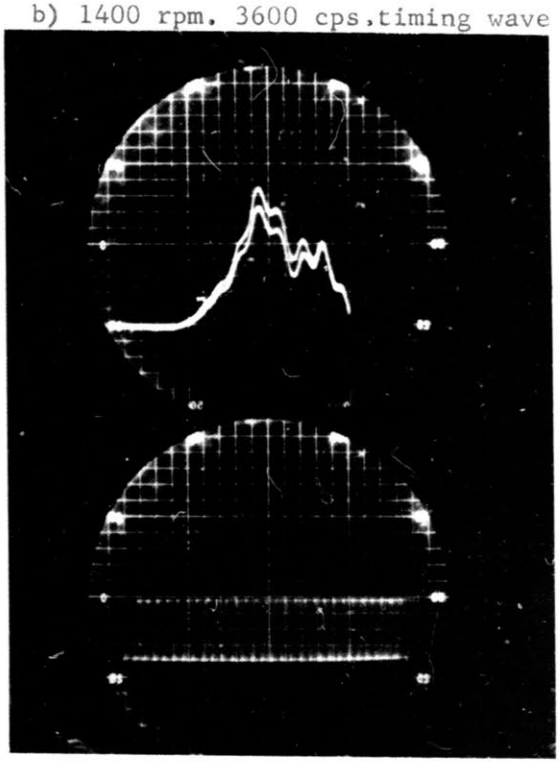

c) 1450 rpm. 3600 cps.timing wave

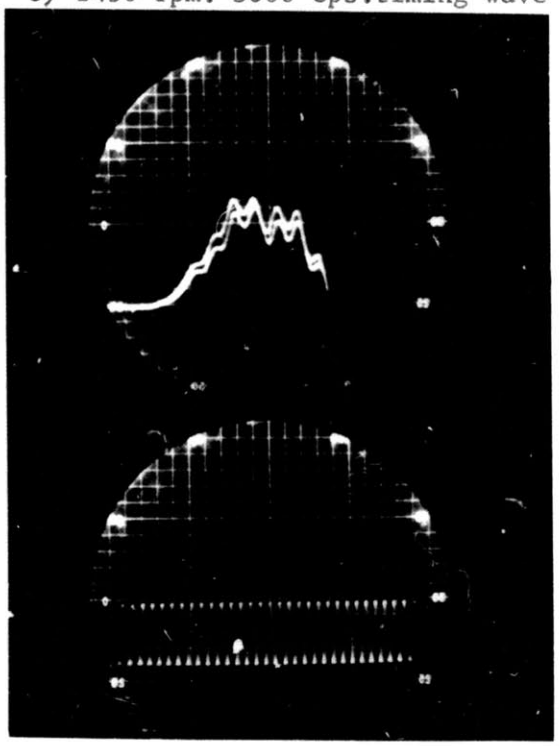

d) 1650 rpm. 3600 cps.timing wave

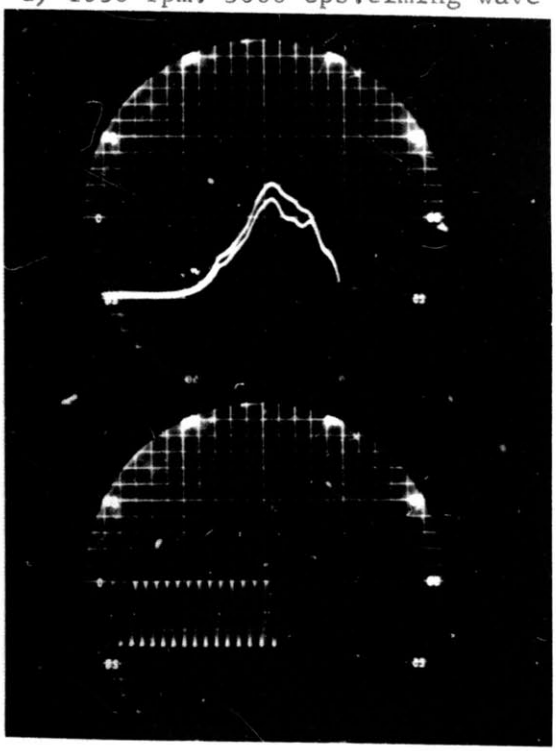

Fig. 71. Dynamic Stress Cycles for Precision Test Gears, at a Transmitted Load of 2830 lbs/inch.

1.25×10^6 lbs/in. Thus the natural frequency ω_n is predicted to be approximately 1500 cps. The frequency of oscillation in the vicinity of the pitch point was observed to be approximately 1560 cps (see Figs. 69 to 71).

The computed value of the frequency-ratio β for single load-transfer dynamics varied from about 0.22 in Fig. 69a to about 0.9 in Fig. 71d. However, the continuous increase of dynamic increment load from zero at low speeds to one half of the static transmitted load at $\beta \approx 0.4$ was not observed. In fact, in all of the dynamic stress measurements that were run, an increment load in excess of about 15 per cent of the transmitted load was never observed. Oscillations in the dynamic stress occurred but these oscillations never resulted in very large increment loads.

As the rotational speed of the gears was increased, the maximum dynamic stress exhibited slight successive increases and decreases. These variations were apparent both in the appearance of the dynamic stress cycles and in the intensity of sound which emanated from the test-gear box. The maxima of sound intensity corresponded with the most oscillatory stress cycles. For example, the stress cycles shown in Fig. 71a and d corresponded to minima in sound intensity while the cycles shown in Fig. 71b and d corresponded to maxima in intensity. Generally, the maxima of dynamic stress were near to, although not coincident with, the maxima of sound intensity.

The qualitative behavior exhibited by the measured dynamic stress cycles is described by the variable-elasticity model presented in Chapter 3. The measured results cannot be compared quantitatively with the theoretical predictions of Figs. 49 and 50 because the operating contact-ratio for the measured cycles differs considerably from the contact ratio assumed in computing the theoretical curves. Qualitative comparison can be made between the measured stress cycles and the load cycles sketched on Figs. 49 and 50 by observing the shape of the vibration that occurs in the region of single tooth-pair contact. For example, Fig. 70a corresponds

qualitatively to $q_a \approx 780^\circ$ in Fig. 50, Fig. 70c corresponds to $q_a \approx 670^\circ$ in Fig. 50, and Fig. 71c corresponds to $q_a \approx 375^\circ$ in Fig. 49. The value of effective damping ratio (ζ_a) appears from the preliminary test results to be appreciable; that is, of the order of 0.3.

In all cases the measured dynamic stress cycles were extremely consistent. Most of the photographs shown in Figs. 69 to 71 are time exposures of several different stress cycles. In the majority of these pictures, two different shapes of stress cycles appear. These two shapes occur because the instrumented tooth on the gear mates with two different teeth on the pinion (due to the 1.5 to 1 ratio). Owing to a small amount of pitch-line runout in the test and loading gears, the transmitted torque in the tandem gear circuit varies slightly as the gears rotate. The variation in torque during one load cycle is negligible, but the variation during one revolution of the large gear is sufficient to cause the variation in stress that is observed in Figs. 69 to 71.

The sudden jump in stress which occurs at the pitch point under static conditions (see Fig. 36) disappears completely at a relatively low speed. In Fig. 69a, a slight amount of this static friction effect still is visible near the pitch-point, but in Fig. 69b it essentially has disappeared.

The tentative conclusions are reached, as a result of the preliminary dynamic stress measurements discussed in this paragraph, that the variable-elasticity phenomenon is a significant factor in dynamic loads in accurately machined, heavily loaded gearing. The single-engagement theory does not appear to describe the behavior of such heavily loaded gear systems. It is therefore suggested that further analytical and experimental studies be made of the variable elasticity phenomena.

3. Tests of Production-Grade Gears

A set of shaved, heat-treated gears were provided by the Caterpillar Tractor Company for use in setting-up and checking-out the test machine and instrumentation prior to installation of the precision test gears described in paragraph 2. The characteristics of the production-grade test gears are described in Paragraph 12.2 of Chapter 2.

3.1. Static Stress Measurements

The static stress cycles shown in Fig. 37 were measured as described in Paragraph 2.1 of this Chapter. Comparison between the measured and calculated static stress cycles is given in Figs. 38 and 39 of Chapter 2. These gears had manufactured errors of the order of 2×10^{-3} inches; however, most of this error was in the form of profile errors, and had the effect of making the static stress cycle much smoother than it would be if no manufactured errors were present.

3.2. Dynamic Stress Measurements

The dynamic stress cycles for the gears just described behaved in the same manner as the stress cycles for the precision test gears. In this case no dynamic increment loads in excess of about 10 per cent of the static loads were observed, and in most instances almost no increment load was observable.

4. Dynamic-Load Measurements of Rettig

Rettig[46] has completed an extensive program of measurement of dynamic loads in gearing. Tests were run on precision ground gears which had controlled amounts of spacing error.

Rettig found that in very heavily-loaded gears, no appreciable dynamic increment loads occurred. However, in lightly- or moderately-loaded gears increment loads of considerable magnitude were observed.

A series of "average" curves were presented (Ref. 49, p. 131) which give conservative estimates, over most ranges of parameters of the dynamic increment loads. These increment loads were plotted as functions of pitch-line velocity for three different values of load and four different values of spacing error. The controlled spacing errors were machined only into one tooth of one of the test gears. The data from Rettig's dynamic load curves have been plotted in Fig. 72. The increment load W_i as given by Rettig has been divided by the effective error, as indicated by Eqs. (3.49) and (3.57) of Chapter 3. The abscissa of Fig. 72 is plotted in terms of the ratio of the pitch-line velocity to the square root of the effective error ($v/\cos\theta\sqrt{e}$). According to the single-engagement theories presented in Chapter 3, all of the data presented in

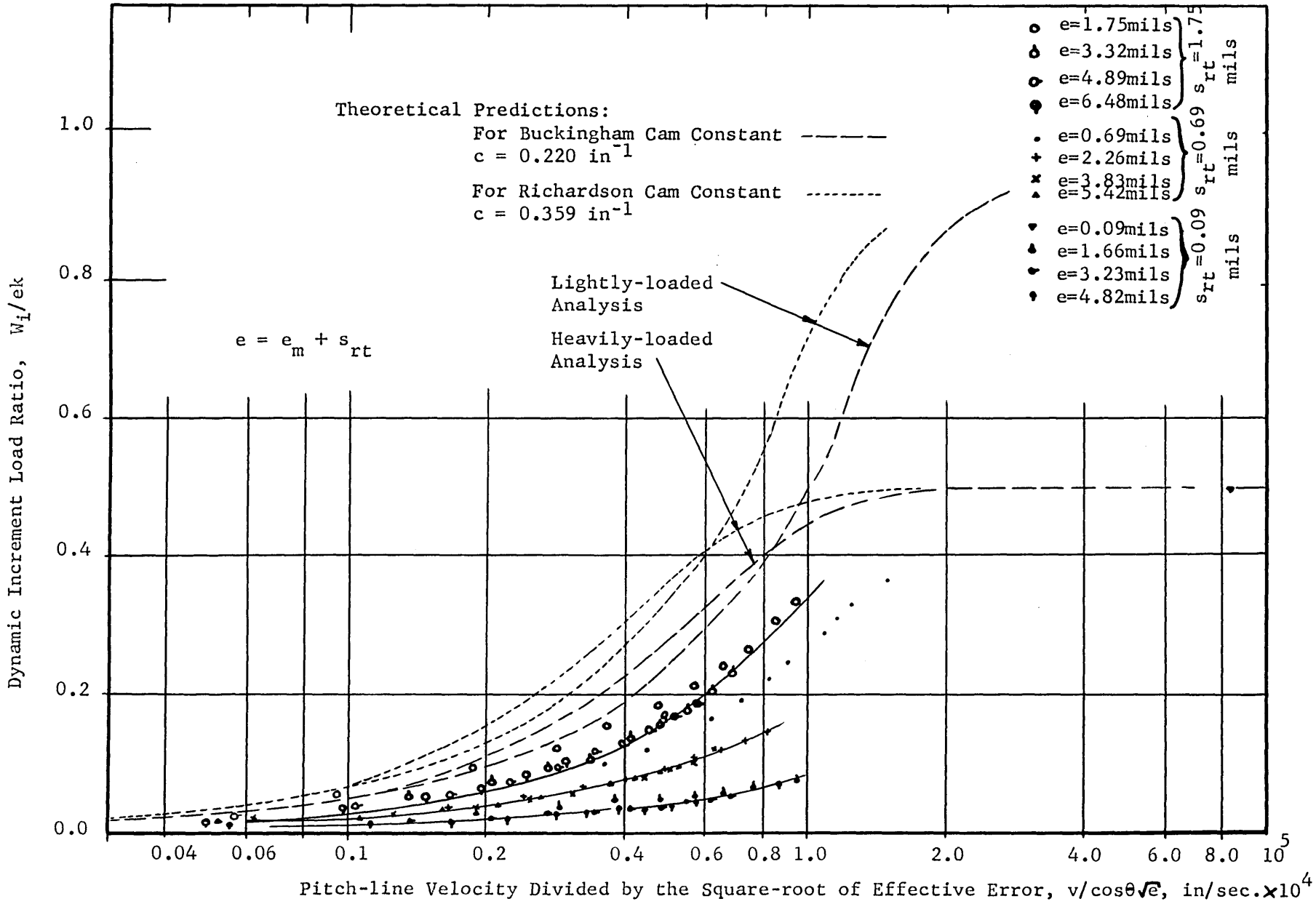

Fig. 72. Comparison Between Measured Dynamic Loads of Rettig[46] and Predicted Dynamic Loads According to the Single-Load-Transfer Theories.

Fig. 72 should lie on one curve. That is, the frequency ratio β was varied by changing pitch-line velocity, load (hence s_{rt}), and manufactured error (e_m). For any given value of load, Rettig's data for different manufactured errors and pitch-line velocities appear to correlate rather well; however, as the transmitted load increases, the increment-load curve appears to shift to the left in Fig. 72. The broken-line curves shown in Fig. 72 are curves of theoretical dynamic increment load, predicted from the results of Chapter 3. The dashed curves were computed using the cam constant c as given by Buckingham (Eq. 3.53), and the dotted curves were computed using a cam constant c obtained from the no-load separation curves of Fig. 18. The value of the cam-constant given by Buckingham was 0.220 in.$^{-1}$, and that given by the no-load separation was 0.359 in.$^{-1}$. The frequency ω_n was computed to be 3760 cps for the gears employed in Rettig's work. The dynamic increment loads predicted by the single-engagement analysis using available values for the cam constant are in all cases substantially larger than the increment loads observed by Rettig. The general trends of increment load versus pitch-line velocity were observed to correspond with predictions. Unfortunately, Rettig's tests did not extend to pitch line velocites at which the asymptotic dynamic loads predicted by the single-engagement analyses should be reached.

5. Tentative Conclusions Regarding Dynamic Loads

On the basis of measurements made by this author on precision gearing and by Rettig on gearing which had controlled amounts of error, the following tentative conclusions are reached.

1. In heavily-loaded, accurate gearing where pitch-line velocities are not too high ($q_a > 300^\circ$, but β has any value,) dynamic loads can be neglected.

2. In lightly-loaded gearing, where manufactured errors are large, the single load-transfer theories apply, and dynamic increment loads can become very large compared with static transmitted loads. The theoretical analyses for single load-transfer presented in Chapter 3 appear to give conservative estimates of dynamic load.

These conclusions must be considered tentative until more carefully controlled experiments have been carried out on gear systems in which all parameters that are significant to dynamic loads are varied. The results presented in Chapters 3 and 4 of this thesis have served to determine these significant parameters and to find ranges in which certain parameters appear to be important while others can be neglected.

CHAPTER 5. SUMMARY, CONCLUSIONS, AND RECOMMENDATIONS

The subject matter of this thesis has been concerned with the loads and significant stresses that the teeth of spur-gear systems experience under operational conditions. This document does not constitute a complete solution to the problem of predicting dynamic contact loads and stresses in any gear system, but is intended to be a reasonably thorough preliminary investigation of the problem. Specifically, the following accomplishments are claimed.

1. A general theory has been developed and useful charts, equations, and other data have been presented which permit computation, in a relatively simple manner, of the static load, stress, or deflection cycles for any gear system, real or contemplated. All prior published information of this nature has not been derived rigorously from first principles, and has neglected completely the significant effects of elastic deformation during load transfer and of friction. The analysis presented here has been derived in the most rigorous manner that appeared possible, and the results were verified by comparison with measurements made by this author and by Rettig of Germany. The results presented should be valuable in making refined stress analyses in gear design, and will make possible the computation of more suitable profile-modification forms than are currently in use.

2. Two physical phenomena which appeared to be the major controlling influences in gear dynamics have been analyzed, and qualitative predictions regarding dynamic tooth loads and stresses have been derived from these analyses. A single-load-transfer mechanism was found to predict that dynamic loads would increase monotonically as a function

of the ratio (β) of system-natural period to engagement or disengagement time and would reach constant asymptotic loads (see Figs. 43 and 47). The analyses of the single-load-transfer phenomena were extensions of Reswick's work[45]. In high-speed, accurate gearing, it was found that the effective time-varying elasticity of the gear mesh could produce steady-state periodic oscillations of the two gears and thus cause dynamic loads. The amplitudes of these dynamic loads were found to be limited only by the magnitude of the effective damping that exists between the mating members. The dynamic load was found to vary with the ratio (q_a) of the gear-system natural frequency to the tooth-engagement frequency (see Figs. 49 and 50). As pitch-line velocity increases, the dynamic load increases and decreases successively. At very high pitch-line velocity an asymptotic load is reached which is less than the average static load.

3. An experimental technique has been developed for measuring dynamic loads in an operating gear system. The method is simple and the transducers are plain wire strain gages which are inexpensive to purchase and are easy to install.

4. Preliminary comparison has been made between measured dynamic stress cycles (of this author and of Rettig) and the predictions of the simplified analyses. This comparison indicates that the single-load-transfer theories presented in Chapter 3 will give somewhat conservative predictions of dynamic loads in lightly-loaded or inaccurate gearing. However, in the case of accurately-machined, heavily-loaded gears, the dynamic loads behave in the manner predicted by the variable-elasticity model. For the precision gears tested in this investigation, measured dynamic increment loads never exceeded 15 per cent of the static loads.

On the basis of the preliminary comparisons between the simplified analyses and the observed results, the following recommendations are made for future investigation.

1. Extensive measurements of dynamic load should be made on accurate and inaccurate gear systems under conditions where load, mass, error, speed, pitch, and lubricant characteristics are varied. The test set-up for making these measurements is currently available and operable. These tests should cover ranges of frequency-ratio β from 0 to 3, and of frequency ratio q_a from infinity to 80°.

2. The simplified variable-elasticity model should be extended to cover a range of contact ratios from 1 to 2.

3. More refined models for gear dynamics which combine the single-load-transfer behavior with the variable-elasticity behavior should be established and analyzed, perhaps with the aid of digital computation techniques. The equations upon which a comprehensive numerical analysis could be based are presented in this thesis. Such an analysis would be a logical extension of the results presented in Chapter 2 for the static-load situation.

APPENDIX A. COMPUTATION OF HERTZIAN COMPRESSION OF GEAR-TOOTH SURFACES

1. Determination of the Potential Functions

When the assumed load distribution, Eq. (2.19), is substituted into Eq. (2.21), the following integral is obtained.

$$\Phi = \frac{W_o}{\pi b^2 j} \int_{-b}^{b} \frac{\sqrt{b^2 - t^2}\, dt}{t + z} \tag{A.1}$$

or when the integration is carried out,

$$\Phi = - \frac{W_o j}{\pi b^2} \left(- z + \sqrt{z^2 - b^2} \right) \tag{A.2}$$

$$\frac{d\Phi}{dz} = - \frac{W_o j}{\pi b^2} \left[- 1 + \frac{z}{\sqrt{z^2 - b^2}} \right] \tag{A.3}$$

When Eqs. (A.3) and (2.22) are combined

$$\Psi = \frac{W_o j}{\pi b^2} \left[- z + \frac{z^2}{\sqrt{z^2 - b^2}} \right] \tag{A.4}$$

2. Plane-Strain Solution for Deformation

When Eqs. (2.22), (2.24), (2.25), and (2.26) are combined, the strain in the direction of the contact load (ϵ_y) is found to be

$$\epsilon_y = \frac{ds_{rH}}{dy} = \frac{1 + \eta}{E} \mathrm{Re} \left[(2 - 4\eta)\, \Phi - \frac{(\bar{z} - z)}{z} \right] \tag{A.5}$$

Since the deformation in the direction of the load is required, the substitution can be made

$$z = iy \tag{A. 6}$$

Then Eq. (A. 5) takes the form

$$\frac{ds_{rH}}{dy} = -\frac{1+\eta}{E} \operatorname{Re}\left[(2 - 4\ \ )\Phi + 2\Psi\right] \tag{A. 7}$$

When Eqs. (A. 2), (A. 4), (A. 6), and (A. 7) are combined,

$$\frac{ds_{rH}}{dy} = \frac{1+\eta}{E}\ \frac{W_o}{\pi b^2}\left[4y + (2 - 4\eta)\sqrt{y^2 + b^2} - \frac{y^2}{\sqrt{y^2 + b^2}}\right] \tag{A. 8}$$

The integral of Eq. (A. 8), between the limits y = 0 and y = h, is

$$s_{rH} = -\frac{2(1+\eta)(1-\eta)\,W_o}{\pi E}\left[\frac{\eta}{2(1-\eta)} + \log_e \frac{b}{2h}\right] \tag{A. 9}$$

Examination of Eq. (A. 9) shows that as h becomes large, the deformation s_{rH} tends to infinity. Hence, the integration must be limited to finite values of h. In this case it is assumed that

$$h = \frac{p_n}{4} \tag{A. 10}$$

The total Hertzian compression is the sum, as given by Eq. (A. 9), of the deformation for the two mating teeth. When Eqs. (A. 9) and (A. 10) are combined, the assumption is made that both mating teeth are of the same material, this total compressive deformation is

$$\frac{s_{rH}}{p_n} = \frac{W_o}{Ep_n} \frac{2(1 - \eta^2)}{\pi} \left[\log_e \frac{p_n^2}{4b^2} - \frac{\eta}{1 - \eta} \right] \tag{A.11}$$

Equation (2.20) aan be rewritten in the form

$$\frac{b^2}{p_n^2} = \frac{W_o}{Ep_n} \left[\frac{\frac{r_1}{p_n} \quad \frac{r_2}{p_n}}{\frac{r_1}{p_n} + \frac{r_2}{p_n}} \right] \frac{8(1 - \eta^2)}{\pi} \tag{A.12}$$

If s is the distance of the point of contact between mating teeth from the pitch-point, the radii of curvature are given by

$$\begin{aligned} r_1 &= R_{B1} \tan\theta + s \\ r_2 &= R_{B2} \tan\theta - s \end{aligned} \tag{A.13}$$

When Eqs. (A.13) and (A.12) are combined, and the definition of normal pitch is utilized, Eq. (A.12) becomes

$$\frac{b^2}{p_n^2} = \frac{W_o}{Ep_n} \frac{4(1 - \eta^2) \tan\theta}{\pi^2} \frac{i_1 i_2}{i_1 + i_2} \left(1 + \frac{2\pi s}{i_1 \tan\theta \, p_n} \right) \left(1 - \frac{2\pi s}{i_2 \tan\theta \, p_n} \right) \tag{A.14}$$

where i_1 and i_2 are the numbers of teeth on gears 1 and 2, respectively. Define

$$i_e = \frac{i_1 i_2}{i_1 + i_2} \tag{A.15}$$

When Eqs. (A.11), (A.14), and (A.15) are combined, the following expression for the Hertzian compression is obtained

$$s_{rH} = \frac{2(1-\eta^2)}{\pi} \frac{W_o}{Ep_n} \left[\log \frac{\pi^2}{16(1-\eta^2)\tan\theta} - \log i_e - \log\left(\frac{W_o}{Ep_n}\right) \right.$$

$$\left. - \frac{\eta}{1-\eta} - \log\left(1 + \frac{2\pi}{i_1 \tan\theta} \frac{s}{p_n}\right) - \log\left(1 - \frac{2\pi}{i_2 \tan\theta} \frac{s}{p_n}\right) \right] \qquad (A.16)$$

For pitch-point contact, Eq. (A.16) becomes

$$\left(\frac{s_r}{p_n}\right)_H = \frac{2(1-\eta^2)}{\pi} \frac{W_o}{Ep_n} \left[\log \frac{\pi^2}{16(1-\eta^2)\tan\theta} - \log i_e - \log\left(\frac{W_o}{Ep_n}\right) - \frac{\eta}{1-\eta} \right]$$

(A.17)

Equation (A.17) is plotted as a dashed line in Fig. 11 for 20° pressure-angle steel gears (= 0.3). This function is not linear, but can be approximated over the practical operating range of the load variable (W_o/Ep_n) by the linear relationships tabulated in Fig. 11. Thus the Hertzian compression for pitch-point contact can be expressed approximately as

$$\left(\frac{s_r E}{W_o}\right)_H = w_H \qquad (2.29)$$

When contact is away from the pitch point, a correction must be applied to account for the change in radii of curvature of the mating members. Comparison of Eqs. (A.17) and (A.16) shows that such corrections can be expressed in the form

$$\Delta w_H = \Delta\left(\frac{s_r E}{W_o}\right)_H = -\frac{2(1-\eta^2)}{\pi} \left[\log\left(1 + \frac{2\pi}{i_1 \tan\theta} \frac{s}{p_n}\right) + \log\left(1 - \frac{2\pi}{i_2 \tan\theta} \frac{s}{p_n}\right) \right]$$

(A.18)

Equation (A. 18) is expressible in two forms, depending on the sign of s/p_n:

$$\Delta w_H = CR_2\left(i_2, \frac{s}{p_n}\right) - CR_1\left(i_1, \frac{s}{p_n}\right); \quad \frac{s}{p_n} > 0$$

$$\Delta w_H = CR_2\left(i_1, \frac{s}{p_n}\right) - CR_1\left(i_2, \frac{s}{p_n}\right); \quad \frac{s}{p_n} < 0 \tag{A. 19}$$

where

$$CR_1 = \log\left(1 + \frac{2\pi}{i \tan\theta}\,\frac{s}{p_n}\right)\frac{2(1-\eta^2)}{\pi}$$

$$CR_2 = -\log\left(1 - \frac{2\pi}{i \tan\theta}\,\frac{s}{p_n}\right)\frac{2(1-\eta^2)}{\pi} \tag{A. 20}$$

These correction factors depend only on the contact position, the numbers of teeth in the mating gears, and the pressure angle. The deformation corrections are linear functions of the load variable W_o/Ep_n. The total deformation is given by Eq. (2. 30)

$$\left(\frac{s_r E}{W_o}\right)_H = w_H + \Delta w_H\left(\frac{s}{p_n}\right) \tag{2. 30}$$

3. Plane-Stress Solution for Deformation

When Eqs. (2.22), (2.24), (2.25), and (2.27) are combined the strain is tound to be

$$\epsilon_y = \frac{ds_{rH}}{dy} = \frac{1}{E} \operatorname{Re} \left[2(1 - \eta)\Phi - (1 + \eta)\Psi \frac{(\bar{z} - z)}{z} \right] \tag{A.21}$$

The combination of Eqs. (A.2), (A.4), (A.6), and (A.21) gives

$$\frac{ds_{rH}}{dy} = \frac{1}{E} \frac{W_o}{\pi b^2} \left[4\eta y + 2(1 - \eta) \sqrt{y^2 + b^2} + 2(1 + \eta) \frac{y^2}{\sqrt{y^2 + b^2}} \right] \tag{A.22}$$

When Eq. (A.22) is integrated between the limits y = 0 and y = h,

$$s_{rH} = - \frac{2W_o}{\pi E} \left(\frac{\eta}{2} + \log_e \frac{b}{2h} \right) \tag{A.23}$$

Equation (A.23) can be put in the same form as Eq. (A.16), in order to determine the total compression for two mating gear teeth.

$$\frac{s_{rH}}{p_n} = \frac{2}{\pi} \frac{W_o}{Ep_n} \left[\log \frac{\pi^2}{16(1 - \eta^2) \tan \theta} - \log i_e - \log \left(\frac{W_o}{Ep_n} \right) - \eta \right.$$

$$\left. - \log \left(1 + \frac{2\pi}{i_1 \tan \theta} \frac{s}{p_n} \right) - \log \left(1 - \frac{2\pi}{i_2 \tan \theta} \frac{s}{p_n} \right) \right] \tag{A.24}$$

Equation (A.24) is plotted in Fig. 11 as solid lines, for the case of pitch-point contact, steel gears, and 20° pressure angle.

The corrections for change in radii of curvature are given by Eqs. (A. 19), where the correction factors have the slightly different form:

$$CR_1 = \left[\log\left(1 + \frac{2\pi}{i \tan\theta} \frac{s}{p_n}\right)\right] \frac{2}{\pi}$$

$$CR_2 = -\left[\log\left(1 - \frac{2\pi}{i \tan\theta} \frac{s}{p_n}\right)\right] \frac{2}{\pi} \tag{A. 25}$$

These correction factors have been plotted in Fig. 12 for 20° pressure-angle gears.

The total Hertzian compression is determined from Figs. 11 and 12, as given by Eq. (2. 30). For most practical purposes, the corrections given by Fig. 12 can be neglected if the number of teeth in each gear is greater than 24.

APPENDIX B. GEOMETRY OF THE NO-LOAD SEPARATION OF IDEAL INVOLUTE GEAR TEETH

Figure 73 shows the geometrical configuration of a pair of gear teeth that are approaching contact. The no-load separation is defined as the amount of rotation required of one gear, when the other member is held fixed, to cause contact between the pair of teeth that is almost touching. The assumption is made that the gear teeth are ideal; that is, manufactured errors are neglected in the region of imminent contact. Under these conditions, the contact will occur between the tip of one gear and a point on the profile of the other tooth. If rounding of the tip of the contacting tooth is assumed, the analysis of no-load separation becomes extremely difficult, due to the fact that the location of the contact point on either tooth is unknown initially and must be located by trial and error.

Case I. Gear Which Engages at its Base Held Fixed

The various terms which will be used in the following development are defined on Fig. 73. In this figure, the no-load separation is zero when the tip of gear 2 lies at point A on the line of action. Conditions at this point will be designated by (*).

When the contact-point of gear 2 is at the pitch point, the tip of gear 2 lies an angular distance δ_o to the left of the pitch point. The origin of the involute curve of gear 1 then lies an angular distance β_o to the left of the pitch point. According to the definition of the involute function

$$\beta_o = \tan\theta - \theta = \text{inv}\,\theta \tag{B.1}$$

The origin of the involute curve for gear 2 lies an angular distance β_o to the right of the pitch point.

$$\cos\phi_2 = \frac{R_{B2}}{R_{o2}} \tag{B.2}$$

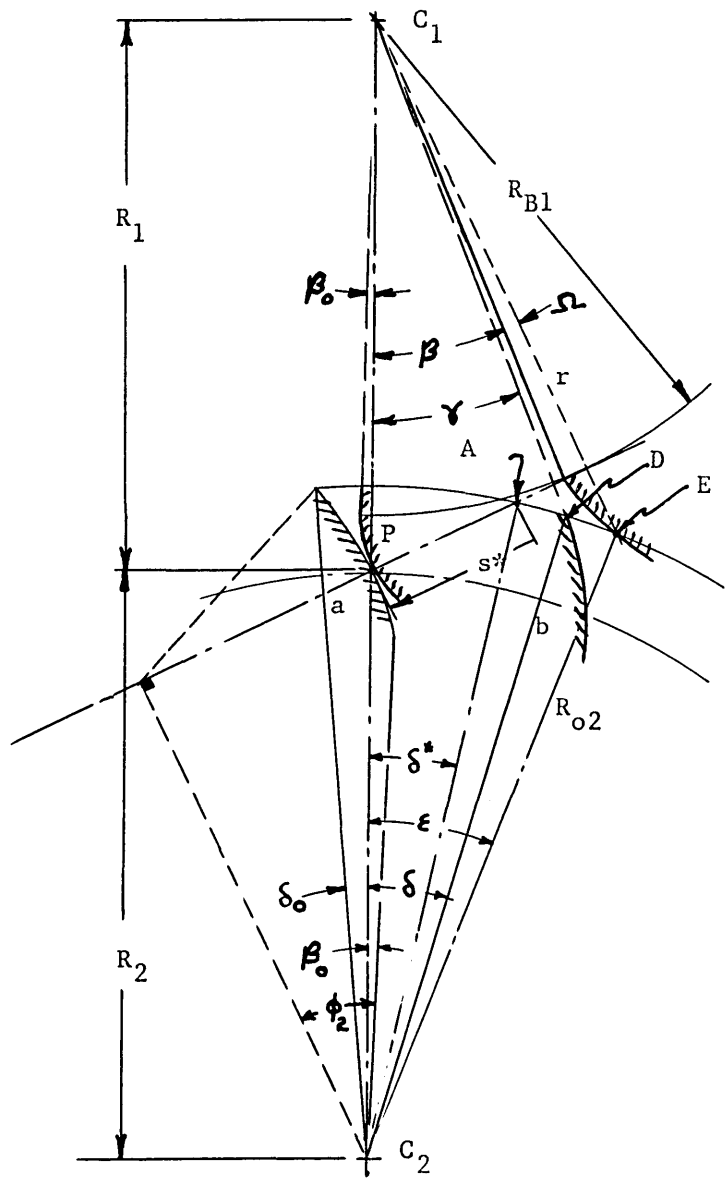

Fig. 73. Geometry of No-Load Separation.

By standards:

$$\frac{R_{o2}}{R_2} = 1 + \frac{2a_a}{i_2} \tag{B.3}$$

Therefore

$$\frac{R_{o2}}{R_{B2}} = \left(1 + \frac{2a_a}{i_2}\right) \frac{1}{\cos\theta} \tag{B.4}$$

Then

$$\delta_o = \text{inv}\left[\cos^{-1}\left(\frac{\cos\theta}{1 + \frac{2a_a}{i_2}}\right)\right] - \beta_o \tag{B.5}$$

Under no-load conditions, the gears operate without pitch-circle slip. Therefore, the angular rotations of the two gears are related according to the following equation

$$(\delta + \delta_o)\ R_2 = (\beta + \beta_o)\ R_1 \tag{B.6}$$

or

$$\beta = (\delta + \delta_o)\ \frac{i_2}{i_1} - \beta_o \tag{B.7}$$

In order to bring tooth-pair b into contact, when gear 1 is held fixed, gear 2 must be rotated through an angle $(\epsilon - \delta)$. Thus the no-load separation for gear 1 held fixed, measured along the pressure line is

$$\left.\frac{\Delta s}{p_n}\right|_1 = (\epsilon - \delta)\ R_{B2}\left(\frac{i_2}{2\pi\ R_{B2}}\right) = \frac{i_2}{2\pi}\ (\epsilon - \delta) \tag{B.8}$$

The absolute position of the gears can be referred conveniently to the position (*) where the no-load separation is zero. From the geometry of Fig. 73, when the tip of gear 2 lies at point A.

$$\tan\theta = \frac{R_{o2}\cos\delta^* - R_2}{R_{o2}\sin\delta^*} \tag{B.9}$$

When Eqs. (B.3) and (B.9) are combined,

$$\tan\theta\sin\delta^* = \cos\delta^* - 1 - \frac{2a_a}{i_2} \tag{B.10}$$

The solution of Eq. (B.10) for $\cos\delta^*$ is

$$\cos\delta^* = \frac{1}{1 + \frac{2a_a}{i_2}} \; \frac{1 + \sqrt{1 - (1 + \tan^2\theta)\left[1 - (1 + \frac{2a_a}{i_2})\tan^2\theta\right]}}{(1 + \tan^2\theta)} \tag{B.11}$$

The absolute position of the gears now can be specified in terms of distance along the pressure line from the point where the no-load separation is zero.

$$\frac{s - s^*}{p_n} = \frac{i_2}{2\pi}(\delta - \delta^*) \tag{B.12}$$

The no-load separation can be determined from Eq. (B.8) if the point of intersection of the addendum circle of gear 2 with the involute curve of gear 2 is known. The equation of the involute curve for gear 1 is, in terms of the involute function,

$$\frac{r}{R_{B1}} = \frac{1}{\cos\left(\mathrm{inv}^{-1}\Omega\right)} \tag{B.13}$$

Now consider the geometry of the figure $\overline{C_1 E C_2}$:

$$r = (R_1 + R_2) \cos (\beta + \Omega) - \sqrt{R_{o2}^2 - \left(\frac{R_1 + R_2}{R_{B1}}\right)^2 \sin^2 (\beta + \Omega)} \tag{B.14}$$

Let

$$dr = \frac{R_{o2}}{R_1 + R_2} = \left(1 + \frac{2a_a}{i_2}\right) \frac{i_2}{i_1 + i_2} \tag{B.15}$$

Then Eq. (B.14) can be written as

$$\frac{r}{R_{B1}} = \frac{i_1 + i_2}{i_1 \cos \theta} \left[\cos (\beta + \Omega) - \sqrt{d_r^2 - \sin^2 (\beta + \Omega)}\right] \tag{B.16}$$

From the law of sines,

$$\frac{r}{\sin \epsilon} = \frac{R_{o2}}{\sin (\beta + \Omega)} \tag{B.17}$$

When Eqs. (B.17), (B.15), and (B.4) are combined,

$$\frac{r}{R_{B1}} = d_r \frac{i_1 + i_2}{i_1 \cos \theta} \frac{\sin \epsilon}{\sin (\beta + \Omega)} \tag{B.18}$$

From Eqs. (B.18) and (B.16)

$$\sin \epsilon = \frac{1}{d_r} \sin (\beta + \Omega) \left[\cos (\beta + \Omega) - \sqrt{d_r^2 - \sin^2 (\beta + \Omega)}\right] \tag{B.19}$$

When Eqs. (B.13) and (B.16) are equated,

$$\cos \ \mathrm{inv}^{-1}\Omega = \frac{\cos\theta}{1 + \frac{i_2}{i_1}} \left[\frac{1}{\cos(\beta+\Omega) - \sqrt{d_r^{\,2} - \sin^2(\beta+\Omega)}} \right] \tag{B.20}$$

The value of $(\beta + \Omega)$ when the no-load separation is zero is given by the relation

$$\tan(\beta+\Omega)^* = \frac{\sin\delta^*}{\frac{1}{d_r} - \cos\delta^*} \tag{B.21}$$

The no-load separation curve,

$$\frac{\Delta s}{p_n} = f\left(\frac{s - s^*}{p_n}\right) \tag{B.22}$$

must be generated in a step-by-step fashion in the following way.

a. Compute the values of

β_o from Eq. (B.1)

δ_o from Eq. (B.5)

$$1 + \frac{2a_a}{i_2}$$

d_r from Eq. (B.15)

δ^* from Eq. (B.11)

$(\beta+\Omega)^*$ from Eq. (B.21)

b. Choose a value of $(\beta+\Omega) > (\beta+\Omega)^*$

c. Compute $\cos \ \mathrm{inv}^{-1}\Omega$ from Eq. (B.20) and hence determine the value of Ω. Subtract Ω from the assumed $(\beta+\Omega)$ to obtain β.

d. Compute ϵ from Eq. (B.19)

e. Compute δ from Eq. (B.7)

f. Substitute ϵ, δ, and δ^* into Eqs. (B.8) and (B.12) and determine the corresponding values of $\Delta s/p_n$ and $s - s^*/p_n$. Figure 16 shows the no-load separation curve, expressed in the form defined by Eq. (B.22), for $i_1 = 27$ and $i_2 = 36$. In every case, the i_2 value refers to the gear which engages (or disengages) at its tip.

Case II. Gear Which Engages at its Tip Held Fixed

Figure 74 shows the geometry for determining the no-load separation when gear 2 is held fixed. In this case point C of gear 1 will move into contact with the tip of gear 2.

$$\frac{r}{\sin\delta} = \frac{R_{o2}}{\sin\gamma} \tag{B.23}$$

$$\frac{r}{R_{B1}} = \frac{r}{R_{o2}} \frac{R_{o2}}{R_2} \frac{R_2}{R_1} \frac{R_1}{R_{B1}} = \frac{r}{R_{o2}} \left(1 + \frac{2a_a}{i_2}\right) \frac{i_2}{i_1} \frac{1}{\cos\theta} \tag{B.24}$$

Therefore

$$\frac{r}{R_{B1}} = \frac{\sin\delta}{\sin\gamma} \left(1 + \frac{2a_a}{i_2}\right) \frac{i_2}{i_1 \cos\theta} \tag{B.25}$$

$$R_1 + R_2 = r\cos\gamma + R_{o2}\cos\delta \tag{B.26}$$

hence

$$\frac{r}{R_{B1}} = \frac{(R_1 + R_2)}{R_{o2}} \frac{R_{o2}}{R_2} \frac{R_1}{R_{B1}} \frac{1}{\cos\gamma} - \frac{R_{o2}}{R_2} \frac{R_2}{R_1} \frac{R_1}{R_{B1}} \frac{\cos\delta}{\cos\gamma} \tag{B.27}$$

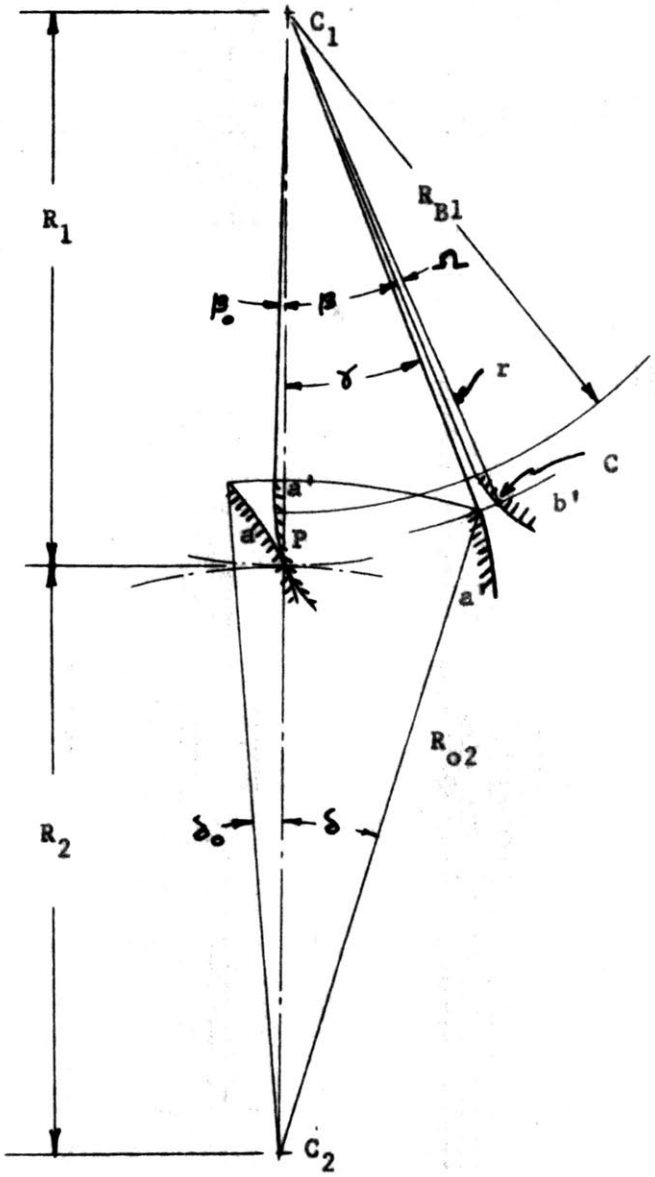

Fig. 74. Geometry of No-Load Separation.

Therefore, when the definition of d_r is employed from Eq. (B.15)

$$\frac{r}{R_{B1}} = \left(\frac{1}{d_r} \frac{1}{\cos\gamma} - \frac{\cos\delta}{\cos\gamma}\right)\left(1 + \frac{2\alpha_a}{i_2}\right) \frac{i_2}{i_1 \cos\theta} \tag{B.28}$$

When Eqs. (B.28) and (B.25) are equated,

$$\tan\gamma = \frac{\sin\delta}{\frac{1}{d_r} - \cos\delta} \tag{B.29}$$

When Eqs. (B.24) and (B.15) are combined + (B.23)

$$\frac{r}{R_{B1}} = \frac{\sin\delta}{\sin\gamma} \; d_r \; \frac{i_1 + i_2}{i_1 \cos\theta} \tag{B.30}$$

From the definition of the involute function

$$\cos\phi_1 = \frac{R_{B1}}{r} \tag{B.31}$$

or, equating Eqs. (B.31) and (B.30),

$$\cos\phi_1 = \frac{\sin\gamma}{\sin\delta \; d_r} \; \frac{\cos\theta}{\left(1 + \frac{i_2}{i_1}\right)} \tag{B.32}$$

Also

$$\Omega = \text{inv}\,\phi_1 \tag{B.33}$$

From Eq. (B.7)

$$\beta = \frac{i_2}{i_1} (\delta + \delta_o) - \beta_o \tag{B.7}$$

The no-load separation along the pressure line can be expressed in the form

$$\left.\frac{\Delta s}{p_n}\right|_2 = \frac{i_2}{2\pi} (\beta + \Omega - \gamma) \tag{B.34}$$

and according to Eq. (B.12)

$$\frac{s - s^*}{p_n} = \frac{i_2}{2\pi} (\delta - \delta^*) \tag{B.12}$$

The steps involved in computing the no-load separation for gear 2 held fixed can now be outlined.

a. Compute the values of δ^*, δ_o, β_o and d_r as described under Case I above.

b. Assume a value of δ, substitute this value into Eq. (B.29) and solve for γ.

c. Using the values of γ and δ, determine ϕ_1 from Eq. (B.32).

d. From Eq. (B.33), compute the value of Ω.

e. Calculate β from Eq. (B.7).

f. Substitute β, Ω, γ, and δ into Eqs. (B.34) and (B.12) to determine a point on the no-load separation curve.

Exact solutions for the two no-load separations designated as Case I and Case II above are plotted in Fig. 16 for one combination of 20° full-depth involute gear teeth. Over the operating range shown in this figure, the difference between the two curves is rather small. Therefore, either of the two curves may be used with acceptable accuracy in the gear system analysis.

For future calculations of no-load separation, it is suggested that the equations for Case II be employed, since the calculation procedure is simpler in this case than in Case I.

It is possible to approximate the arc distances involved in the no-load separation calculations by straight lines over the short distances involved, and thus arrive at simpler equations for the no-load separation than have been presented in this Appendix. Approximations of this nature lead to predicted curves which are almost identical with the exact curves. However, since the calculations must be carried out to at least 6 decimal places in order to obtain 3-place accuracy in the resulting curves, a calculating machine normally will be used. Under these conditions the exact solution for Case II is almost as easy to work out as the approximate solution. For this reason the Case II exact solution is recommended over an approximate calculation, and the approximate analysis is not included here.

APPENDIX C. ANALYSIS OF GEAR-TOOTH ENGAGEMENT

Figure 75 shows the geometrical situation when a tooth-pair b is engaging. The diagram is drawn for no-load conditions, but at the position shown, the deflection of tooth-pair a due to transmitted load is sufficient to bring tooth-pair b into contact.

The following assumptions are made.

a. Friction is negligible.

b. The spring constant of the engaging pair of teeth is not significantly affected by small deviations of the contact force from the line of action.

c. The input and output torques τ_1 and τ_2 are nearly constant, but may vary enough to permit the engagement process to occur.

d. Initial contact occurs at the tip of one of the engaging teeth.

e. Engagement geometry depends only on the relative displacements of the two gears for given proximity of the engaging tooth-pair. That is, a unique no-load separation curve is assumed.

Assuming that gear 2 is held fixed in defining the no-load separation, tooth pair b will come into contact at point G on tooth b'.

The equilibrium equations for the two gears are, in terms of the symbols defined on Fig. 75,

$$\tau_2 - W_a R_{B2} - W_b(X - \epsilon^*) = J_2 \ddot{\psi}_2 \qquad \text{(C.1)}$$

$$\tau_1 - W_a R_{B1} - W_b (R_{B1} + \epsilon^*) = - J_1 \ddot{\psi}_1 \qquad \text{(C.2)}$$

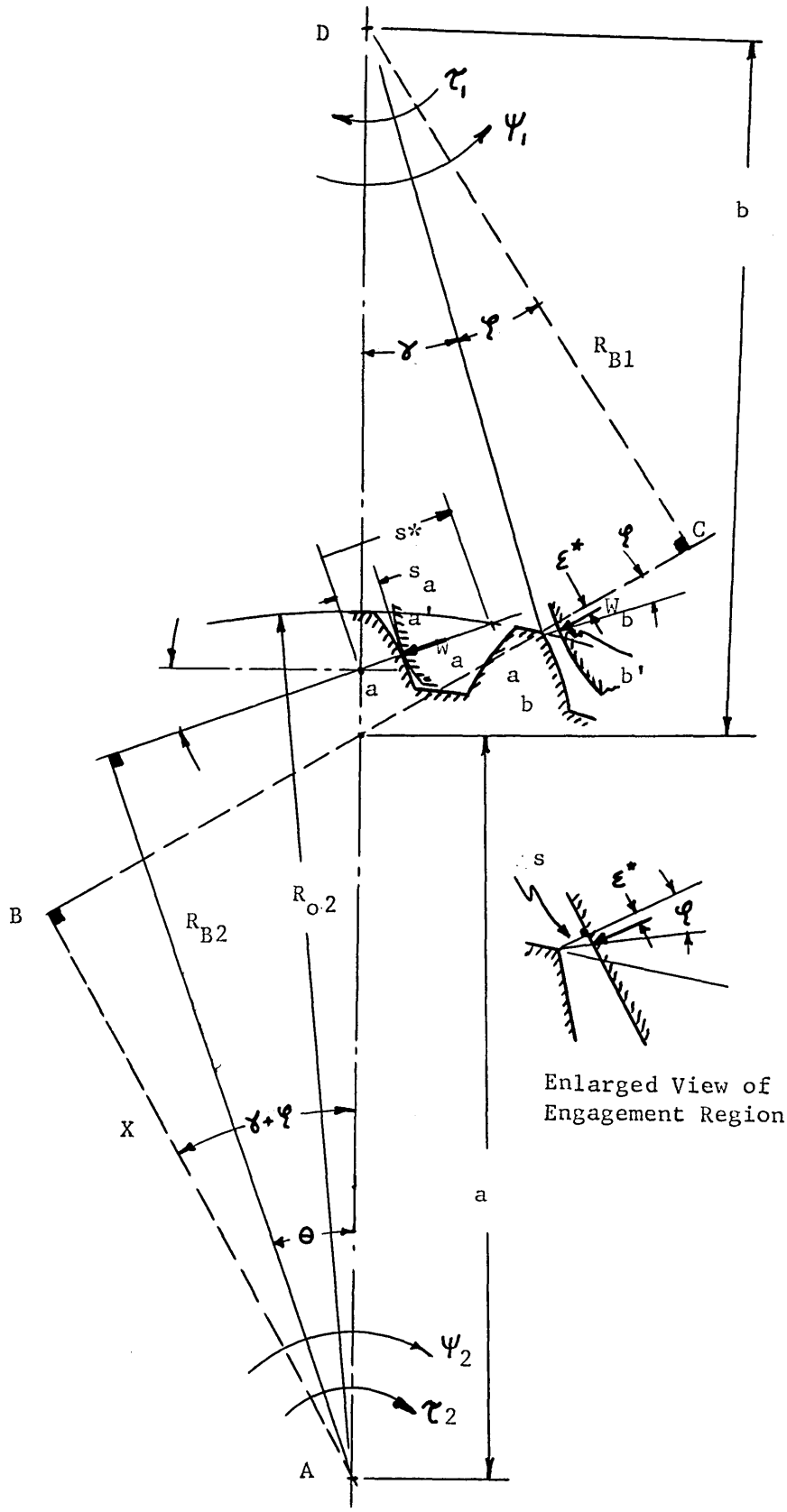

Fig. 75. Gear-Tooth Loading and Engagement Geometry.

From the geometry of figure ABCD,

$$b \cos (\gamma + \varphi) = R_{B1} \tag{C.3}$$

$$a \cos (\gamma + \varphi) = X \tag{C.4}$$

$$a + b = \frac{R_{B1} + R_{B2}}{\cos \theta} \tag{C.5}$$

Therefore,

$$X = \frac{R_{B1} + R_{B2}}{\cos \theta} \cos (\gamma + \varphi) - R_{B1} \tag{C.6}$$

According to assumption 5,

$$\epsilon^* = \Delta s \, \varphi \tag{C.7}$$

The angular rotations of the gears are referred to linear motion along the line of action by the equations

$$\begin{aligned} s_1 &= R_{B1} \Psi_1 \\ s_2 &= R_{B2} \Psi_2 \end{aligned} \tag{C.8}$$

If k_a and k_b are spring constants for tooth-pairs a and b, respectively,

$$\begin{aligned} W_a &= k_a (s_2 - s_1) \\ W_b &= k_b \quad (s_2 - s_1) - \Delta s && \text{if } \Delta s = (s_2 - s_1) \\ &= 0 && \text{if } \Delta s = (s_2 - s_1) \end{aligned} \tag{C.10}$$

Now assume that the inertias J_1 and J_2 are negligible, When Eqs. (C.1) (C.6) and (C.7) are combined

$$\tau_2 - W_a R_{B2} - W_b \left[\frac{R_{B1} + R_{B2}}{R_{B1}} \left(\frac{\cos \gamma + \varphi}{\cos \theta} - 1 \right) + \frac{R_{B2}}{R_{B1}} - \frac{\Delta s \varphi}{R_{B1}} \right] R_{B2} = 0 \tag{C.11}$$

Since

$$\frac{R_{B1}}{R_{B2}} = \frac{i_1}{i_2}, \tag{C.12}$$

equation (C.11) can be written

$$\frac{\tau_2}{R_{B2}} - W_a - W_b - W_b \left[\left(1 + \frac{i_2}{i_1} \right) \left(\frac{\cos \gamma + \varphi}{\cos \theta} - 1 \right) - \frac{\Delta s \varphi}{R_{B2}} \right] = 0 \tag{C.13}$$

From Eqs. (C.2) and (C.7)

$$\frac{\tau_1}{R_{B1}} - W_a - W_b - W_b \, \Delta s \, \varphi = 0 \tag{C.14}$$

Let

$$\frac{\tau_1}{R_{B1}} = \frac{\tau_{10}}{R_{B1}} - \frac{\Delta \tau_1}{R_{B1}} \tag{C.15}$$

$$\frac{\tau_2}{R_{B2}} = \frac{\tau_{20}}{R_{B2}} + \frac{\Delta \tau_2}{R_{B2}} \tag{C.16}$$

where the subscript (0) refers to conditions when contact is on the pressure line. Then $\Delta s = 0$ and $\cos \gamma + \varphi / \cos \theta = 1$ and therefore

$$\frac{\tau_{10}}{R_{B1}} - \frac{\tau_{20}}{R_{B2}} = \frac{\Delta \tau_1}{R_{B1}} + \frac{\Delta \tau_2}{R_{B2}} \tag{C.17}$$

Assuming that τ_1 and τ_2 are constant when engagement is not occurring,

$$\frac{\tau_{10}}{R_{B1}} = \frac{\tau_{20}}{R_{B2}} = W \tag{C.18}$$

Then Eqs. (C.13) and (C.14) become

$$\frac{\Delta \tau_2}{R_{B2}} + W - (W_a + W_b) - W_b \left[\left(1 + \frac{i_1}{i_2}\right)\left(\frac{\cos \gamma + \xi}{\cos \theta} - 1\right) - \frac{\Delta s\, \xi}{R_{B2}}\right] = 0 \tag{C.19}$$

$$-\frac{\Delta \tau_1}{R_{B1}} + W - (W_a + W_b) - W_b \frac{\Delta s\, \xi}{R_{B1}} = 0 \tag{C.20}$$

Equations (C.19) and (C.20) may be replaced by the sum and difference equations

$$\frac{\Delta \tau_2}{R_{B2}} - \frac{\Delta \tau_1}{R_{B1}} + 2W - 2(W_a + W_b) - W_b \left[\left(1 + \frac{i_1}{i_2}\right)\left(\frac{\cos \gamma + \xi}{\cos \theta} - 1\right) - \frac{\Delta s\, \xi}{p_n}\left(\frac{1}{i_2} - \frac{1}{i_1}\right)\right] = 0 \tag{C.21}$$

$$\frac{\Delta \tau_2}{R_{B2}} + \frac{\Delta \tau_1}{R_{B1}} - W_b \left[\left(1 + \frac{i_1}{i_2}\right)\left(\frac{\cos \gamma + \xi}{\cos \theta} - 1\right) - \frac{\Delta s\, \xi}{p_n}\, 2\pi\left(\frac{1}{i_1} + \frac{1}{i_2}\right)\right] = 0 \tag{C.22}$$

Equation (C.22) shows that, for any finite load W_b, a change in one or both torques τ_1 and τ_2 is necessary to force the tooth-pair b into engagement.

In Eqs. (C.21) and (C.22) the angle $(\gamma + \varphi)$ is very close to the angle θ, and the angle φ is a very small angle. Similarly the no-load separation $\Delta s/p_n$ is an extremely small quantity. Thus, for practical purposes, the changes in torques can be neglected.

This conclusion also can be reached by comparing the change in potential energy of the tooth-springs to the work done by the variations of input and output torques over the angular distances traversed during engagement.

Since, according to the no-load separation curves, the gears rotate a very large distance in order to change the no-load separation by a small amount, a very small torque change will produce sufficient work to compress the engaging tooth-pair spring.

APPENDIX D. RELATIONSHIP BETWEEN GEAR TOOTH LOAD AND NOMINAL BENDING STRESS

1. Bending Moment

Figure 76 shows a gear tooth located at a distance s from the pitch-point, measured along the line of action. The bending moment at a distance (gR) above the base can be expressed in terms of the quantities defined on Fig. 76.

$$M = W(h - gR) \tag{D. 1}$$

$$R = \frac{R_B}{\cos\phi} + (R - R_i) - h \tag{D. 2}$$

By standards (see Table 1, p. 23),

$$R - R_i = \frac{a_d p_c}{\pi} = \frac{a_d 2R}{i} \tag{D. 3}$$

When Eqs. (D. 3), (D. 2), and (D. 1) are combined,

$$M = W \cos\phi \, R \left[\frac{2a_d}{i} + \frac{\cos\theta}{\cos\phi} - 1 - g\right] \tag{D. 4}$$

This moment can be nondimensionalized in the following way. Let

$$M_o = W \cos\theta \, (R - R_i) = W \cos\theta \, R \, \frac{2a_d}{i} \tag{D. 5}$$

Thus

$$\frac{M}{M_o} = \frac{i}{2a_d} \cos\phi \left[\frac{1}{\cos\phi} - \frac{\left(1 + g - \frac{2a_d}{i}\right)}{\cos\theta}\right] \tag{D. 6}$$

The moment at the base of the tooth is obtained by setting $g = 0$ in Eq. (D. 6).

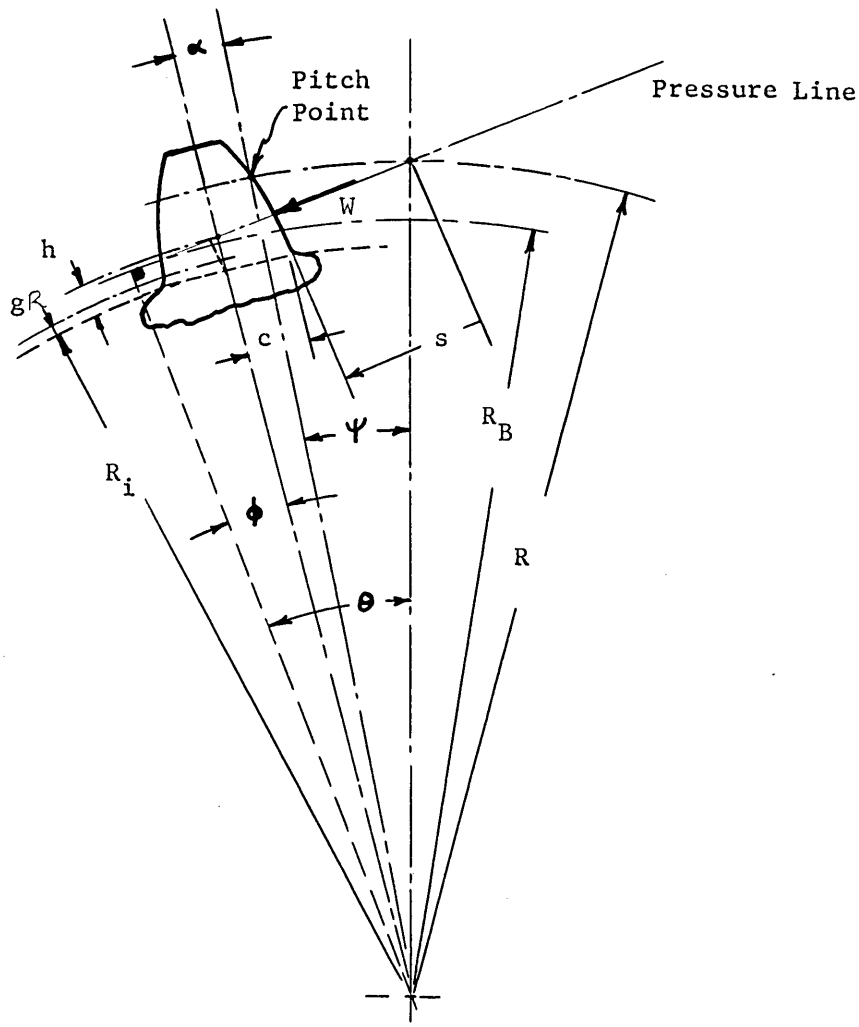

Fig. 76. Geometrical Relationships for a Loaded Gear Tooth.

2. Cross-Sectional Area

In a determination of the cross-sectional area of the base of a gear tooth, two cases must be distinguished depending on whether the base circle lies inside or outside of the dedendum circle. The base circle lies inside the dedendum circle if

$$R \cos \theta < R \left[1 + \frac{2a_d}{i} \right] \tag{D.7}$$

For 20° pressure-angle full-depth involute gears, the condition stated in Eq. (D.7) reduces to

$$i > 38 \tag{D.8}$$

Case I. More than 38 Teeth in the Gear

For this case, the tooth thickness is determined by the intersection of the involute curve and the dedendum circle. Let

$$a_1 = \text{inv}\ \theta \tag{D.9}$$

$$a_2 = \text{inv} \left[\cos^{-1} \frac{R_B}{R_i} \right] \tag{D.10}$$

Then the tooth thickness 2c is given by the equation

$$\frac{2c}{R_B} = \frac{2R_i}{R_B} \left[a_1 - a_2 + \frac{\pi}{2i} \right] \tag{D.11}$$

or

$$\frac{2c}{R_B} = \frac{2(1 - 2\frac{a_d}{i})}{\cos \theta} \left[\text{inv}\ \theta - \text{inv} \left\{ \cos^{-1} \left(\frac{\cos \theta}{(1 - 2\frac{a_d}{i})} \right) \right\} + \frac{\pi}{2i} \right] \tag{D.12}$$

Case II. Less Than 38 Teeth in the Gear

In this case the assumption is made that the tooth surface is straight below the base circle. Thus the tooth thickness is determined by the thickness at the base radius. The desired result may be obtained from Eq. (D. 1) by setting $a_2 = 0$.

$$\frac{2c}{R_B} = \frac{2(1 - 2\frac{a_d}{i})}{\cos\theta}\left(\text{inv}\,\theta + \frac{\pi}{2i}\right) \tag{D. 13}$$

3. Lewis Form Factor

The Lewis factor is defined by Eq. (1. 1)

$$Y = \frac{W\cos\theta\, p_d}{\sigma f} \tag{1. 1}$$

The stress σ can be expressed as

$$\sigma = \frac{Mc}{\frac{1}{12} f(2c)^3} = \frac{3}{2}\left(\frac{M_o}{fc^2}\right)\left(\frac{M}{M_o}\right) \tag{D. 14}$$

When Eqs. (D. 5), (D. 6), and (D. 14) are combined, and g is set equal to zero

$$\sigma = \frac{3}{2}\,\frac{W\cos\theta\, R}{fc^2}\,\cos\phi\left[\frac{1}{\cos\phi} - \frac{(1 - 2\frac{a_d}{i})}{\cos\theta}\right] \tag{D. 15}$$

The combination of Eqs. (1. 1) and (D. 15) yields the expression

$$\frac{1}{Y} = 3\,\frac{R^2}{c^2}\,\cos\phi\left[\frac{1}{\cos\phi} - \frac{(1 - 2\frac{a_d}{i})}{\cos\theta}\right] \tag{D. 16}$$

When Eqs. (D. 16) and (D. 12) are combined

$$\frac{1}{Y} = \frac{3 \cos \phi \left[\frac{1}{\cos \phi} - \frac{\left(1 - 2 \frac{a_d}{i}\right)}{\cos \theta} \right]}{i \left(1 - 2 \frac{a_d}{i}\right)^2 \left[\text{inv}\, \theta - \text{inv} \left(\cos^{-1} \frac{\cos \theta}{\left(1 - 2 \frac{a_d}{i}\right)} \right) + \frac{\pi}{2i} \right]^2} \; ; \; i > 38 \qquad \text{(D. 17)}$$

and when(D. 16) and (D. 13) are combined

$$\frac{1}{Y} = \frac{3 \cos \phi \left[\frac{1}{\cos \phi} - \frac{\left(1 - 2 \frac{a_d}{i}\right)}{\cos \theta} \right]}{i \left(1 - 2 \frac{a_d}{i}\right)^2 \left[\text{inv}\, \theta + \frac{\pi}{2i} \right]^2} \; ; \; i < 38 \qquad \text{(D. 18)}$$

From Fig. 75,

$$\phi = \theta - \psi - a \qquad \text{(D. 19)}$$

$$a = \frac{\pi}{2i} \qquad \text{(D. 20)}$$

$$s = R_B \psi = \frac{i p_n \psi}{2\pi} \qquad \text{(D. 21)}$$

Therefore,

$$\phi = \theta - \frac{i}{2\pi} \psi \frac{s}{p_n} - \frac{\pi}{2i} \qquad \text{(D. 22)}$$

Equations (D. 22), (D. 18), and (D. 17) have been employed to compute the curves given in Fig. 22 of the inverse Y factor versus normalized position along the line of action. The various curves apply for different numbers of teeth, as indicated, and have been plotted for 20° pressure-angle full-depth involutes.

APPENDIX E. BIBLIOGRAPHY

1. Lewis, Wilfred, "Investigation of the Strength of Gear Teeth," Proceedings of the Engineers' Club, Vol. 10, Philadelphia, 1893.

2. Lasche, Oscar, "Elecktrischer Antrieb mittels Zahnradübertragung", V.D.I. Zeit., 1899.

3. Logue, C. H., "Influence of Impact on Gears," American Machinists, Vol. 35, 1910.

4. Marx, G. H., "Strength of Gear Tooth," Trans. A.S.M.E., Vol. 34, 1912.

5. Cutter, L. E., and Marx, G. H., "The Strength of Gear Teeth," Trans. A.S.M.E., Vol. 37, 1915.

6. Lewis, W., "A New Method for Determining the Effect of Speed on the Strength of Gear Teeth," Mechanical Engineering, Vol. 44, 1922.

7. Lewis, W., "Modern Problems in Gear Testing and a Proposed Testing Machine," American Machinist, December 13, 1923.

8. Nicholas, John E., The Influence of Elasticity and Errors in Tooth Shape on Stresses in Gears, Thesis, S.M., Dept. of Mech. Engr., Mass. Inst. of Tech., Cambridge, Mass., 1926.

9. Timoshenko, A., and Baud, N.V., "Strength of Gear Teeth," Mechanical Engineering, Vol. 48, 1926.

10. Cushman, P.A., Spur Gear Strength as Influenced by Pitch, Material, Attached Flywheels, Tooth Errors, and Tooth Forms, Thesis , Dept. of Mech. Engr., Mass. Inst. of Tech., Cambridge, Mass., 1927.

11. Ortiz, S., and Castellanos, M.R., Effect of Mass on Tooth Load of Gears, Thesis, S.B., Dept of Mech. Engr., Mass. Inst. of Tech., Cambridge, Mass., 1927.

12. Buckingham, E., Spur Gears, McGraw-Hill Book Company, Inc. New York, N.Y., 1928.

13. DuVernet and Shedd, "Limiting Wear Loads on Gear Teeth," Thesis, S.M., Dept. of Mech. Engr., Mass. Inst. of Tech., Cambridge, Mass., 1928.

14. Progress Reports Nos. 4 - 14, A.S.M.E. Special Research Committee on the Strength of Gear Teeth, Mechanical Engineering Vols. 49 to 51, 1927 - 1929.

15. Baud and Peterson, "Load and Stress Cycles in Gear Teeth," Mechanical Engineering, Vol. 51, N. 9, 1929, p. 653.

16. Diefendorf and Wyman, Impact Factors for Nitrided Gears, Thesis, S.M., Dept. of Mech. Engr., Mass. Inst. of Tech., Cambridge, Mass., 1930.

17. Peterson, R.E., "Load and Deflection Cycles in Gear Teeth," Proc. 3rd. Intern. Appl. Mech. Cong., 1930, p. 382.

18. Schulze, C., Dynamic Loads on Gear Teeth, Thesis, S.M., Dept. of Mech. Engr., Mass. Inst. of Tech., Cambridge, Mass., 1930.

19. Buckingham, E., Dynamic Loads on Gear Teeth, Report of Special Research Committee on the Strength of Gear Teeth, A.S.M.E., New York, 1931.

20. Black, P. M., "An Investigation of the Relative Stresses in Solid Spur Gears by the Photoelastic Method," Univ. of Illinois Bulletin No. 288, December 1936.

21. Blok, H., "Measurement of Temperature Flasks on Gear Teeth Under Extreme Pressure Conditions," Proc. Inst. Mech. Engr., 1937.

22. Walker, H., "Gear Tooth Deflections and Profile Modifications," The Engineer, Vol. 166, 1938, and Vol. 170, 1940.

23. Dolan, T. J., "Influence of Certain Variables on the Stresses in Gear Teeth," Jour. Applied Physics, Vol. 12, August 1941, p. 584.

24. Dolan, T. J., and Broghamer, E. I., "A Photoelastic Study of the Stresses in Gear Tooth Fillets," Univ. of Illinois Engr. Expt. Sta. Bull., Ser. 335, Vol. 39, N 31, March 1942.

25. Portsky, H., Sutton, A. D., and Pernick, A., "Distribution of Tooth Load Along a Pinion," Jour. Applied Mech., A. S. M. E. Vol. 12, N 2, June 1945.

26. "Strength of Spur Gear Teeth," A. G. M. A. Standard 220.01, December 1946.

27. "Gear Tooth Wear," A. G. M. A. Standard, Machinery, Vol. 52, N 8, April, 1946, p. 166.

28. Blok, H., "Gear Wear as Related to the Viscosity of the Gear Oil," Proc. of the Summer Conference on Mechanical Wear, Mass. Inst. of Tech., Cambridge, Mass., June 1948.

29. Buckingham, E., Analytical Mechanics of Gears, McGraw-Hill Book Co., Inc., New York, 1949.

30. Weber, C., "The Deformation of Loaded Gears and the Effect on Their Load-Carrying Capacity," Part I, Dept. of Scientific and Industrial Research, Sponsored Research Report No. 3, London, England, 1949.

31. Dudley, "Modification of Gear Tooth Profiles," Product Engineering, Vol. 20, N. 9, September 1949, p. 126.

32. Mills, K. N., "Gearing, How to Reduce Noise and Increase Efficiency with Modified Tooth Forms," Machine Design, Vol. 21, N. 1, January 1949, p. 89.

33. Leopold, W. R., "Gear Wear Load," Machine Design, Vol. 22, N. 7, July 1950, p. 159.

34. Tuplin, W. A., "Gear-Tooth Stresses at High Speed," Proc. Inst. Mech. E., Vol. 163, 1950, p. 162.

35. Durham, H. M., "Designing Spur and Helical Gears for Durability," Machine Design, Vol. 23, N. 1, January 1951, p. 149.

36. Mills, K. N., "Gears- Improving the Resistance of Heavy Duty Gearing to Service Damage," Machine Design, Vol. 23, N. 5, May 1951, p. 116.

37. A. G. M. A. Progress Report by Automative Gearing Committee, Sec. II, P. V. T. Valves of Gear Teeth, A. G. M. A. Pub. 101.02, October 1951.

38. Kelley, B. W., "A New Look at the Scoring Phenomena of Gears," Trans. S. A. E., 1952.

39. Merritt, H. E., "Gear Tooth Stresses and Rating Formulae," Proc. Inst. Mech. E 1952.

40. Poritsky, H., "Lubrication of Gear Teeth, Including the Effect of Elastic Displacement," Fundamentals of Friction and Lubrication in Engineering, First A. S. L. E. Symposium, Published by A. S. L. E., Chicago, Ill., 1952.

41. Van Zandt, R. P., "Beam Strengthof Spur Gears," Quarterly Trans. S. A. E., Vol. 6, N. 2, April 1952, p. 252.

42. Dudley, D. W., "Discussion of B. W. Kelley Paper," Trans. S. A. E., 1952.

43. Tuplin, W. A., "Dynamic Loads on Gear Teeth," Machine Design, Vol. 25, October 1953, p. 203.

44. Degner, V. R., "Gear - Wear Evaluation in High-and Low-Speed Instrument Gear Trains," North American Aviation, Inc., Report EM-686, A. S. T. I. A., No. AD-49952, 1954.

45. Reswick, J. B., "Dynamic Loads on Spur-and Helical-Gear Teeth," Trans. A. S. M. E., Vol. 77, N. 5, July 1954, p. 635.

46. Rettig, H., Dynamische Zahnkraft, Thesis, Dr.-Ing., Techn, Hochschule, München, 1956.

47. Spur Gear Design Standard, Applied Physics Laboratory, Univ. of Washington, Seattle, Washington, October 1956.

48. Kelley, B. W., and Pedersen, R., "The Beam Strength of Modern Gear Tooth Design," S.A.E. Preprint, presented at the Annual Earthmoving Conference, Peoria, Illinois, March 26, 1957.

49. Niemann, G., and Rettig, H., "Dynamische Zahnkräfte," V.D.I. Zeit, Bd. 99, Nr. 3, S. 89, und Nr. 4, S. 131, 1957.

50. Zeman, J., "Dynamische Zusatzkräfte in Zahnradgetrieben," V.D.I. Zeit, February 21, 1957, p. 244.

51. Brickman, A.D., The Effect of Tooth Deformation and Profile Inaccuracy on Operating Loads in Gearing, Thesis, Mech. E., Dept. of Mech. Engr., Mass. Inst. of Tech., Cambridge, Mass., 1956.

52. Muskhelishvili, N.I., Some Basic Problems of the Mathematical Theory of Elasticity, P. Noordhoff, Groningen, Holland, 1953, pp. 410 - 415.

BIOGRAPHICAL NOTE

The author, son of Walter B. and Isabel E. Richardson was born in Lynn, Massachusetts, on September 24, 1930. He attended the public schools of Bridgton, Maine, and graduated from Bridgton High School in June, 1948. He attended Colby College in Waterville, Maine for one year, 1948 -1949, and transferred to M.I.T. as a freshman in September of 1949. He was admitted to the Honors Course in Mechanical Engineering in 1951, and received the degrees of Bachelor of Science and Master of Science simultaneously in February, 1955.

During his period of graduate work, the author combined his studies with teaching and with research activities at the Dynamic Analysis and Control Laboratory. Since 1953, he has been involved in research and development work concerned with hydraulic and pneumatic control systems, dynamics, instrumentation, and combustion. He holds the rank of First Lieutenant in the U. S. Army Reserve.

He was appointed Instructor in Mechanical Engineering in 1957 and Assistant Professor in 1958. Teaching activities have included courses in Machine Design, Fluid Control Systems, and Applied Mechanics.

Activities as a consultant have included work with the University of Virginia, Pantex Manufacturing Co., Bryant Chucking Grinder Co., General Electric Company, and others, in connection with hydraulic control systems, gas-lubricated bearings, and various design problems.

Marriage to Estelle French of Waltham, Massachusetts took place in 1953, and a child, Gale Ann, was born in 1955. The family now lives in Waltham.

PRINCIPAL NOMENCLATURE

b	effective damping at the pressure line, lb-sec/in.
	or half-width of local contact band between mating teeth, in.
B	rotary damping, in-lb-sec.
c	cam constant, in^{-1}
	or half-width of the base of a gear tooth
C	a constant
CR	contact ratio or correction factor
d_r	ratio of addendum radius to center distance for a pair of gears
e	total error, manufactured plus elastic deformation, in.
e_m	total manufactured error, in.
e_p	profile error, in.
e_s	spacing error, in.
E	Young's Modulus, psi
f	face width, in.
i	number of teeth
I	operator which varies between 1 and 2, periodically
j	$\sqrt{-1}$
J	moment of inertia, in-lb-sec^2
k	tooth-pair spring stiffness, lb/in.
K	wear factor, psi
m	effective mass at the base circle, lb-sec^2/in.
n	stress correction factor
N	radial component of gear-tooth load, lbs.
p_c	circular pitch, in.
p_d	diametral pitch, in^{-1}
p_n	normal pitch, in.
P	pressure, psi
q_a	tooth-engagement frequency ratio
r	radius of curvature of a gear tooth, in.
r_f	fillet radius of a gear tooth, in.

PRINCIPAL NOMENCLATURE (Continued)

R	pitch radius, in.
R_B	base-circle, radius, in.
R_i	dedendum radius, in.
R_o	addendum radius, in.
s	displacement along the line of action, measured from the pitch-point, in.
s_r	relative motion between two gears, measured along the pressure line, in.
s_{rt}	deflection of a single pair of teeth due to the transmitted load, in.
t	time, sec.
T	tangential component of gear-tooth load, lbs.
T_c	time for one pair of teeth to pass through the gear mesh, sec.
v	average circumferential velocity of the base circle, in/sec.
V	velocity, in/sec
w	nondimensionalized compliance
W	effective static load acting along the pressure line, lbs.
$W_{a,b,c}$	total loads acting on tooth-pairs a, b, c, lbs.
W_d	dynamic tooth load, lbs.
W_f	friction force, lbs.
W_i	dynamic increment tooth load, lbs.
W_o	load per unit of face width acting on a gear tooth, lbs/in.
x	coordinate axis
y	coordinate axis
Y	Lewis form factor, dimensionless
z	complex variable $x + iy$
Z	number which has magnitude unity and the sign of s

PRINCIPAL NOMENCLATURE (Continued)

α_a	dimensionless factor determining addendum distance
α_d	dimensionless factor determining dedendum distance
β	frequency-ratio for single load transfer
γ	angle, degrees
δ	pitch-circle slip, in.
Δs	no-load separation, measured along the pressure line, in.
ϵ	small quantity
ϵ_y	strain in the y-direction
ξ	angle, degrees
η	Poisson's Ratio
θ	pressure angle, degrees
μ	coefficient of friction
π	3.14159
σ	stress, psi
τ	torque, in-lb.
τ_{xy}	shear stress in the x-y plane, psi
ϕ	angle, degrees
Φ	potential function
ψ	angle of rotation of a gear, degrees
Ψ	potential function
ω	angular velocity, rad/sec
ω_n	natural frequency of gear system oscillating on one tooth-spring, rad/sec
Ω	angle, degrees
ζ	damping ratio